PhD Thesis

SAPIENZA
UNIVERSITÀ DI ROMA

Faculty of Mathematical, Physical and Natural Sciences

Department of Earth Sciences

Multiphysical modelling for thermo-mechanical behaviour of rock masses in slope-scale gravitational dynamics

Candidate: Gian Marco Marmoni

Cycle: XXX Curriculum: Geosciences

Advisor: Prof. Salvatore Martino

A.A. 2017/2018

DIPARTIMENTO
DI SCIENZE DELLA TERRA

SAPIENZA
UNIVERSITÀ DI ROMA

DOTTORATO DI RICERCA
IN SCIENZE DELLA TERRA

Summary

Acknowledgements

This research was supported and funded by the following institutions in the frame of the projects:

- "Sapienza" University of Rome - "Landslide triggering in areas affected by intense morphodynamics due to volcanism, seismicity and erosional processes" (Anno: 2012 - prot. C26A12MT4F) P.I. Prof. S. Martino.
- Italian National Antarctic Research Programme (PNRA) PdR 2013/B2.01- "How climate changes and crustal thermo-mechanic variations interact in driving East Antarctic glacial evolution since late Cenozoic?" (P.I.: C. Baroni).
- "Sapienza" University of Rome - "Influence of geothermal systems and related thermal regime variations on the onset and development of large slope instabilities in the island of Ischia" (Year 2015 - prot. C26A15FH3L - P.I. Dr. Carlo Esposito);
- Partenariats Hubert Curien (PHC) and Università Italo Francese, "Galileo 2016-2017" grant (project number 37180VC) "Landslide-triggered tsunami hazard in the Mediterranean: improving risk mitigation strategies by understanding natural processes" (P.I. Dr. Michael Heap and Prof. Salvatore Martino).
- Starting Research 2016 "Sapienza" University of Rome "Influenza delle proprietà termo meccaniche di ammassi rocciosi fratturati ai fini della stabilità e della mitigazione del rischio da frana" (P.I. Matteo Fiorucci).

Thanks to my mentor and guide Prof. Salvatore Martino. He deserve my respect, my esteem and gratitude.
All this work would not have been possible without his original idea, his constant guidance, his commitment and his professionalism. Thank you for trust in me and for all the opportunities you gave me and still gives me today, thanks for the constant presence in times of difficulty, thanks for the laughs and the nice moments shared together during all the activities carried out.

I wish to thank Profs. Carlo Baroni and Maria Cristina Salvatore for the support to the formulation of the Antarctic case study and the reconstruction of the morpho-evolutionary model of Priestley glacier, and to Prof. Gianni Musumeci for the validation of geological cross-section of Priestley glacier.

A special mention is regarded to Prof. Mario Gaeta, Dr. Cristina Perinelli e Dr. Gianluca Sottili for the essential contribution to volcanological surveys and

petrographic analysis. A thanks goes to B. Renaudié, Dr. J.I. Farquharson, Prof. P. Baud, and T. Reuschlè for their useful suggestions and support during the laboratory work. A good luck to L. Griffiths for his PhD defense and a sincere thanks for your friendship and the time spent together in Strasbourg.

I would like to express my gratitude to Dr. Michael Heap who gave me the opportunity to have a formative research experience during a not-easily forgettable internship. Thanks for the teachings and all the "sugar-coated" comments.

I express my sincere thanks to Dr. Andrea Calabriso and Dr. Paolo Venturini for the support on physical formulation numerical thermo-hydrodynamical model of Ischia Island and the time spent to teach me the code.

The most important acknowledges must be expressed to my family, my love and all my best friends, support and reference in every stage of my life.

Abstract

Volcanic and glacial valley systems are geological context where Deep Seated Gravitational Slope Deformations (DSGSDs) frequently evolve. These areas experienced in their geological history significant variation in stress field due to the rapid growth of volcano flanks or glacial debuttressing rebound, respectively. In addition to these effects, a less importance have been given to multi-physical interactions between the slopes and the natural systems in which the DSGSD can evolved.

In order to evaluate the role of physical or multi-physical interaction in dictating time-dependant slope-scale gravitational deformation processes, a numerical analysis has been approached reproducing by stress-strain and thermo-hydrodynamical modelling, the mutual interaction between thermal and mechanical processes in slope stability. With the purpose to evaluate and constrain the inner forcings related to deep systems which can influence the gravitational process acting in the slopes, the combination of models at different geometric-scales have been experimented.

Basing on two selected case study, representative of two thermal end-member (i.e. warm and cold systems) the influence of thermo-mechanical processes in gravity-induced deformations was evaluated by adopting different solving schemes as function of the stationarity or transiency of the systems within an observation time-window. Coupled or Uncoupled solution between two or more physics were experimented reproducing sequential evolution of slope system with the support of FDM and FEM numerical codes. A process of validation of the Thermal and the Mechanical models defined for both deep- and slope-scales were achieved by means of sensitivity and parametric analysis. The validated models were then used for the formulation of physically-based scenarios, defined to evaluate the role of multiple factors in the onset or time-evolution of slope deformation. The adopted approach

represented an useful tool to evaluate the proneness of DSGSDS to paroxysmal tertiary failure and in the definition multi-hazard scenarios related to slope instabilities.

1. Introduction

Deep Seated Gravitational Slope Deformations (DSGSDs Auct.) are one of the most impressive processes related to gravity that can be observed in mountain areas or volcanic systems. These processes can frequently represent major threats, because they can involve huge slope sections causing even catastrophic failures (i.e. high magnitude events in terms of volume and/or run-out distances).

The scale of such deformations ranges from slow rock-slope deformations to fast massive rock-slope failures, with the latter frequently representing the local acceleration of a long-term time-dependent process. These landforms, in fact, evolve on a time span of the order of thousands of years and are frequently located in geological and morpho-structural contexts characterised by steep slopes with considerable extensions and involved volumes. The geological setting of the slope, the joint conditions and mechanical properties of the rock mass may influence the development and evolution of such phenomena, representing a predisposing factor for slope instabilities.

Literature widely recognizes this kind of slope instability as a mass rock-creep process (Bozzano et al., 2012; Chigira, 1992; Della Seta et al., 2017; Petley et al., 2005) responsible for peculiar micro- and macro-scale landforms -Fig. 1- (Agliardi et al., 2001; Pánek et al., 2017).

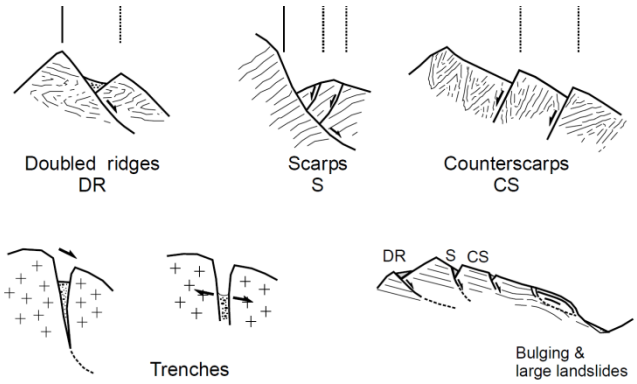

Fig. 1 - Morpho-structural features typical of a DSGSD (after Agliardi et al., 2011).

The above processes are normally retained as expression of a slow and continuous evolution (Chigira, 1992; McCalpine and Irvine, 1995), but may be locally reactivated or accelerated by the combined action of endogenous and exogenous phenomena (Del Ventisette et al., 2012; Moro et al., 2007; Palis et al., 2016) leading to a generalised collapse (Bianchi Fasani et al., 2011; Esposito et al., 2013; Scarascia et al., 2006; Semenza and Ghirotti, 2000), triggered by internal or external transient actions (Benko and Stead, 1998; Bozzano et al., 2011; Del Ventisette et al., 2012). These disturbances may affect the deformative response of the slope-system, resulting in acceleration or deceleration of a continuous process, thereby influencing the evolution of the same gravitational process and affecting possible risk scenarios associated with it (Haque et al., 2016; Petley, 2012).

It follows that, in complex geological systems (i.e. volcanic and hydrothermal systems, glacial and periglacial zones, high seismicity areas), the role of endogenous processes cannot be underestimated and a multidisciplinary approach able to take into account multiple physical interactions is required. In this context, temperature conditions related to the geothermal gradient as well as to specific anomalies connected to local heat sources, may affect the mechanical and rheological behaviour of the rock mass involved, potentially anticipating time to failure.

To this aim an integrated thermo-mechanical modelling of the deformative behaviour of natural slopes involved in peculiar geological context where strong thermal interaction exist cannot be disregarded.

By means of numerical models through Finite Element Methods (FEMs) and Finite Difference Methods (FDMs) (Zienkiewicz, 1971; Smith, 1978) these influences will be analysed, defining the role of complex physics in the slope scale gravitational dynamics, in the frame of definition of primary and residual risk conditions.

The main steps performed in dealing with slope-scale gravitational dynamics by multi-physical approach will be discussed in this doctoral thesis, starting from the definition of an engineering geological model based on a pure geomechanical

approach, moving to an integrated field- and laboratory-based numerical modelling as follows:

Chapter 2: It provides a literature review regarding slope-scale gravitational deformations, analysing thermo-mechanical effects both in laboratory and slope scales, and discussing implications for long term evolution of dynamic systems in multi-hazard scenarios.

Chapter 3: It focuses on a numerical approach in the definition of an inclusive multi-physical analysis capable to describe the thermodynamics of complex systems with the purpose of validating thermo-mechanical or thermo-hydro-mechanical models devoted to the formulation of predictive analysis of future scenarios.

Chapter 4: It introduces experimental materials and the working approach adopted for numerical analysis. This chapter illustrates the importance of definition of an engineering geological model and conceptual models for the best description of natural systems in stationary or transient conditions, by numerical analysis.

Chapter 5: Following the methods mentioned above, this chapter introduces the two selected case studies, which, for their characters, are representative and functional for the topic and finality of this research. Case studies dealing with conductive and/or convective heat transfer systems were chosen, reproducing through thermal mono- and multi-phase models the thermalisation conditions where DSGSD can evolve.

Chapter 6: It reports the numerical solutions adopted in both case studies, such as function of thermal and fluid flow regimes, as much as the spatial and temporal scale of evolution for the reconstructed slope scale processes. A comparison of mechanical and thermo-mechanical models was provided, analysing the sensitivity to variable thermal scenarios and rheological parameters assumptions.

Chapter 7: It illustrates the main inferences derived by numerical modelling results, highlighting the outcomes of thermo-mechanical models and the suitability of multi-physical approaches dealing with slope-scale gravitational deformation topics.

Chapter 8: It summarise the general work approach used, providing general conclusions and perspectives for modelling of slope deformations and gravitational dynamics at slope scale.

The preliminary contributions to this Thesis (here presented in Chapter 5) have been published in the following journal papers or conference proceedings:

- *Della Seta M., Esposito C., Marmoni G.M., Martino S., Paciello A., Perinelli C., Sottili G. (2015).Geological constraints for a conceptual evolutionary model of the slope deformations affecting Mt. Nuovo at Ischia (Italy). Italian Journal of Engineering Geology and Environment (2) DOI: 10.4408/IJEGE.2015-02.O-02*
- *Marmoni G.M., Martino S., Heap M.J., Reuschlé T. (2017). Multiphysics laboratory tests for modelling gravity-driven instabilities at slope scale. Procedia Engineering 191: 142 – 149*
- *Marmoni G.M., Martino S., Heap M.J., Reuschlé T. (2017). Gravitational slope-deformation of a resurgent caldera: new insights from the mechanical behaviour of Mt. Nuovo tuffs (Ischia Island, Italy). J. Volcanol. Geotherm. Res. 345: 01 – 20.*
- *Marmoni G.M., Calabriso A., Martino S., Borello D., Della Seta M., Esposito C., Fiorucci M., Venturini P. (2016). Hydrothermal system influencing slope-scale deformations at Mt. Nuovo (Ischia, Southern Italy):preliminary results from 2D-multiphysics numerical modeling. Atti 35th GNGNTS.*
- *Baroni C., Gaeta M., Marmoni G.M., Martino S., Perinelli C., Salvatore M.C. & Scarascia Mugnozza G. (2016). 1D Numerical modelling of crustal heat transfer in the Antarctic glaciers of Northern Victoria Land. Abstract S35th IGC, Cape Town.*
- *Baroni C., Gaeta M., Marmoni G.M., Martino S., Perinelli C., Salvatore M.C. & Scarascia Mugnozza G. (2016). Crustal heat transfer in the Antarctic glaciers: From*

1D- to 2D-multiphysics numerical modelling. Rend. Online Soc. Geol. It., Suppl. n. 1 al Vol. 40.

The fundamental contribution represented by thermal, mechanical and thermo-mechanical numerical modelling of both case studies (Chapters 3-6-7), remains nowadays an unpublished work.

2. Gravitational slope deformations: thermo-mechanical interactions in slope dynamics

2.1. State of the Art

Since the second half of the last century and the milestone works of Zischinsky (1966, 1969) and Varnes (1978), a considerable part of slope stability researches focus on the mechanics of gravitational slope deformations, starting from the description of its morphostructural and geomechanical features (Mencl, 1968; Feda, 1973; Mahr, 1977; Savage and Varnes 1987; Hutchinson, 1988; Dramis and Sorriso-Valvo, 1994).

These studies introduced the concept of *sackung* referring to continuous flow-like deformations along planar, biplanar, or listric surfaces, leaving room to the more constructed definition of mass rock creep and gravitational mass rock creep (Radbruch-Hall, 1978; Chigira, 1992; Beck, 1968). These phenomena are reflected in peculiar features as double ridges, multiple trenches and counterslopes in the upper slope where tensile stress occurs, while a marked bulging or diffuse minor landslides at lower sectors (i.e. toe of slopes) guarantee the balance of slope masses (Crosta, 1996). At meso- and micro-scale compressional features are usually expressed by shearing, banding or buckling folding (Chigira, 1992).

The main geomorphological evidences derived by DSGSD processes often testify a marked structural control on the onset and development of slope deformations (Agliardi et al., 2001; Esposito et al., 2007), which inherited the anisotropic settings and the kinematic predisposition where the deformation can evolve (Di Luzio et al., 2004; Zorzi et al., 2014). The jointing conditions can compromise the mechanical response of the rock mass negatively affecting the overall strength and deformability (Hoek, 1983; Ramamurthy, 1994), as much as its rheological behaviour and time series of deformative processes (Discenza et al., 2013).

The morpho-structural setting and tectonic evolution of mountain fronts can also actively control the onset of large-scale slope deformations acting as dynamic

disequilibrium brought by the action of oriented geodynamic stress field variations (Bianchi Fasani et al., 2011; Pan et al., 1995).

In the last decades the scientific interest shifted toward the analysis of factors controlling the occurrence of DSGSDs and the definition of static and dynamic forces capable of influencing the temporal evolution of creep processes. Among these, the topographic stress due to tectonic dislodgment or continuous phases of uplift, plays a predominant role in the induced stress and consequently in gravitational disequilibrium (Molnar, 2004). A complete analysis of the role of slope gradient and geometry was performed by Ambrosi and Crosta (2011) via numerical modelling approaches.

In the catalogue of the forces acting on the slope system, the groundwater circulation and its regimes should be mentioned. The flow discharge of regional aquifer at the foot of a slope induces destabilising actions able to influence the gravity-induced deformation (Maffei et al., 2005) and cause small-scale secondary instabilities (Discenza et al., 2011; Pisani et al., 2010).

The tensile stress distribution and the opening of deep trenches can also favour fluid percolation in the upper slope enhancing weathering and karsts dissolution (Casini et al., 2006; Maffei et al., 2005). At the toe of the slope where water table crops out, the combined presence of local impermeable layers (i.e. shear zones, geological or tectonical contacts) can led to a superimposed water table with different flow net geometries, inducing stationary or transient fluid overpressure (Pisani et al., 2010; Crosta et al., 2013 and references therein).

The geological evolution of valley systems can also be the main factor responsible for major topographic variations, as consequence of erosion and sedimentation in intramontane basins and valleys (Della Seta et al., 2017). The latter in high mountain areas could have undergone periodic glacial fluctuations which can induce repeated cycle of loading and unloading, altering the stress state acting on the

slopes. The ice load and the following rebound could led to progressive slope failure (Eberhardt et al., 2004; Terzaghi, 1972).

The high stress release, combined with local geo-structural controls, can facilitate the onset of gravitational deformation (Ballantyne, 2002; Holm et al., 2004), leading the slope to accelerating creep stage, where the timing of tertiary slope failure can be delayed, confirming the time-dependency of the process (Bigot-Cormier et al., 2005; Cossart et al., 2008). This is proved by the time-space occurrence of deep-seated gravitational slope deformations in deglaciated valley and high mountain area, as reported in the inventory summarised in Crosta et al., (2013).

Fluctuations in ice masses and the consequent debutressing can condition the mechanical response of underlying rock masses driving progressive rock mass failure along discontinuity (Grämiger et al., 2017), acting as fatigue process at slope scale (Jia et al., 2015).

A not less important effect is represented by the thermal contribution played by glacial masses (Baroni et al., 2014). The presence of ice masses interacts with the rock mass inducing repeated cycles of freezing and thawing which can condition the stability of rock slopes (Davies et al., 2001). Thermal expansion and contraction clearly reflect in elastic deformations, leading to fracture opening, stress concentration and crack propagation (Draebing et al., 2014, 2017).

Thermal effects in glacial areas can play their role at different scales, operating both at surficial levels and slope scale, respectively through seasonal thermal variations or by the actions of advancing or retreating glacial masses (Baroni et al., 2014).

However a marked thermal control on small scale instabilities has been demonstrated, an investigation of the stress-strain slope response to the thermalisation of the whole rock mass by regional and local heat sources has never been addressed before.

Although debutressing is one of the predominant controlling factors and large parts of DSGSDs evolved in glacial environment (Crosta, 1996; Crosta et al., 2013), slope deformations can evolve even in different morphoclimatic (Pánek et al., 2015) and geological context.

Geothermal and volcanic systems are predisposing backgrounds for gravitational instability at slope-scale due to their intrinsic structural instability and the continuous rejuvenation operated by impulsive magmatic feeding (Gudmundsson, 2012). Fluid overpressures are ascribed as one of the causes of slope instabilities and major mass failures in young unstable volcanic flanks (Gudmundsson, 2012; McGuire, 1996) where they can modify the local gravitational force equilibrium. Given the large scale of mass movements, ranging from hundreds of thousands of cubic meters up to a few million cubic meters (Ablay and Hürlimann, 2000; Gudmundsson, 2009; Van Wyk de Vries et al., 2000; Voight and Elsworth, 1997), high stress level must be invoked due to dikes intrusion (Bonaccorso et al., 2013) or magmatic cryptodomes emplacement (Sherrod et al., 2008) as well as magmatic/hydrothermal pressurization. In these cases dynamic transient input must be called in action (Reid, 2004; Thomas et al., 2004).

Meanwhile, aggressive acidic fluids can promote the alteration of rock masses modifying their physical (mineralogy, porosity), mechanical (cohesion and friction angle), and hydraulic (permeability) properties (Frolova et al., 2014; Wyering et al., 2014), prejudicing their stability (Del Potro et al., 2013; del Potro and Hürlimann, 2009, 2008; John et al., 2008; Lopez and Williams, 1993; Reid et al., 2002).

The relevant geothermal gradient itself can have a direct impact on thermo-mechanical properties of rocks, such as changes of mechanical and rheological parameters that can occur at high temperatures.

Despite broad exhaustive discussions and the documented interplay between deep seated instabilities and magmatic hydrothermal system (Lénat et al., 2012; Poland et al., 2017; Rosas-Carbajal et al., 2016), not so extensive discussions on preparatory

(sensu Gunzburger et al., 2005) and controlling factors on volcanic slope deformation exist (Del Potro et al., 2013).

Recently, first analytic (Borselli et al., 2011) and numerical approaches to volcanic stability has been proposed, analysing the role of magmastatic pressure and dikes intrusions (Apuani et al., 2013; Apuani and Corazzato, 2009), or simulating seismic, hydrothermal (Currenti et al., 2017) and magmatic scenarios (Bozzano et al., 2013).

Nowadays a comprehensive analysis of the role of geothermal fields in slope scale gravitational dynamics by conductive and convective heat transfer lacks, and an investigation of thermal effects on mechanical time-dependant behaviour of rock masses has been disregarded or underestimated. For this reasons, relations between large scale instabilities and thermal anomalies in volcanic and glacial environment where most of gravitational slope deformation found their maximum expression should be considered, and a time-dependent thermo-mechanic and thermo-hydro-mechanical analysis can no longer be omitted.

2.2. Thermo-mechanical interactions in slope stability

Short-term transient and impulsive phenomena (e.g. earthquakes, intrusions, fluid pressurisation) may be responsible of stress and strength variations capable of leading the slope to failure by the lowering of reacting forces and rapid increasing of destabilising forces.

All these dynamics can be generally ascribed to *triggering factors*, which act directly on slopes ultimately leading to irreversible collapse (Gunzburger et al., 2005). Such disturbances are not able to explain the evolution of large-scale systems over a wider time-scale (from tens of thousands to millions of years) where massive gravitational deformations evolve.

Thermal interactions with rock masses are generally referred to preparatory factors (Gunzburger et al., 2005), where cumulated effects add up over longer time-scales. Gunzburger et al., (2005) analyse these effects by thermo-mechanical (TM) modelling on rock blocks exposed to cyclic daily and seasonal thermal variations, observing a marked influence of surface temperature changes in plastic deformations.

Thermo-mechanical forcing act on slopes inducing thermal expansions and, consequently, thermal stresses, enhancing the opening of fractures (Collins and Stock, 2016) and leading to the mechanical damaging of rock masses and joint failures (Bakun-Mazor et al., 2013; Bérard and Cornet, 2003; Vargas et al., 2013).

Cyclic thermal stresses over time are thus regarded to be responsible for thermal fatigue processes (Vargas et al, 2009; Hall, 1999; Villarraga and Gendre, 2016) extended in depth below the thermal active layer (Gischig et al., 2011).

This phenomenon has already been cited as microscopic thermo-mechanic effect on rocks under repeated thermal loads due to the differential thermal expansion along contacts at mineral boundaries (Ferrero et al., 2014).

Systematic laboratory tests have demonstrated that temperature can promote thermal micro-cracking (Homand-Etienne and Houpert, 1989; David et al., 1999; Fredrich and Wong, 1986), consequently increasing rock permeability (Vinciguerra et al 2005; Reuschlé et al., 2006; Nara et al., 2011) and decreasing material strength (e.g., Alm et al., 1985).

Thermal stress induced on materials from high temperature (> 500 °C) may result in a progressive modification in chemical, physical, mechanical and rheological properties (Heap et al., 2013, 2011; Rocchi et al., 2004, 2003).

Although it may be thought that these are related short-term effects of high thermal stress, even at lower temperature the heating conditions have a significant effect on the strain rate and in the viscous time-dependent behaviour of rocks (Brantut et al., 2013; Chen et al., 2014; Heap et al., 2009; Ye et al., 2015)

Long-term strength of rocks might be significantly influenced by in-situ temperatures (e.g. geothermal systems) as low as 80 °C, conditioning brittle creep by temperature-sensitive stress corrosion cracking (Kranz et al., 1982; Meredith and Atkinson, 1985), anticipating time-to-failure (Ye et al., 2015). For these reasons volcanic or geothermal systems are the most suitable context where correlation with thermal heating exists (Bonaccorso et al., 2010) and continuous creep-like deformations evolve.

The first progress in coupled thermo-mechanic approaches are reconnected to studies conducted on the design of radioactive waste repositories (Giraud and Rousset, 1995) and geothermal exploitation (Bruel, 1995; Rutqvist et al., 2001). Only in recent time, the thermo-mechanic approach found applications for rock joints and rock mass deformations, focusing on the research of thermally-induced elastic and plastic deformations (Bakun-Mazor et al., 2013; Greif et al., 2016; Gunzburger et al., 2005; Pasten et al., 2015; Vargas et al., 2013; Vlcko et al., 2009) as direct response to solar radiation (Gunzburger and Merrien-Soukatchoff, 2011), limiting the analysis within thermal active layers and focusing exclusively on small-scale planars or wedge failures (Gischig et al., 2011).

Thermo-mechanic interactions have been invoked to justify high velocities and run-out of large rapid landslides (Voight and Faust, 1982), accounting temperature rise due to frictional heat production and pressurisation (Cecinato et al., 2011; Cecinato and Zervos, 2012) generated by planar or compound sliding (Alonso and Pinyol, 2010). These interactions happen at the scale of sliding surfaces and are able to explain strain rate softening, accelerating creep and its transition to failure (Alonso et al., 2016; Pinyol and Alonso, 2016).

Numerical stress-strain simulations at slope scale demonstrate that thermo-mechanical viscous behaviour cannot be neglected over thousands of years' time scales, because the resulting strains are significantly higher than those obtained by elasto-plastic (Currenti et al., 2017) or visco-plastic behaviour (Baroni et al., 2014). Despite the growing interest in these topics, the application of thermo-mechanic numerical model to the rock mass-scale is still limited.

The here presented research is focused on numerical modelling of multi-physical systems involving slope-scale time-dependant process. This multi-physical approach to slope deformations deal with the coupling of different physical process acting on a complex slope-system and evolving with own time-scales. To this aim coupled or uncoupled solutions to multi-physical problem were experimented in relation to the steady or transient state of the system in the temporal scale of evolution of deep-seated slope deformation. These multi-physical interactions in landslide-process were tested combining modelling of different dimensional scale (i.e. deep/shallow crustal- and slope-models) with the purpose to defining its significance in the spatial and temporal evolution of deformative process.

This PhD research also provides, for each case study, a contribution to the role played by the thermo-mechanical behaviour for the evolution of gravitational deformation processes. In this sense, slope systems or gravitational deformations involved in conductive and convective heat transfers will be considered, prefiguring evolutionary scenarios potentially leading to slope failure.

Starting from selected case studies, representative of the two different thermal context mentioned above, the temperature control on the temporal evolution of slope deformations will be defined, evaluating its significance in slope-scale rheology and dynamics.

3. Multiphysical approach for numerical modelling

In its general definition a "model" consists in a theoretical scheme that describes, usually at smaller scale, a phenomenon or set of phenomena by highlighting its most relevant characteristics. The concept also extends to the study of processes, considered schematically in their essential aspects, so that they can be translated in mathematical terms with the aim of analysing, studying, understanding, quantifying and elaborating the phenomenon in question.

Em. Prof. John Burland in his definition of the famous triangular engineering-geological approach (Burland, 1987), puts emphasis on the importance of the conceptualisation of an appropriate model, highlighting how modelling represents "the process of idealising the full-scale project", extending and integrating the interlinking between geological, geotechnical and engineering features with the idealisation and evaluation of physical models. In this process, modelling is more than a mere execution of an analysis, but the understanding, evaluation (and simplification) of complex processes. Its faithful reconstruction requires the most accurate description of the forms and the processes forming and characterising it, which relies heavily on the information obtained from the other parts of the triangle.

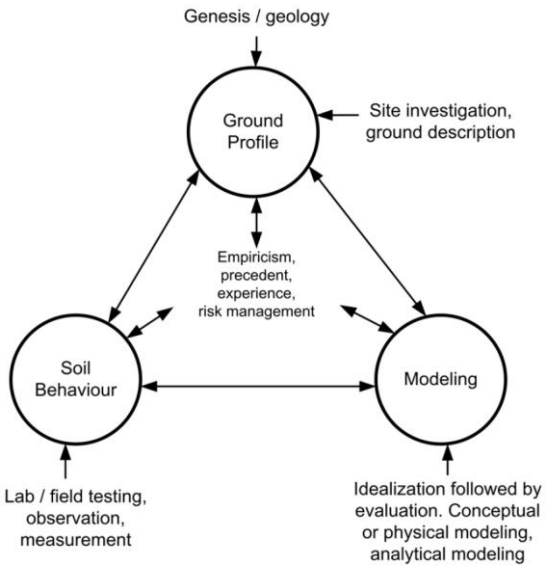

Fig. 2 - Expanded Burland Triangle (after Burland, 1987).

Geologists and Geotechnical Engineers have to face these reconstructions with variable stochastic processes evolving on large spatial and temporal scales, dealing with geological complexities within natural systems (Ingebritsen et al., 2009).

For this reason, in natural systems, a full comprehension of variables and processes that characterise it represents a tricky task for the formulation of an accurate model. Therefore modelling is the process by which we construct a simplified (mathematical/analogue) representation from a more complex physical reality (Barbour and Krahn, 2004). In this process we make use of numerical methods in order to more fully describe a complex physical reality by the discretisation of the time and space domain, solving sets of partial differential equation by algebraic expressions at discrete point of space, given initial and boundary conditions within different solution methods (FDM, FEM, DEM, etc) and, most importantly, under conceptual basic assumptions.

The computational code sets the dynamic matrix relating stress to strain through the constitutive laws attributed to the materials. The dynamic problem is solved by the numerical code on all discrete spaces, seeking, in a cyclic calculation, an equilibrium solution considered acceptable if less than an unbalanced force (equal to a predetermined value).

The solution to heat-transfer or fluid-flow problems invokes the equation of motion and constitutive relations too, together with Fourier's law for conductive heat transfer and Darcy's Law for fluid flow in a porous solid, as well as specific boundary conditions.

For time-dependent analysis the discretisation of a numerical model is extended to the temporal domain by means of settings of time-steps within the calculation wave proceeds. The resulting system of ordinary differential equations is solved using two modes of discretisation in time, corresponding to explicit and implicit formulations (Cundall et al., 1976).

The size of the time-step is limited by a stability condition and is, in general, very small. In fact, numerical stability of the explicit scheme can only be achieved if the

time-step remains below a limiting value. On the contrary, in implicit solutions, time-step can be arbitrarily large with unconditionally stable schemes even though iterative procedure are necessary to follow nonlinear constitutive law.

In the definition of numerical solutions, the time domain the analysis refers to must be considered. In stationary analysis, field variables do not change over time. If stationary analysis is conducted, time derivative terms of differential equations are null and the calculation wave is interrupted when the solution reaches static, thermal, flow equilibrium.

Transient analysis are used to compute the propagation of transient fields in the time domain. In this cases (i.e. groundwater flow, heat transfer, dynamic and creep calculation) the variation of a variable over time is computed. In time-dependent analysis time-steps and time limits can be defined, so intermediate transitory solutions are provided.

A process can be defined in a steady-state if the state variables which define its behaviour are unchanging in time. In continuous time, this means that for those properties of the system, the partial derivative with respect to time is zero. In a discretised time, the steady state is reached when the first difference of the variable is null or smaller than an admissible variation. Dealing with stochastic systems, the stationarity is expressed by the constancy of the probability that various states will be repeated in time.

For the dissertation of continuous processes in stationary or transitory states, the definition of observation time-scale (i.e. time-window) is required. Picturing the heating of a cold body by conduction, the mass will undergo a heating proportional in time to the thermal conductivity and the temperature gradient, according to the Fourier law. After a certain time in the system a new equilibrium will be reached asymptotically. At this time the system will tend towards stationarity, which can be defined if a negligible variation of significant parameters is assumed. When the perturbation stops, systems will tend to a new equilibrium, passing from infinite

intermediate transient states. By restricting the time-scale of the observation window, a non-negligible transient variation may occur and a stationary state can no more be assumed.

Instead, if a periodic signal is considered (e.g., temperature variations, tides, aquifer recharges), the perturbation is cyclically repeated over time, thus the stationarity or transiency of the process is a function of both the time-window of observation and the period (or more periods) of the considered process. Taking into account daily thermal cycles, if we analyse the process on an hourly time-window the process is always transient. However, if the time-scale extends to multiples of characteristic periods (T; -days-), the process is cyclically stationary. The same happens when considering seasonal thermal cycles on monthly or annual time-windows of observation (Fig. 3).

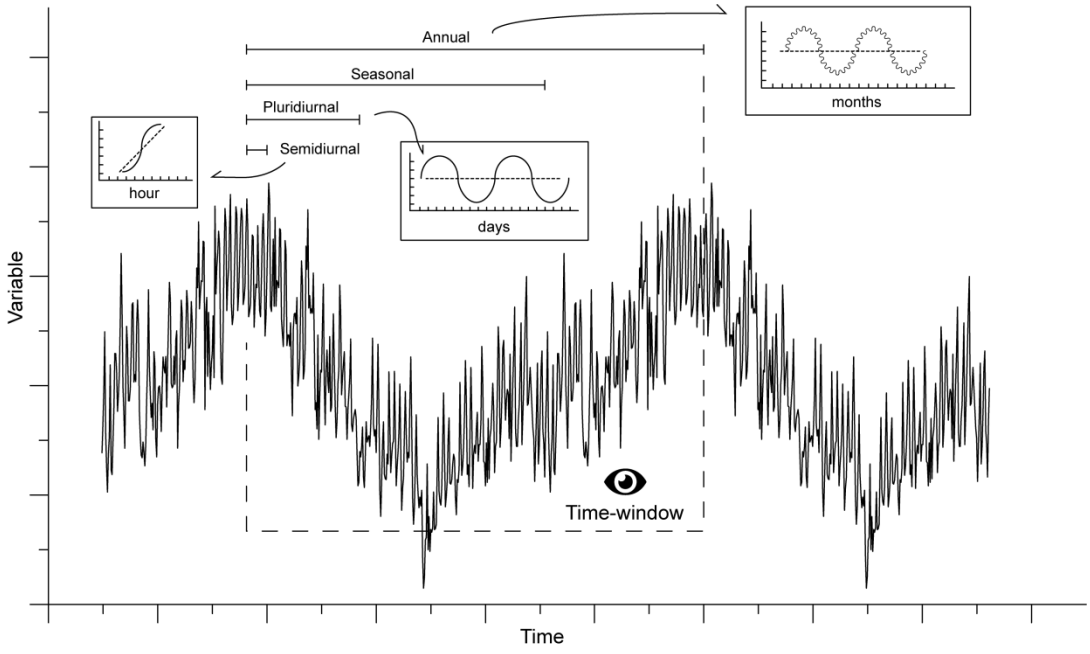

Fig. 3 - Steady- and transient-state of a time series respect the temporal scale of observation (time-windows).

On the contrary, if the time scale of observation is infinitesimally small, the process can instantly be assumed stationary. Therefore, the state of the dynamic system varies according to the time-window we are going to investigate.

On the other hand, if a perturbation acts on a time-scale larger than the observation window (i.e. time-window), within the latter the process is sufficiently slow to allow the achievement of stationary conditions at any moment. For this reason, the state of the system can be considered in almost-stationary conditions. In addition, if the perturbation is so small with respect to the variations of a variable in the observation time-window, it can be defined irrelevant to the equilibrium conditions reached by the system, and a stationary state can be assumed.

In the evolution of a complex slope system, the progression of the gravitational deformation is regulated by the concomitant actions of several internal and external processes (i.e. thermal flux, groundwater flow, rheological flow, dynamic inputs), each one of them acting with its own time-scale.

Thus the definition of the observation time-window is a function of the studied process and the purpose of the investigation. In the slope instabilities field study the scale of the observation time-window is regulated by the time required for the evolution of the deformative process and the time interval in which morpho-climatic or thermo-baric boundary conditions remain unchanged.

It follows that the definition of the time-window to refer the analysis (Fig. 3) it is based on a geological and morpho-evolutionary approaches, which considers the conceptual model at the base of the study and the concurrent physical processes that condition the evolution of slopes.

The time-scale within natural processes take place and the observation time-window in which our analysis is referred, concurrently act to the definition of a characteristic time-scale of the analysis, which express the ratio between the two entities and define a time-range functional to the observation of the investigated process (i.e. gravitative process). By this characteristic time-scale depends the sensitivity of the modelled system to natural perturbations: the wider is the characteristic time-scale, the less sensitive is the model to small perturbations (inner or external), and vice versa.

For these reasons, from the definition of the characteristic time-scale derives the stationarity or transiency of processes acting during the period of activity of slope-scale gravitational deformations (Fig. 4Fig. 4. Coupled or Uncoupled solutions can be adopted in virtue of the mutual physical interactions existing between two or more processes over a simulated time-interval.

The time-interval simulated in the model can be also reproduced by means of different stages, where significant variations to inner or boundary conditions occurred. Single- or multi-stage (i.e. sequential) modelling can be solved coupling or combining different stages and physics. Further detail about coupled and uncoupled solution are discussed in the following chapter.

By these assumptions comes out the choice of the most appropriate numerical solution to be used in the modelling phase (Fig. 4). Coupled or Uncoupled solutions can be adopted in virtue of the mutual physical interactions existing between two or more processes over a simulated time-interval.

The time-interval simulated in the model can be also reproduced by means of different stages, where significant variations to inner or boundary conditions occurred. Single- or multi-stage (i.e. sequential) modelling can be solved coupling or combining different stages and physics. Further detail about coupled and uncoupled solution are discussed in the following chapter.

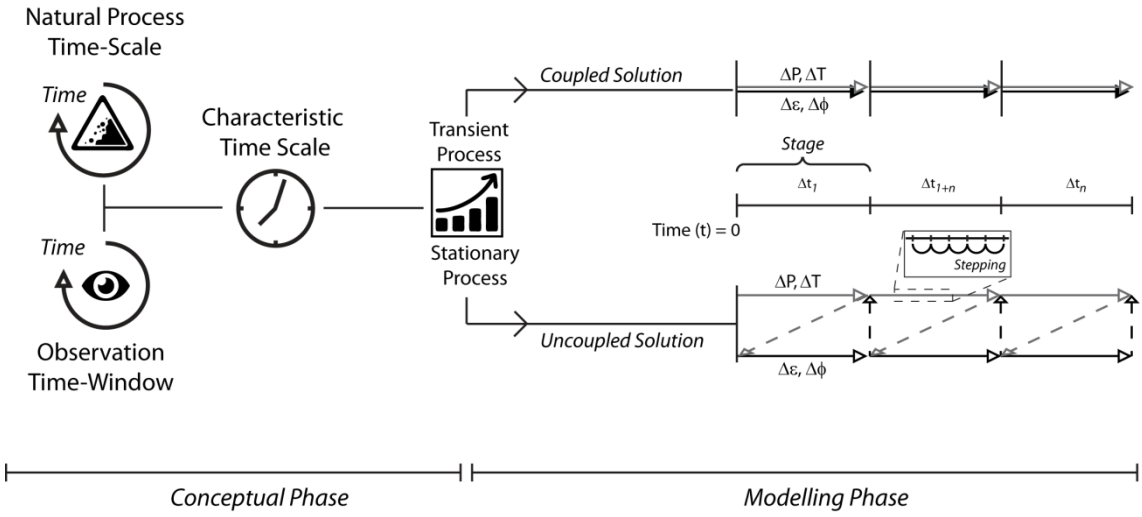

Fig. 4 - Flow chart representing the comparison between time-scale of natural process and observation time-window of the analysis for the definition of characteristic time-scale preparatory for the numerical modelling phases.

In the numerical analysis of complex systems where multiple physics react within the slope, a correct definition of time-window and an appropriate decision of the transient or stationary state of the process is mandatory.

The following chapter will then discuss the working approach used in the multi-physical treatment of gravitational deformations at slope scale as function of the peculiar characters of the case studies.

3.1. Coupled and uncoupled schemes for numerical modelling

The treatment of complex natural systems, and in particular slope systems, necessarily requires the coupling of physics that work simultaneously. Numerical models allow the coupling of more physics together by the combined solution of equations of motions and constitutive relations for different materials, and energy-balance equations and transport laws derived from Darcy's (groundwater flows) or Fourier's (thermal fluxes) laws.

Although the numerical coupling between different physics mainly depends on the mathematical formulations of the codes, it mainly resides in the wide difference in the numerical time-steps (e.g. dynamic actions acting over a short to a very short time and continuous slow creep processes).

In the following the main physical interactions which may occur in gravitational deformations processes mentioned above (DSGSDs Auctt.) are summarised, where groundwater flows of thermal fluxes can interact with the slope dynamics, conditioning its short and long term evolution.

For these processes physical interactions and related coupled mechanisms in numerical modelling can be divided in three groups:

- mechanical behaviour and thermal conditions;
- mechanical and groundwater flow;
- thermal conditions and groundwater flow.

The first group includes stress changes induced by temperature variations. These effects are proportional to the thermal expansion coefficient according to (Eq. 1).

$$\frac{\partial \epsilon_{ij}^{T}}{\partial t} = \alpha_t \frac{\partial T}{\partial t} \delta_{ij} \qquad \text{Eq. } 5Eq.\ 1$$

Mechanical properties can also be a function of temperature, depending on the range they are exposed to. Mechanical changes in a body can result in changes to its thermal properties, influencing temperature variations in turn. However, in the stress-strain analysis performed by FLAC (Itasca Cons., Cundall et al., 1988) codes (see Materials and Methods chapter), the coupling is one-way and mechanical changes do not affect thermal properties of the materials, which remain unchanged.

The second one encompasses all types of fluid/solid interactions which can occur in rocks and soils. Fluids within voids in rock/soil matrixes react to mechanical volume changes by changing in the pore pressure which can cause changes in the effective stress affecting the response of the solid (up to last stage of failure). This is the

interaction at the basis of consolidation processes, where the slow pore pressure dissipation causes displacements in a soil (Terzaghi and Fröhlich, 1936). Dynamic overpressure can be generated as response to volumetric strain after transient shaking (see liquefaction processes).

The latter group of physical interactions encloses the pore pressure variations induced by thermal expansions of both fluid and solid matrixes. Groundwater flows can also influence heat transfers considering the thermal dependency of fluid density which can condition fluid transports by advection/convection processes and thus heat propagation.

As previously discussed, the interactions between two or more physics can be resolved combining the ongoing processes through two different resolving schemes, considering the time-window of analysis and the transiency or stationarity of impulsive or continuous forcings.

The one-way or two-way coupling can be achieved resorting different algorithms referred to two solutions procedure approaches identified as fully coupled and segregated (i.e. sequentially coupled or uncoupled) algorithms (Fig. 5).

Fully coupled approaches assume that all of the couplings between physics must be considered at the same time (Fig. 5). With coupled methods, equations for all the variables are solved at the same time for a given cell, and that process is then repeated for all cells in the numerical domain.

The segregated (i.e. sequentially coupled or uncoupled) approach treats each physics sequentially (Fig. 5), using the results of the previously solved physics to evaluate the loads and material properties for the next physics to solve. The algorithm is continued until convergence is achieved. With segregated methods an equation for a certain variable is thus solved for all cells, transferring sequentially the results to solve the equation for the next variable for all cells.

The Fully Coupled is useful, and generally needed, for multi-physical problems that have very strong interactions between the various physics being solved. On the other hand, the uncoupled approach assumes that all physics can be solved independently, and will iterate through the various physics in the model until convergence. Although the fully coupled approach guarantees the solution of strict interactions between different physics, its computation is intensive and time- and memory-consuming.

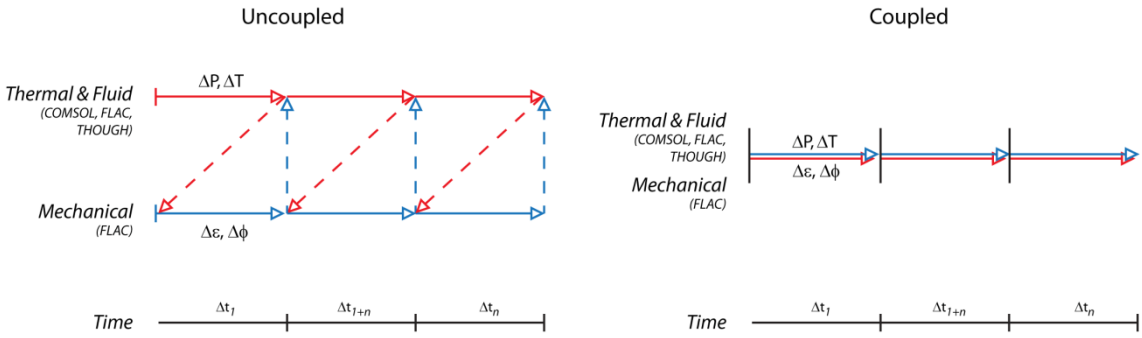

Fig. 5 - Uncoupled and coupled algorithm used linking single- or multi-codes solving schemes (modified after Rutqvist et al., 2011).

In this context, numerical modelling solutions will be structured and defined according to the specificity of the case studies, considering a time-window representative of the time-scale of the gravitational process, and based on the conceptual model postulated.

3.2. *Thermodynamic and thermo-mechanical analysis*

The discussion on gravitational slope deformations involved in conductive or convective heat transfer systems together with developed fluid circulations entails in a correct definition of a thermodynamic model of the slope system within which the deformation evolves.

Thermo-baric fields can interact with the slope equilibrium modifying the stress-strain response of the rock mass to short- and long-term forces. In the short-term, a rapid thermal variation, in the presence of a low-permeability trap and undrained

conditions (i.e. timescale that precludes fluid movement), might reflect in a fluid overpressure that can negatively influence rock strength and provide new internal forcing on the slope, promoting slope instabilities (Day et al., 1996; Voight and Elsworth, 1997; Reid et al., 2004).

On a wider time-scale (the ones we are focusing on), constant thermal anomalies can condition the rheological behaviour of the rock mass acting on both the elasto-plastic and the visco-plastic influencing strength and stiffness as well as static and dynamic viscosity, and thus strain-rates. These perturbations can alter the evolution of continuous deformative processes, potentially leading to acceleration towards the last stage of failure.

For these reasons a full description of physical interactions in a deforming slope for a complete definition of risk scenarios is required, and a definition of a thermodynamic model of the slope is necessary.

The thermodynamic and mechanical models of the slope will be constructed starting from geological and thermal forces derived by geological, hydrogeological, geophysical and thermal laboratories and field-based investigation (Fig. 6).

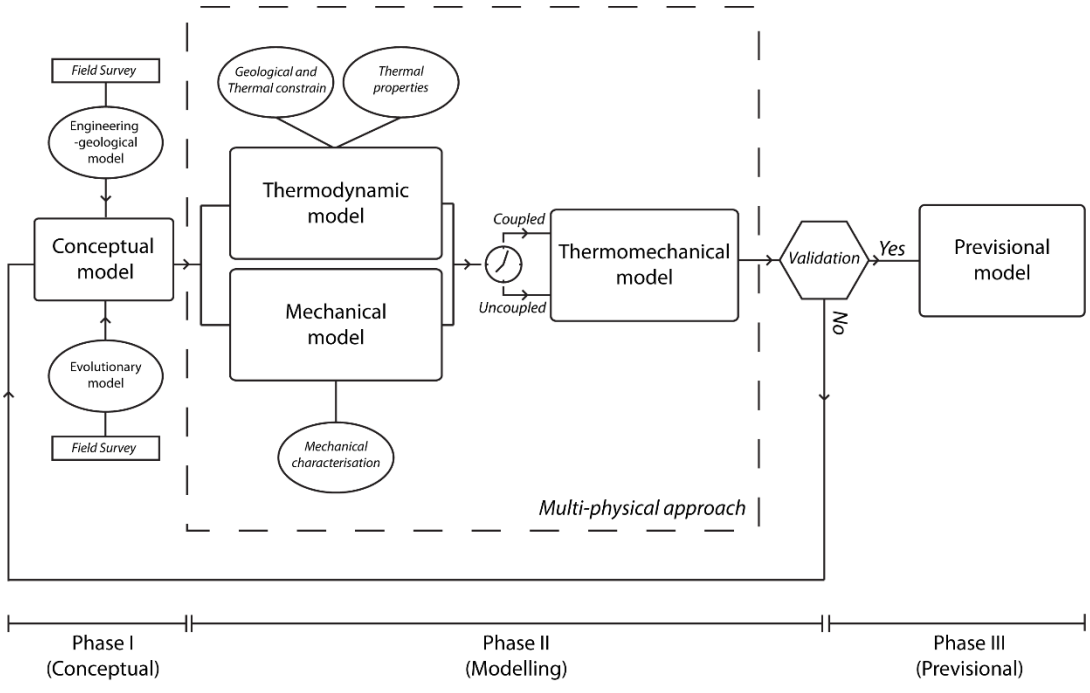

Fig. 6 - Flow chart of the multi-physical numerical approach adopted for slope deformation analysis.

Thermodynamic modelling has been solved using FDM and FEM numerical codes as FLAC® (Itasca Consulting) and COMSOL Multiphysics®, able both to resolve coupled calculation of heat transfer in porous media and give solutions to groundwater flow models by solution of energy-balances equations and specific transport law for heat (Fourier's law) and fluids (Darcy's or Brinkman's laws).

On the other hand, taking into account the size of the slope scale numerical model, the computation of pure mechanical solutions has been resolved by only using of FLAC 7.0 and 8.0, capable of resolving stress-strain analysis. This choice resides in the impossibility to manage rock matrix and joints separately because the modelling scale, which requires to simulate the rock mass as a continuum medium to which equivalent properties are attributed.

The mechanical model can be defined by the definition of a conceptual model based on an accurate engineering geological model defined by field investigations. The full description of an accurate engineering-geological model, and then of a mechanical model, requires the implementation by field-geomechanical and lab-mechanical characterisations, aimed at deriving mechanical parameters able to descript the chosen constitutive model and to relate applied stress to deformations.

Elastic, elasto-plastic, visco-elastic or visco-plastic constitutive models can be attributed to simulate static and dynamic inputs even by time-dependent analysis (see Chapter 4 for a detailed description).

The definition of thermal or thermo-dynamical models is based on the solution of Fourier's law on heat conduction, which states that the conductive heat flux, q, is proportional to the temperature gradient, by a proportionality constant k which is the thermal conductivity (SI unit: W/(m·K):

$$q_i = -k \frac{\partial T}{\partial x_i} \qquad Eq.\ 2$$

Thermal conductivities, as much as hydraulic conductivities, can be anisotropic differing their magnitude in three direction of space. k can be expressed by a tensor in all the combination of direction k_{xx}, k_{yy}, k_{zz}.

The equation of heat conduction in 2D can be solved for temperatures and two components of the heat flux relating heat transport law to energy-balance equation, given a specific boundary and initial conditions.

The equation assumes that mass is always conserved, which means that density (ρ) and velocity (v) must be related through:

$$\frac{\partial \rho}{\partial t} + \nabla \cdot (\rho v) = 0 \qquad Eq.\ 3$$

Substituting Eq. 2 in Eq. 3 and solving the equation for the temperature, T. If velocity is set to zero, the equation governing the pure conductive heat transfer is obtained:

$$\rho\, C_p \frac{\partial T}{\partial t} + \nabla \cdot (-k \nabla T) = Q \qquad Eq.\ 4$$

where:

- ρ is the density (SI unit: kg/m^3)
- Cp is the specific heat capacity at constant pressure (SI unit: J/(kg·K))
- T is the absolute temperature (SI unit: K)
- t is time (SI unit: s)
- Q contains volumetric heat sources terms (SI unit: W/m^3)

The coupling with mechanical constitutive laws requires the solution of thermal-stress problems which involve the formulation of the stress-strain rate relations. In isotropic materials free thermal expansion results in no angular distortion, so the shearing strain increments are unaffected. The thermal-strain rate associated with the

free expansion in i,j Cartesian plane, corresponding to temperature rate $\partial T/\partial t$ has the form:

$$\frac{\partial \epsilon_{ij}^{T}}{\partial t} = \alpha_t \frac{\partial T}{\partial t} \delta_{ij} \qquad Eq.\ 5$$

where α (SI unit: 1/°C) is the coefficient of linear thermal expansion, and δij is the Kronecker delta.

Considering an elastic material, as reported by the numerical formulation of FLAC code, the mechanical constitutive equation under thermal perturbation is given by:

$$\frac{\partial \sigma_{ij}}{\partial t} + \alpha \frac{\partial P}{\partial T} \delta_{ij} = 2G \left(\frac{\partial \epsilon_{ij}}{\partial t} - \alpha_t \frac{\partial T}{\partial t} \delta_{ij} \right) + \left(K - \frac{2}{3} G \right) \cdot \left(\frac{\partial \epsilon_{kk}}{\partial t} - 3\alpha_t \frac{\partial T}{\partial t} \right) \delta_{ij} \qquad Eq.\ 6$$

where σij and εij are total stresses and strains, α is Biot coefficient, K and G are Bulk and Shear moduli, and δij is the Kronecker delta.

Stress changes in natural slopes are often due to fluid flow in porous or fractured media. The structure where fluids are able to move strongly controls velocity and fluid regimes, according to the magnitude of Reynolds number (Ra), which expresses the ratio between inertial and viscous forces:

$$Ra = \frac{F_{iner}}{F_{visc}} = \frac{\rho u L}{\mu} \qquad Eq.\ 7$$

where ρ is the density (SI unit: kg/m^3), μ is the dynamic viscosity (SI unit: Pa·s), u is the velocity of the fluid (SI unit: m/s), and L denotes a representative length (SI unit: m).

The Reynolds number represents the ratio between inertial and viscous forces. At low Reynolds numbers, viscous forces dominate leading to laminar flow. At high Reynolds numbers, the damping in the system is very low and the flow field switches to a chaotic state called turbulence.

Porous media reflect in slow laminar flows, where fluids move in the interstices of the rock/soil matrixes. In this condition the flow is regulated by the pressure gradient and is mostly influenced by the frictional resistance within the pores. On the

contrary, fractured and discontinuous rock masses results in turbulent channelized fast flows mainly located in the fracture network, described by Navier-Stokes equations.

The first case, proper of laminar and stationary flows, is fully mathematically described by Darcy's law, which relates velocity field pressure gradients by means of fluid viscosity and intrinsic permeability (controlled by the structure of the porous medium). Darcy's law together with the continuity equation and the pore fluid state equation provides a complete mathematical description, useful for numerical solutions of groundwater flows in laminar regime, as follow:

$$\frac{\partial}{\partial t}(\rho n) + \nabla\cdot(\rho u) = Q_m \qquad Eq.\ 8$$

where ρ is the density of the fluid (kg/m^3), n is the porosity (dimensionless), u is the velocity (m/s) and Q_m (kg/(m^3·s)) is a mass source term. If the Darcy's Law interface is coupled to an energy balance, then the fluid density can be a function of the temperature, pressure, and composition.

An alternative to Darcy's equation is what is commonly known as Brinkman's equation. With inertial terms omitted it takes the form:

$$\beta\nabla^2 q + q = -\frac{k}{\mu}\nabla p \qquad Eq.\ 9$$

where β is an effective viscosity term, q is the discharge per unit area,∇p is the pressure gradient vector (Pa/m). We now have two viscous terms: The first is the usual Darcy term and the second is analogous to the Laplacian term that appears in Navier-Stokes equations.

The Brinkman equation (Brinkman, 1949) treats both pressure and flow velocity vectors as independent variables and is used to compute fluid velocity and pressure fields of single-phase flows in porous media in the laminar flow regime. The physics interface extends Darcy's law to describe the dissipation of kinetic energy by viscous shear, similar to the Navier-Stokes equations, and is used to define for transitional flows between boundaries (introduced by Brinkman in 1949).

The second case, with regard to fast flows in channels (i.e. fracture network), can be described by free turbulent flows of single-phase within open regions by the Navier-Stokes equations.

Both thermal and hydrodynamic processes acting on the considered case studies, can contribute as preparatory (or triggering) factors to the slope deformation processes, influencing both short- and long-term behaviour of rock masses.

Given the scale of here analysed gravitational processes, the numerical modelling of rock mass involved in DSGSDs, will be treated through equivalent continuum approach, attributing mediated properties to the overall rock mass consisting of a porous matrix separated by a dense fracture network.

For each case study a comprehensive thermal or thermo-hydro-dynamical model of the slope will be defined. After a validation on monitoring data and field-survey observations (Fig. 6), the model will led to the definition of a thermo-mechanical model of the slope, solved by coupled or uncoupled schemes as function of the previously defined characteristic time-scales.

The adopted multi-physical approach, consisting on the definition of a complete analysis of all the concurrent physical processes capable of influencing the evolution gravitational slope deformations, moves one step ahead with respect to the consolidated geomechanical approach on the analysis of slope scale instabilities, where models are insensitive or at least invariant in relation to the thermo-baric boundary conditions.

3.3. Analysis of Scenario and Forward analysis

The approach summarised in Fig. 6 involves the definition of a thermo-mechanical model based on a thermodynamic numerical model of the groundwater

flow and thermal flux within the slope and elastic, elasto-plastic, and visco-plastic mechanical constitutive laws.

The thermo-mechanic model, in order to be consistent and useful for predictive analysis (Fig. 6), must be validated on independent datasets, based on geological and geomorphological evidences as well as on monitoring data of characteristic parameters, considered as output variables of the modelled systems. As an example, thermal models can be validated by verifying the consistency of numerical thermal profiles or outlet heat fluxes, in relation to the observed (i.e. monitored) data. For mechanical models of DSGSDs the validation can be achieved back-analysing the deformative process in terms of kinematic and magnitude of ground deformations.

Once validated, the model can be exploited for the formulation of previsional analysis (Phase III on Fig. 6), analysing the influence of variation in physical boundary conditions (i.e. analysis of scenarios) or generally, to evaluate effects produced by the progression over time of ongoing processes (i.e. forward analysis). Previsional analysis will be defined adopting the above described multi-physical approach and considering mutual interactions between thermal, hydrodynamic and mechanical processes. The physical coupling between different physics will be achieved, by steady-state or transient analysis after the definition of a time-window of observation specific for the evaluation of different scenarios. For instance, if short-term effects related to transient pressurisation of hydrothermal fluids on large gravitational slope deformations are analysed, the dependent variables changes over time must be considered and a transitory analysis adopted. On the contrary, if the role of thermal perturbations on stationary gravitational processes evolving on wider time-scales are evaluated, a steady-state analysis can be assumed. Thus, by these time intervals, even in the formulation of scenarios, derives the choice of coupled or uncoupled multi-physical solutions.

For this purpose, basing on validated thermo-mechanical model physically commensurate scenario analysis will be performed to compute stress-strain effects

induced by variation of heating conditions induced by variation of geothermal gradients or heat fluxes.

4. Materials and Methods

In order to deal with the so defined multi-physical analysis, a consolidated multi-modelling approach (Martino et al., 2017) based on the experiences of stress-strain sequential modelling defined by the reconstruction of an engineering geological model was considered and adopted (Discenza et al., 2011; Esposito et al., 2007; Scarascia et al., 2006).

A geological model of the slope system based on detailed geological surveys was preliminary defined. From this preparatory activities, rock samples were collected in order to characterise the mechanical behaviour and thermal response of rocks involved in gravitational deformative processes. The combined geomechanical investigation of the jointing conditions of rock masses allowed the complete characterisation of rock masses and the definition of an engineering-geological model of the slope, joining geological formations into homogeneous litotechnical units, characterised by having an analogous response to thermal and mechanical stresses.

The defined engineering geological model was then transferred in a numerical domain settled in both thermal and mechanical configurations, in order to verify the consistency of the defined conceptual model and to prove the effects of thermal perturbations on the evolution of gravitational deformations.

4.1. Engineering geological modelling

Preliminary activities for the numerical modelling of rock masses involved in heat transfer systems consist in the definition of engineering-geological models of slopes, with a resolution and accuracy function of the length scale of the modelled domain (i.e. rock cliffs, whole slope, wide valleys). First step was the investigation of specific features of geological-framework of the selected study areas, in order to derive a robust basic geological model, preparatory for the engineering geological modelling.

The reconstruction of the engineering geological model was based on field surveys and also supported by bibliographic geological, geomorphological and geophysical data. These data also sustain the definition of conceptual and evolutionary models on each case study, which will be exhaustively discussed in Chapter 5.

Where possible, geological and geomechanical field surveys were achieved to characterise geological settings of the slopes where deformations can evolve. Geological surveys were carried out on scales consistent with the purpose of the modelling, trying to distinguish the main morpho-structural features of interest. Geological maps or synthetic geological cross sections were then defined, on the basis of which engineering geological model was constrained by *in-situ* laboratory analysis.

In particular, through geomechanical field survey a detailed picture of the jointing condition of the rock mass was completed by the description of the main sets of discontinuities. Geomechanical characterisation was conducted according to ISRM standards (2007) measuring dip direction, dip, spacing, aperture and persistence of the main joint set deriving geomechanical index as I_b (Block Dimension Index) or J_v (Volumetric Joint count), derived according to relations proposed in literature (e.g. Palmstrom, 1995):

$$J_v = (1/S_i + 1/S_{i+1} + \cdots + 1/S_{i+n}) \; ; \qquad I_b = \frac{S_i + S_{i+1} + \cdots + S_{i+n}}{n} \qquad Eq.\ 10$$

The main discontinuity sets were then investigated in terms of strength and roughness by means of Joint wall Compressive Strength (JCS -Aydin, 2009-) tests and definition of Joint Roughness Coefficient (JRC -Barton and Choubey, 1977-) by the use of Schmidt Hammer and Barton comb profilometer.

The complete characterisation of the rock mass behaviour has been achieved through the physical and mechanical characterisation of the rock matrix performed, depending on the case study, by a set of porosity and permeability tests together with uniaxial, triaxial, and tensile strength tests, at pressure conditions characteristic for the

deformative process. The performed tests are summarised within each case studies discussed in Chapter 5.

Given the thermo-mechanical modelling that is going to be approached, the physical characterisation was implemented by the characterisation of thermal transmission properties in solids, such as thermal conductivity (Guarded-Hot-Plate methods – ASTM C177–13), specific heat capacity (DSC calorimetry -ASTM E1269–11-) and linear thermal expansion coefficient (ASTM E831–14).

The geomechanical spatial distribution and laboratory tests allow us to define a detailed engineering-geological model, distinguishing or combining litotechnical units in virtue of their litotechnical features.

The engineering geological model reconstructed was then transferred into a numerical domain by the discretisation of geological structures and tectonic elements and by the zoning of litotechnical regions.

4.2. From lab- to slope-scale: the equivalent continuum approach

Rock masses are constituted by the joining and the mutual interaction between rock matrix and discontinuities (primary -i.e. depositional- and secondary -i.e joints-). The latter has a significant influence on the stress distribution within the slope and thus on the stress-strain behaviour (Amadei et al., 1988) often controlling the evolution of gravitational deformation to slope failure (Di Luzio et al., 2004). Starting from the theoretical model proposed by Lekhnitskii (1963), Amadei et al., (1988) demonstrating that in transversally isotropic media (as example a stratified rock mass) horizontal stress may be greater than vertical stress (i.e. lithostatic load), proving two distinct solutions based on "discrete" or "equivalent continuum" modelling.

In the second approach an equivalence of the rock mass is defined, considering densities assumed as the mean values of the layers constituting the transversally

isotropic rock mass. In an equivalent continuum approach, rock mass deformation moduli and gravitational stresses are obtained by taking into account the contribution of both matrix and discontinuities.

The equivalent deformability of jointed rock masses is derived by empirical relations based on fracture density or generally by means of rock mass classifications (e.g. RMR - Bieniawski, 1988).

An empirical relation was proposed by Verman et al. (1997) based on the RMR index as follows:

$$E_d = 0.4H^{\alpha}10^{(RMR-\frac{20}{38})} \qquad Eq.\ 11$$

where E_d identifies the equivalent rock mass deformation modulus, α is a coefficient that is a function of the RMR, and H is the height of the excavation.

Another empirical set of relations were proposed by Zhang and Einstein (2004), using the rock quality designation index (RQD) defined by core drilling, having the general form of:

$$E_m/E_r = c10^{0.0186RQD-1.91} \qquad Eq.\ 12$$

where E_m is the rock mass modulus, E_r is the intact rock modulus and c is a variability coefficient with values between 0.2 and 1.8.

The definition of the rock mass moduli can be also addressed by the definition of geomechanical parameters obtained from exposed rock surveys. In our analysis, because we manage exposed rock mass outcrops, the definition of rock mass deformability was addressed by the empirical relations proposed by Ramamurthy (1994) and Sridevi and Sitharam (2000) at null confining pressure:

$$E_{j0} = exp\left(-1.15 * 10^{-2}J_f\right)E_{i0} \qquad Eq.\ 13$$

where E_{j0} is Young's modulus of the jointed rock, E_{i0} is the is the Young's modulus of the intact rock at zero confining pressure and J_f is the Joint Factor (Ramamurthy, 1994).

The Joint Factor expresses the ratio between the volumetric joint count (J_v), defined as the number of discontinuities per cubic meter of rock, considering an additional inclination and strength parameters *n* and *r* as follows:

$$J_f = \frac{J_v}{nr} \qquad Eq.\ 14$$

where n, the inclination parameter, depends on the joint attitude (β), and r is an additional parameter depending on the unconfined compressive strength (UCS) measured on the rock joints (Sitharam et al., 2001; Sitharam and Latha, 2002).

Elastic moduli of fractured rock masses can be derived at non-zero confining pressure (E_j) by the following relations:

$$E_j = E_{j0}/1 - exp[-0.1\,\sigma_{cj}/\sigma_c] \qquad Eq.\ 15$$

where σ_c represents the confining pressure and σ_{cj} express the UCS of the jointed rock, calculated by negative exponential function by the UCS of intact rock (σ_{ci}) as reported below:

$$\sigma_{cj} = \sigma_{ci}[0.04 + 0.89\,exp(-J_f/161)] \qquad Eq.\ 16$$

In this work the equivalent continuum approach proposed by (Sridevi and Sitharam, 2000) was adopted and the parameters required were quantified by integrating on-site geomechanical measurements with uniaxial and triaxial laboratory tests (Bozzano et al., 2008; Esposito et al., 2007).

Elastic moduli and compressive strength values of the intact matrix were obtained directly from uniaxial compressive strength tests or, alternatively, from triaxial tests performed at variable confining pressure levels, consistent with ones acting within the slope and representative for the evolution of gravitational

deformations (Della Seta et al., 2017). The derived values of elastic moduli were then scaled in relation to the jointing conditions according to the equivalent continuum approach above defined, starting from the stiffness of the intact rock derived by triaxial test at increasing confining pressure (i.e. increasing depth). This method allowed the zoning of the rock mass in distinct geomechanical zones, in virtue of both their joint conditions and confining pressure levels.

Strength parameters were attributed by triaxial tests according to the Hoek-Brown criterion (Hoek et al., 2002). The strength contribution of major anisotropies in rock masses was also considered attributing frictional strength according to the Barton and Choubey (1977) criterion. The defined physical and mechanical parameters were attributed to the different litotechnical unit and transferred in numerical domain for the stress-strain analysis in mono- or multi-stage modelling.

4.3. From conceptual to sequential numerical modelling

To better constrain the numerical analysis to be performed, a correct definition of the morpho-evolutionary model of the slope and slope-to-valley systems, as much as external or internal forcing acting on the slope and able to guide the onset and evolution of gravitational slope deformations is necessary.

The evolutionary model of slope systems has been defined by the quantification of morphological variations representative of the main relevant stage of a natural continuous evolution. The continuous evolution of slope systems has been reproduced in the numerical domain by discrete sequential variations assumed as instantaneous in comparison to the evolution time-scale of deformative processes.

In other words, it was necessary to assume that the main morphological changes related to the salient stage of the evolutionary model (e.g. erosion, deposition, tectonic displacements, glacial advance or retreat) have occurred much faster than the

ones naturally required, or that, following morphological variations, the deformative processes can evolve in a steady-state without any variations in boundary conditions.

With regards to internal or external forces, an analogous assumption of stationarity or quasi-stationarity of the processes in relation to the observation time-window was addressed. If thermal boundary conditions (i.e. temperatures, heat fluxes) can be assumed as constant within the time-scale of evolution of gravitational processes (i.e. the observation time-windows of our analysis) a stationarity or quasi-stationarity can be assumed and a time-independent analysis can be performed.

The timing of discrete geometric variations and/or changes of thermal boundary conditions have been defined by means of geomorphological evidences or absolute dating specific for each case study, which will be discussed in the following chapters. These variations in geometric or physical boundary conditions naturally reflect and evolve in own time-scales as transient or continuous processes, which acts while deformative processes take place. From these assumptions derives the choice of numerical solving approach, which is the reflection of the transitory or steady-state of the system. As summarised in Chapter 3 about the statement of the state of the system in the time-window of analysis, results the choice of coupled or uncoupled multi-physical solving schemes and the attribution of constant or variable boundary conditions.

Based on the defined evolutionary models and the basic assumptions above described, thermal, mechanical and thermo-mechanical analysis will be described by numerical FDM and FEM methods modelling.

The numerical analysis was based on restored engineering-geological cross-sections, which was transferred to a numerical domain consisting of a regular grid with a regular square or triangular mesh resolution. The spatial resolution of the model was defined considering the dimensions of the littlest reconstructed elements or geometrical variations.

Starting from conditions of gravitational equilibrium, a mono-stage or multi-stage sequential evolution of the slope systems were reproduced (cf. Chapter 3) availing of the reconstructed morpho-evolutionary models.

For time-dependant analysis an appropriate computational time-discretisation (i.e. time-stepping - Fig. 4 -) was chosen to guarantee numerical stability respect both thermal and viscous creep processes. In particular, for thermal analysis, if an explicit finite-difference numerical formulation is selected, the temperature (T) at a node (n) is assumed to vary linearly over an incremental time interval (Δt). Starting from an initial temperature, the nodal temperature after Δt becomes:

$$T^{n}_{(t+\Delta t)} = T^{n}_{(t)} + \Delta T^{n}_{(t)} \quad Eq.\ 17$$

To ensure calculation stability, the numerical time-step must remain below a critic value of time (Δt_{cr}), corresponding to a measure of the characteristic time needed for the diffusion to propagate throughout the domain. This critical value is proportional to the smallest triangle characteristic length (L_c) of the domain, thermal diffusivity (κ), density (ρ), specific heat at constant volume (C_v) and a geometrical constant (m) according to:

$$\Delta T_{cr} = \frac{1}{m}\left[\frac{\kappa}{L_c^2} + \frac{h}{\rho C_v L_c}\right]^{-1} \quad Eq.\ 18$$

where L_c is equal to the ratio between the volume of the solid and the area of the exchanging heat surface. This number can be large enough that the solution by explicit method can be unaffordable, therefore the use of an implicit formulation contemplating simultaneous solving of equations at each time step is required.

Time-dependant creep deformations (ε) were modelled by a visco-plastic Burger rheological model (Karato, 2008) combining in series visco-plastic (i.e. Maxwell) and visco-elastic (i.e. Kelvin-Voigt) elements:

$$\varepsilon = \frac{\sigma}{E_1} + \frac{\sigma}{\eta_1} t + \frac{\sigma}{E_2}\left(1 - e^{-\left(\frac{E_2}{\eta_2}\right)t}\right) \quad Eq.\ 19$$

In this case, in order to ensure numerical stability, the maximum duration of the creep time-step was defined considering the ratio between the lowest viscosity of the model (η) and the correspondent shear modulus (G).

In the attribution of parameters for the Burger model it was assumed that visco-elastic Kelvin-Voigt properties were representative of the rock matrix, while visco-plastic Maxwell parameters stand for the behaviour of the fractured rock mass (Bozzano et al., 2012). For damper viscosity (η), the value attributed to the Kelvin-Voigt rheological element ($\eta_2=\eta_{rock}$) was fixed to an order of magnitude greater than the ones on the Maxwell element ($\eta_1=\eta_{joint}$) (Della Seta et al., 2017). In addition, a sensitivity analysis regarding the attributed viscosity values was conducted to calibrate the rheological properties of the rock-mass involved in the deformational process.

A thermo-mechanical numerical analysis was performed, with the purpose of analysing the effects of thermal anomalies on the evolution of slope scale gravitational deformation processes by using different codes in a two coupled or uncoupled solving scheme depending on the physics and stationarity of the processes respect to the gravitational slope dynamics.

To this purpose the combined use of licensed COMSOL® and FLAC® codes were experimented for thermo-dynamical and mechanical analysis. The impact of thermo-mechanic interactions on DSGSD was quantified by comparison of pure visco-plastic and thermo-mechanic time-dependent modelling.

5. Case Studies

The onset and development of DSGSD have been widely recognised in literature, nevertheless the influence of factors controlling the long-term evolution of these processes are still the object of researches. In case of multiple complex physical agents (thermal, hydraulic, mechanical, dynamic etc.) acting simultaneously on a slope, an accurate description of all the internal or external forcings and conditioning is required. Nevertheless, a parallel coupled solution of physical processes evolving with own velocities might be tricky and computationally intensive. For these reasons working simplification or assumption must be undertaken. In order to deal with this systems, the validity and feasibility of coupled/uncoupled multi-physical analysis will be tested.

To this aim, two representative case studies were selected because of their functionality respect to the research project. Sequential or mono-stage analysis were conducted with respect to morphological and boundary conditions variations. In particular, case studies of natural slopes involved in a peculiar geological context, characterised by conductive or convective heat transfer and by a proneness to gravitational slope deformation, were selected.

The two case studies are at different stages of the evolution, spanning from incipient to advanced phases of deformation. This distinctive character allows to evaluate the influence of thermal boundary or inner conditions on slope masses, directly analysing or back-analysing the impact on spatial and temporal progression of deformative processes. In both cases, gravitational processes can evolve, evolved or still evolve, in relation to variations of geological (then reflected in thermal) and morpho-climatic conditions, therefore, they prove to be appropriate for the purpose of the research. These gravitative deformations could be influenced by thermal variations within the observation period, therefore a comparative mechanical and thermo-mechanical analysis was performed. The influence of geothermal fields and heat

transfer processes on the behaviour of rock masses has been also investigated for each case study, trying to assess their significance in slope stability.

5.1. Warm Systems: The Ischia case study

The first case study has been identified in the north-western slopes of the volcanic island of Ischia, which, for its features, it is the seat of an intense thermal perturbation induced by hydrothermal activity. The island experienced several slope-scale gravitational instabilities in its history as feedback of the renewal of volcanic activities. Part of this sector is undergoing gravitational deformation, which affect a considerable portion of the slopes involving volumes of hundreds of Mm^3 (Della Seta et al., 2012; Della Seta et al., 2015; Marmoni et al., 2017b). The concomitant presence of an enhanced hydrothermal system with high thermal gradients and a large DSGSD over this thermal perturbation, makes the case study a unique opportunity to back-analyse the deformative processes and to deduce the weight of thermo-mechanical deformations in the slope dynamics.

5.1.1. Ischia Volcanic and Hydrothermal System

The island of Ischia represents the westernmost part of the Phlegraean Volcanic District (Central Italy; Fig. 7). The formation of this district is related to the ascent of magma along the Tyrrhenian margin of the Apennine chain (Orsi et al., 2003). Volcanic activity on Ischia Island began prior to 150 ka (Rittmann, 1930; Vezzoli, 1988; Sbrana and Toccaceli, 2011) and continued until the beginning of the 14th century with small volume events characterised by effusive and sporadic explosive magmatic and hydro-magmatic style eruptions (the Arso lava flow in 1302 A.D.) (Vezzoli, 1988; de Vita et al., 2006; Orsi et al., 1996; Vita et al., 2010). The erupted products belong to the LK-series (low potassium series; Appleton, 1972) and vary in composition (mainly trachytic and alkali-trachytic rocks) (Civetta et al., 1991) and eruptive style.

Fig. 7 - Location of the study area (Ischia Island, Italy) with respect to the Campanian Plain. Inset shows a map of Italy. The caldera rims for the Phlegraean Fields and the island Ischia are shown by dashed white lines (Marmoni et al., 2017).

The main event which characterised the geological history of the island was dated 55 ka, when a major explosive caldera-forming eruption led to the emplacement of the Mt. Epomeo Green Tuff (MEGT) (Brown et al., 2008; Orsi et al., 1991; Tibaldi and Vezzoli, 1998), with a total estimated volume of 40 km^3 (Tomlinson et al., 2014). MEGT consists of a massive greenish alkali-trachytic pyroclastic flow deposit which emplacement was assumed to be within a seawater environment (Rittmann, 1948).

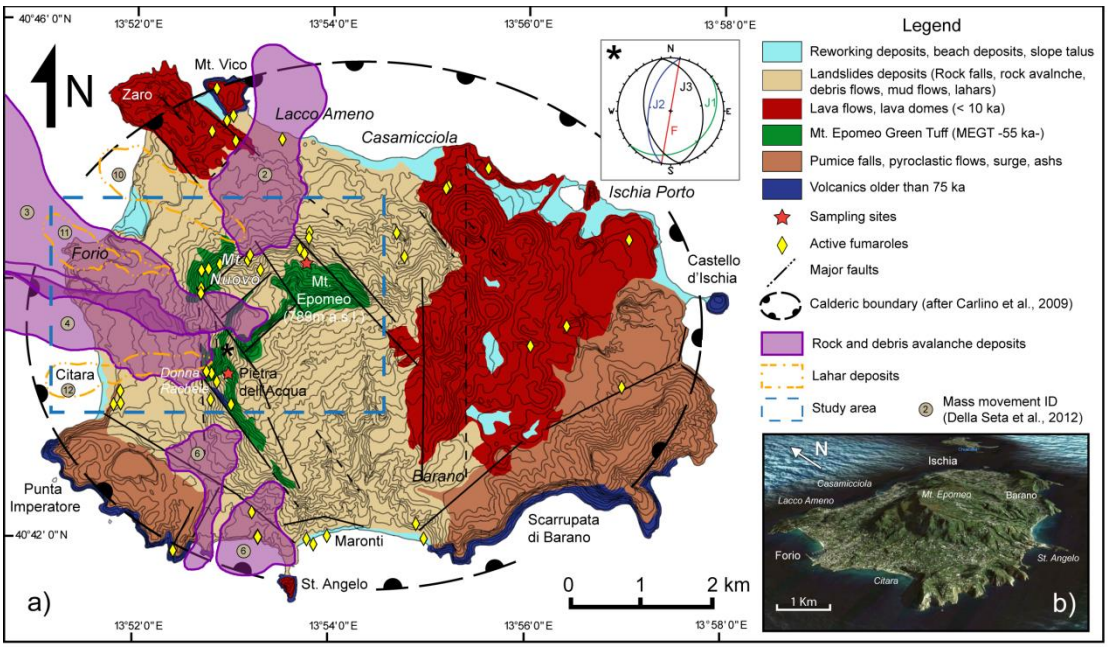

Fig. 8 - Geological sketch map of Ischia Island. Major mass movements in NW sector are reported here as classified by Della Seta et al. (2012). The study area is indicated by the dashed blue rectangle. b) ENE–WSW satellite photograph of Ischia Island (Marmoni et al., 2017b).

The collapse of the caldera was followed by the asymmetric and discontinuous resurgence of the Mt. Epomeo block (Fig. 8), which along high-angle NW–SE and N–S trending faults (Molin et al., 2003), isolate the polygonal shape of the Ischia resurgent block (Acocella and Funiciello, 1999).

The resurgence produced a maximum net uplift of about 900 m in the last 28–33 ka which occurred with intermittent style, as documented by the current elevation of marine sediments and the temporal clustering of landsliding (Buchner et al., 1996; Della Seta et al., 2012; Orsi et al., 1991; Tibaldi and Vezzoli, 1998). The resurgence resulted in the formation of differentially displaced and tilted polygonal blocks that can clearly be seen in satellite or aerial photos (Fig. 8). The resurgence could have been generated by the emplacement of a shallow laccolith (Rittmann, 1930; Carlino, 2012) or by an increase in volume or pressurisation of the shallow magmatic systems (Orsi et al, 1991; Tibaldi and Vezzoli, 1998).

The present-day state, revealed by Differential Interferometry Synthetic Aperture Radar (DInSAR) and geodetic measurements, shows a general trend of deflation (Manzo et al., 2006; Sepe et al., 2007).

The shallow magmatic body produced in addition a vapour dominated hydrothermal system characterised by high heat fluxes (200-400 mW/m^2) and geothermal gradients ranging between 180 and 220 °C/km (Cataldi et al., 1991; AGIP, 1987). The underground fluid circulation mainly occurs within a layering of tuffs and lavas in a multilayered aquifer. The fluid migration occurs through a dense network of cracks separated by low-permeability layers and impermeable horizons (Carlino et al., 2014).

The principal surficial evidences of the presence of vigorous hydrothermal circulation are several thermal springs and fumaroles with temperature up to 100°C, among which most vigorous localised in the western sector of the island, in the Donna Rachele fumarolic field (Fig. 9).

Fig. 9 - Donna Rachele fumarolic field.

The structural alignment, which drove the resurgence, strongly controlled the hydrothermal circulation, conditioning the lateral extension of aquifers and geothermal reservoirs, controlling the geometry of convective cells, fluid velocity, and thermal anomalies distributions of the geothermal system (Bächler et al., 2003; McKenna and Blackwell, 2004). Tectonic elements also represent preferential pathways for upwards migrations of fluids, where maximum heat discharge occurs (Carlino et al., 2014), as inferred by Chiodini et al. (2004) through CO_2 measurements.

The vertical distribution of the geothermal system was acquired by means of drilling of deep wells conducted by SAFEN-AGIP company. The coring highlights the vertical distribution of the system and allowed to derive geothermal gradients in the most active area of the island in the municipality of Forio (NA), where temperatures higher than 200 °C were measured at depth of about 1100 m (Pc46 well - Fig. 10-).

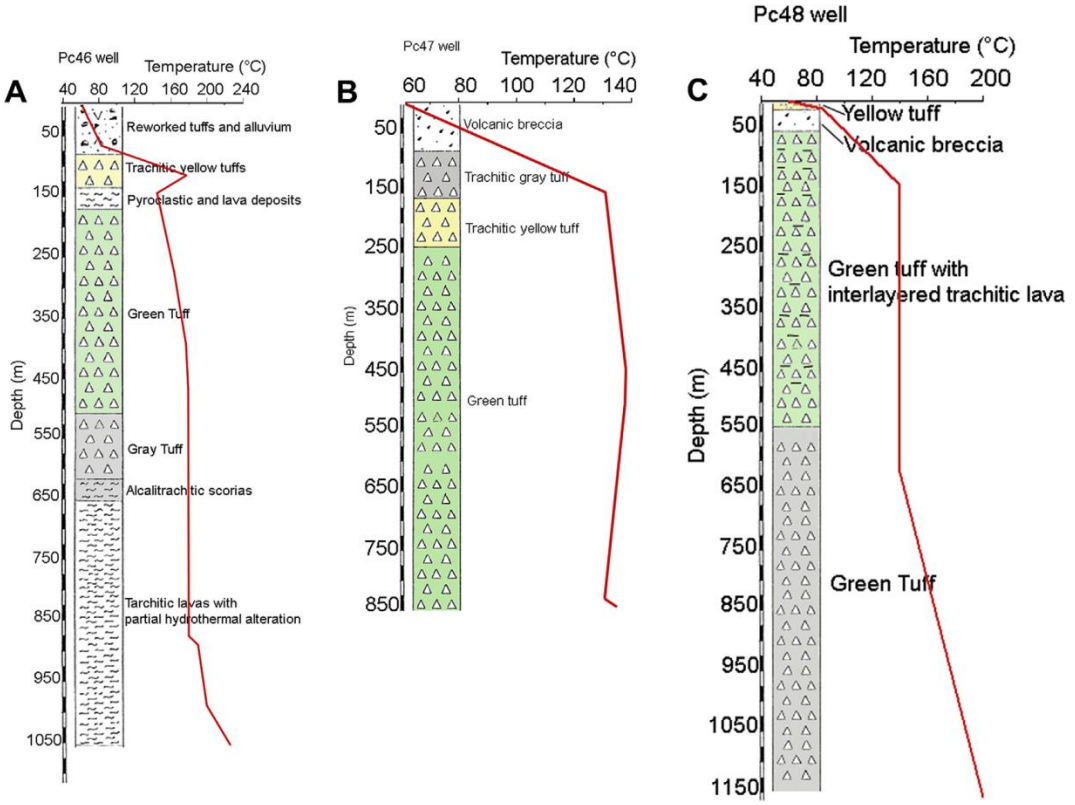

Fig. 10 - Comparison between temperature vs depth measurements (red lines) and the stratigraphy for Pc46, Pc47 and Pc48 wells (AGIP, 1987) (Carlino et al., 2014).

The analysis of temperature/depth curves (Fig. 10), supported by analytical calculation and geothermometric analysis, allowed Carlino et al. (2014) to obtain a conceptual model of the south-western sector of the island. Geotherms obtained in all the deep wells show a first part, from 0 to -180 m b.g.l., characterised by a pure conductive path, which is referred to as impermeable argillitic cap (Carlino et al., 2014). Below this level to about 800 m, gradients become null and the temperature remains stable at around 140-150°C, as a results of the convective regime related to (fluid) mass transfers.

At lower depth gradients become high showing features typical of conductive systems. The third part of the geotherms has good fit with temperatures calculated by the equation of a one-dimensional unsteady heat conduction in an infinite region (Carlino et al., 2014), proving that the heat transfer below this depth is dominated by conduction as a result of permeability reduction.

With the support of integrated geophysical and geochemical investigations, Di Napoli et al. (2009, 2011, 2013) and Chiodini et al. (2004) support the hypothesis that fluid circulation takes place in a layered reservoir.

On this basis, Carlino et al. (2014) proposed a conceptual model based on the definition of a tripartite layering with the purpose to simulate the extraction of fluids for geothermal exploitations. The presence of an advective intermediate (approximately from 105 to 800 m depth) zone contributes to the thermal state of shallow crusts, with increasing of temperature to up to 60 °C at 400 m of depth (Carlino et al., 2014). The thermal perturbation reflects in an higher heating of the slope, through which the heat flux propagates. The heating results in surficial temperatures ranging between 40 and 90 °C (Castaldo et al., 2016; Di Napoli et al., 2009) (Fig. 11) and heat fluxes of 200-400 mW/m^2 (Cataldi et al., 1991).

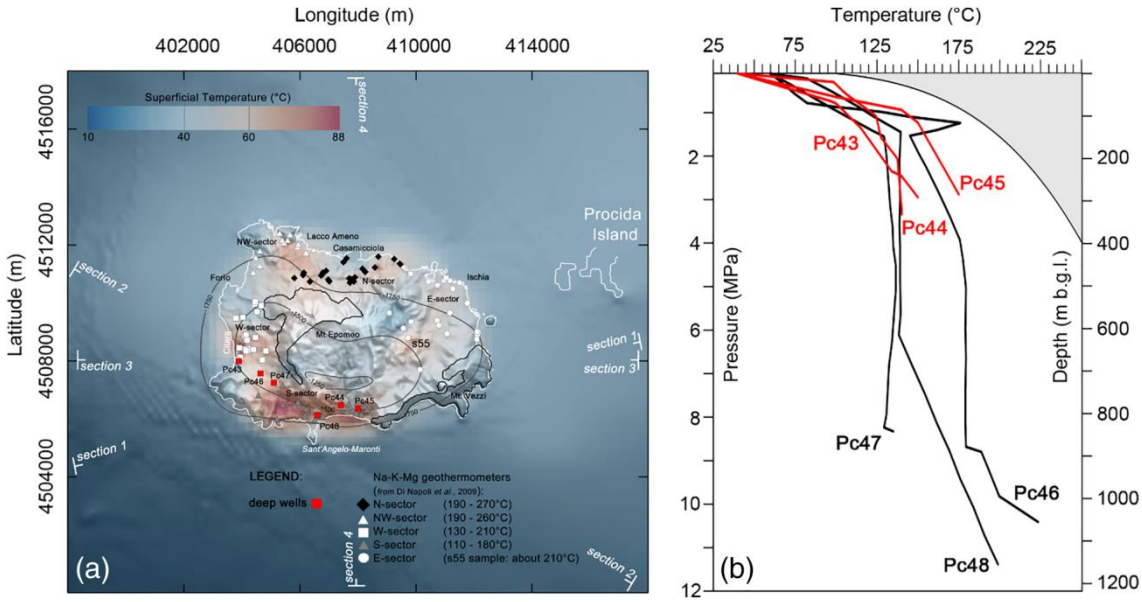

Fig. 11 - a) Superficial temperature distribution of Ischia Island with locations of water samples and deep wells (from Di Napoli et al., 2009) are showed. b) Temperature-depth profiles of the six deep boreholes cored by SAFEN-AGIP (from Carlino et al., 2014; Penta and Conforto, 1951). The boiling curve (black line) derives from the pressure-temperature phase diagram for pure water and it separates the steam field (grey area) from the liquid one (white area). Modified after Castaldo et al., 2017.

Comparison with stratigraphy derived by deep wells (Fig. 10) underlines how deeper MEGT and trachytic lavas represent the major reservoir where fluids circulate in a fractured porous media, heated from below by a magmatic source (Carlino et al., 2014). The convective "layer" seems not to be strictly controlled by lithologies, which indistinctly interest pyroclastic and lava deposits, and it appears mostly controlled by pressure/temperature conditions.

Conceptual models proposed in literature (Chiodini et al., 2004; Di Napoli et al., 2011, 2009) highlight the presence of a multilayered aquifer where the thermal circulation occurs in at least two distinct superimposed reservoirs (

Fig. 12).

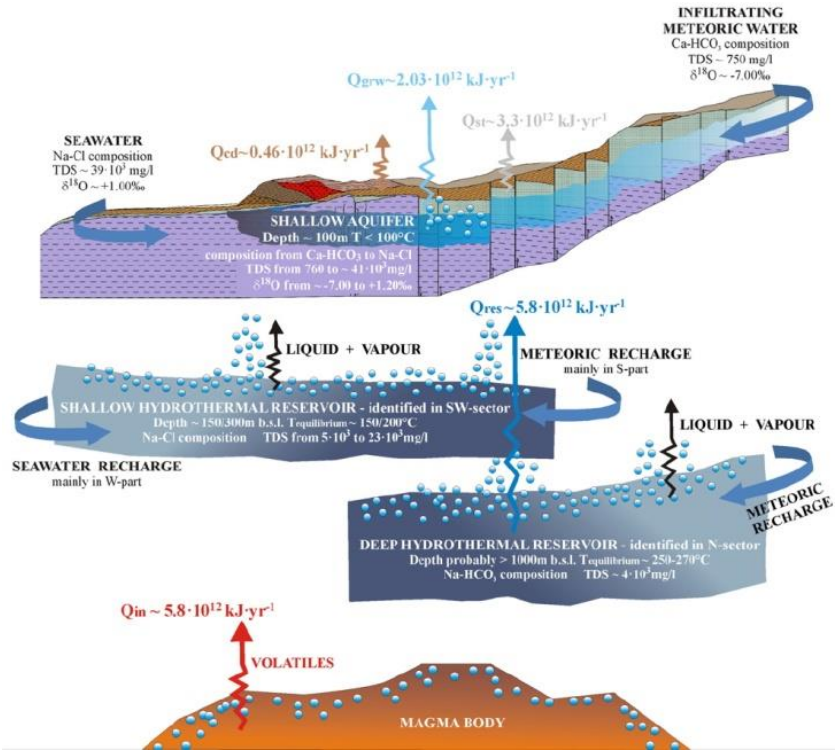

Fig. 12 - Geochemical conceptual model of the chemical–physical structure of Ischia's hydrothermal system. Degassing of a cooling magmatic body at depth sustains the activity of Ischia's hydrothermal system, providing heat Qin (transferred by a volatiles flux) to the deep and shallow hydrothermal reservoirs. In a steady state, the same heat amount is supplied to the shallow aquifer from beneath hydrothermal reservoirs (Qres= Qin) by rising liquid and vapour phases. This amount of heat is (i) dissipated by the shallow groundwater system to warm shallow infiltrating waters (meteoric and seawater) up to boiling temperature (Qgrw), (ii) lost by conduction to the overlying rocks (Qcd), and finally (iii) spent by steam transport and condensation in the very shallow levels of soil in active fumarolic fields (Qst). After Di Napoli et alii (2013).

These models reinforce the hypothesis of close relationship existing with the structural settings, where uprising fluids found their way-out along high-angle normal faults bounding the sides of the Mt. Epomeo resurgent block (e.g. Donna Rachele fumaroles - Chiodini et al., 2004 -) (Fig. 13).

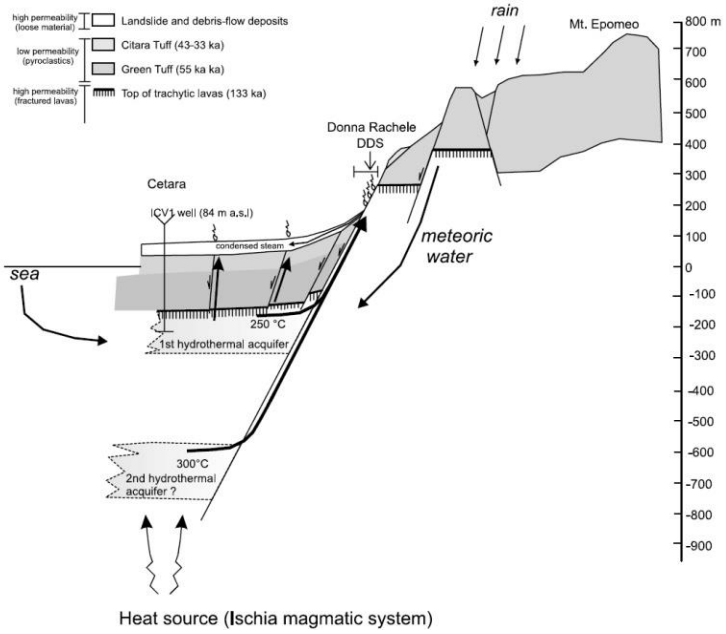

Fig. 13 - Conceptual model of Donna Rachele fumarolic emissions. Model thickness are constrained by geological (Vezzoli, 1988) and shallow well (Penta and Conforto, 1951) data.

In order to obtain more detailed information about spatial distribution and potential time-variation of hydrothermal emissions and to derive relations with the gravitational slope deformation, an annual thermal monitoring of the major fumarolic gas emission was carried out by indirect and direct sensing techniques, using a TESTO® 885-2 IR-thermal camera and a portable thermocouple, respectively.

The monitoring was conducted with a monthly cadence on groups of fumarolic emissions located at different altitudes around the Mt. Nuovo DSGSD (Fig. 14). The derived data show a general stability of the system revealed by the constancy of fluid temperature and the absence of seasonality in the signal (Fig. 15). The temperature of fluid emissions ranges in value between 90 and 100 °C, showing no clear relation with the altitude of fumaroles.

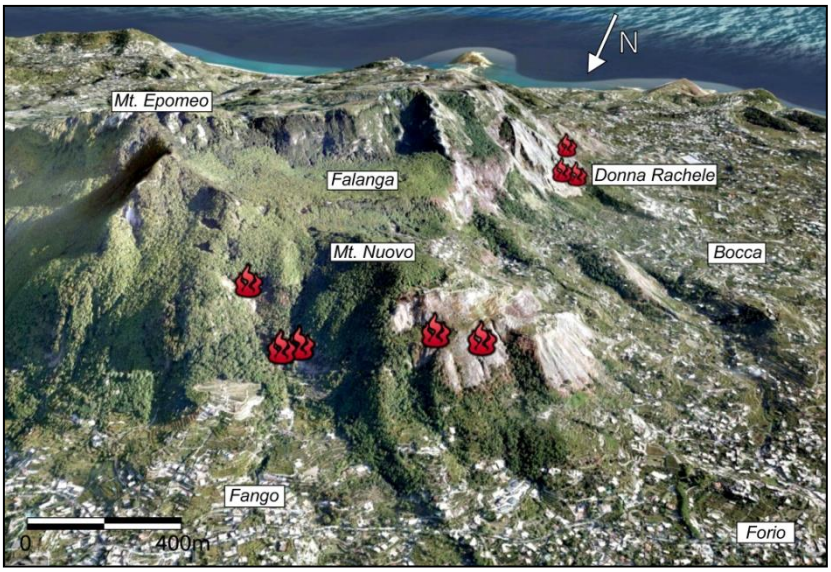

Fig. 14 - Location of monitored fumarolic gas emissions respect to the Mt. Nuovo slope deformation.

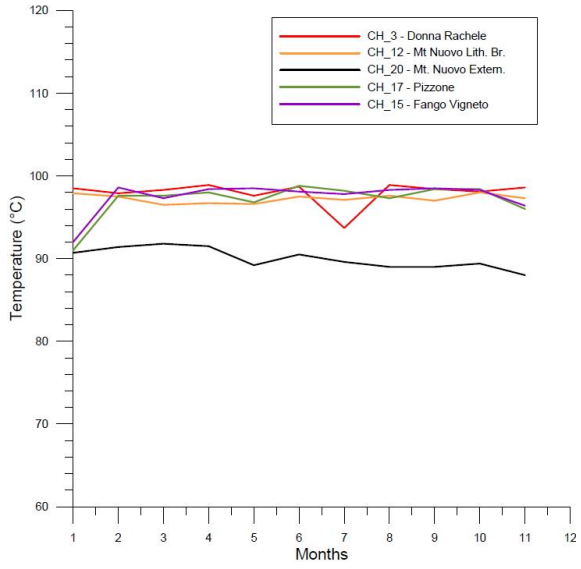

Fig. 15 - Temperature of fumarolic gas emission derived by annual monitoring. No marked seasonal effects were recognised.

The monitoring of hydrothermal emissions is currently going ahead to better constrain relations between fluid circulation and the Mt. Nuovo DSGSD. Measurements of heat fluxes will be conducted in order to constrain and validate single- or multi-phase thermal modelling.

5.1.2. *The Mt. Nuovo Gravitational Slope Deformation*

The volcano-tectonic activity and, in particular, the resurgence generated a landform prone to slope instabilities. In the last 3 ka, the island experienced several large-scale mass-wasting phenomena, including large lahars, debris avalanches, rock avalanches, and slumps (Buchner, 1986; de Vita et al., 2006; Vezzoli, 1988). In particular, large-scale mass movements (Della Seta et al., 2012) appear to be strictly related to volcano-tectonic processes (de Vita et al., 2006).

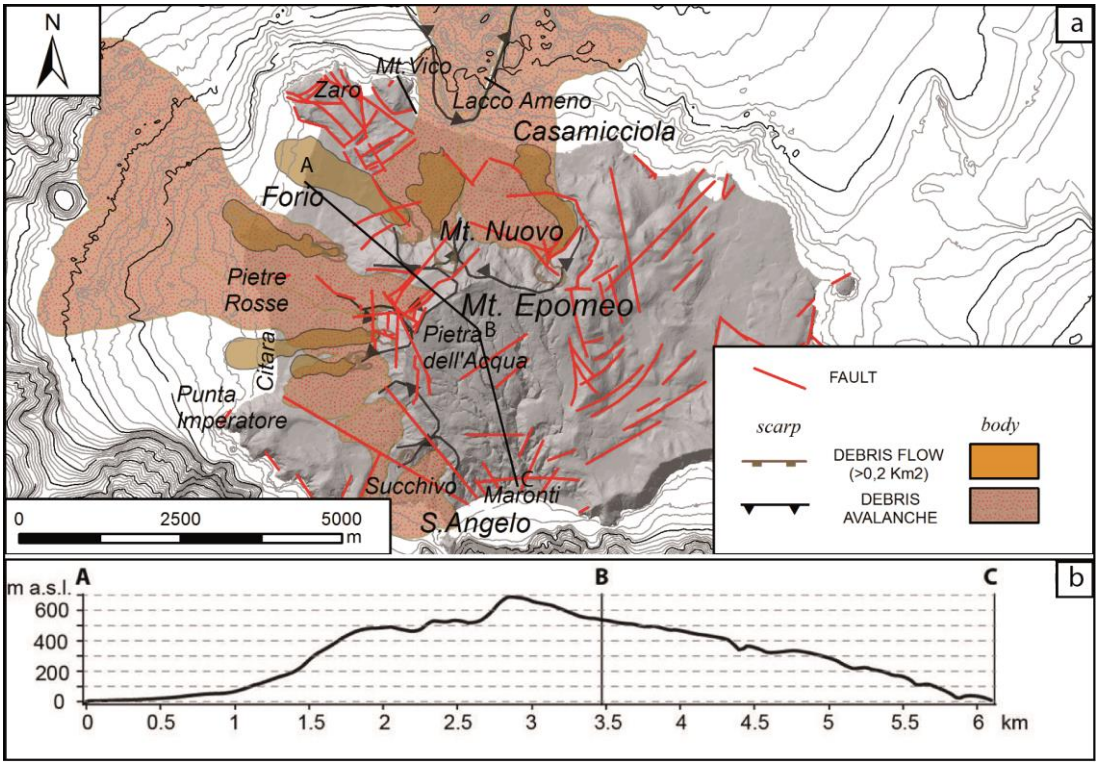

Fig. 16 - Distribution of the major volcano-tectonically triggered slope instability landforms. b). Topographic profile across the Mt. Epomeo resurgent block (Della Seta et alii, 2015)

A new magmatic injection, as hypothesised by de Vita et al. (2006), would result in a reawakening of the resurgence and consequently uplift and slope over-steepening, which together with seismicity (Cubellis, 1985; Alessio et al., 1996), provide the conditions required for slope instabilities. Larger events, which have volumes ranging between 0.5 and 1.5 km^3 ("Ischia Debris Avalanche" (IDA); de Alteriis, 2010; "Pietre Rosse Avalanche"; Della Seta et al., 2012) and which have affected the intensely jointed

and hydrothermally altered rock masses of most of the uplifted sectors of Mt. Epomeo, were often associated to the intersection of resurgence-related fracture systems and associated fumarolic emissions (Della Seta et al., 2015).

The most unstable slopes are located to the north, northwest, and southwest of Mt. Epomeo, where large debris avalanches, documented by their huge deposits, detached from the outer edge of the resurgent block (Fig. 16). In details, these deposits detached from the hanging wall of NE–SW- and NW–SE-trending faults, which provide the kinematic arrangement for slope deformation (Della Seta et al., 2015). The temporal occurrence and geometric relation of major mass movements attest the close connection between volcano-tectonic activity, local seismicity, and flank instabilities (Tibaldi and Vezzoli, 2004; de Vita et al., 2006) (Fig. 17).

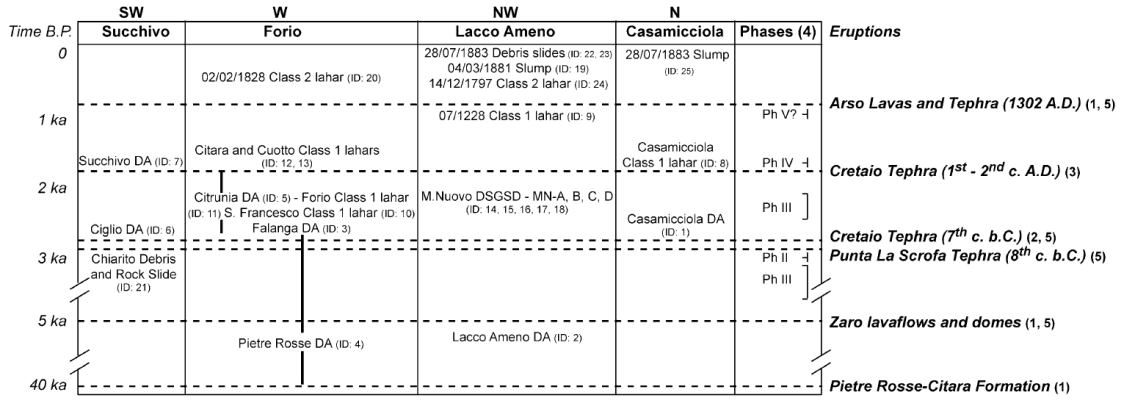

Fig. 17 - Chronological and stratigraphical relationships between mass movements and primary volcanic deposits (Della Seta et al., 2012).

The biggest debris avalanches expanded into the lowlands south of the town of Forio and into the Serrara Fontana basin, as testified by scar areas and submarine hummocky deposits (Chiocci and de Alteriis, 2006; de Alteriis and Violante, 2009). Part of proximal facies of these deposits outcrops in the Rione Bocca (Fig. 8), close to the Donna Rachele fumarolic field. The topography of the Rione Bocca area consists of typical marginal and distal cliffs, linear ridges, and a distinctive hummocky morphology (Fig. 19) due to the megaclasts contained within the massive chaotic matrix of MEGT (Siebert, 1984; Glicken, 1998). A large volume of this debris avalanche

reached the sea and spread into the continental shelf, configuring significant Tsunami-risk conditions (Tinti et al., 2011).

In addition to these large landslides, which represent the major catastrophic mass movements occurred in the island since the Holocene, a still active deep seated gravitational slope deformation (DSGSD) takes place in the western sector of the island in the Mt. Nuovo area, located on the downslope further west of the Mt. Epomeo relief.

This process involves the most unstable slope of the island where the largest debris and rock avalanche and minor volcaniclastic flows (i.e. lahar) detached (Fig. 18), expanding downwards to the coastal plain and the sea (Fig. 19).

Morphological evidences of slope deformation and its geo-structural and geomorphological similarities with the adjacent historical debris avalanche (Della Seta et al., 2015), suggest that an ongoing slope deformation involves the residual portion of a wider deforming block that had only partially achieved the conditions for paroxismal collapse.

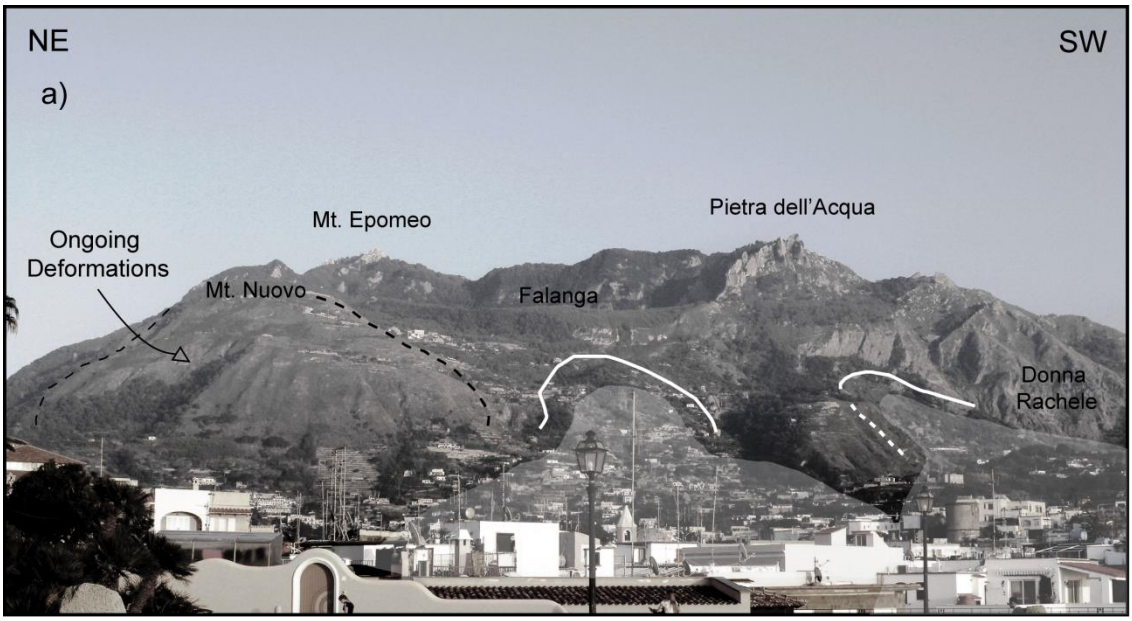

Fig. 18 - Panoramic view of the Mt. Epomeo relief from the Forio Plain; the Mt. Nuovo area, involved in the ongoing gravitational deformation is clearly visible on the left side of the picture (Della Seta et al., 2015). The apical zone and proximal deposits of the documented rock avalanches are presented.

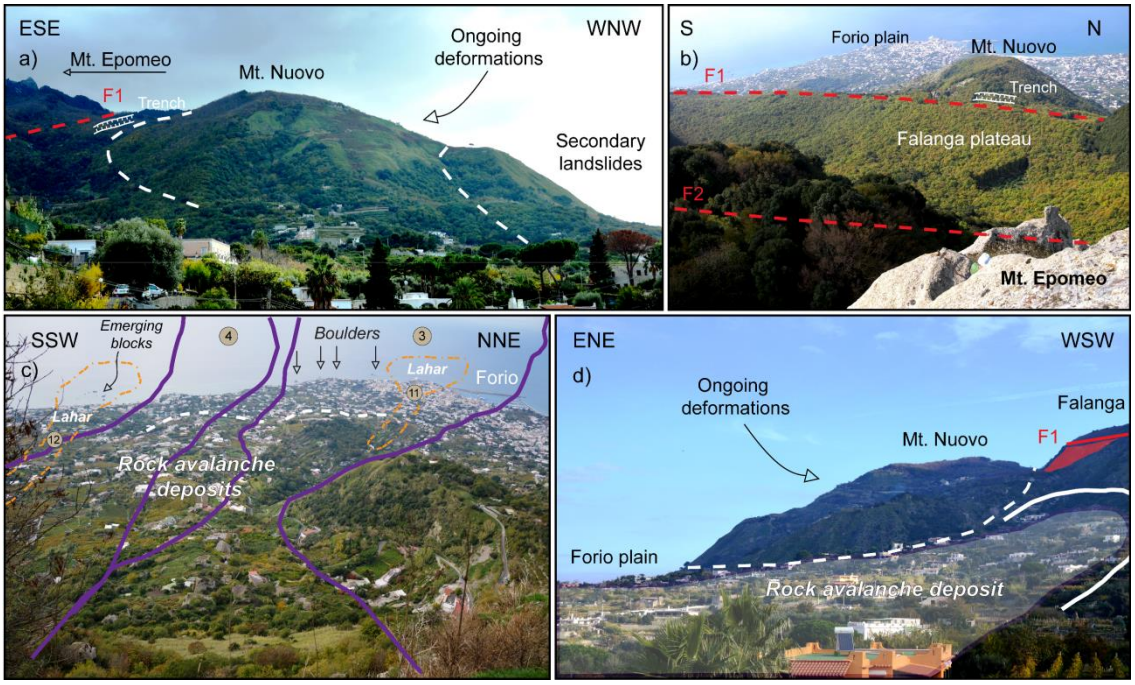

Fig. 19 - a) ESE-WNW view of the Mt. Nuovo area involved in the ongoing gravitational deformation. Schematic traces of gravitational shear zone are shown as white dashed lines. b) View from the top of Mt. Epomeo showing tectonically displaced blocks. Faults that displace the Mt. Nuovo block and Falanga plateau are indicated by F1 and F2, respectively. c) View from the top of the scar area of rock avalanche deposits (deposit trace delineated by the purple line). Hummocky morphology and linear ridge within the landslide deposits are delineated by a white dashed line. Large blocks and boulders are also indicated. Secondary lahar deposits outcrop in Citara shore and Forio Town (shown in orange). Both the lahars and the avalanche deposit reached the sea. Mass movement ID (grey circles) are shown following the classification proposed by Della Seta et al. (2012). d) Lateral view of the ongoing deformation and apical zone of rock avalanche deposits. (after Marmoni et al., 2017b).

The DSGSD at Mt. Nuovo covers an area of 1.6 km^2 (Fig. 20) and is located on the NW of Mt. Epomeo (i.e. downslope of Falanga plain) in the most uplifted part of the resurgent block (Della Seta et al., 2012) (Fig. 20). The DSGSD was reported as triggered by a catastrophic volcano-tectonic event that took place around 460÷470 BC (Della Seta et al., 2012; Buchner, 1996).

The main diagnostic features of such a deformational process consist in counter-slope terraces and open deep trenches with a direction almost parallel to the slope face (Della Seta et al., 2012).

Similarly to the IDA, an analogous tsunamigenic potential for the slope collapse of Mt. Nuovo (Fig. 20) was depicted by Zaniboni et al. (2013), on the basis of the

geometry and diagnostic features of ongoing deep-seated gravitational slope deformation identified by Della Seta et al., (2012).

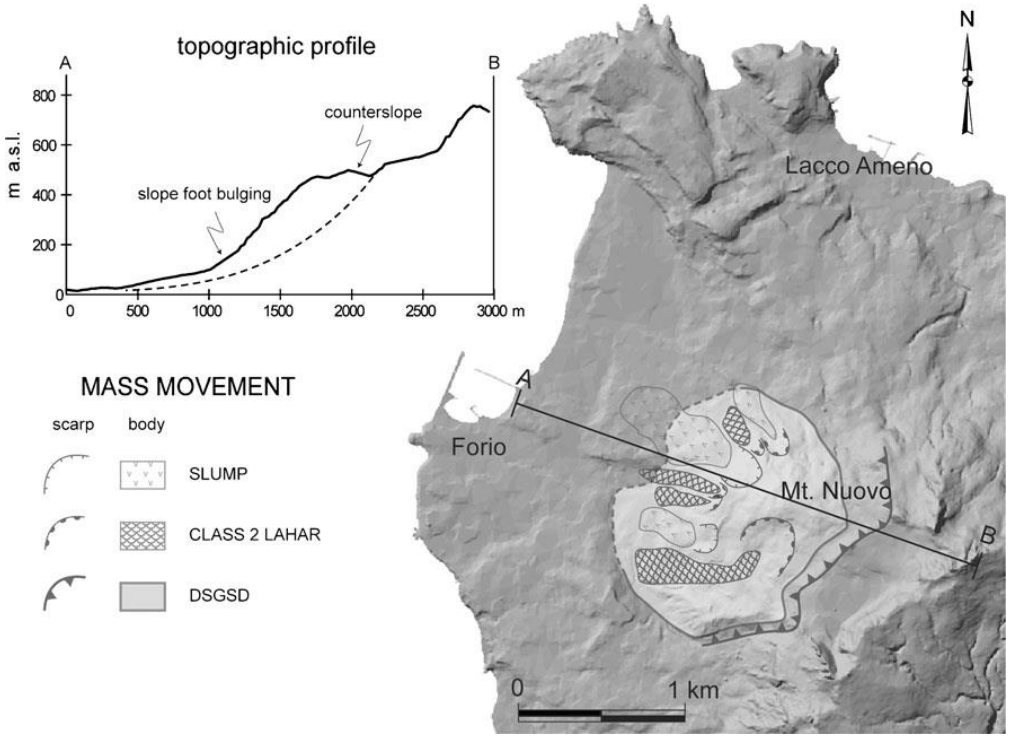

Fig. 20 - The Mt. Nuovo DSGSD and its corollary of minor mass movements with a radial pattern, detached from the deformed mass. Diagnostic features, such as a significant counterslope scarps (delimited by major fault segments) and bulging of the slope foot of the deformed block, are evidenced in plain view and in the topographic profile. (after Della Seta et al., 2012)

In order to identify the geometries that currently drive the gravitational slope deformations of Mt. Nuovo and infer mechanisms and volumes associated with this gravity-induced process, in the frame of this PhD research, an high-resolution engineering-geological model was obtained through a multidisciplinary approach including geological, geomorphological, geomechanical and geophysical investigations.

By means of geological and geomechanical surveys the geological framework of Mt. Nuovo was identified. The geological survey focused on the identification and mapping of the MEGT deposits and the distinction of two ignimbritic units of which MEGT is composed of. The performed survey allowed to reconstruct at detailed scale the stratigraphic setting in which the Mt. Nuovo DSGSD took place (Della Seta et al.,

2015). At the same time, a geomechanical survey was carried out to assess the role of tectonic elements on the gravity-induced slope deformation and to derive the properties of the outcropping jointed rock mass. Through geomorphological surveys and terrain analyses (in GIS environment), scarps, terraces, saddles, trenches and morphological counter-slopes were also identified (Fig. 19).

Seismic measurements of ambient noise were also carried out to characterise the local seismic response of the Mt. Nuovo slope as well as to acquire other constrains to the geological model (Della Seta et al., 2015). An high-resolution geological model of the Mt. Epomeo western slope was defined and reproduced through a 1:10000 geological map and four engineering-geological cross sections (Fig. 21) (Della Seta et al., 2015).

These sections intercept three distinct gravitational shear surfaces: the main one is about 250 m deep, while the two minor ones are located downslope (Fig. 22). The geometric evidence allows to classify the slope deformation as a "type E" structurally-defined compound "constrained at toe" slide (Hungr & Evans, 2004) driven by translational mechanism. The main rupture surface follows an high angle joint set at scarp while a basal shear zone cuts the rock mass. By geometry of failure surfaces, counter-slope terraces and depositional features (i.e. tilted elongated scoria), a minor rotational component in the landslide mass movement can be deduced. A marked structural control is revealed by the alignment of tectonic elements and gravitational landforms: joint trends have, in fact, a direct correspondence in the morphological trenches observed upslope the deformed volume (Fig. 19).

The bi-planar compound setting of the main sliding surface involves a rock mass volume of about 190 Mm^3 with a total horizontal displacement of about 65 m.

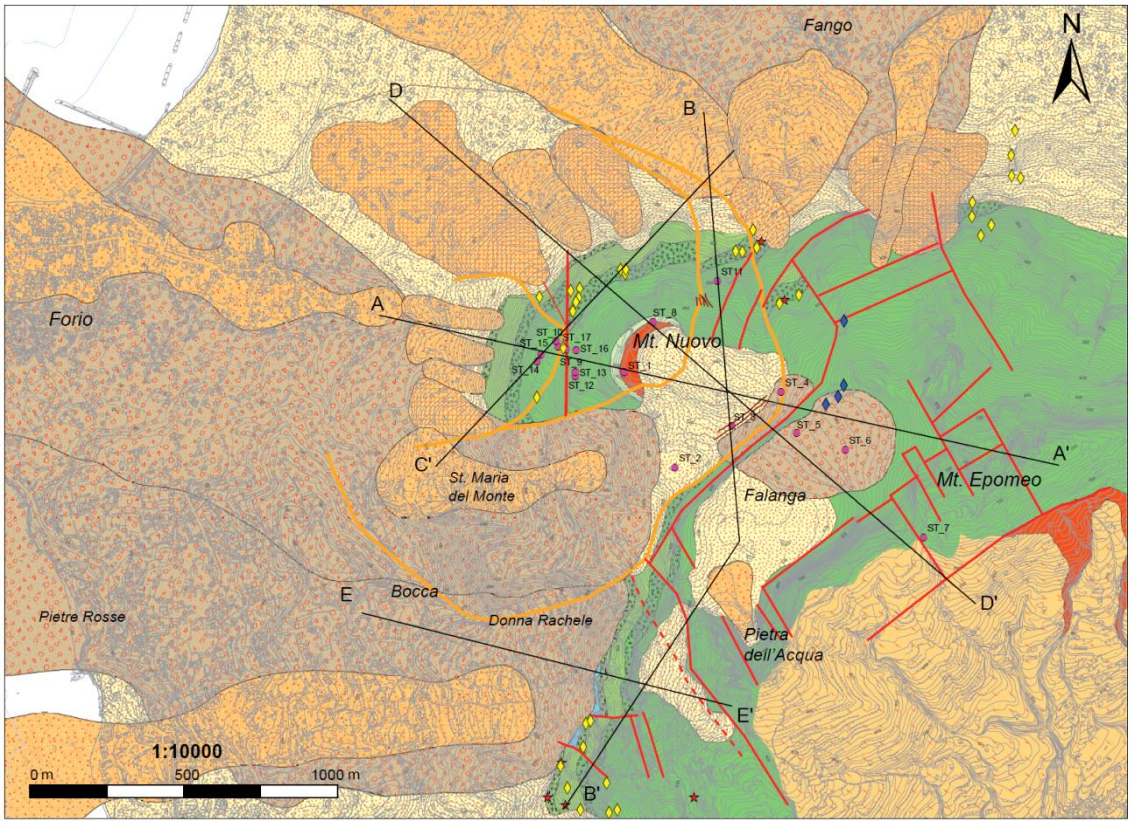

Fig. 21 - Geological Map of Mt. Epomeo Western Slope (Ischia), from Della Seta et al., 2015. Location of active and relict fumarolic emission are reported by yellow and blue rhombus, respectively. Distribution of noise measurements is evidenced by magenta circles. All the reconstructed geological cross-section are presented in Della Seta et al., 2015.

HVSR measurements show resonance peak at 0.8 Hz without spatial directivity at stations ST_1, ST_3 and ST_8 (Fig. 22), which could be related to an impedance contrast between a soft-rock layer and a bedrock. This contrast has been attributed to approximately 250 m of thick soft layer constituted by the MEGT involved in landsliding and overlaying the trachytic lavas constituting the landslide bedrock (Fig. 22). Such a seismic resonance is no more evident moving upslope from Mt. Nuovo towards the Falanga plain where the MEGT is not involved in the landslide process. Moreover, the proposed geological model highlights that hydrothermal emissions are strictly related to both stratigraphic and structural settings of the area, in which breccia layers and fault zones represent preferential escape paths for the ascent of fluids.

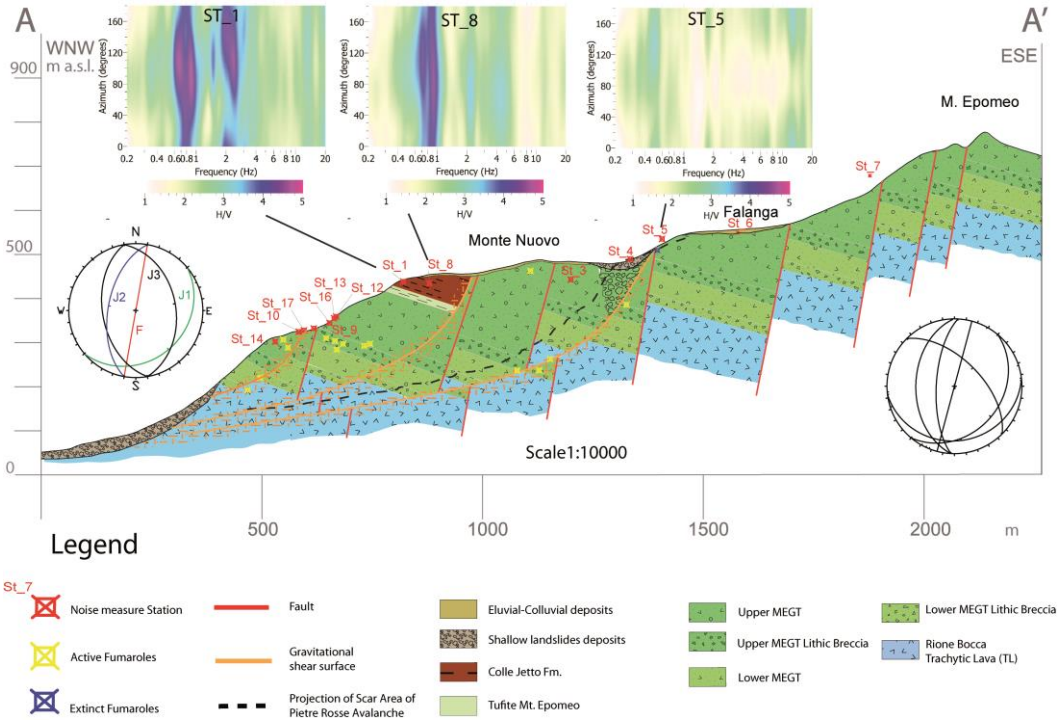

Fig. 22 - Geological section of the gravitational deformation affecting the Mt. Epomeo western slope. Fumaroles as well as seismic noise measurement locations are projected from the surface position to the cross-section. The dashed black line represents the shape of the already detached avalanche of Pietre Rosse scar area, shifted 150 m eastward. The synthetic stereographic plot of the main joint sets measured in the Mt. Nuovo area (left) and in the scar area of the historical Pietre Rosse rock avalanche (right) are also shown.

Monitoring deformative data deriving from GPS levelling or DInSAR interferometry do not provide useful information to constrain the deformative style and mechanism of slope deformation.

5.1.3. Laboratory characterisation of Mt. Nuovo Tuffs

To better understand the mechanism responsible for driving the DSGSD on Mt. Nuovo, as well as to constrain possible factors that can trigger or accelerate the ongoing gravity-induced process and to comprehend the role of confining pressure on the mechanical behaviour and failure mode of the MEGT, a physical and mechanical characterisation of the MEGT was performed (Marmoni et al., 2017a, 2017b). Brown et al. (2008) divided the MEGT in two pyroclastic flow deposits (the Upper and Lower MEGT) separated by a volcanoclastic member with a thickness varying from 20 to 50

m. This unit constitutes a large part of the Mt. Nuovo slope and is widely involved in the gravitational deformation. For this reason, intact blocks of rock of both the Upper MEGT (hereafter named UGT) and the Lower MEGT (hereafter named LGT) were collected from representative outcrops (Fig. 8).

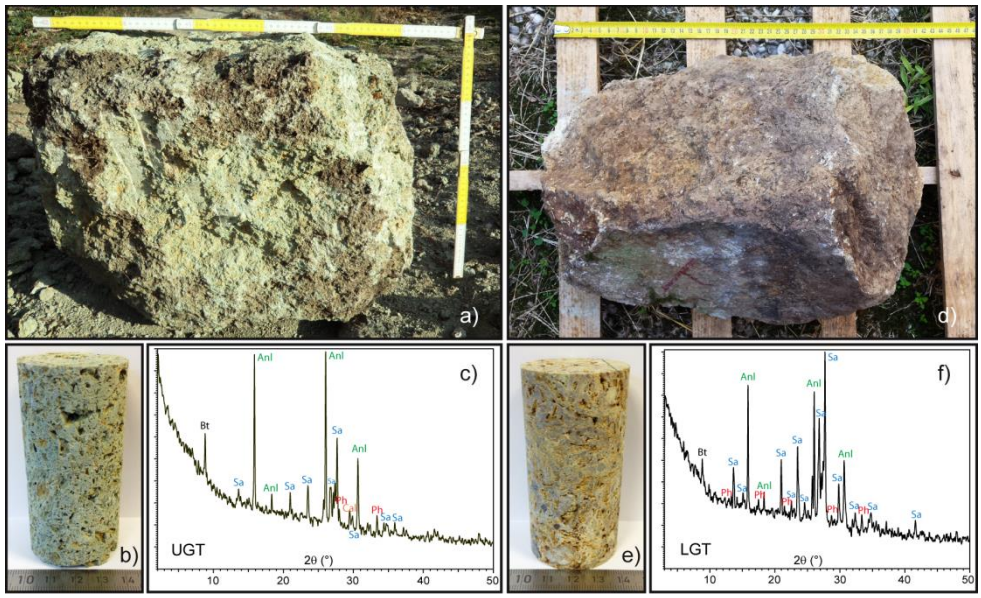

Fig. 23 - Photographs of exemple collected blocks of UGT (a) and LGT (d) and respective laboratory samples (D = 40 mm) (Fig. 4b-4e). X-ray powder diffraction performed on UGT (c) and LGT (f) reveal the presence of biotite (Bt), sanidine (Sa), analcime (Anl), calcite (Ca), and minor phillipsite (Ph)(panels (c) and (f)).

Physical properties as density, shear wave velocity, connected porosity, and permeability were measured prior to deformation. A set of Uniaxial Compressive Strength tests (UCS) and Triaxial tests were after performed on 20 mm-diameter dry (dried in a vacuum oven at 40 °C for at least 24 hours) and water-saturated samples. Triaxial tests were performed under drained conditions over a range of effective pressure (P_{eff}) conditions (analogous to depth) relevant for the gravity-driven slope deformation on Mt. Nuovo. Axial load, axial displacement, pore volume change (in the wet experiments), and confining volume change were all monitored during deformation using a load cell, an LVDT, and a pore pressure intensifier/volumometer, respectively.

The obtained results show that the presence of water dramatically reduced the strength of the MEGT, in both the uniaxial and triaxial cases, suggesting that meteoric water or the movement of fluids within the hydrothermal system could dramatically impact slope stability (Marmoni et al., 2017a, 2017b).

Our triaxial experiments also prove that the UGT shows compactant (i.e. ductile) behaviour at effective stresses of ~1 MPa (Fig. 24,Fig. 25), corresponding to a depth between ~100-200 m. The onset of compactant behaviour occurs at a higher effective pressure of ~10 MPa for LGT (Fig. 24, Fig. 25), a consequence of its lower porosity. Below these pressure levels the rock deforms in a dilatant (i.e. brittle) mode, with negative volumetric deformations related to the opening of microcracks up to failure (Fig. 24, Fig. 25). This transition in failure mode occurs at a depth relevant for the Mt. Nuovo slope, and could influence gravity-induced strain deformation. For this reason, inelastic compaction may occur at shallow depths and may be the mechanism responsible for driving the present-day slope deformation (Marmoni et al., 2017b).

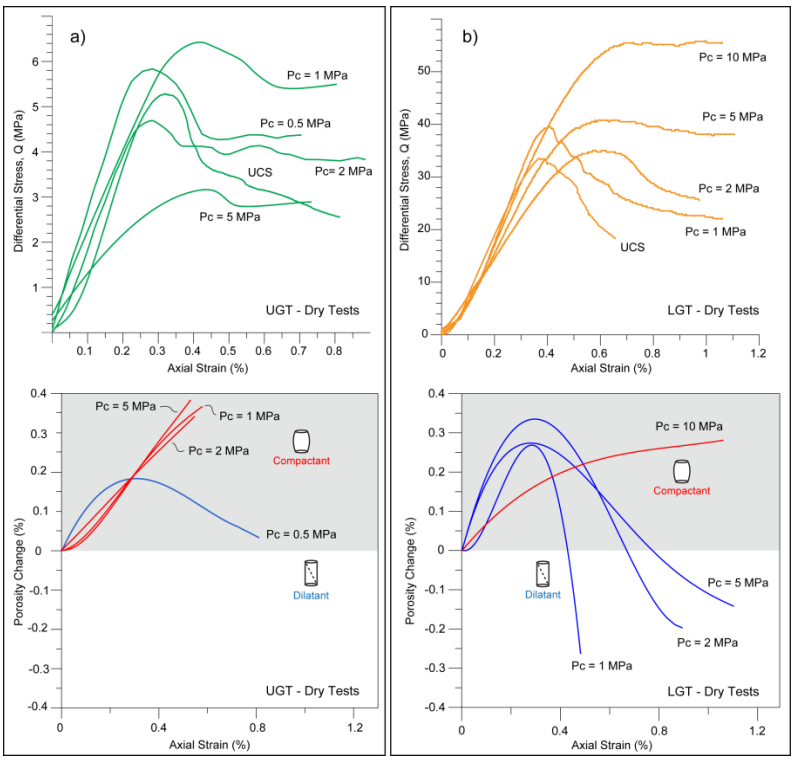

Fig. 24 - Dry triaxial tests on UGT (a) and LGT (b). The effective pressure of the experiment is labelled next to each curve. The porosity change was estimated using the change in confining fluid volume. Dilatant porosity change curves are shown in blue and compactant porosity change curves are shown in red. The grey and white zones highlight net compaction and net dilation in the porosity change graphs, respectively (Marmoni et al., 2017b).

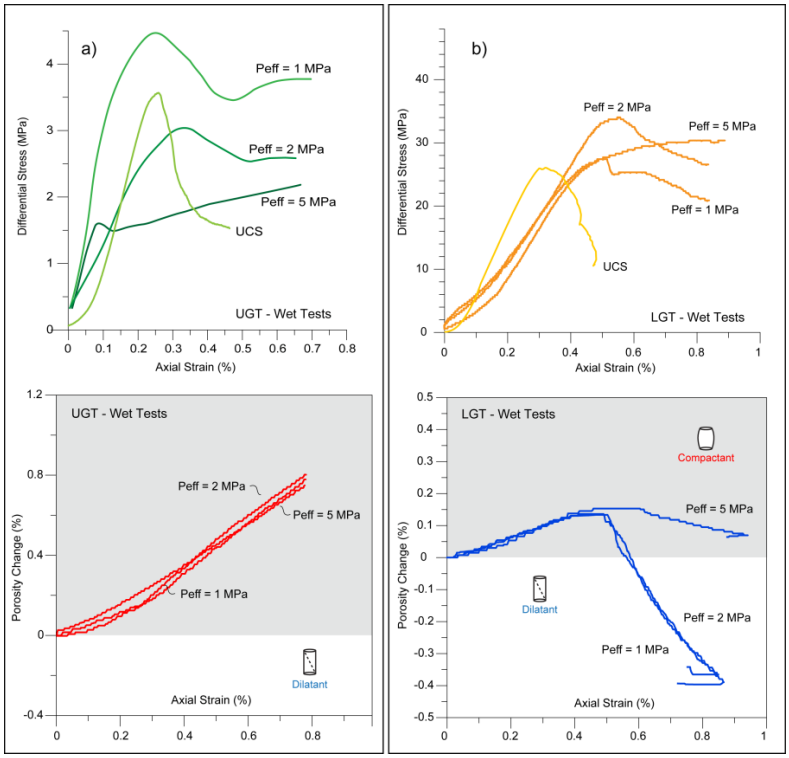

Fig. 25 - Wet triaxial tests on UGT (a) and LGT (b). The effective pressure of the experiment is labelled next to each curve. The pore pressure for all experiments was 10 MPa. Dilatant porosity change curves are shown in blue and compactant porosity change curves are shown in red. The grey and white zones highlight net compaction and net dilation in the porosity change graphs, respectively (Marmoni et al., 2017b).

All laboratory investigations were conducted at room-temperature. Because of the limitation of triaxial press and other laboratory facilities no proper thermo-mechanic tests (i.e. triaxial test under controlled temperature) were performed.

The laboratory characterisation was completed by the definition of thermal properties (i.e. thermal conductivity, specific heat) governing heat propagation in solids by differential guarded hot plate and calorimetry methods according to ASTM or UNI EN standards. The definition of thermal conductivity was achieved on three samples measuring 150 x 150 x 70 mm (Fig. 26) by the use of Lambda Meter EP500 (Lambda Messtechnik GmbH Dresden).

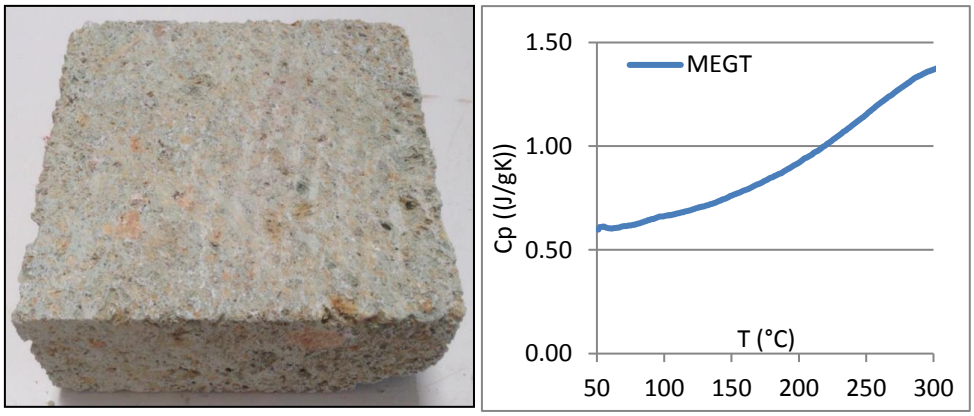

Fig. 26 –Sample of MEGT tested with guarded hot plate method (left), Graph of Differential Scanning Calorimetry test performed on MEGT sample.

In order to output thermo-mechanical effects on the rock mass, measurements of the linear thermal expansion coefficient were achieved according to standards (UNI EN 14581:2005). Samples measuring 250 x 50 x 20 mm were heated inside an oven measuring the linear expansion in a temperature range between 20 and 80°C. All thermal tests were conducted by the Ecam Ricert Laboratory (Vicenza, Italy). All of the other laboratory tests were performed at the Géophysique Expérimentale laboratory at the Institut de Physique du Globe de Strasbourg (IPG Strasbourg). Further details about experimental methods and materials can be found in references (Marmoni et al., 2017b). A summary of the experimental results is provided annexed to this document (Annexe Table 1).

The derived thermal and mechanical data, that can be considered representative of the sample length-scale, will be fundamental for mechanical zoning of rock masses which, following equivalent continuum approaches (Hoek et al., 2002; Sitharam et al., 2001), will allow laboratory results to be up-scaled to longer length-scales like those proper of slopes. The derived parameters will be directly exploited through an engineering-geological model that includes mechanical zoning of rock masses where depth zones are distinguished by stress level according to experimental results. Mechanical and thermal parameters will be then transferred to numerical modelling to evaluate the contribution of heat transfer in the mechanical behaviour of rock masses involved in slope scale gravitational deformation.

5.1.4. *Conceptual model of the Mt. Nuovo DSGSD*

Based on the high-resolution of the engineering-geological model of Mt. Nuovo, a preliminary conceptual model was attained to justify ongoing gravity-induced slope deformations. This model ensures that slope deformation initiates with the nucleation of crack and fracture propagation at the foot of the slope (i.e. where low confining pressures exist) caused by stress field variation related to the hydrothermal system.

At higher stress levels within the slope, joints evolve in a proper shear zone propagating upslope up to the intersection with pre-existing discontinuities related to volcano-tectonic elements, originated by resurgence events (Fig. 27).

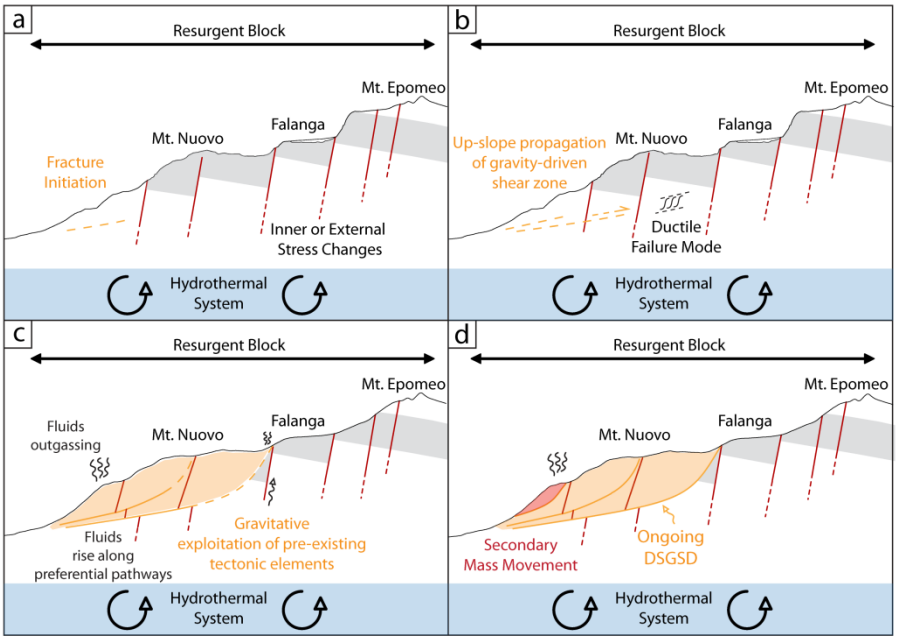

Fig. 27 - Conceptual evolutionary model of the Mt. Nuovo slope deformation (modified after Della Seta et al., 2015).

The hypothesis of enucleation of a basal shear zone has been supported by the laboratory investigations conducted on MEGT (Fig. 24, Fig. 25), which evidenced a brittle-ductile transition in charge of porous tuffs at depth relevant for slope deformation.

On the basis of the theoretical approaches proposed so far (Mencl, 1968; Feda, 1973; Mahr, 1977), Marmoni et al. (2017b) assume that the combination of brittle and ductile behaviour may be responsible for the large-scale slope deformation. In this hypothesis, compactive flow-like deformation occurs in the internal part of the slope, where the shear zone is under a higher lithostatic pressure, while brittle failure takes place downslope, where failure surface is more surficial and low confining stress operates (Fig. 28). Based on this conceptual model, the progressive slope failure migrated upslope on Mt. Nuovo, generating a compactant shear zone that terminates on the inherited sub-vertical fault zones (Fig. 28).

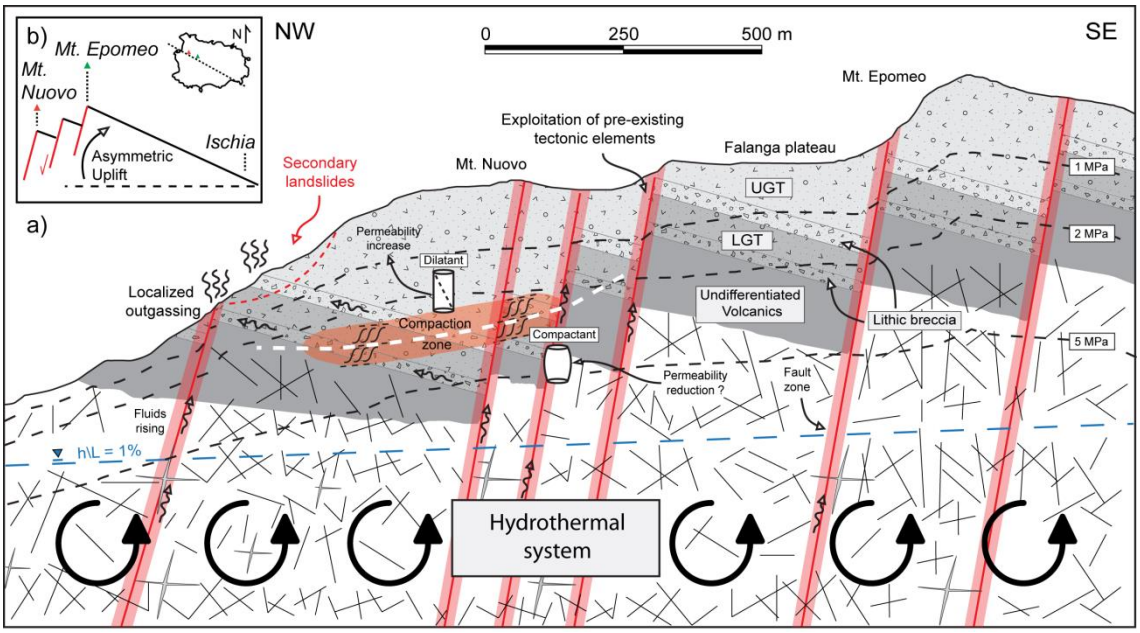

Fig. 28 - Schematic cross section of the Mt. Nuovo (NWflank Mt. Epomeo) slope before the onset of deep-seated gravitational slope deformation. The failure mode transition (brittle to ductile) occurs at a shallow level, where a compaction zone favours shear zone nucleation. Isobars of lithostatic (i.e. confining pressure) obtained by preliminary stress-strain numerical modelling are shown by black dashed lines. Fluids rise from the shallow convective hydrothermal system along tectonic elements and can move laterally within more permeable levels of lithic breccias when they reach the LGT, which is characterised by a much lower permeability. Modified after Marmoni et al. (2017).

5.2. Cold Systems: The Priestley Glacier (Antarctica) case study

The second selected case study was defined in the slopes bounding the Priestley glacier valley (Northern Victoria Land, Antarctica), belonging to the East Antarctic Ice Sheet (EAIS -Fig. 29-), which, because of its features, presents opposite thermal conditions comparing to the warm Ischia case study, i.e. presence of negative thermal anomalies due to the existence of a cold glacial mass. No evidence of DSGSDs exists in this area, however the morpho-structural evolution and the geological context represent the predisposing settings for the development of gravitational slope deformations.

The case study area includes a wide sector of the Transantarctic Mountains and the Mt. Melbourne Volcanic Province and it represent a key site for investigating the effects of past ice volume variations and geothermal perturbations.

Since its formation, in fact, the valley and the slope's wallrocks experienced variations of geothermal heat fluxes as direct reflection of rifting and volcanism of the Ross Sea.

Fig. 29 – Antarctica overview map. Modified by official mapping source available at: http://lima.usgs.gov

Such endogenous forces may have affected the thermalisation of the slope system, altering the rock mass mechanical and rheological behaviour and, secondarily, influencing the energy balance and ice dynamics of the glacial system. The role of geothermal contribution on the glacial physical state and dynamics is still object of discussion in the scientific community (e.g. Engelhardt et al., 1990; Fisher et al., 2015; Gudlaugsson et al., 2016; Larour et al., 2012; Pollard et al., 2005).

Similarly to the "warm" case study, thermal, mechanical and thermo-mechanical analysis will be conducted trying to directly evaluate the influence of thermal conditions in the onset and progression of slope deformations.

Despite no documented landforms attributable to gravitational slope deformation were identified in literature, the proneness of the glacial valley to gravitative deformations and the double contribution of deep geothermal heat fluxes and local thermal anomalies played by glacial masses, make the specific case study interesting for the main purpose of the research.

It is worth to note that all the activities of this research are framed in Line-B of the Antarctic research project and are funded by the Italian National Antarctic Research Program (PNRA). This research is based on experimental and on field data obtained by previous Antarctic expeditions and no on-field activities were carried out.

5.2.1. Thermal evolution in Northern Victoria Land

The geological evolution of the Antarctic continent, confined above the 60° S of Latitude, is the consequence of a long and complex geological history, began ~140 Ma with the fragmentation of the Gondwana supercontinent (Veevers, 2012) and the drifting of Antarctica towards polar latitudes (reached in the early Cretaceous, c. 120 Myr), and the opening of deep ocean passages around the continent (Kennett, 1977), which led to the establishment of the Antarctic Circumpolar Current (ACC).

However, dating estimations of this onset span over an extremely wide time range, in which the ACC would have been established after the Eocene-Oligocene boundary (Lyle et al. 2007). If this is true, the switching-on of the ACC did not contribute to the ice sheet formation and it widely anticipated the middle Miocene climate cooling (Zachos et al., 2001; Baroni, 2013;). The first continental-scale Cenozoic glaciation in Antarctica is in fact registered about 34 Myr ago (Denton et al., 1991; Hambrey et al., 2007; DeConto and Pollard, 2003; Young et al., 2011).

It is widely accepted that the inception of polar-desert conditions on East Antarctica occurred about 14 Myr ago (Marchant et al., 1993; Sugden and Denton, 2004; Lewis et al., 2007), when EAIS shifted from wet- to cold-based regime (Lewis et al., 2008).

In Northern Victoria Land (NVL) a change in glacial dynamics delayed to the Late Miocene (Armienti and Baroni, 1999; Smellie et al., 2011), when hyperarid polar climatic conditions began, preserving either glaciated and deglaciated areas from erosion. K–Ar and Rb–Sr dating testify that erosion of alpine topography (i.e. truncated spurs, trimlines, etc.) associated with valley glaciers occurred until about 8.2 and 7.5 Myr (Armienti and Baroni, 1999). Since that period, cold basal ice conditions characterised glacier dynamics in northern Victoria Land. These evidences have been interpreted as a change in climatic conditions which could have moved the glacier states from a condition allowing the development of a wet-base (Baroni and Fasano, 2006; Baroni et al., 2008) to one favouring the presence of polar glaciers (Baroni, 2013).

The distribution of wet- or cold-based glaciers and the amount of melted water at the base of ice masses have been widely proved as a factor controlling glacial dynamics in terms of mobility (Alley et al., 1989), erosion rates (Rippin et al., 2003), and hydrology (Boulton et al., 1995).

Several studies have systematically analysed the role of geothermal fluxes beneath glacial masses to define the role of deep thermal perturbations in ice volumes and extent variations (Ritz, 1997, 2001), basal pressure melting conditions (Hansen and Greve, 1996; Takeda et al., 2002) and ice-flows (Larour et al., 2012), up to the possible role in the onset of major glaciations (Pollard et al., 2005).

Subglacial heat-fluxes can reach extremely high values (Della Vedova et al., 1992; Fisher et al., 2015; Schroder et al. 2011) because of active rifting, volcanism, or heat production by intrusive rocks (Carson et al., 2014).

Armienti and Perinelli (2010), with the support of thermo-barometric data obtained by the study of spinel-peridotites xenoliths, inferred a geothermal gradient rise from 0.5 to ~3 °C/km during the development of the Ross Sea rift system. This warming would have caused the upward movement of isotherms, providing significant perturbation of the local thermal regime (Perinelli et al., 2017, 2011).

The thermal variation in the geothermal regime, as well as ice thickness fluctuations, could have also conditioned the response of the slope system to gravitative forcing, potentially enhancing deformations and fostering the onset of incipient slope deformations.

Starting from the definition of an engineering-geological model of selected glacial valleys, a morpho-evolutionary model of the slope-to-valley system has been defined, reconstructing past ice volume variations and thermal boundary conditions.

Thermo-mechanical modelling of both the rocky bedrock and the ice mass will be thus performed, aiming at the evaluation of stress-strain effects on rock mass behaviour, with an eye to the effects on the kinematic of the glaciers.

5.2.2. The Priestley Glacier and Ice-Sheet dynamics

The territory of Victoria Land (Fig. 29) extends from Williams Head (69°, 11' S) to the Mc Murdo shelf (77° S). In this area the Terra Nova Bay, between Drygalski Tongue in the south and Cape Washington in the North, represents a limit separating two different zones from a geomorphological and glaciological point of view (Orombelli et al., 1990). South of Terra Nova Bay glaciers reaching the coast drain the EAIS, contrary to the northern sector where local glaciers with alpine morphology are not directly related to the ice-sheet (Armienti and Baroni, 1999; Orombelli et al., 1990).

The geologic basement of the NVL has been divided into three different overimposed terranes displaced since Early Palaeozoic along NW-SE trending faults (Salvini et al, 1997; Salvini and Storti, 1999; Dowe and Neall, 1974): the Wilson Terrane, the Bowers Terrane and the Robertson Terrane (Carmignani, 1989). The study area is totally comprise within the Wilson Terrane, composed of a granitoid complex (Granite Harbour Intrusive Complex -GHIC-) intruded within low- to high-grade metamorphic rocks (?Precambrian – ?Early Ordovician) of the Wilson Metamorphic Complex, mostly outcropping along the slopes of the Priestley glacier (Pertusati et al., 2012; Carmignani et al., 1989). During the Cenozoic a diffuse magmatism involved the NVL, with dominant volcanism starting since ~12 Ma (Mt. Melbourne, Mt. Overlord)(Armienti and Baroni, 1999).

The Priestley glacier, together with the David and the Reeves glaciers, with ~ 96 km of length, represents one of the largest outlet glacier draining the portions of ice-sheet in Dome C and Talos Dome, over an area of 250'000 km^2 (Frezzotti, 1994). The glacier drains southeast between the Deep Freeze and Eisenhower ranges to enter the northern end of the Nansen Ice Sheet. The maximum thickness is about 1600 m in the external area in close proximity to the grounding line (Baroni et al., 2004).

The Priestley glacier represents a key site for the reconstruction of past ice-sheet fluctuations, directly reflecting advance or retreat phase in glacial the troughs.

With the support of geological literature observation (Pertusati et al., 2012; Carmignani et al., 1989) and quantitative geomorphic analysis (Bastoncelli, 2004; Baroni & Salvatore, in progress), together with geophysical data related to bedrock topography (BEDMAP2 - Fretwell et al., 2013; Tabacco et al., 2002, 1999) and Digital Elevation Model (DEM) of the free surface (RAMP-RADARSAT), a synthetic geological section crossing the Priestley valley has been reconstructed (Baroni & Salvatore, in progress).

The section extends from Black Ridge (1510 m a.s.l.) to Lowry Bluff (1070 m a.s.l.) crossing granitoid rocks belonging to GHIC and anfibolitic metasediments of the Wilson Metamorphic Complex (Fig. 30). The position and orientation of the geological cross-section has been defined considering the location respect to the grounding line and on the basis of geomorphological constrain (i.e. edges of glacial trough and LGM morain dated at 11.2 ± 0.9 kyr - Oberholzer et al., 2003 -).

The geological cross section has been then transposed to engineering-geological cross section, defined on the basis of litotechnical and geomechanical features, by the merging in engineering geological units, characterised by analogous response to thermal and mechanical stresses.

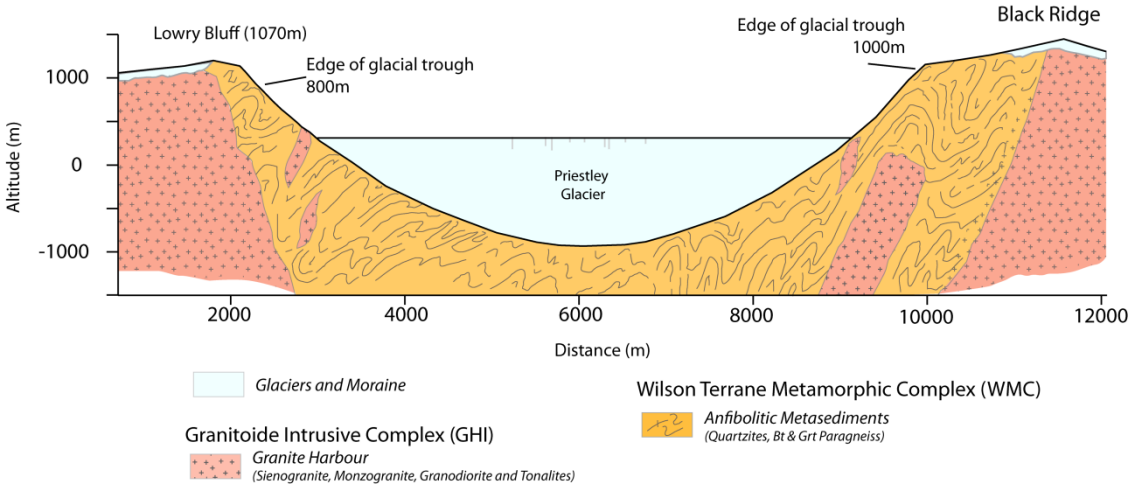

Fig. 30 - Geological cross section of the Priestley glacier valley. Parabolic profile of glacial trough is derived by geomorphic quantitative analysis and BEDMAP2 bedrock elevations data.

5.2.3. *Laboratory characterisation of Priestley valley rocks*

With the intention of constrain the geomechanical parameters of rocks, prerequisites of stress-strain and thermal numerical modelling, a complete physical and mechanical characterisation has been achieved on the lithologies outcropping in the study area.

The thermal and mechanical characterisation has been performed at the Rock Deformation Lab, facility of the Institut de Physique du Globe (IPGS) of the University of Strasbourg, and at the Petrology laboratory of the "Roma Tre" University of Rome.

Laboratory physical and mechanical characterization has been achieved on a rock sample collected in a previous Antarctic expedition and stored at the rock repository of the National Museum of Antarctic (MNA) in Siena, Italy. The sample was directly cored at the IPGS laboratory (Fig. 31). All the physical properties of the cored specimens, including density, porosity, permeability and elastic wave velocity were investigated.

Fig. 31 - Antarctic Rock samples as provided by MNA (left) and cored laboratory specimens (right) at the IPGS laboratory.

The laboratory mechanical characterisation consisted in a suite of uniaxial compressive strength (UCS) tests on cylindrical rock samples with diameter D=20 mm and aspect ratio ≥ 2.

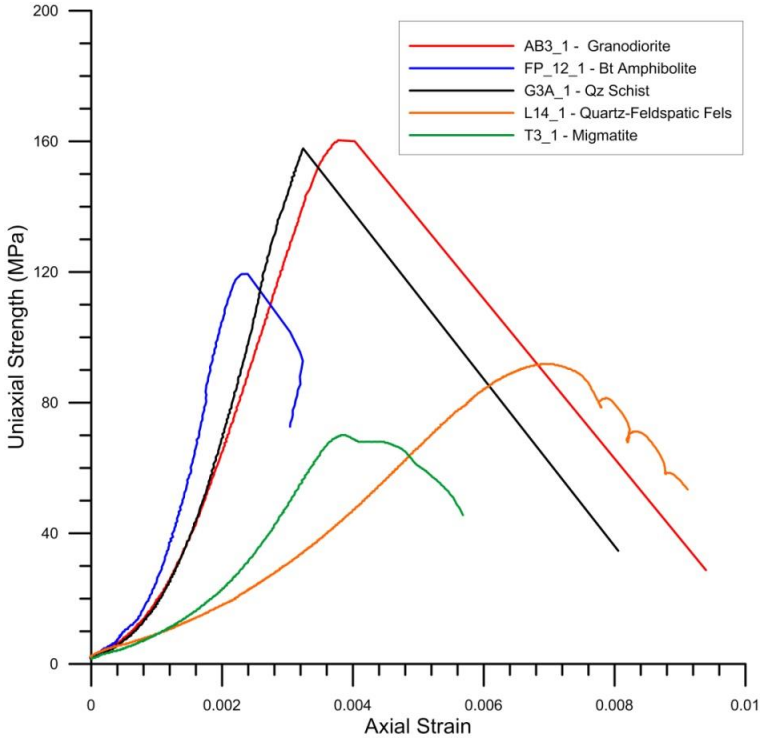

Fig. 32 - Example of the UCS vs Axial Strain curves derived by compression of selected lithologies.

Due to high strength of the tested intrusive and metamorphic rocks characterising the bedrock of the Priestley glacier valley and the size limitation of rock samples (Fig. 31), considering the maximum admissible strength and stiffness of the triaxial device at IPGS, compressive tests at controlled confining pressures have not been feasible. All the uniaxial tests were conducted at room-temperature.

The derived curves have been used to define of maximum uniaxial strength and stiffness of the analysed lithologies. This characterisation represents the basic input for the attribution of mechanical parameters in the stress-strain numerical modelling phases. Other strength parameters required for numerical analysis (i.e. friction angles, cohesion, tension) have been obtained from by literature.

Because no geomechanical (i.e. fracture density) data was available by direct field investigation, the laboratory deformability data derived by UCS was scaled respect to the only confining pressure condition by the relation proposed by Arora et

al. (1987), without considering jointing conditions (see equivalent continuum approach in Chapter 4.2).

Thermal properties of rocks (i.e. specific heat) were derived by Differential Scanning Calorimetry (DSC) tests (Salari, 2017). These tests were conducted on a wide range of lithologies at the University of Rome "Roma Tre", calibrating the measures on a standard Sapphire crystal.

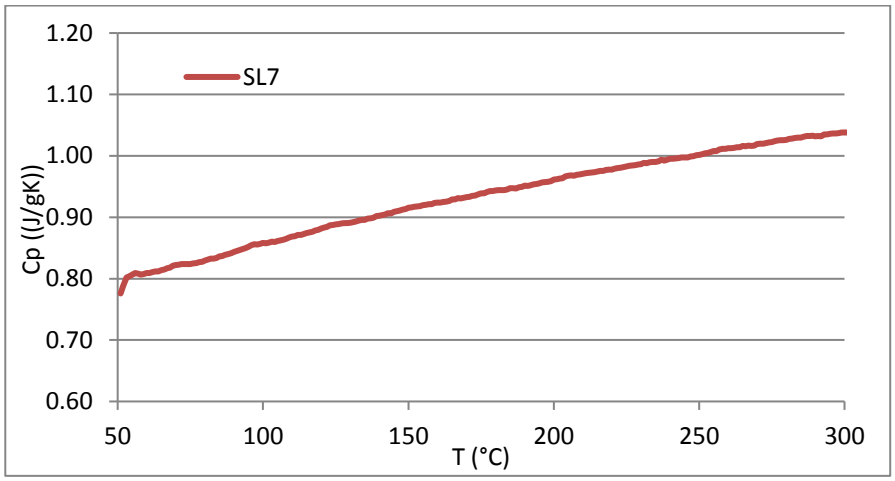

Fig. 33 - Example of calorimetric test performed on Schist samples (SL7), after Salari (2017).

Because no thermal conductivity test could be executed, conductivity values (κ) were derived starting from experimental specific heat (C_P) and density (ρ), assuming a reference thermal diffusivity (K) according to the following equation:

$$\kappa = K\rho C_p \qquad Eq.\ 20$$

Thermal, physical and mechanical parameters of glaciers, as well as pressure-temperature melting conditions, were obtained from by literature (Petrenko and Whitworth, 1991; Wagner et al., 1994; Bader et al., 1964).

The dependency of κ and C_P on the absolute Temperature and the thermal conductivity on density were computed and taken into account by the application of Paterson (1994) and Van Dusen (1929) relations.

5.2.4. Conceptual and evolutionary model of the Priestley glacier system

The definition of conceptual and evolutionary models of the glacier system represents an essential step for the estimation of the effect of thermal perturbation in gravitational slope- and glacial- dynamics.

With the purpose to evaluate the role of thermal fluxes as well as ice mass fluctuations on the slope deformation and physical and kinematic state of the glacier, the dimensioning of heat perturbations and the reconstruction of glacial thickness in different phases of the glacial history is required.

Starting from the hypothesis of crustal underplating or formation of high-temperature intrusive bodies near the mantle-crust boundary (Perinelli et al., 2017), a working hypothesis has been proposed.

The textural evidence in clinopyroxenes of some cumulate xenoliths suggests that infiltration of hot primary magmas in the uppermost part of the mantle led to the storage of a hot and hydrous primary lasted long enough to create a local "wet and hot deep zone" (Perinelli et al., 2017) reflected in high heat fluxes (left part of Fig. 34). The initiation of dominant volcanism after 14 Ma (Armienti and Baroni, 1999) and transition toward the crystallisation of hot hydrous primary magma (right of Fig. 34) would have been reflected in a decrease (rapid or slow) of total heat fluxes, which could have been responsible of the observed variation in melting condition at the base of the glacier (Pollard et al., 2005; Hansen and Greve, 1996; Takeda et al., 2002).

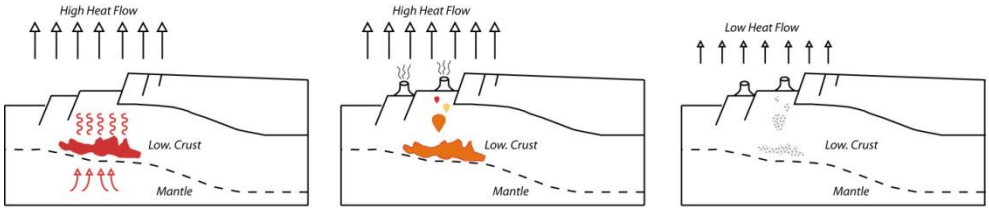

Fig. 34 - Conceptual model of deep-source heating in the Northern Victoria Land.

Moving from this working hypothesis, the effect of heat flux variation in the heat propagation in the upper crust has been investigated through 1D thermal modelling by parametric approach of analysis. The derived results have then been applied as a thermal boundary condition of the surficial slope system, which was modelled under 2D conditions reproducing ice mass and bedrock geometries.

In order to constrain past glacial thickness attributable to different phases of glacial history and to infer the effects of local thermal anomalies in the enhancement of slope deformation, a morpho-evolutionary model of the Priestley glacier system in the last 1.2 Ma has been reconstructed in the framework of PNRA research group activity (RU1-Pisa) of the PdR 2013/B2.01 ("How climate changes and crustal thermo-mechanic variations interact in driving East Antarctic glacial evolution since late Cenozoic?"). The reconstruction of former glacial topography and glacial thickness has been defined through the analysis of erosional trimlines and glacial deposits along longitudinal profiles of tributary or outlet glaciers.

The timing of past ice sheet elevation derived by trimlines and drift limits has been reconstructed by geomorphic analysis and radionuclide (SED) dating. Surface Exposure Dating (SED) is a geochronological technique for estimating the length of the time that a rock has been exposed. This technique was crucial to better define the chronology of Antarctic ice volume variations and to reconstruct landscape evolution and the main steps of glacial history. Combined studies on multiple cosmogenic nuclides also allowed to differentiate surfaces that experienced continuous or complex exposure history.

Available dates supplied so far (Oberholtzer et al 2003, 2008; Di Nicola et al 2009, 2012; Strasky et al., 2009) have been used for the timing of major ice advance or

retreat phases. The morpho-evolutionary model here presented also made use of the undated samples collected during past PNRA expedition and recently processed (Baroni et al., in progress).

The most recent phase (25-8 ka) is constrained by a glacial morain located at elevation of 950 m a.s.l., dated by SED in Oberholzer et al. (2003) and referred to a maximum ice stationing at 11.2 ± 0.9 kyr. A further phase during Late Pleistocene (before 50ka) is identified on Mt. Keynath and Mt. Kring in David Glacier (42 ±10.4 – 40 ±2.2 kyr and 33.9±2.8 yr - sample K5 Oberholzer et al., 2003 -). In this phase an increase of thickness of 380 m above the actual level is unmistakable on Mt. Keynath, similar to that observed at Northern Foothills. This phase is also confirmed by samples at Ricker Hills (RH06/01) where exposure ages of 70±8 kyr [Ne] and 49±3 kyr [Be] were derived. The same elevation of LGM has been applied at this phase.

An older phase, prior 140 ka, was derived by exposure ages at Northern Foothills with a continuous exposure history (BROW8 128±12 kyr - 146±kyr and 147±33, Oberholzer et al., 2003), and at Vantage Hills (164±15kyr - Baroni et al., in progress -). A thickness of ~ 600 m can be assumed at this phase, however, around the location of the reconstructed cross section, the advance and raise of ice masses cannot exceed 50 m above Last Glacial Maximum (LGM).

Moving back in time, a phase older than 310 ka was fixed by SED at minimum age of 305±16 [Be] - 309±32 [Ne] kyr. This phase is also confirmed also by SequenceHills06 samples (294 ±18.4ka - Baroni et al., in progress -). and it was attested at elevation comparable to the following 140 ka stage. Same elevation can be assigned to a previous stage dated at 500ka (Di Nicola et al., 2009). A further vigorous phase leaving evidences of landforms and sediments was dated around 1.4 Ma, at Ricker Hills (Strasky et al., 2009) and Vantage Hills (Baroni et al., in progress).

The activation of Mc Murco Volcanic Field (2.96 Ma, Armienti et al., 1991) and Mt. Merlbourne (2 Ma, Kyle, 1990, Giordano et al., 2012) precedes the last modelled glacial phase.

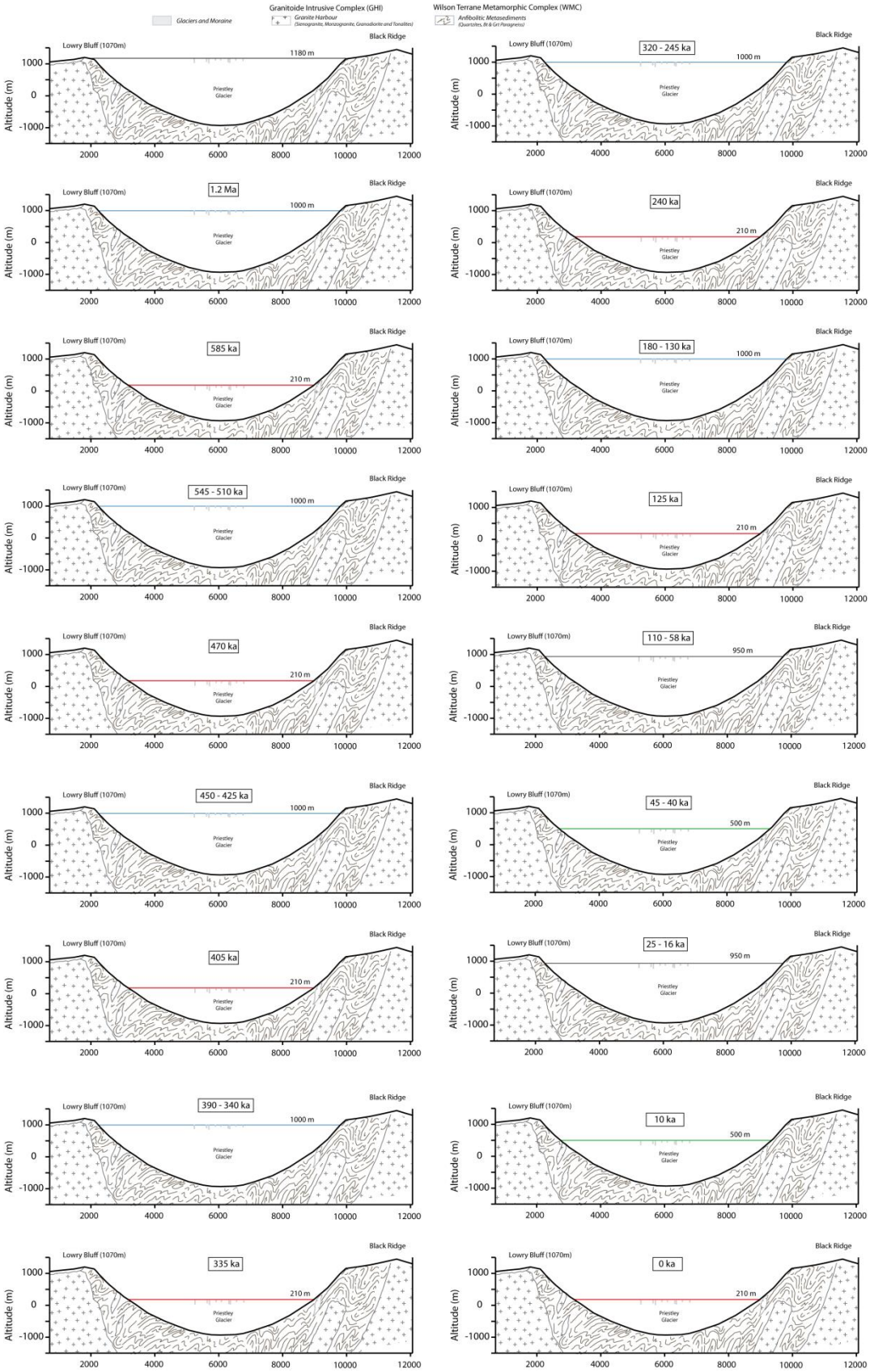

Fig. 35 - Morpo-evolutionary model of the Priestley glacier valley defined according to SED dating (Baroni et al., in progress).

Surface exposure dates at the top of Mt. Keynath or Chisolm Hills also evidenced areas that did not undergo any glacial erosion from several Ma (Oberholzer et al., 2008, 2003). Such evidence confirm that the ice-sheet goes through a long lasting stability (6 ± 2 Myr -Di Nicola et al., 2012-), and the related glaciers experienced an increase in thickness limited upward by the sampling elevation.

The derived main stages of a morpo-evolutionary model, supported by temperature variation derived by EPICA-DOME C (EPICA community members, 2004), has been summarised in (Fig. 35).

By means of the defined model, starting from two different thermal (i.e. heat flux) "hypothesis", distinct evolutionary sequences have been analysed, varying thermal boundary conditions and keeping invariant the morphological evolution of the glacial system, analytically expressed through timing and elevation of glacial stages.

Once defined temporal, geomorphological and glaciological constrains, as well as hypothesis of thermal perturbations, specific numerical modelling solutions were identified in relation to the peculiarity of the case study and the physics involved.

6. Numerical modelling solutions

In this chapter the numerical solutions adopted for modelling the effects of conductive and convective heat transfer processes in the gravitational deformations process will be discussed, detailing the modelling performed in the case studies of Mt. Nuovo and Priestley glacial valley.

The resolving schemes and the numerical assumptions adopted to combine multiple physical models acting on slope deformation processes at shallow or deep scales (e.g. heating by deep geothermal or hydrothermal fields) will be examined.

All the step performed in the definition of multi-physical approach, from the conceptual phase (Fig. 4, Fig. 6) to the full description of thermo-mechanical model of the slope will be examined. The peculiar features of the two case studies and the boundary conditions applied to the slope systems, intended as the set of physical and mechanical characteristics and the internal or external forcing acting on a slope, are also reported.

Two sub-chapter will detail the numerical modelling phases (Fig. 4) of each case study, beginning from the conceptual phase, preliminary to the multi-physical modelling approach (Fig. 6), analysing the solutions adopted in the modelling to reproduce physical interactions at slope scales in the long-term temporal evolution of slope deformations. To this aim, the use of different codes in coupled or uncoupled schemes will be discussed depending on the nature and typology of the physical interactions and stationarity/transiency of the studied processes.

6.1. Ischia case study

First step in the definition of a comprehensive numerical model representative of the multiple physics acting on the Mt. Nuovo slope was the definition of the thermal model of the NW sector of the Ischia hydrothermal system. Because the hydrothermal circulation is driven by convective heat and fluid transfer process the thermal model was supported by the computation of a hydrodynamic model of the deep multilayer geothermal system (see Chapter 5.1.1).

The model of the deep hydrothermal system so defined, has been then transferred as input boundary condition to a second shallower slope-scale model, in which the gravitational slope deformation take place. With the support of 2D mechanical model of the Mt. Nuovo slope a 2D thermo-mechanical model has been constructed assuming a conductive heat-transfer and a time-dependant rock mass rheology.

6.1.1. 2D Thermal modelling of the Ischia hydrothermal system

In order to define the thermal model of the Ischia hydrothermal system, basing on geological and geophysical data used by Carlino et al. (2014) to define the conceptual model of the geothermal reservoir, a 2D thermo-fluid dynamic simulation was performed. The modelling was performed using COMSOL® code on a closed domain 3000 m wide extended in depth from the sea level up to -2000 m. The used code lends itself well to the simulation of modelling heat and fluid flow in porous media allowing the consideration of discrete fracture network, free flow in channels, and complex fluid and heat transfer physics in single and two-phase flow.

The three layers of 3D model defined by Carlino et al. (2014) was reproduced in a 2D section, where geometries and stratigraphic settings were preserved. A multilayer

aquifer was thus defined, fixing the hydrodynamic parameters of a reservoir located at depth ranging between 150 and 800 m u.s.l. (Fig. 36) (Carlino et al., 2014).

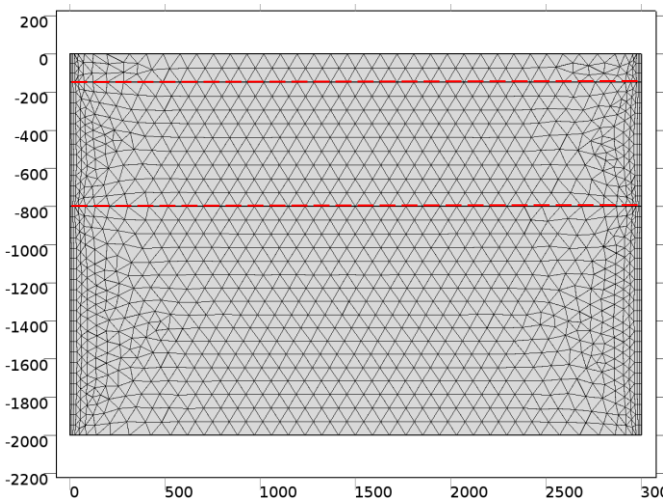

Fig. 36 - Mesh generated by COMSOL for the 2D numerical model of Ischia hydrothermal deep system.

A numerical analysis was performed, assuming a stationary, conductive geothermal heat flux combined with a convective fluid flow in porous medium, assuming the heat transfer in a solid porous media and a Brinkmann flow model, extension of Darcy's law, to simulate the flow along interfaces and high porosity medium. Because of the strict mutual interaction in the physics driving convective fluid circulation, a fully coupled solution was adopted.

The 2D thermo-fluid model was validated by matching experimental thermal data obtained from deep wells (AGIP, 1987), i.e. verifying the coherence of the numerical thermal output respect with the path of measured temperature and the amount of discharged heat flux.

The numerical best-fitting was achieved by means of parametric analysis performed on reservoir permeability and temperature at the base of the model. Temperature field in depth was calculated fixing appropriate Dirichlet and Neumann thermal and fluid boundary conditions, summarised as follows:

- ✓ fixed temperature of 120 °C at top of the model (0 m a.s.l.), derived by the Pc46-47-48 wells (Fig. 10) considering the borehole elevation;
- ✓ variable temperature at base of the model, ranging from 300 to 600 °C. Temperature equals to 400 °C can be derived extrapolating at depth the pure conductive gradient of the third branch of the well's temperature vs. depth profiles;
- ✓ linear thermal gradient at lateral boundary to simulate an infinite thermal lateral extension;
- ✓ hydrostatic pressure initial condition (Di Napoli et al., 2009; Celico, 1999);
- ✓ wall conditions (i.e. no flow) on lateral boundary.

According to Castaldo et al. (2017), under the statement of hydrostatic conditions within the hydrothermal system, we assumed a deep single-phase fluid convection controlling the large-scale thermal structure.

The free-convection problem was solved introducing a Boussinesq buoyancy term to the Brinkman's momentum equation, and then linking the resulting fluid velocities to the Heat Transfer in Porous Media interface, thus accounting for the lifting force due to thermal expansion of fluid (Hossain and Wilson, 2002).

The Boussinesq buoyancy term that appears on the right-hand-side of the momentum equation accounting for the lifting force due to thermal expansion is directly proportional to the fluid density (ρ), gravitational acceleration (g), thermal expansion coefficient (β), and a temperature difference:

$$\rho g \beta (T - Tc) \qquad Eq.\ 21$$

where T and Tc are respectively the local and initial temperature derived from heat transfer solution.

The steady-state solution of fully coupled heat transfer and fluid flow in porous media highlights a well-developed convection in the shallow reservoir, with four convective cells developed at depth between 100 m and 900 m u.s.l. (Fig. 37), in which fluids moves upwards with maximum velocity of about $2 \cdot 10^{-9}$ m/s (approximately 0.1 m/yr), capped by an impermeable layer (Fig. 37).

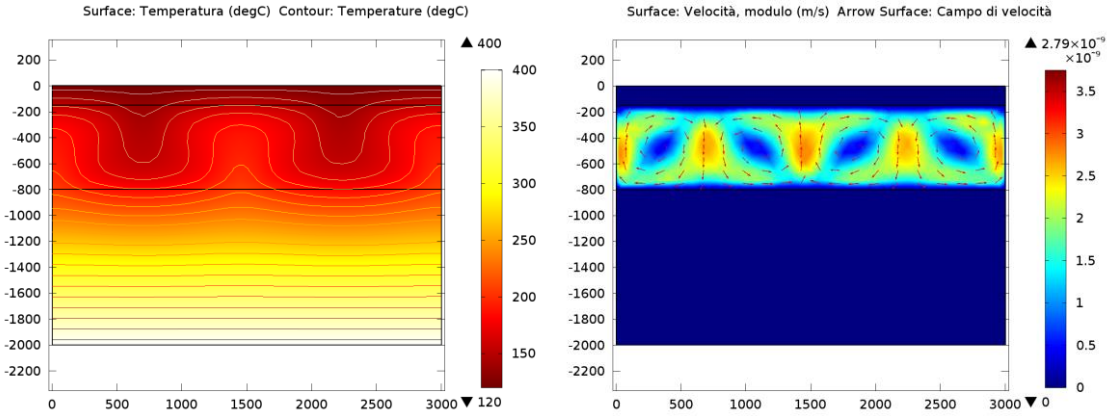

Fig. 37 - Temperature (left) and fluid velocity (right) fields derived by deep hydrothermal model.

The obtained volume lifting force (i.e. buoyancy term) deriving by thermal expansion effects shows a maximum contribution in the lower part of the model, where maximum temperature differences occurred (blue arrows in Fig. 38). Despite this forces distribution, the fluid convective circulation (expressed by red arrows) is strictly controlled by the rock mass permeability.

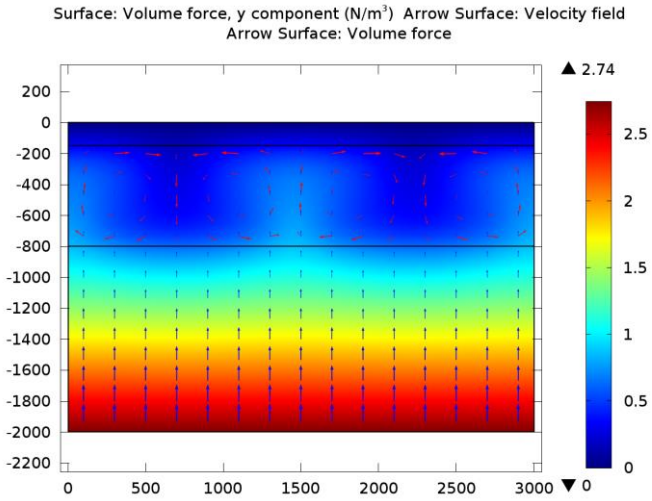

Fig. 38 - Volume forces field due to fluid thermal expansion (blue arrows). Red arrows show the fluid directivity and velocity by graduated symbols.

Temperature vs. depth logs for different permeability value (right on Fig. 39) clearly demonstrate this effect, showing the onset of convection from permeability $1E^{-11}$ m^2, which appears to be orders of magnitude lower than ones derived by Carlino et al. (2014) and Castaldo et al. (2017). This value is not far from gas permeability values of fractured porous MEGT tested by Marmoni et al. (2017a, 2017b). In addition, size-scaling dependency of rock mass permeability should be considered.

Temperature vs. depth distribution shows the effect of rise in deep thermal perturbations, expressed by temperature rise at the basal boundary of the model (shown on x-axis of left graph on Fig. 39). Fixing the temperature value at top of the model (constrained by deep-wells data), an ascend in deep temperatures reflects in a raise of conductive gradient in the less permeable layer, and a temperature increase in the reservoir (left of Fig. 39).

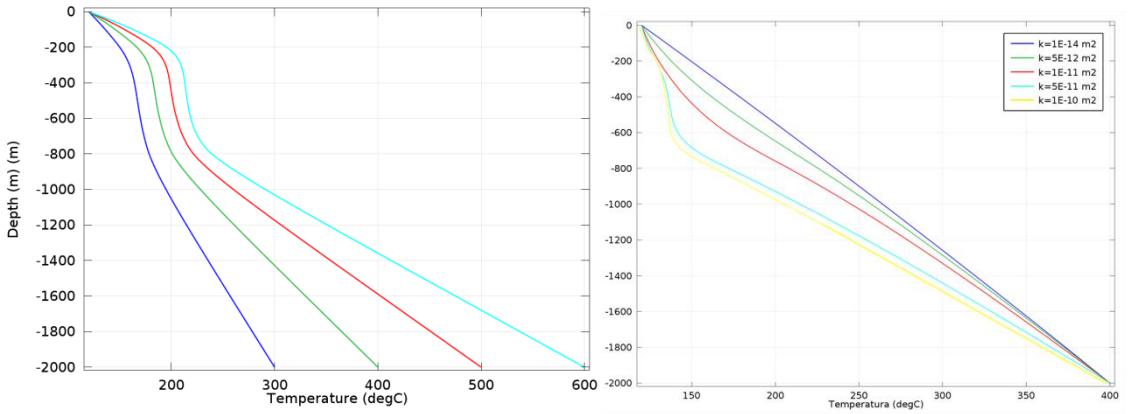

Fig. 39 - Temperature vs. depth log respect boundary temperature conditions (left) and reservoir permeability (right).

The derived gradient and temperatures allows the validation of numerical output, which has been realised verifying the coherence of the numerical thermal output respect to the wells temperature vs. depth profiles. The validation of the model by parametric analysis will be discussed in the following paragraphs, after the complete definition of a combination of deep- and slope-models.

The defined deep circulation within geothermal reservoir can be assumed as representative of the Ischia south-western sector, where deep wells were drilled. No

geophysical or direct information are available for the north-western sector. Because of lacks interpretation about the lateral extension of hydrothermal reservoir, the model was transposed below the Mt. Nuovo area. Hence, the hydrothermal deep model was jointed to slope-scale model, derived by retro-deforming the main discontinuities and the dislodged blocks to restore a 32-28 ka scenario (predating the onset of gravitational slope deformation).

In order to assess the role of structural elements in the development and characteristics of thermal convection, fault zones were implemented, by introducing linear permeable zones. The permeability of fault zones and breccias layers opening the member of which MEGT is composed, was assumed an order of magnitude higher than the surrounding rocks. Physical parameters of MEGT (density, porosity, permeability), as much as thermal conductivities and heat capacities, needed in the formulation of heat and fluid transfer equations were derived by laboratory investigations.

A Mean annual temperature of 25 °C and an open frontier for fluid flow was assumed as boundary conditions at the slope surface. A physics controlled triangular fine mesh was applied by COMSOL embedded meshing code. The resolution of the mesh was defined ensuring the discretisation of finer elements by at least two cells.

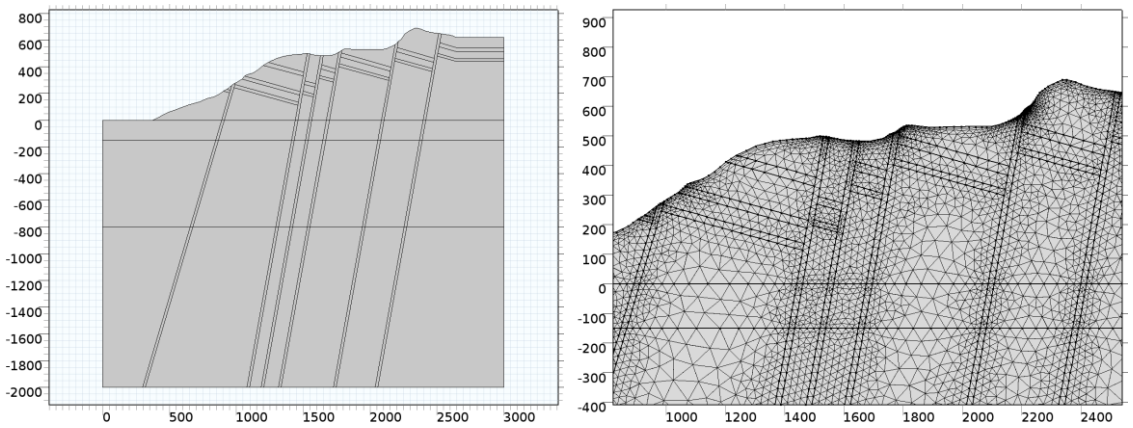

Fig. 40 - Domains defined by the combination of deep- and slope-model (left). Triangular fine mesh applied by COMSOL meshing code. Persistent permeable layer (sub-vertical faults) was implemented in the model.

The numerical modelling extended to the slope system of Mt. Nuovo, highlight the well-developed steady-state convection in the reservoir, allowing to define the thermo-baric conditions at shallower levels within the slope.

The contour plot of temperature distribution shows the influence of temperature boundary conditions on geometries of hydrothermal circulation (Fig. 41), underlying the clear role of tectonic elements in the ascent of fluids from the deep hydrothermal system (Fig. 42).

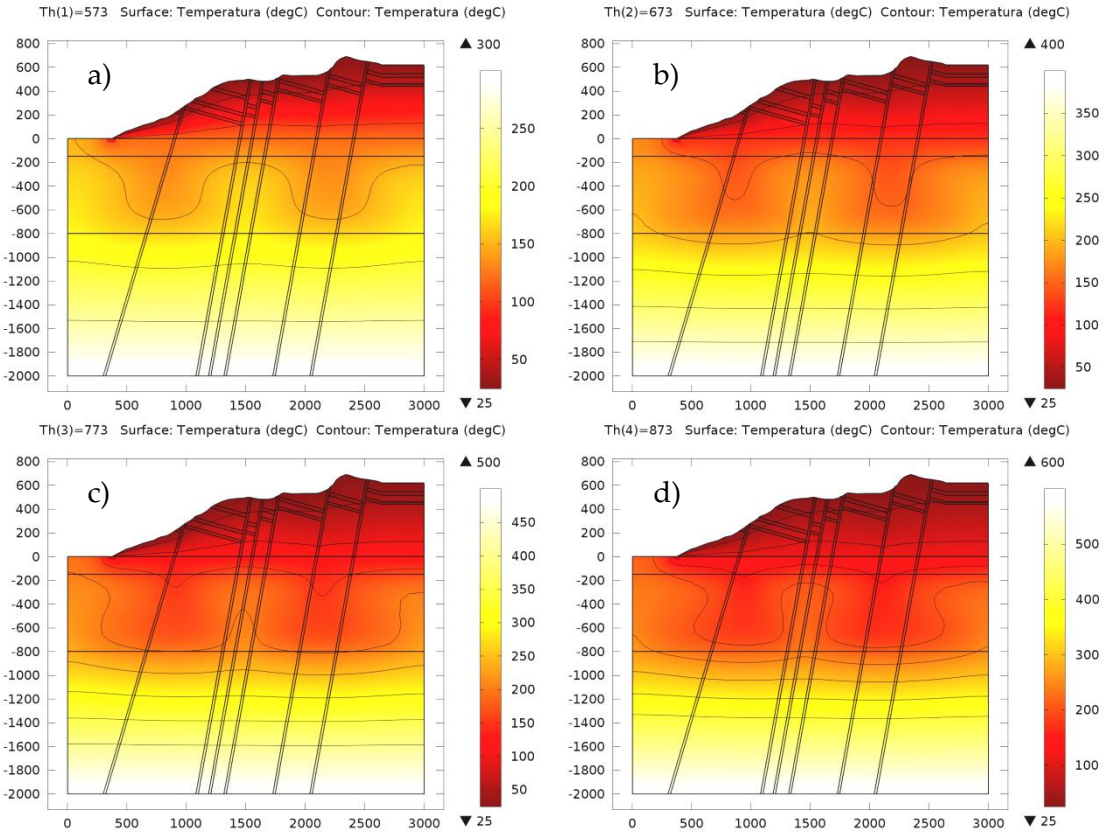

Fig. 41 - Temperature fields derived under bottom temperature of 300 (a), 400 (b), 500 (c), and 600 °C (d).

The fluid flow model results reported on Fig. 42 show the effect of thermal perturbation on fluid velocity, which doubles as result of a rise in temperature at the base of the model from 300 °C (a) to 600 °C (d).

The fluid pathways confirm the hypothesis of strict relation to both the stratigraphic and structural settings advanced by Della Seta et al. (2015) and Chiodini et al. (2004) (Fig. 43).

The hydrothermal fluids rise along the permeable fault zone, degassing directly at surficial level in correspondence of fault line outcrop, or moving laterally within permeable breccias levels, feeding the fluid emissions at fumarolic fields (Fig. 43). The location of major fluid outlet, located in correspondence of the lithic breccias layer, appear consistent with elevation of the major hydrothermal manifestations (Fig. 43).

Preferential paths for fluid rising may also have played a dual role in controlling the pore-pressure distribution and localising hydrothermal chemical-alteration in the rock mass.

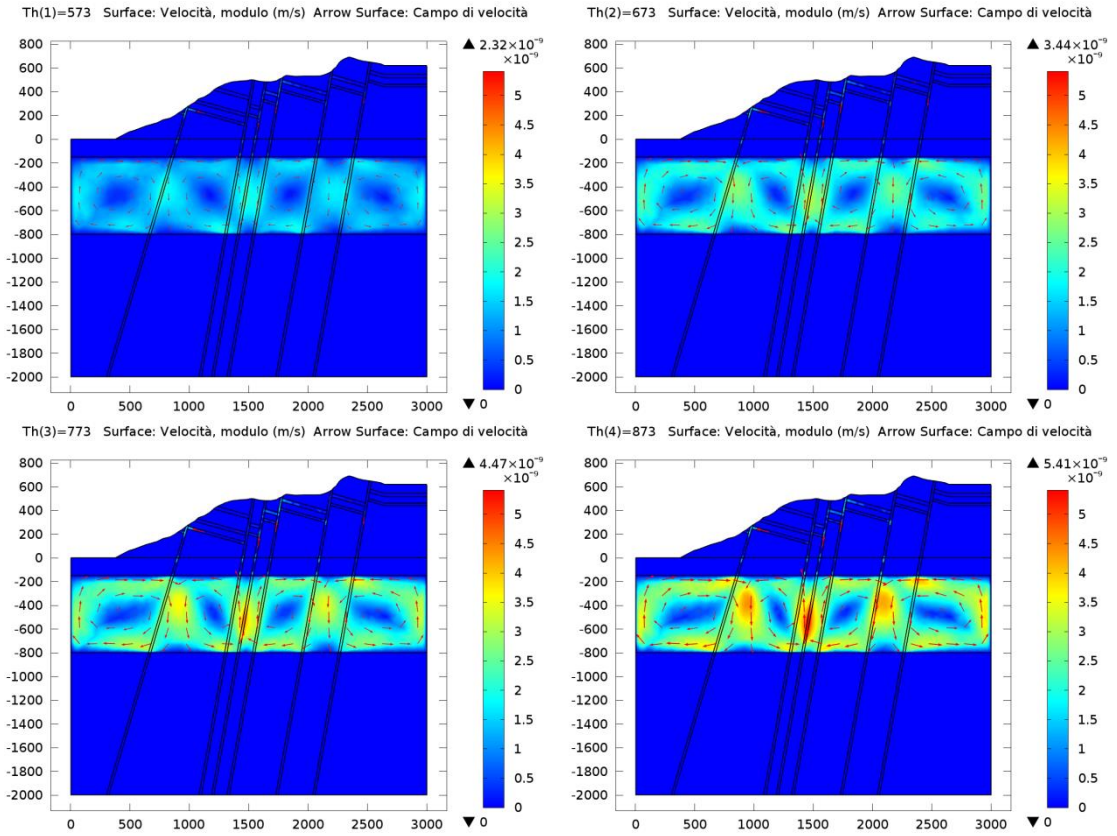

Fig. 42 - Fluid velocity distribution at increased boundary temperature conditions.

The thermo-fluid dynamic solution derived assuming bottom temperature of 400 °C (the one obtained extrapolating a pure conductive gradient at depth) fits the temperature log-profile measured in deep borehole, and shows the thermal-baric field and the fluid velocity distribution within the Mt. Nuovo slope.

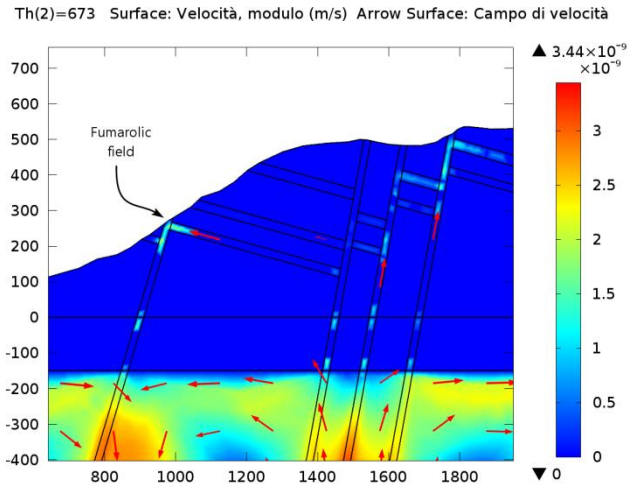

Fig. 43 - Detail of fluid migration along permeable domain of numerical model (i.e. faults and lithic breccias layers) expressed by red arrows.

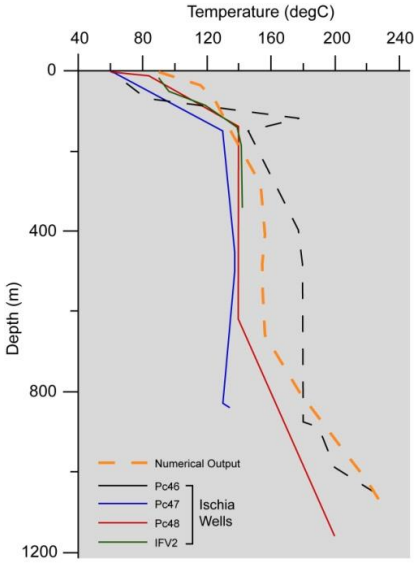

Fig. 44 - Comparison of temperature vs. depth resulting from Ischia deep wells with the output of performed simulation.

The modelling was then improved to take into account the vapour phase transition at shallower depth, where conductive layer guides the heat transfer toward the surface. The surficial slope model was conditioned imposing, in a cascade sequence of models, the thermal output of the deep model as boundary condition of the surficial one. Physical and thermal parameters of both water and vapour were defined, imposing relative gas permeability curves and fixing fluid saturation conditions at the top (100% Vapour) and bottom (100% Water) boundaries of the model.

The fluid pressure-density distribution highlights the presence of high pressure in the foot of slope, where low lithostatic load exist (Fig. 45).

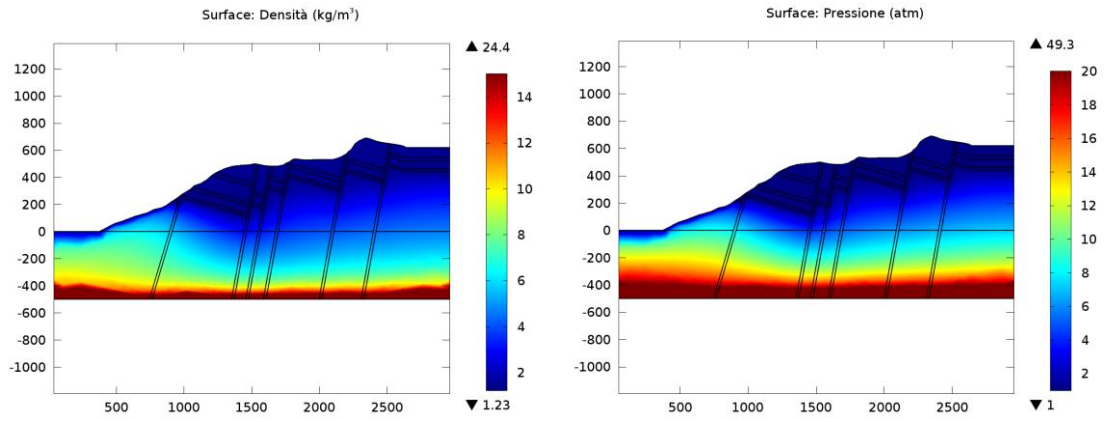

Fig. 45 - Fluid density (left) and fluid pressure (right) deriving by multiphase flow modelling.

The output heat flux confirms the role of breccia layers in the lateral migration of heat and vapour moisture (Fig. 46), already established by the mono-phase model. The vertical (y) component of the heat flux (Fig. 46) shows a maximum value of 450-500 mW/m² in the foot of slope, values in good agreement with data reported in literature for the coastal plain of Forio town. In the horizontal component the maximum value of heat flux is located in correspondence of the outcrop of breccia layers, where one of the fumarolic fields exists (Fig. 46).

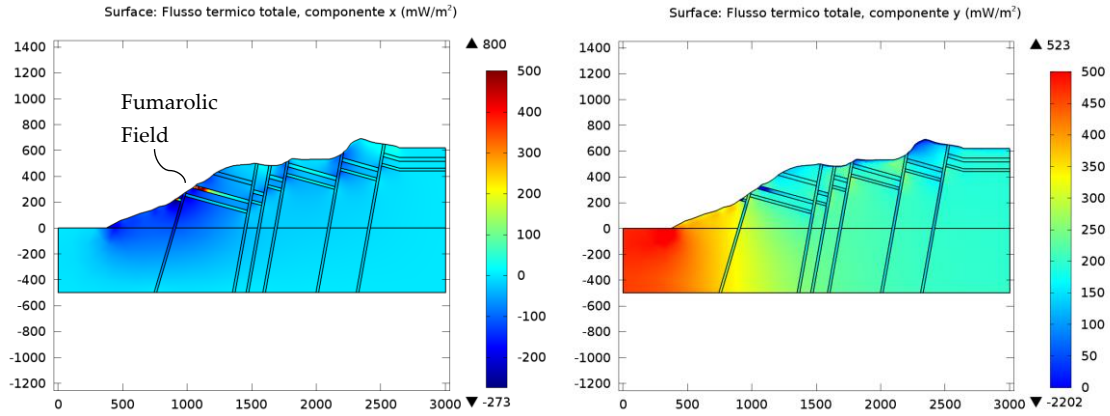

Fig. 46 - Horizontal (left) and vertical (right) heat flux component derived by multiphase flow modelling.

Because in both mono- and multi-phase flow model a fluid thermal non-equilibrium was not considered, the surficial temperatures derived by monitoring of gas emissions at fumaroles were not considered for the validation of numerical results.

6.1.2. 2D Elasto-plastic modelling of Mt. Nuovo slope

Parallel to the validation of the model of the deep hydrothermal system a 2D mechanical model of the Mt. Nuovo slope was defined under elasto-plastic and visco-plastic rheological behaviours.

The 2D mechanical model of the Mt. Nuovo slope has been defined using the FDM code FLAC® 7.0 (Itasca Cons.), software for advanced geotechnical analysis of continuum in rocks and soils, which allows the definition of numerical model able to consider groundwater and thermal flows. Given the size scale (i.e. entire slope) and the adopted equivalent continuum approach, the code lends itself for the purpose of the research.

The numerical analysis was based on the retro-deformed geomechanical cross-section of Mt. Nuovo slope (Fig. 28), representative of the geological setting existing at the end of resurgence (32-28 ka). This section was transferred to a numerical domain consisting in a 250 x 200 grid with a square mesh resolution of 5 m. The numerical domain was laterally extended by about 40 m at both left and right sides of the model to avoid boundary effects. A 500-m thick base representing the shallow part of the hydrothermal system was implemented in the numerical domain to extend the model to the deep convective zone and take into account heat transfer from the deeper levels. In this elasto-plastic model the role of thermal perturbations was initially not considered.

Because an infinite half-space was assumed appropriate boundary conditions were fixed. In particular, horizontal displacements were avoided along the lateral boundaries, while both vertical and horizontal displacements at the base of the numerical domain were not allowed. An initial static equilibrium was reached under perfectly-elastic and elasto-plastic conditions by applying the gravitational acceleration.

The zoning and parameterisation of the model has been addressed according to the defined engineering geological cross section and the laboratory mechanical investigations conducted in this PhD thesis and summarised in Chapter 5.1.3. The deformability parameters were scaled in virtue of pressure levels and jointing conditions according to Sridevi and Sitharam (2000) approach.

Strength parameters were derived by Mohr circles construction for both Upper (UGT) and Lower (LGT) Mt. Epomeo Green Tuff (Fig. 47, Fig. 48). The deformability parameters (i.e Bulk and Shear modulus) were distinguished in discrete pressure levels of 1,2 and 5 MPa. The derived values at increasing stresses, were attributed by automatic FISH scripting, after a check of the magnitude of confining pressures. The deep basement was assumed as elastic medium. A summary of the adopted strength and deformability parameters in numerical modelling are reported as Annexed Table (Annexed Table 2).

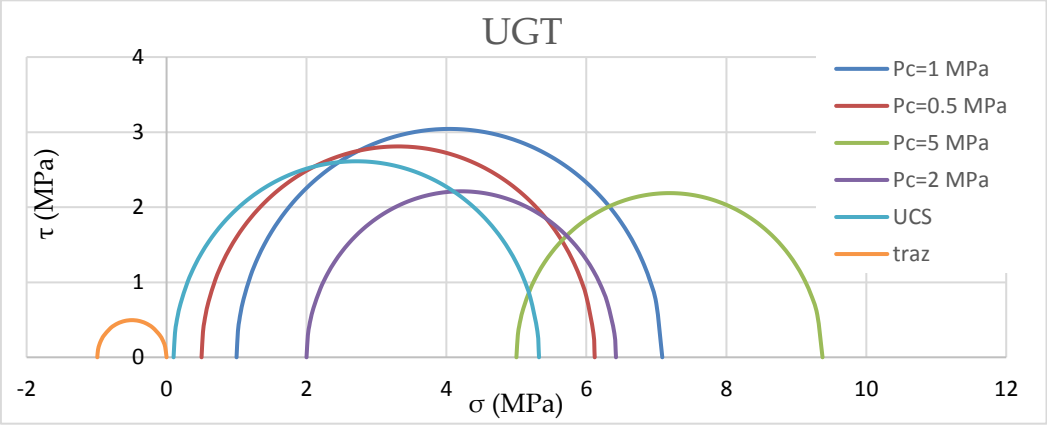

Fig. 47 - Mohr circles derive by a suite of mechanical tests on UGT.

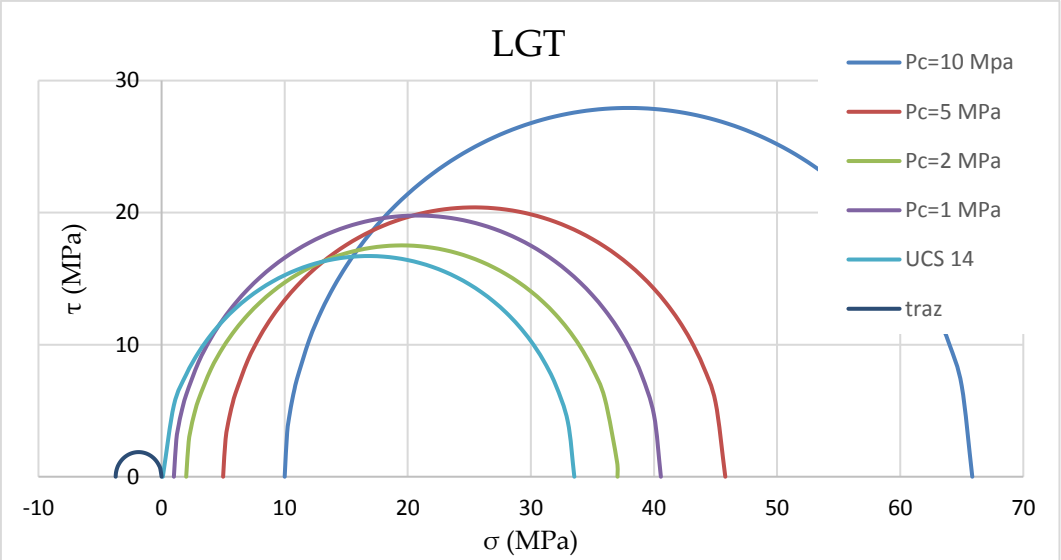

Fig. 48 - Mohr circles derive by a suite of mechanical tests on LGT.

Horizontal and vertical displacements, as well as stress distribution were monitored along five equally spaced vertical (Fig. 49), to derive stress/strain fields distribution under the sole effect of lithostatic load (Fig. 50). Lithostatic pressure within in the shallow part of the slope grow up to 5 MPa at depth of about 250-300 m, where ongoing gravitational slope deformation take place.

In the numerical modelling no morphological variations or sequential stages was assumed (Fig. 3) after the end of calderic resurgence, therefore invariant geometry was kept for the whole simulation, which will configures as a mono-stage modelling.

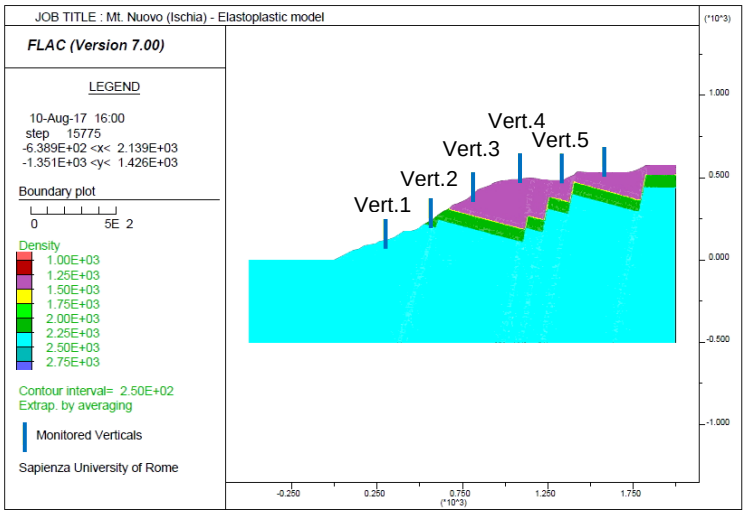

Fig. 49 - Density plot of the reconstructed geological cross section. Location of monitored verticals is also shown.

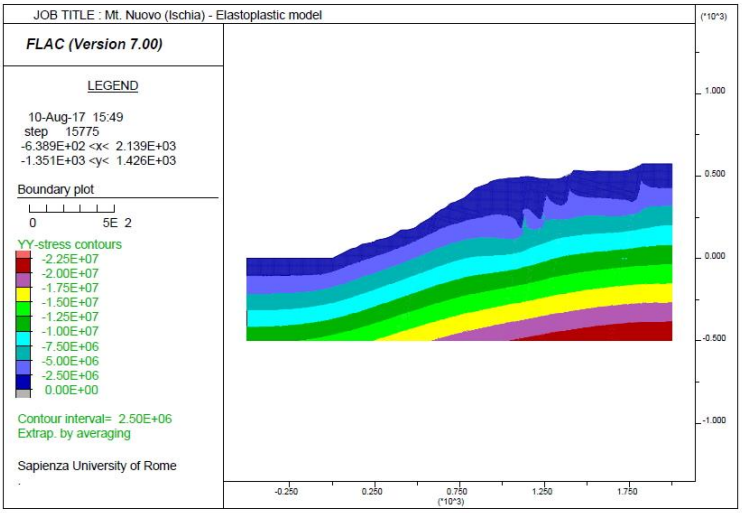

Fig. 50 - Lithostatic load at elasto-plastic equilibrium conditions under gravitational acceleration. Stress in Pa.

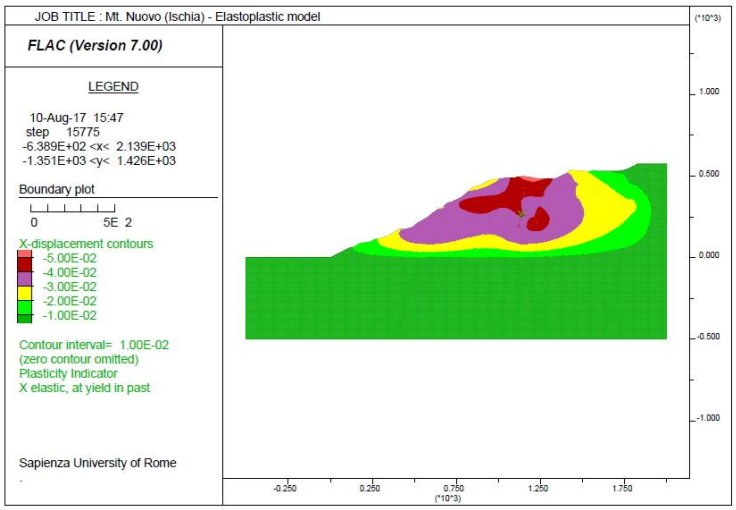

Fig. 51 - Horizontal displacement (X-disp) contours under elasto-plastic gravitational equilibrium.

The horizontal displacements output negligible deformations with displacement enclosed within few centimetres. The displacement contours pointed out an incipient deformation located in correspondence of Mt. Nuovo, downslope to the Falanga plain. Nevertheless, no plasticity conditions occurred and elasto-plastic deformations are not sufficient to justify the observed deformative process.

6.1.3. 2D Visco-plastic modelling

With the aim to back-analyse the Mt. Nuovo slope deformation and infer the role of Mass Rock Creep (Chigira, 1992) in the magnitude of slope-scale gravitational deformation, a pure time-dependent simulation was performed in creep-mode configuration by assuming a visco-plastic rheological model, according to a Burger constitutive law.

A time interval of 30 ka has been simulated, period assumed as the maximum time elapsed from the onset of calderic resurgence, dated 28-32 ka (Tibaldi and Vezzoli, 2004). The initial time of numerical simulation (t_0) thus correspond to different ages in the volcano-tectonic history of Mt. Nuovo as function of the assumed velocity of resurgence.

Time-dependent numerical solutions were obtained assuming a time-step duration of 15Ms (almost equal to 6 months). Deformability of rock mass was updated every 5ka to encompass the effect of stress field variation, by the introduction of apposite FISH script.

For this purpose, a sensitivity analysis was performed on both Kelvin and Maxwell viscosity values, trying to back-analyse the slope-scale process. The sensitivity analysis was performed in a range of viscosity between 10^{16} and 10^{19} Pa·s.

Because of lacks deformative data deriving by interferometry or direct geotechnical survey, the validation criteria of the back-analysis were assumed on the basis of the kinematics of the process by means of comparison between numerical results and field geological and stratimetric reconstruction. The validation of numerical output was based on the definition of Validation Index (Iv) given by the summing of partial coefficient based on: i) magnitude of horizontal displacements (X-disp) respect the stable bedrock, ii) elevation of the shear zone and iii) entity of rotational contribution of the mass movement. For each control points (i.e. Monitored vertical within the rock mass -Fig. 49-) a binary score was attributed. For every viscosity

hypothesis, the kinematic convergence score was given by the sum of three kinematic criterion totalised for each of the 5 monitoring verticals, as follows:

$$Iv_{(\eta)} = TF \cdot \sum_{i=1}^{5} C_{(\Delta x)_i} + C_{(h)_i} + C_{(\beta)_i} \quad Eq.\ 22$$

$$TF = \begin{cases} 0, & t_f > 5\ ka \\ 1, & t_f \leq 5\ ka \end{cases} \quad (age\ b.p.)$$

The kinematic admissibility has been then validated based on temporal criterion derived by the occurrence of tertiary slope failure, multiplying the sum of kinematic scores by a binary Temporal Factor (TF). Predated instability respect to the expected time to failure (t_f - ≤ 5ka -) nullify the Validation Index (Iv).

The analysis of kinematic consistency of the modelled slope deformation was performed along five monitoring verticals, at the final time-step of each modelling, proving the similarity of the numerical output respect target values. The target values were fixed considering the reconstructed geometries in the engineering-geological model, in the "locus of points" placed at the intersection between the monitoring verticals and the expected failure zone. At each target value an admissible error was attributed considering the numerical model resolution and the scale of field surveys.

Rotational contribution derived by numerical modelling was calculated at each nodal point by the definition of a rotation angle (β), trigonometrically defined by the arctan of the ratio between the modulus of the vector L (i.e. projection of the resulting nodal displacement on the bow of circumference enveloping the sliding surface) and the radius of the circumference passing through the node (Fig. 52). The rotation angles derived by means of this construction were compared with target expected rotations defined by the engineering geological model.

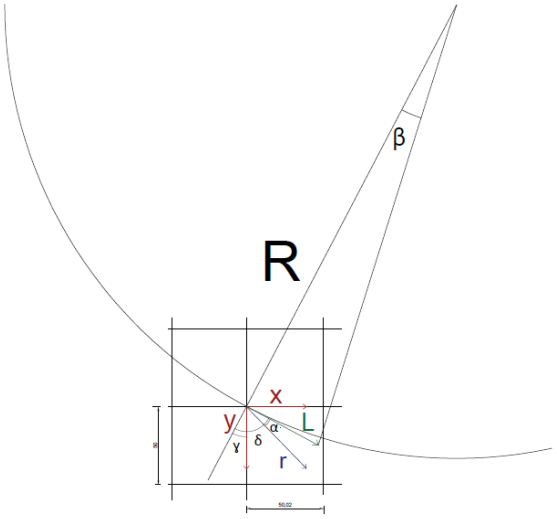

Fig. 52 - Geometric construction for the definition of nodal rotation angle (β) (Coletta, 2017).

The outputs of the sensitivity analysis performed to calibrate the rock mass viscosity show that the viscosity values of 10^{16} and 10^{19} Pa·s can be regarded as out of range end-member of the analysis. In the first case slope failure occurred after 2300 yrs since the end of calderic resurgence (i.e. start of creep time) (Fig. 53), verifying the kinematic criterion of elevation of shear zone (C_h) in only one case (Tab. 1). In the latter (Fig. 53), temporal occurrence of slope deformation was verified, while the kinematics of gravitational process under any circumstances do not fit the reconstructed geometries (Tab. 1).

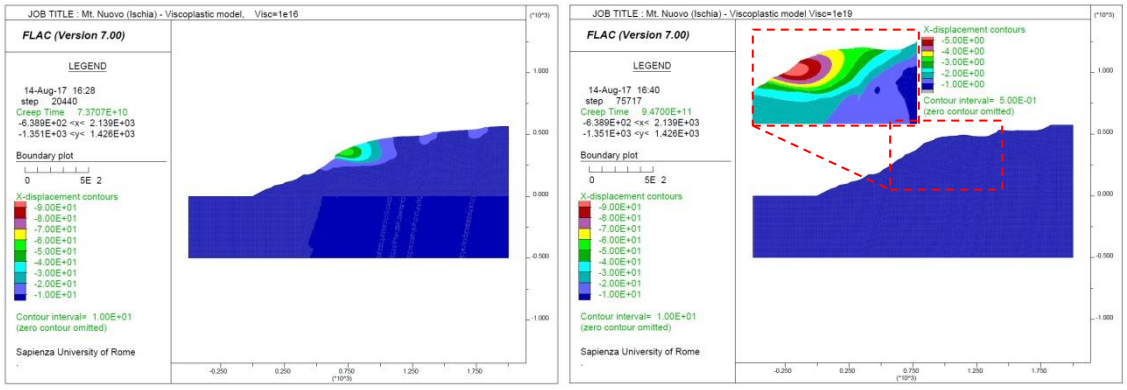

Fig. 53 - Plot of horizontal displacement (X-disp) under viscosity hypothesis of 10^{16} (left) and 10^{19} (right) Pa·s. Detailed view of horizontal displacement for the highest viscosity is shown.

Visco-plastic sequence's results clearly show the onset of a slope deformation in the Mt. Nuovo area, driven by an apparently biplanar mechanism (inlayer of Fig. 53) involving the most external portion of the slope.

Numerical solutions of Burger-creep model with viscosity equals to 10^{17} Pa·s shown considerable deformation, matching the expected horizontal deformation and verifying the displacement criterion ($C_{\Delta x}$) along the shear zone in three cases out of five (Fig. 54, Tab. 1). Failure occurred in this solution after a creep time of ~8200 yr (i.e. age of 21800 ka), which was not consistent respect the morphological and chronological elements (i.e. time-space distribution of mass wasting deposits detached from the edge of resurgent block). This predated occurrence led also to a null score for Temporal Factor (TF) nullifying the Validation Index (Iv).

$Iv_{(\eta)}$						
η	C_h	$C_{\Delta x}$	C_β	TOT	TF	t_f
Pa · s	score					yrs
1E+16	1	0	0	1	0	2335
1E+17	2	3	0	**5**	0	8207
5E+17	2	2	1	**5**	**1**	30000
1E+18	2	0	0	2	1	28138
1E+19	0	0	1	1	1	30000

Tab. 1 Scoring of Validation Index based on kinematic and temporal criteria.

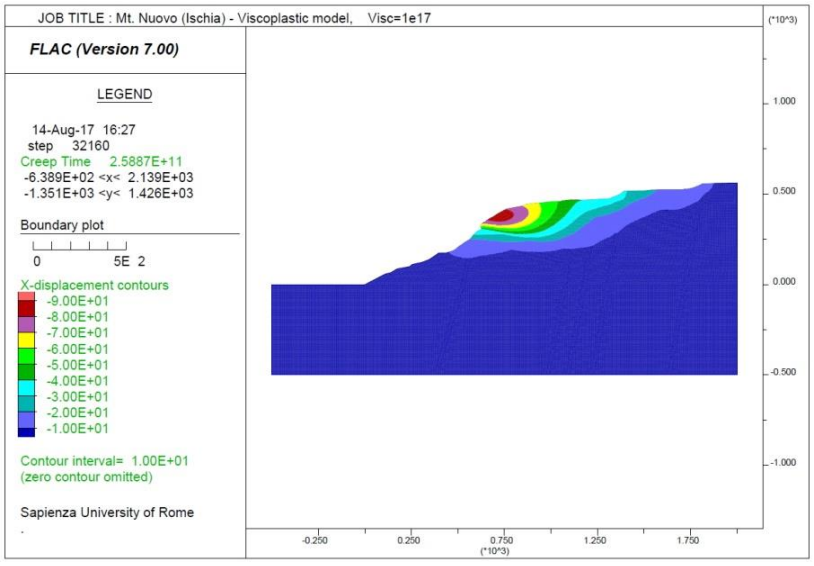

Fig. 54 - Plot of horizontal displacement (X-disp) under viscosity hypothesis of 10^{17} Pa·s.

The log of horizontal displacements (Fig. 55) along the five monitoring verticals shows as much evidenced in Fig. 54, where the higher deformation occurred in the external portion of the slope. The elevation of the shear zone was assumed located in correspondence of the kink of the curves, where deformations rapidly increase above a bedrock assumed as stable (Fig. 55). It follows that the maximum displacements cumulated in the slope, used for the definition of the displacement kinematic criterion, were derived subtracting the dislodgment cumulated below the shear zone.

The analysis of the kinematics of the modelled deformative process at the last time-step (i.e. in this case corresponding to failure), clearly shown the good reproduction of the slope-scale process, in which the elevation of the shear zone and the maximum displacement criteria were satisfied two and three times, respectively (Fig. 56). The kink of the X-disp vs Elevation curves (Fig. 55) falls inside the admissible error for verticals n. 3 and n. 4, located in the central portion of the slope, while the elevation of the shear zone in the Vertical n. 5 (i.e. the uppermost one), is not far from the target value. The expected maximum displacements were verified along three different verticals, reproducing to the best the geometries of slope deformations.

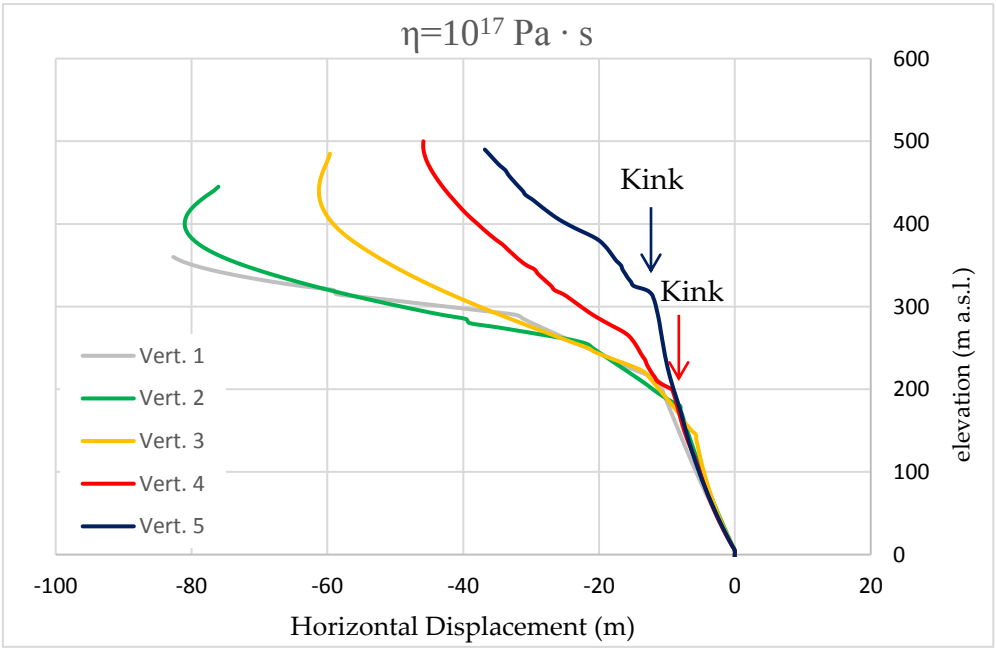

Fig. 55 - Example of horizontal displacement log at the five monitoring verticals for viscosity hypothesis of 10^{17} Pa·s.

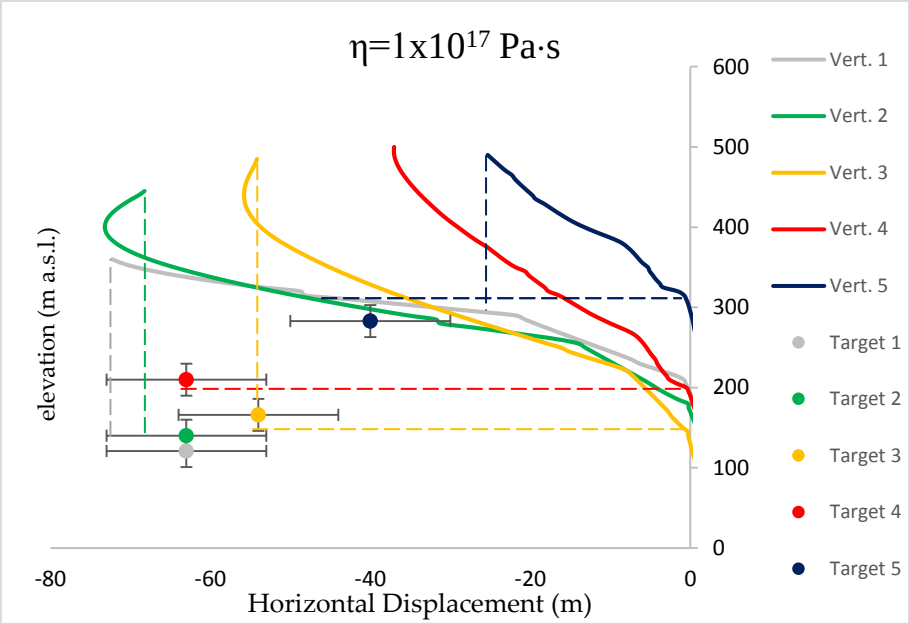

Fig. 56 - Log of horizontal displacement filtered respect the stable bedrock at the five monitoring verticals. A comparison with the elevation (y axes) and maximum horizontal displacement (x axis) is provided under viscosity hypothesis of 10^{17} Pa·s

For viscosity values of to $5 \cdot 10^{17}$ Pa·s and 10^{18} Pa·s (Fig. 57, Fig. 58), the numerical solutions satisfy the temporal criterion, giving no plasticity before 5 ka.

The X-disp contours envelope an ongoing slope deformation controlled by a biplanar compound mechanism, confirming the previously defined conceptual model. The magnitude of horizontal displacements fit the geomorphological reconstruction, highlighting the role of time-dependant deformation in dictating slope scale instabilities.

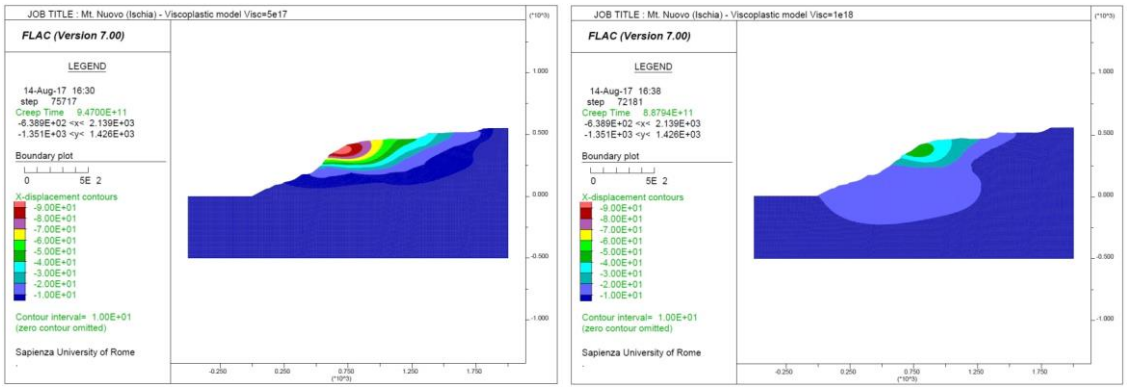

Fig. 57 - Plot of horizontal displacement (x-disp) under viscosity hypothesis of $5 \cdot 10^{17}$ (left) and 10^{18} Pa·s(right).

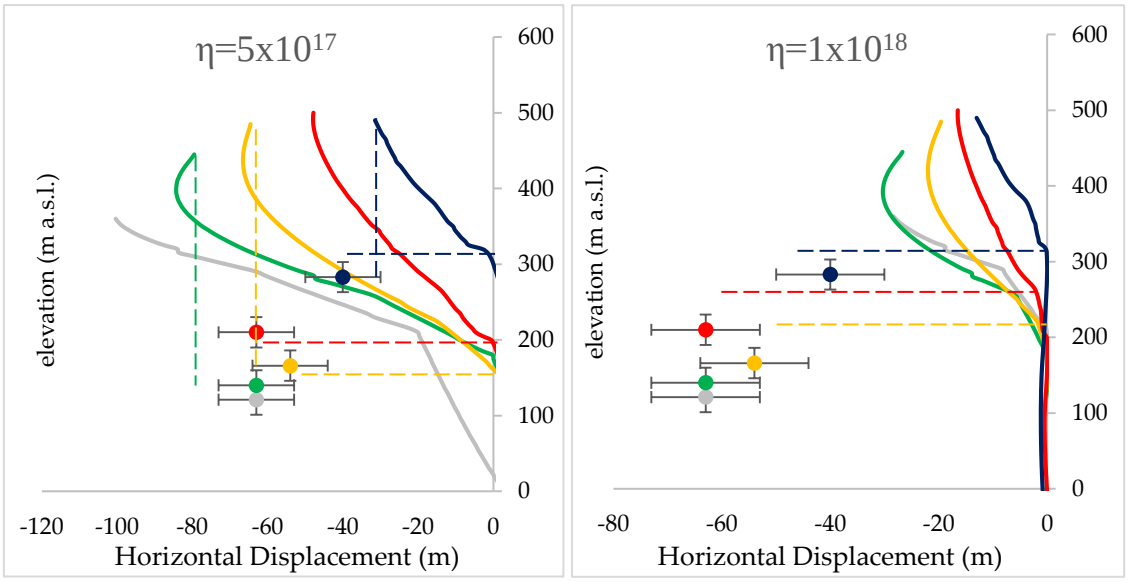

Fig. 58 - Log of horizontal displacement along five monitoring verticals under viscosity hypothesis of 5·10^{17} Pa·s (left) and 10^{18} Pa·s (right).

For viscosity value of 5·10^{17} Pa·s the kinematic of the process was verified along three central monitoring verticals, in which elevations and magnitude of displacements are comparable to the engineering-geological reconstruction. For viscosity equals to 10^{18} Pa·s, the sole shear zone elevation criterion was satisfied at least two times.

For what concerns the most external vertical (Vert. 1), the modelling results emphasize a more surficial shear zone, implying a different geometry and a more sharp circularity of the rupture surface.

The obtained rotation angles verify this inconsistency, indicating no rotation in the foot of slope (Vert. 1-2-3). Under viscosity hypothesis of 5×10^{17} and 10^{19} Pa·s, only in one case the rotation angle, nodally derived by numerical analysis, falls within the rotation target's error bar (Fig. 59).

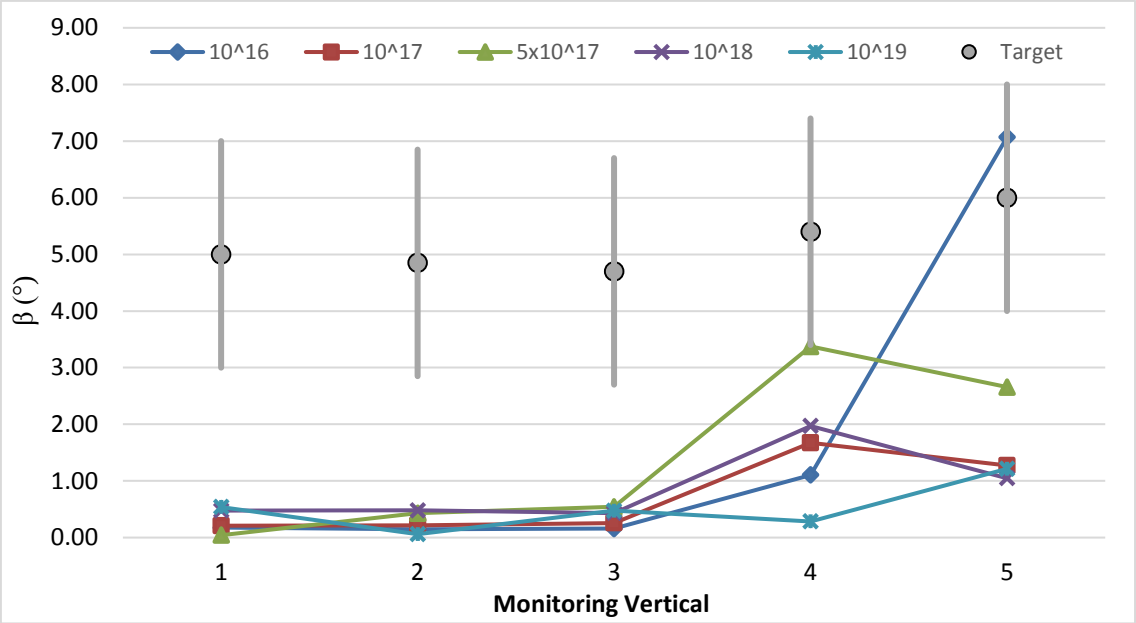

Fig. 59 - Rotational kinematic criterion along the monitoring vertical for each viscosity hypothesis.

6.1.4. 2D Thermo-mechanical modelling

The thermal field in rock slope can interact with the slope equilibrium modifying the stress-strain response of the rock masses, and thus influencing the evolution of deformative processes, potentially leading to acceleration and incremental deformations.

In order to assess the contribution of local thermal anomalies induced by the presence of an active hydrothermal systems on time-dependent processes, a set of thermo-mechanical analysis were conducted by the definition of comprehensive visco-plastic and thermo-mechanical model.

Given the narrow time-window where the seasonal variability of the shallow hydrothermal system take place (derived by thermographic survey of fumarolic gas emission reported in Fig. 15) respect the long-term temporal evolution of slope scale gravitational deformation (i.e. time-window of our analysis), a steady state assumption has been formulated. Starting from this assumption, an uncoupled solving scheme was adopted by the combined use of COMSOL® and FLAC 7.0® codes.

For each time stage (Δt_n), temperature and pressure variations, deriving by the solution of thermo-hydro-dynamic codes (red line on Fig. 5), have been attributed as thermo-baric condition to solve the set of equations defined in mechanical solutions (blue line on Fig. 5).

Because in the conceptual morpho-evolutionary model of the Mt. Nuovo slopes no morphological changes or variations in physical conditions occurred, in this case study, a single-stage analysis was conducted and elasto-plastic and viscous deformative processes evolve under constancy of thermal and hydrodynamic conditions.

The mechanical solution was performed by the use of continuum mechanics code (FLAC®) configured for thermal and mechanical creep analysis. The outputs derived by mechanical solutions in terms of strain and porosity or density variations

were then attributed as conditioning for the following stage of thermal calculation (dashed blue line on Fig. 5) (modified after Rutqvist, 2011).

Because of its formulations, the mechanical calculation was in turn completed by uncoupled solve among visco-plastic and thermo-mechanic equations, switching from creep to thermal configuration at constant time-interval (Δt).

Because the heat transfer process can be assumed at steady-state, a constant thermal condition has been fixed during all the modelled time. In other words, a mono-stage with constant thermal conditions was assumed within the surficial slope system, which was kept invariable during the evolution of time dependent processes. It's worth note that no fluid pressure variations were initially considered, to take into account the exclusive role of thermal perturbations. Therefore, temperature field at steady-state generated by convective processes and derived by thermal modelling, has been transferred in FLAC domain, exporting by the triangular mesh of COMSOL code a regular quadrangular mesh with resolution equals to the one settled in the mechanical FLAC model, and then translating it to the new numerical domain.

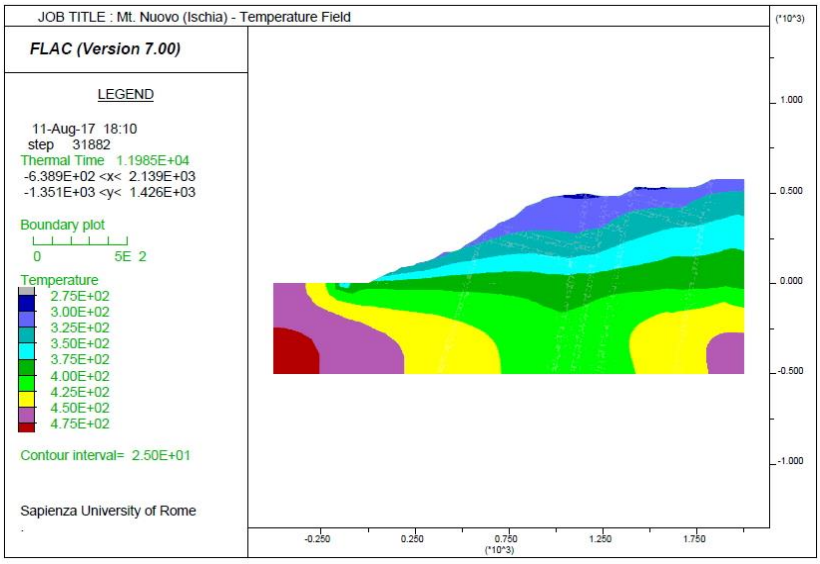

Fig. 60 - Temperature field derived by transfer from COMSOL to FLAC domain. Temperature expressed in Kelvin.

Once the thermal state within the model representative of the steady state free convection in the deep reservoir and the conductive heat transfer in the upper part of the slope was computed, temperature field was fixed in all the numerical domain.

The same time interval of 30ka was simulated under the same viscosity hypothesis, attributing to the rock masses the thermal parameters derived by laboratory characterisation. A thermal insulation was attributed to the lateral boundary of domain. Because no laboratory test was conducted at controlled temperature a thermal independency of the mechanical parameters was maintained and room-temperature data was attributed. It follows that the incremental thermo-mechanic deformations derived only by thermal dilation effect.

An initial static equilibrium was reached under elastic and perfectly-elastic in temperature-dependency conditions. The mechanical calculation was the completed by uncoupled solve among visco-plastic and thermo-mechanic equations, switching from creep to thermal configuration activating and deactivating the thermal modulus (*therm on/off*) at constant time interval (Δt) corresponding to 5ka in age. The viscosity sensitivity analysis under controlled thermal conditions, show negligible effects in the spatial distribution of deformations, which appears mainly controlled by the stress field distribution due to the local geological settings.

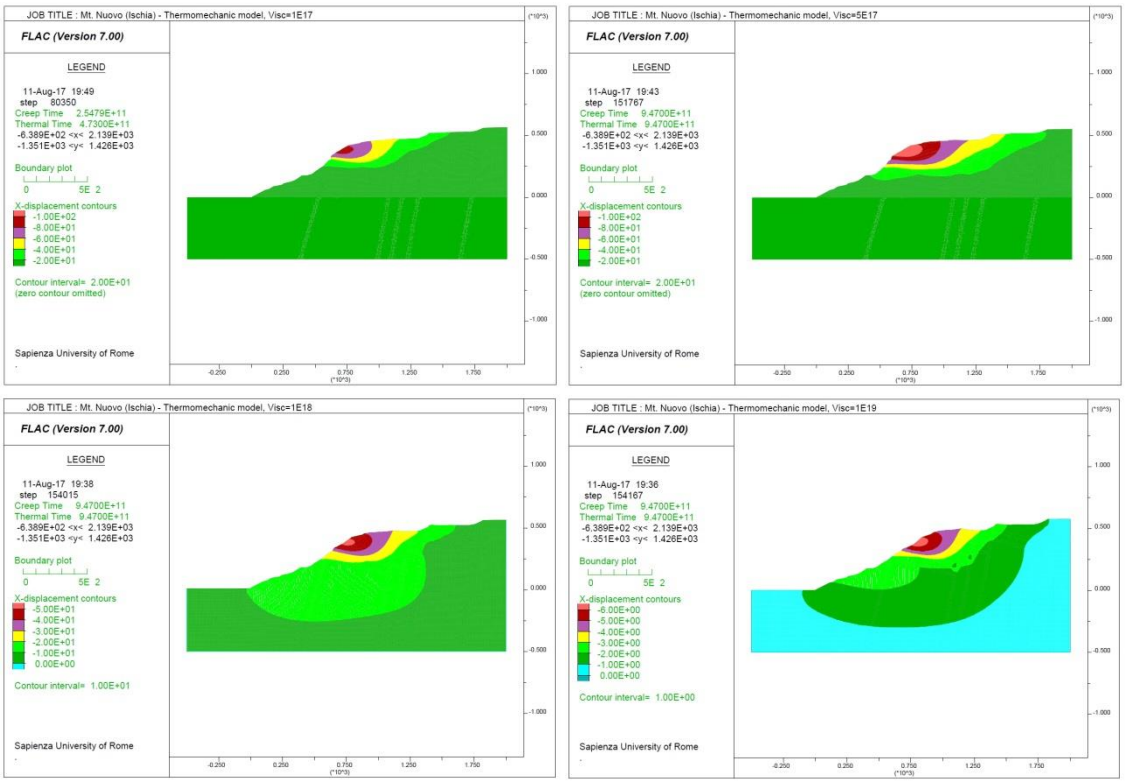

Fig. 61 -Thermo-mechanical model results under viscosity hypothesis ranging between 10^{17} and 10^{19} Pa·s.

Appreciable effects are highlighted in the magnitude of horizontal displacement, as revealed by the comparison of horizontal displacement vs. elevation curve derived by pure visco-plastic rheology (curve from Vert.1 to Vert.5) and thermo-mechanical visco-plastic sequence (Vert._TM curves).

With viscosity equals to 10^{17} Pa·s, the failure time (8088 ka) predates the temporal occurrence derived in creep sequence, while displacement (i.e. deformation) almost reach the same displacement level (Fig. 62). However, after only 8.8 kyr, sensible contribution of thermo-mechanics cannot be appreciated. The elevation of the basal rupture surface remain stable at depth equals to ones derived by visco-plastic creep sequences.

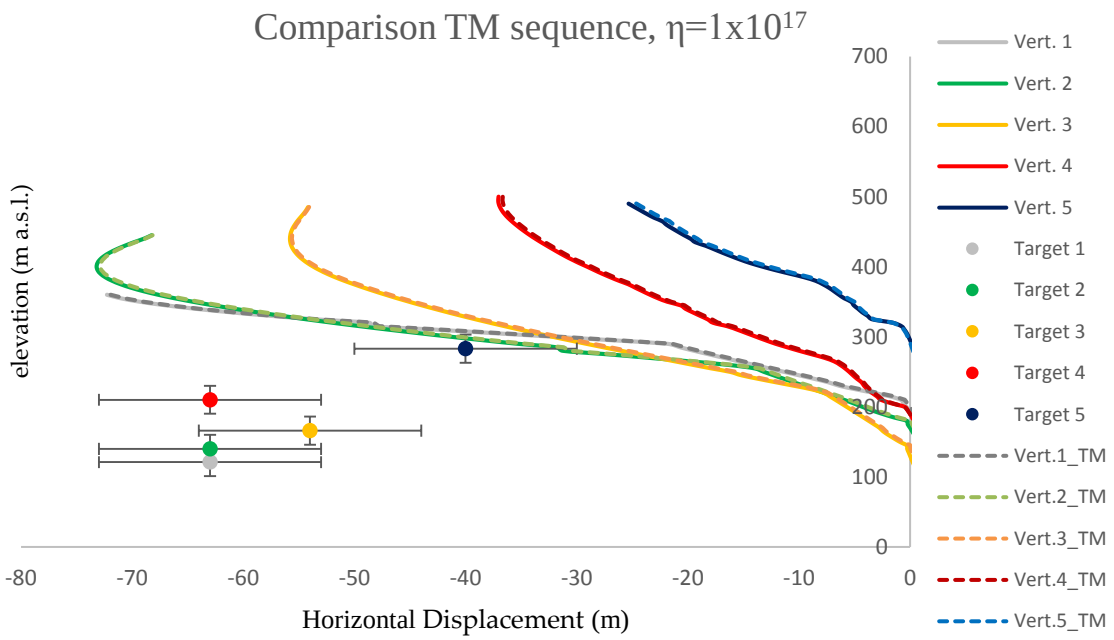

Fig. 62 - Comparison of horizontal displacement results in thermo-mechanic (TM) and creep models along the five monitoring verticals. Viscosity hypothesis of 10^{17} Pa·s.

On the contrary, both thermo-mechanic visco-plastic sequence derived by viscosity hypothesis of $5 \cdot 10^{17}$ and 10^{18} Pa·s, reveal a considerable contribution on displacement field within the rock slope (Fig. 63,Fig. 64), with maximum increment in horizontal displacement along the most external zone (Vertical 1) of 2.8 and 4.4 m, under lower and higher viscosity, respectively.

This contribution appears to be relevant for the higher viscosity, where reach a maximum percentage incremental contribution of about 30% of the total ($\eta=10^{19}$ Pa·s, Fig. 65). At lower viscosity, where high strain rate occurs, the thermo-mechanic effects remain masked by time dependant deformation, representing only the 15% (10^{18} Pa·s) and 3% ($5 \cdot 10^{17}$ Pa·s) of the total horizontal displacement.

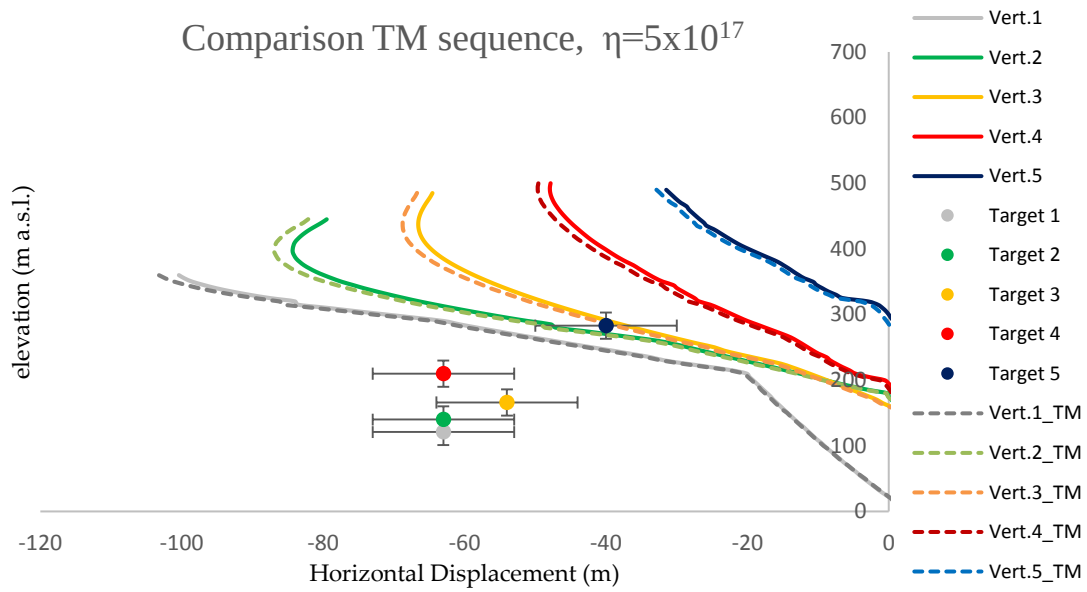

Fig. 63 - Comparison of horizontal displacement results in thermo-mechanic (TM) and creep models along the five monitoring verticals. Viscosity hypothesis of $5 \cdot 10^{17}$ Pa·s.

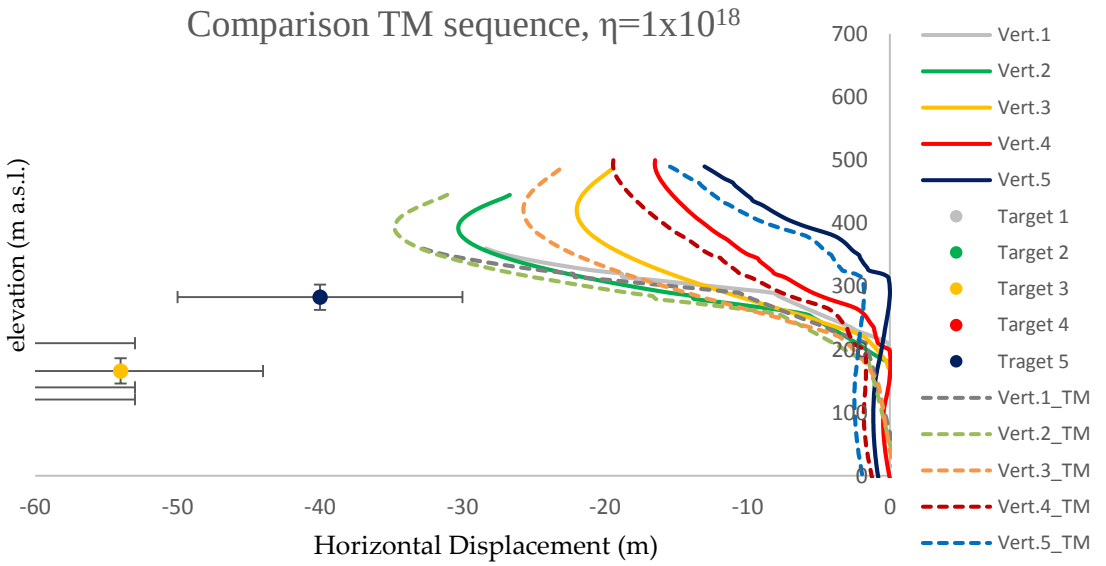

Fig. 64 - Comparison of horizontal displacement results in thermo-mechanic (TM) and creep models along the five monitoring verticals. Viscosity hypothesis of 10^{18} Pa·s.

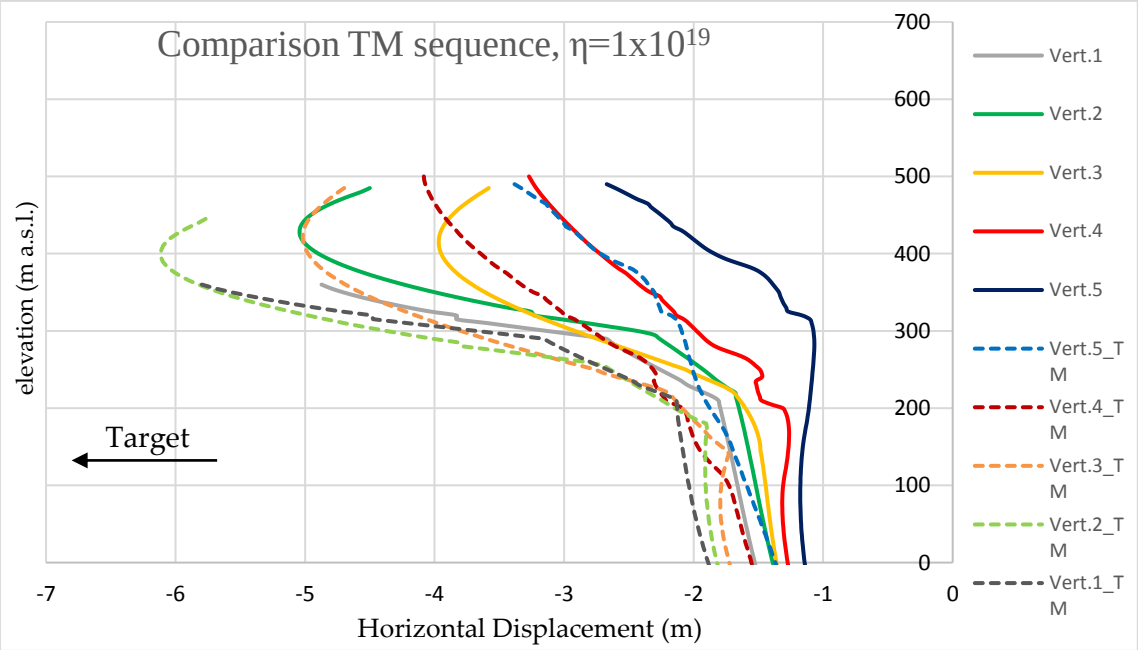

Fig. 65 - Comparison of horizontal displacement results in thermo-mechanic (TM) and creep models along the five monitoring verticals. The obtained horizontal displacement are out of target. Viscosity hypothesis of 10^{19} Pa·s.

The here defined thermo-mechanic (TM) model do not affect the attribution Validation Index scoring (Iv) which, based on kinematic and temporal criteria, remain unaltered because no significant incremental displacement or shear zone elevation variation occurred.

To evaluate the effect of temperature field on the magnitude of deformation and test the response of thermo-mechanic model to temperature variations, the sensitivity analysis was extended toward the consideration of thermal scenarios. The sensitivity analysis to different thermal scenarios was performed reproducing the same time evolution of slope deformation over the last 30ka, under varied temperature conditions, analysing the deformative effects introduced by a rise of thermal perturbations.

Effects of thermal perturbations were evaluated by parametric analysis under two different thermal scenario, the first one commensurate with the physical variability of the system while the latter representative of "extreme" thermal conditions. The first thermal scenario was defined according to the thermal variability of the hydrothermal

systems, deduced by Della Seta et al., 2015 since geo-thermometer analysis. This analysis on alteration minerals assemblage suggested a hydrothermal alteration episode at temperature confined below 160-180°C. Despite this temperature are likely referred to hydrothermal fluids, because fluid thermal non-equilibrium was not implemented in numerical modelling, this target temperature was referred and imposed as maximum temperature within the hydrothermal reservoir. A worst-scenario (i.e. extreme physical conditions) was assumed imputing a doubled geothermal gradient, able to produce temperature greater than 200 °C at depth of failure surface (Fig. 66).

The thermal scenario analysis was performed on the higher viscosity hypothesis of 10^{18} and 10^{19} Pa·s, which in virtue of its lower strain rate and the smaller deformations experienced, it allows to better visualize the thermo-mechanic contribution. With the same approach adopted for thermo-mechanic sequence, thermal solution deriving by COMSOL® code was transferred to FLAC® for the stress-strain analysis (Fig. 67).

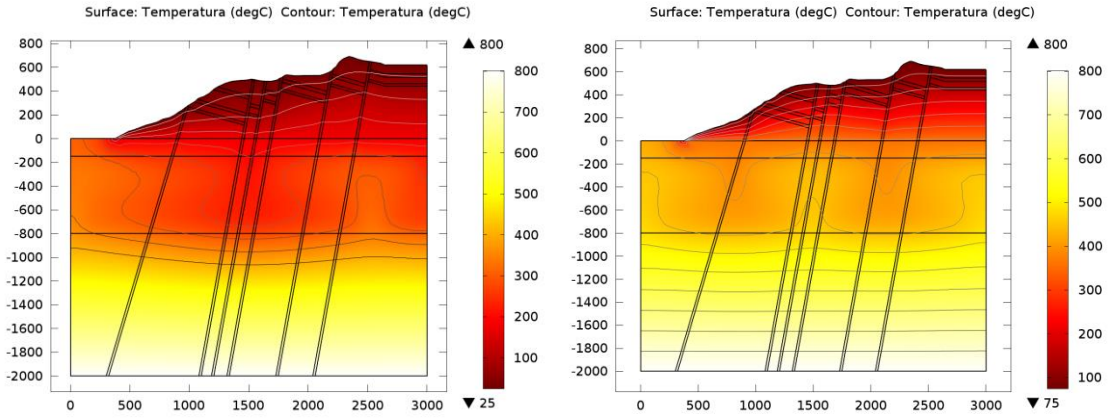

Fig. 66 - Physically-commensurate (left) and extreme (right) thermal scenario derived by thermo-hydrodynamic modelling in COMSOL and transferred to FLAC numerical domain.

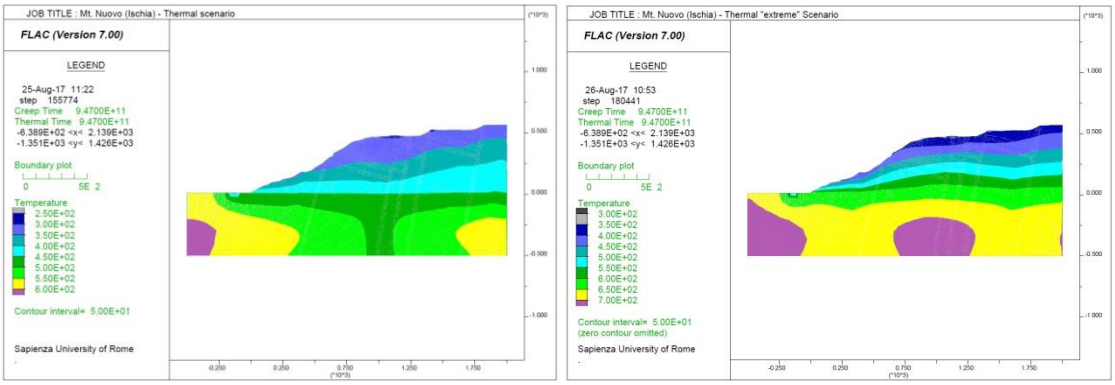

Fig. 67 - Physically-based (left) and extreme (right) thermal scenario defined as input thermal condition in for thermo-mechanical model.

The first physically-based thermal scenario induced slight temperature variation within the first hundred of m in depth within the slope, which led to indiscernible deformations. Under "extreme" gradient conditions the consistent rise of temperature reflected in incremental deformations up to 0.6 m (Fig. 68).

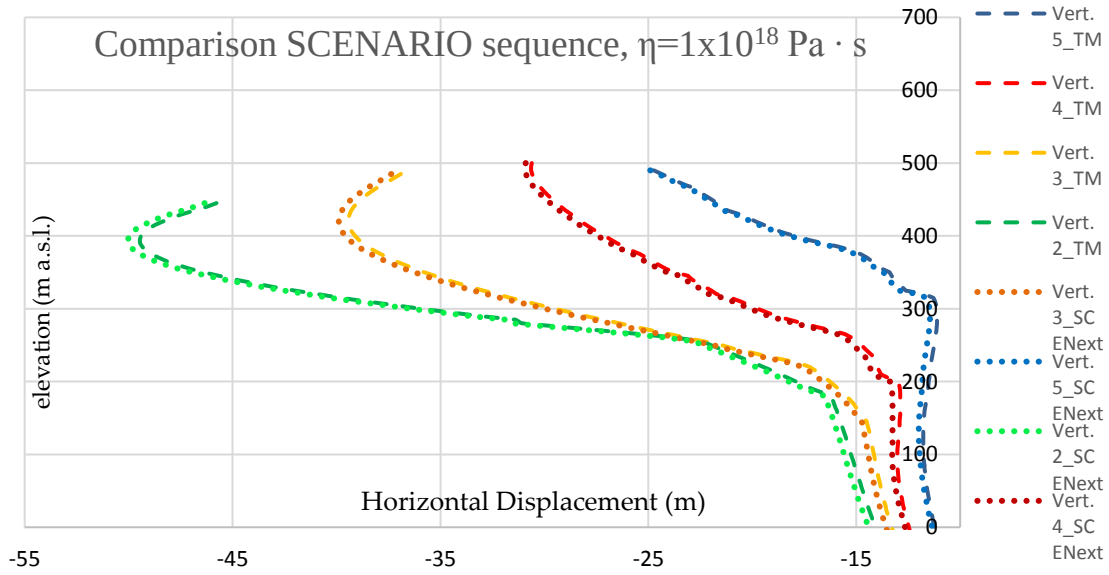

Fig. 68 - Comparison of horizontal displacement results in thermo-mechanic models under natural (TM) and "extreme" (SCENext) thermal conditions. Viscosity hypothesis of 10^{18} Pa·s.

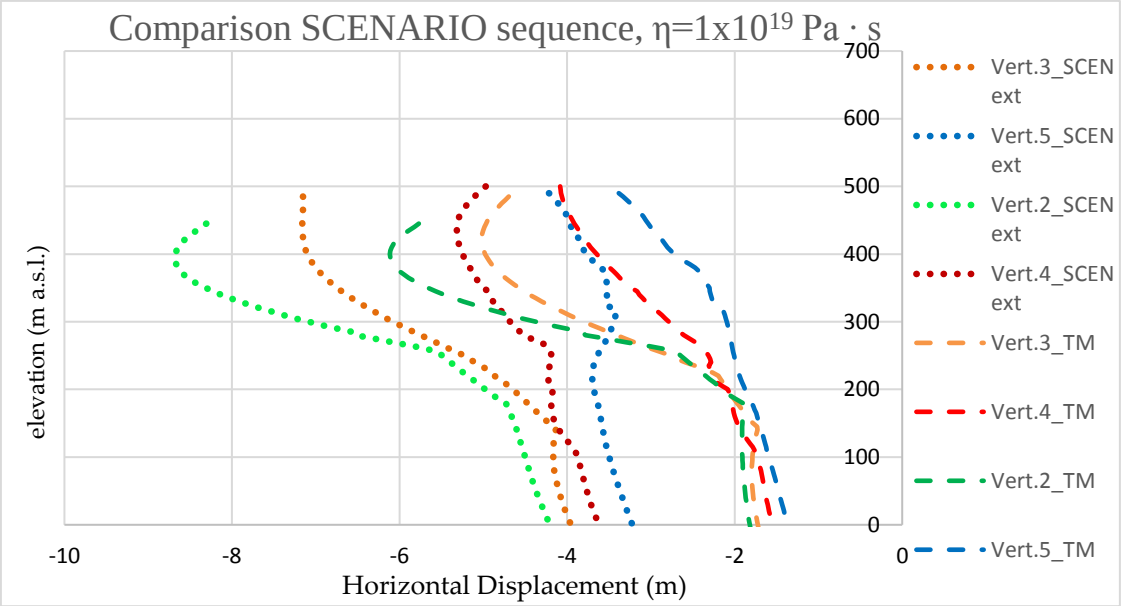

Fig. 69 - Comparison of horizontal displacement results in thermo-mechanic models under natural (TM) and "extreme" (SCENext) thermal conditions. Viscosity hypothesis of 10^{19} Pa·s.

As observed by comparison of visco-plastic and thermo-mechanic results, even by the analysis of thermal scenario results (SCENext curves), where incremental deformation deriving by thermal dilation effects appeared to be predominant at higher viscosity (10^{19} Pa·s). Under this parametric hypothesis, thermally-induced displacement exceeded 2 m, causing a double strain respect to the conditions representative for the thermal state at current time (Fig. 69).

The analysis of time series of horizontal displacement does not reveal significant strain rate variation, which evolve under constant thermal conditions (Fig. 70). The creep rate is temperature-dependent only for the WIPP model, the WIPP-creep visco-plastic constitutive model implemented in FLAC®. No temperature dependency of creep rates was considered in mathematical formulation of Burger creep model.

Because no temperature-induced viscosity variations were considered, the incremental deformation deriving by thermo-mechanic interactions are limited to elasto-plastic or primary stage of creep deformation (Fig. 70, Fig. 71). Time-series of X-disp confirm the speculation of viscosity relevance on thermo-mechanical incremental

deformations, which appear to be predominant under extreme thermal scenario conditions and more influent at higher viscosity.

This counter-intuitive outcome appear related to stress increments related to intermediate thermo-mechanic solution, which given constitutive law of visco-plastic media, under constancy of viscosity, led to consequent incremental deformations.

The comparison of visco-plastic creep and thermo-mechanic sequences (TM), under thermal states corresponding to physically-based (SCEN) and extreme scenario (SCENext), also evidenced the limited effect of slight temperature variation on time-series of deformations. After primary creep stages, the deformations evolved at constant strain rates.

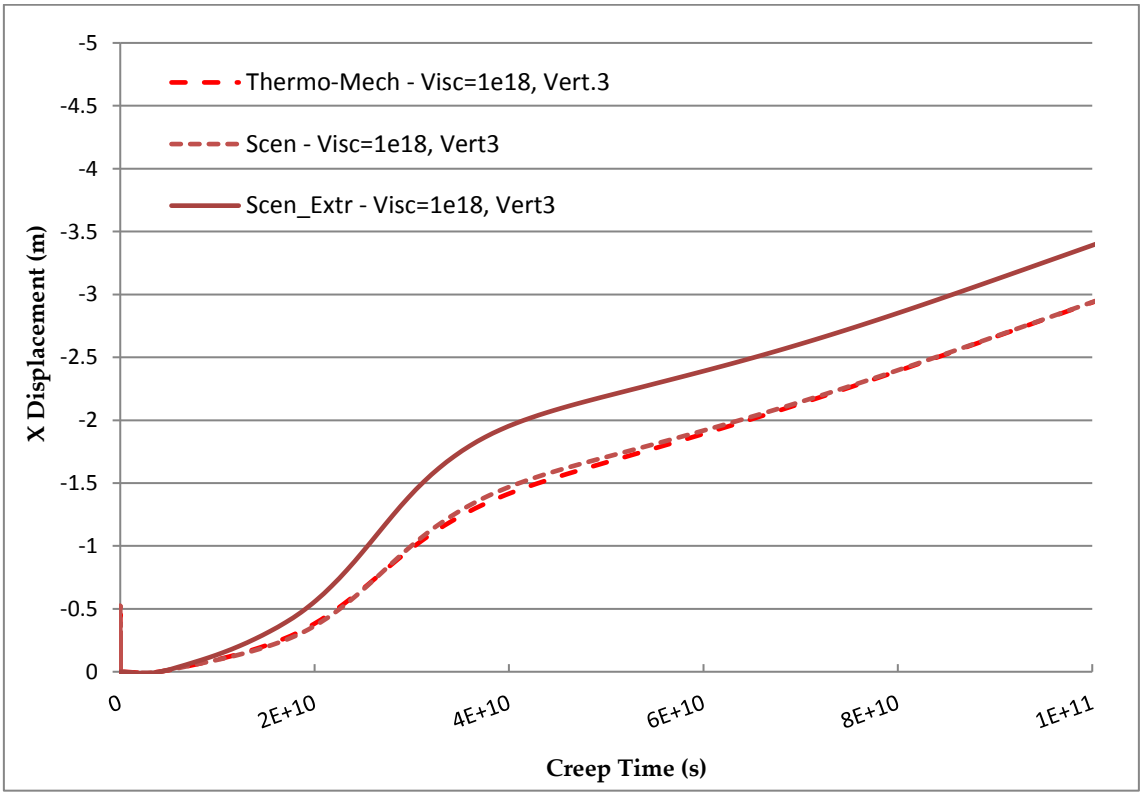

Fig. 70 - Time-series of X-disp in the first stage of creep curves under viscosity hypothesis of 10^{18} Pa·s along the monitoring Vertical 3. A marked influence of thermo-mechanical interaction is revealed under extreme thermal scenario.

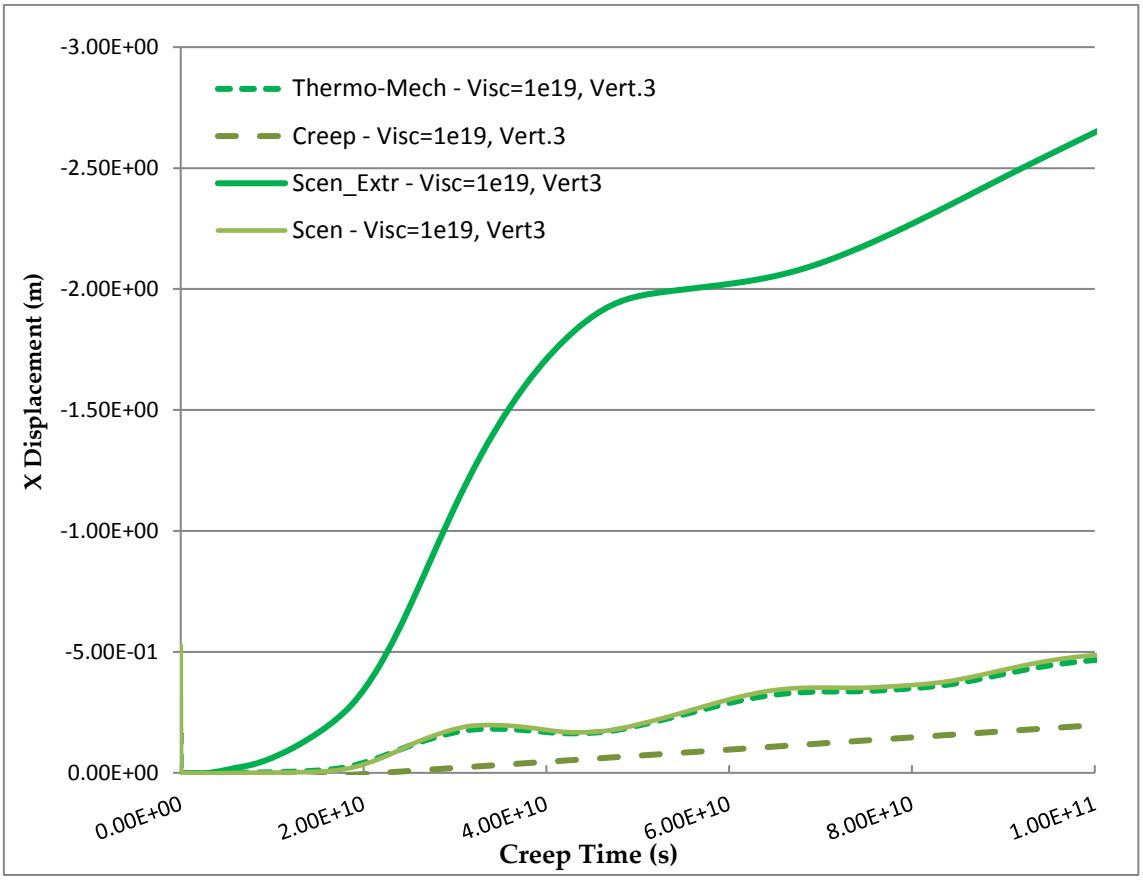

Fig. 71 - Time-series of X-disp in the first stage of creep curves under viscosity hypothesis of 10^{19} Pa·s along the monitoring Vertical 3. A marked influence of thermo-mechanical interaction is revealed under extreme thermal scenario (SCENext).

Lack of a full thermo-mechanical characterisation deriving by temperature-controlled triaxial tests and the non-consideration of changes in mechanical and rheological parameters, results in an underestimation of deformative effects on gravitational slope-scale processes.

The exemplary thermo-mechanical model reproduced under perturbed thermal conditions confirmed the validity and potentiality of this numerical analysis. Further improvement deriving by the definition of a thermo-hydrodynamic-model and thermal-pore pressure coupling will be implemented, to assess the role of fluid pressurisation in slope scale instability. With the same multi-codes uncoupled solution schemes, pore pressure variations deriving by hydrothermal thermalisation will be transferred in thermo-hydro-mechanic model. To better constrain thermal effect on

slope stability a non- isothermal fluid flow will be considered. In addition, all the defined model does not consider thermal degradation effect and changes in mechanical and rheological parameters. In order to assess proper thermo-mechanic effect on slope deformations the model will be implemented by temperature dependency of mechanical and rheological parameters. These effects can control the strain rate evolution of DSGSD dictating and controlling the time-space propagation of deformation, thus influencing time to failure.

6.1.5. Salient features of the Ischia case study

The island of Ischia represents a unique case study to test the above described multi-physical approach and evaluate at the same time the spatial and temporal significance of thermo-mechanics in the behaviour of rock mass involved in slope-scale gravitational deformations.

First step was the definition and validation of a 2D model of the deep hydrothermal systems by the implementation of both hydrodynamic and thermal model. Both physical processes evolve within different time-scales, mainly controlled by the underground circulation dynamics (i.e. drainages and seasonal recharges) and the heating by deep magmatic sources.

The hydrothermal processes act nowadays within time-scales extremely small respect the time-scale of evolution of gravitational slope deformations processes (time-window of observation in our analysis). Because of this wide time-window of observations, a steady-state of thermal and hydrodynamic processes were assumed and a stationary solution was obtained. Due to the strict physical relation in convective hydrothermal circulation a fully coupled algorithm was used. The model was validated on experimental temperature data derived by deep boreholes. The 2D model of the deep hydrothermal system was defined to constrain the thermal state of the deep system and derive the boundary conditions to apply to the slope-scale model, where

the ongoing gravitational process take place (Fig. 72). Because a stationarity of the internal forcing was assumed in the time-scale of evolution of the DSGSD process, an uncoupled multi-physical solution was adopted combining in a 2D Thermo-mechanic model the results of a 2D mono-stage mechanical model (computed by FLAC® code) and a 2D model of the hydrothermal system (solved by COMSOL®). The mechanical modelling at slope-scale was also supported by a detailed physical, mechanical and thermal lab characterisation.

The multi-physical approach was extended to the previsional phases of analysis, using the same cascade of modelling (i.e. from deep-scale to slope-scale) to evaluate scenarios deriving by a more vigorous heating or turbulent flows related to new magmatic feeding. The results of the deep hydrothermal model under physically-commensurate or extreme scenarios was thus reversed in the slope-scale model, evaluating the role of thermal forcing in the slope scale deformation.

The proposed approach will be reproduced to compute the combined role of thermal perturbations and fluids pressurisation in the slope stability, which will be computed by means of coupled or uncoupled schemes in a steady or transient regime as function of the nature of the perturbation.

The approach here applied combining deep- and slope-scales has been revealed a promising approach for the numerical modelling of gravitational slope deformation under geological conditions where several physics act together. The uncoupled solving scheme has revealed a practical way to manage with slope deformations evolving in complex conditions such as the ones of hydrothermal systems, where heat fluxes, fluid flows and rheological flows act concurrently under steady-state regimes.

The uncoupled solving scheme easily allowed to consider mutual physical interactions evolving in a relatively short time-window (30 ka) in a mono-stage simulation, with reduced calculation time. The uncoupled modelling lends itself well also to the definition of sequential model, where multiple stages of analysis must be

defined on wider time-scales (hundreds of thousands years), over which the most of DSGSD processes evolve.

Despite this easy formulation and numerical coupling, the applicability of this schemes seems to be limited to case studies or conditions where stationarity can be assumed. The combination of multiple geometric scale of analysis allowed to better constrain the contribution of deep perturbation on shallow systems and in particular on the evolution of a DSGSD, lending itself for multi-physical scenario analysis.

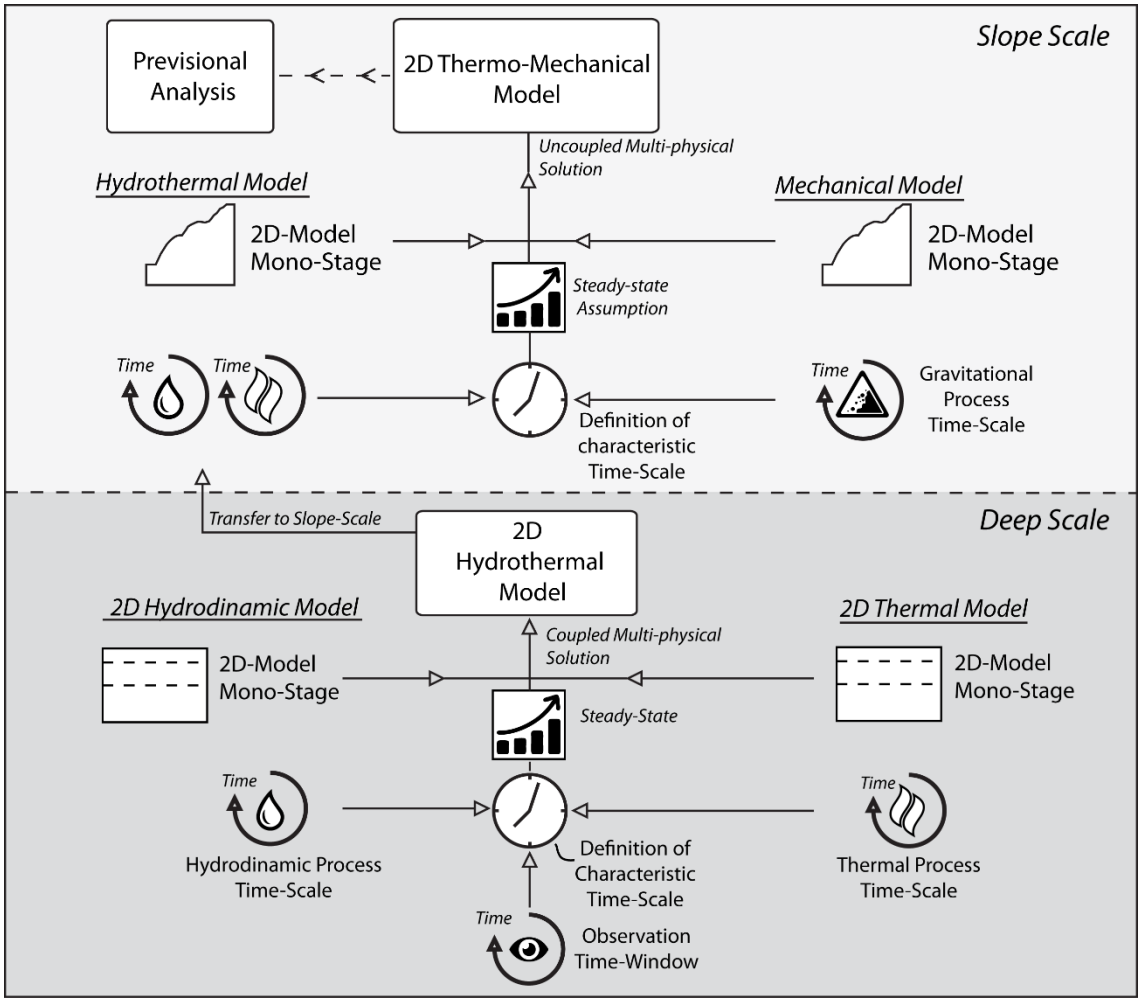

Fig. 72 - Summary flow chart of the multi-physical numerical modelling performed for the Ischia case study.

6.2. Priestley Glacier case study

The second case study, represented by the slope bounding the Priestley glacier valley, experience during the last millions of year sensible variation of heat flux supposed as the response of emplacement of magmatic bodies at deep levels. Such variation, in addition to the local anomalies due to the presence of a cold glacial mass, can have interacted with the slope and glacial systems, respectively influencing the onset and spatial/temporal evolution of gravitational deformation and altering the physics state and thus the kinematics of glacier.

For this purpose, in a first instance, a 1D model of the crustal heat transfer was defined to constrain the effect of geothermal perturbations on shallower glacial systems. The 1D thermal model, once validated on temperature data derived in deep boreholes, has been transferred to the valley system, attributing the output heat fluxes as thermal conditioning to the shallower slope-scale model of the glacial valley.

To constrain thermo-mechanic effects, with the same approach, a 2D thermal model of the slope system was defined, evaluating the sensitivity of the glacier to geothermal perturbations.

Starting from the conceptual and morpho-evolutionary model of the Priestley glacier valley, a multi-stage sequential modelling was defined under pure mechanical and thermo-mechanical configurations.

6.2.1. 1D Modelling of Antarctic crustal heat transfer

First step in the definition of thermal perturbation in complex slope system, was the validation of a 1D crustal thermal model, aimed to constrain, in terms of heat flux, steady-state perturbation to the shallower slope system, modelled in turn by an own 2D model. Such thermal perturbations, resulting from changes in the local and regional heat flow conditions, was applied as thermal boundary conditions for the upper 2D

model. On the basis of geothermometric constrain (Armienti and Perinelli, 2010; Perinelli et al., 2017) and heat flux data reported in literature (Della Vedova et al., 1994; Morin et al., 2010), a validation of a 1D crustal thermal model was carried out, capable of dimensioning heating conditioning at shallower level, below the glacier valley.

A specific numerical model was performed, assuming different geological conditions and stratigraphic proportion along vertical profiles, representative of different thickness of crustal layer and partitioning between granite and gabbroid compositions. For the deep 1D model, an isotropic conductive heat flux propagation under steady-state regime was assumed. By parametric analysis, the influence of thermal conductivities and thickness proportion was then considered. The calibration and validation of the 1D model was achieved by comparison with temperature data derived in deep borehole (ANDRILL-1B) (Morin et al., 2010), where a temperature of about 70°C was reached at depth of about 1000 m below sea floor. Such heating would be the result of the geothermal flux existing in the study area (Della Vedova et al., 1992, 1994), comparable to what observed in the Priestley glacier study area (Fig. 73), belonging to the same rift basin and for which similar geological and heat flow condition can be approximated.

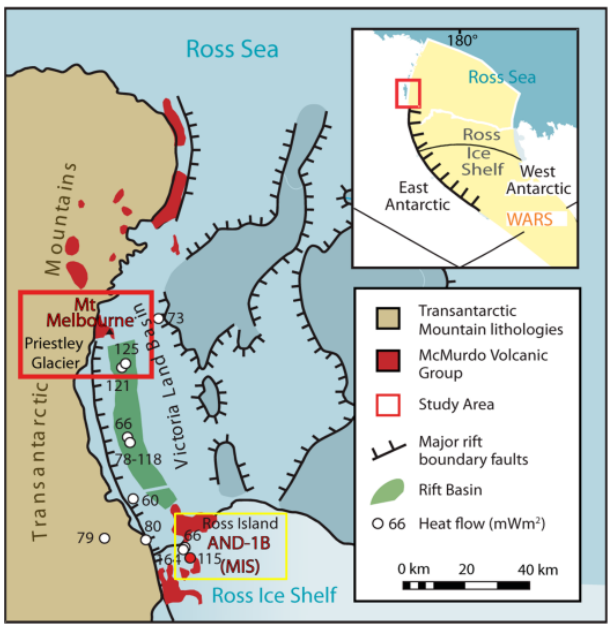

Fig. 73 - Location of AND1-B deep borehole respects the study area. Heat flux measurements results are provided (modified after Morin et al., 2010).

This high flow condition, would be the results of the lithospheric rifting and consequent volcanism, which moved in the last millions of years from the internal area (east of Transantarctic Mountains) to the coast, where the major active volcanism persist in Mt. Melbourne and Ross Island (i.e. Erebus Volcano).

The model was conditioned imposing thermal boundary conditions to top and bottom of the model, while thermal insulation on lateral boundary was attributed to ensure 1D vertical propagation of heat flow. The top of the model (Fig. 74) was fixed at temperature of 2°C, assumed as upper temperature at sea floor (Morin et al., 2010). The mantle thermal gradient of 3°C/km inferred by Armienti and Perinelli (2010) was kept constant. Temperatures at Moho discontinuities were varied in a range of temperature between 750 and 1000 °C, simulating the presence of a deep source of thermal perturbation. This boundary condition likely represents a heat source assimilated to one deriving by the differentiation of cumulate rocks at the mantle-crust transition, where Perinelli et al. (2017) speculates about the development of crustal underplating or a storage of an "hot" and "wet" zone able to influence the thermal evolution of lower crust.

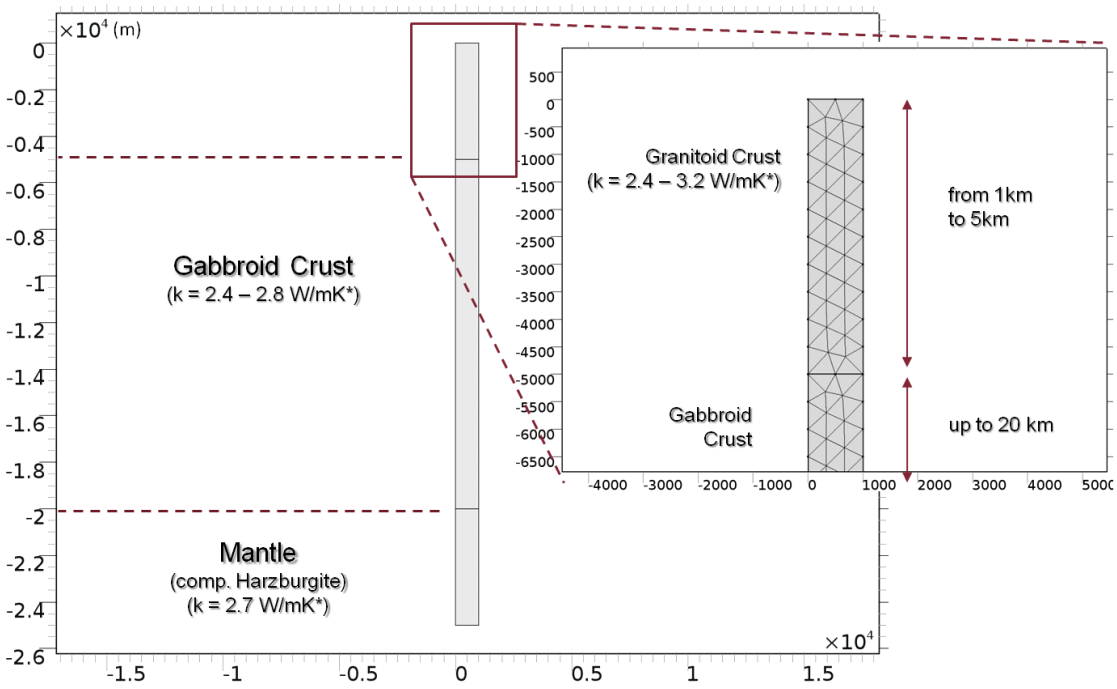

Fig. 74 - Geometries of 1D thermal model. Example of end-member geometry with thickness of granitoid crust of 5 km. A fine physics-controlled mesh was defined.

In a first analysis the exclusive role of thermal conductivities parameters was considered, keeping constant thermal boundary conditions. The parametric analysis clearly shows how this effect is limited within few Celsius degrees, with an excursion at depth of -1000m (target depth for validation of 1D modelling), limited within ± 3 °C (Fig. 75). The parametric analysis was carried out considering a commensurate wide range of thermal conductivities, as reported in literature (Eppelbaum et al., 2014).

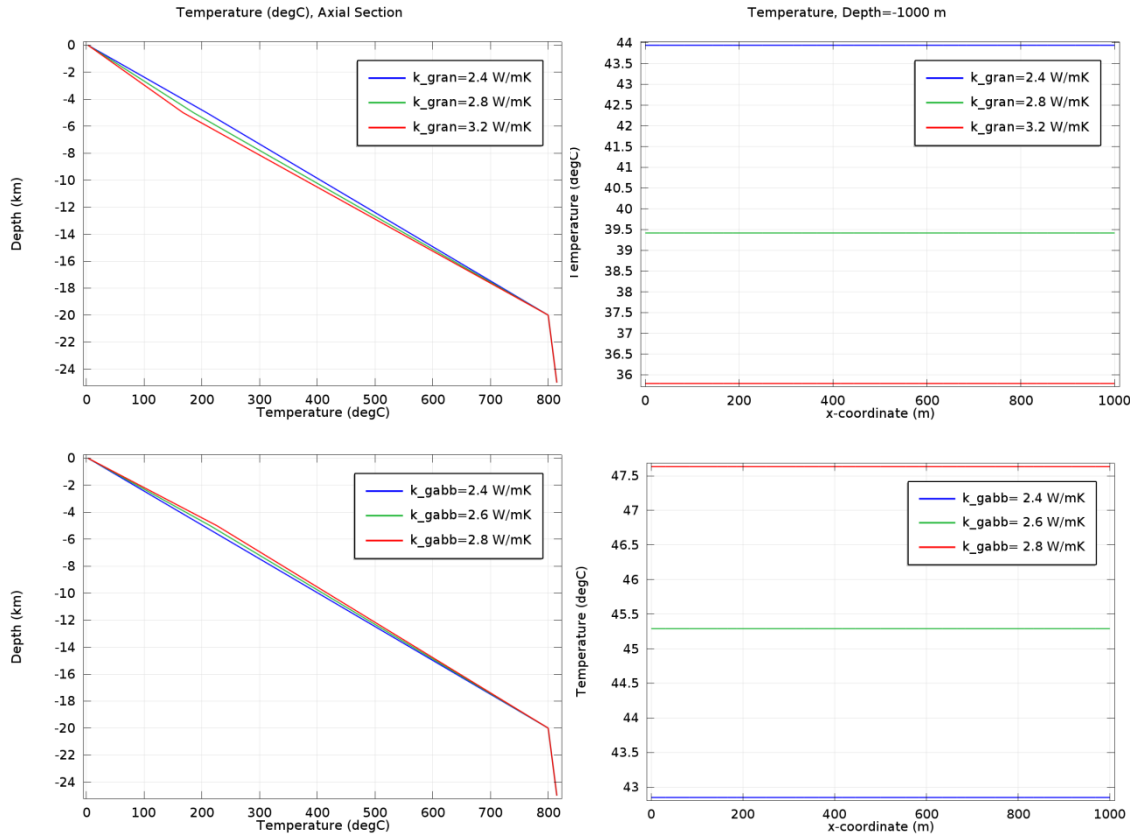

Fig. 75 - Parametric analysis on thermal conductivities performed at constant head boundary conditions. Thermal conductivities of granitoid (k_gran) and gabbroid (k_gabb) crust were varied according to Eppelbaum et al. (2014).

The main contribution was clearly led by deep thermal perturbations, here expressed by temperature variations at depth of 20 km (T_moho), assumed as the depth of Moho discontinuities for the rifting basin of Victoria Land (Wörner, 1999). Geotherms derived along axial section of the 1D model evidence the major contribution of thermal perturbation on temperature vs. depth profiles (Fig. 76). Geotherms paths are influenced by different stratigraphic proportion between granitoid and gabbroid crustal rocks, expressed by variable thickness of the model regions.

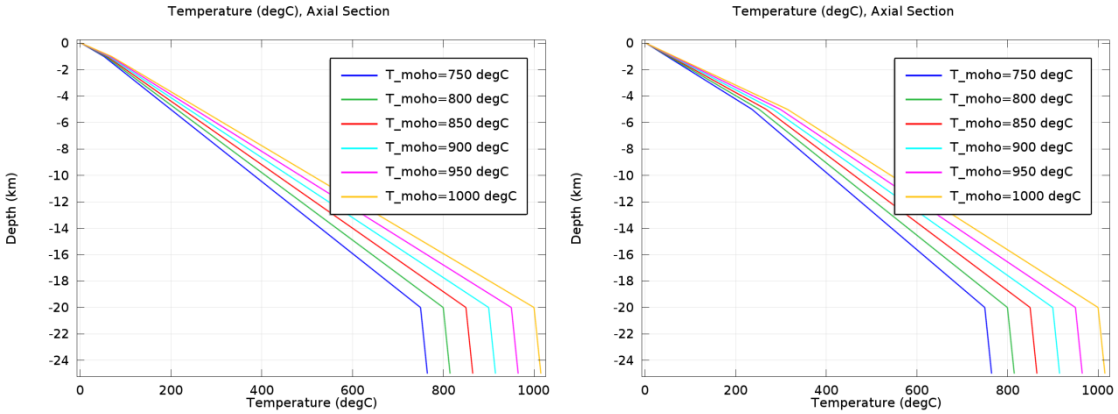

Fig. 76 - Temperature vs. depth profiles at different values of thermal perturbations (T_Moho), assuming a thickness of granitoid crust of 1 km (left) and 5 km (right).

The calibration of the model on experimental borehole data reported by Morin et al. (2010) was reached assuming the minimum and the maximum values of granitoid and gabbroid thermal conductivities respectively, and a temperature at the Moho of ~1000 °C (Fig. 77). This hypothesis results in temperature at depth of 1 km close to the target temperature of 70° C (Morin et al., 2010).

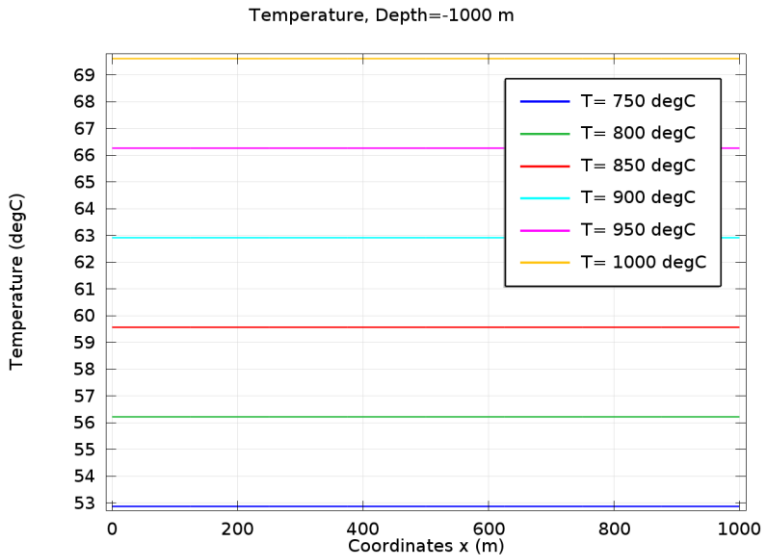

Fig. 77 - Temperature at depth of 1 km, for various thermal boundary conditions. The target temperature of ~70°C was reached by boundary temperature at bottom model equals to 1000°C.

The 1D conduction along the entire stratigraphic profile resulted in output total heat flux, along the vertical (Y) component, ranging between 100 and 135 mW/m² (Fig.

78), values slightly higher than ones obtained by local heat flux measurements (Fig. 73), in which mean values of 120 mW/m² and a maximum of 164 mW/m² (Risk and Hochstein, 1974) were found.

Because thermal contribution of surficial perturbations was not considered, the deep thermal boundary conditions and the resulting outlet heat fluxes can be overestimated. By these assumptions the obtained results have been assumed as representative of the regional heat flux perturbations existing below the study area. The output heat perturbations derived by 1D modelling have been considered in a cascade modelling sequence, aimed to the definition of a 2D-model representative of the shallower glacial system.

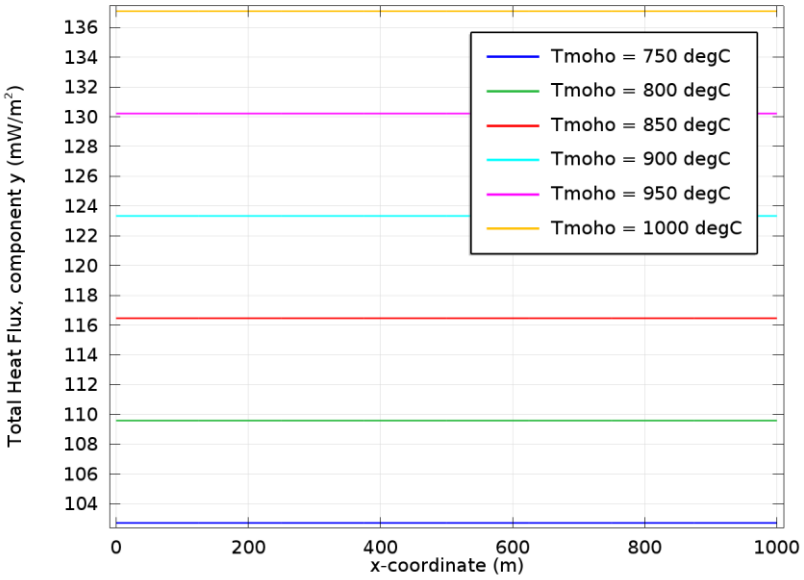

Fig. 78 - Resulting total heat flux in different temperature boundary conditions.

6.2.2. 2D Thermal model of Priestley glacier evolution

The outcomes of 1D thermal model were reported to the specificity of the Priestley glacier valley, applying the output thermal flux as boundary conditioning of a 2D model referred to the entire cross-section of the glacial valley. It's worth remind that the Priestley outlet glacier is continuously feed by the East Antarctic Ice-sheet, of which dynamics is the direct expression. This interconnection reflects in appropriate numerical solution, defined to simulate the continuous thermal non-equilibrium between the bedrock and the glacial mass.

The numerical modelling was performed along the reconstructed engineering-geological cross-section (Fig. 30), with the aim to evaluate the thermo-mechanic response of slope system to geothermal heat fluxes and the presence of local thermal anomalies. The modelling tries also to highlights the sensitivity of the glacial system to geothermal perturbations, evidencing thermal and mechanical interactions between ice and rock masses. According to literature, the glacial system would have experienced heat flux variation potentially responsible of transition at the base of the glacier from wet to dry conditions.

The numerical model was defined by the code FLAC 2D® 8.0 (Itasca Cons. License n. 213–039–0127–18973), through the definition of a discrete domain composed by 1300x300 grid with a square mesh resolution of 10 m, thus extended 13 km up to depth of about 1500 m below sea level.

The model was solved sequentially in mechanical configuration by attribution of elastic (Hooke), elasto-plastic (Mohr-Coulomb) and visco-plastic (Burger) constitutive law. These constitutive laws were coupled with heat propagation law to performed proper thermo-mechanic simulation.

In order to verify the role of geothermal flux on physical state of glacier, the numerical domain was initially equilibrated at constant heat flux of 120 mW/m^2 reaching a steady-state without the presence of the cold ice mass (Fig. 79), imposing an

isotropic heat flow propagation by conduction. Thermal insulation was fixed along lateral boundaries, while surface was maintained at temperature corresponding to the mean annual air temperature measured at Priestley glacier (-22 °C, Baroni et al., 2005).

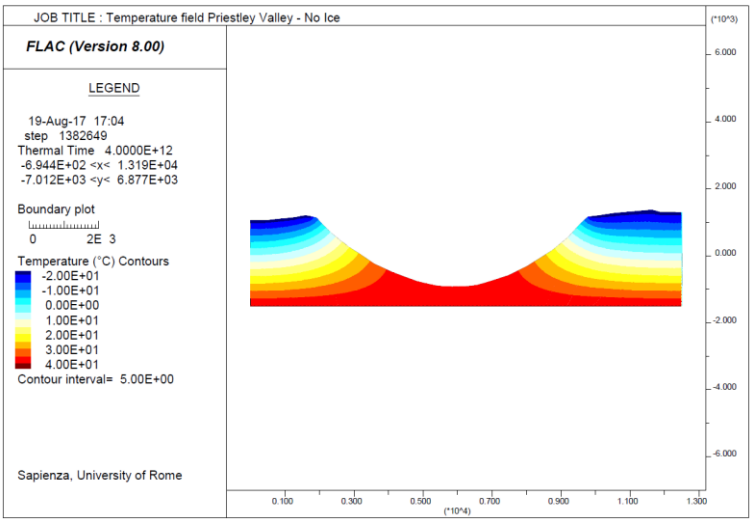

Fig. 79 - Temperature field at steady-state without the presence of the ice-mass.

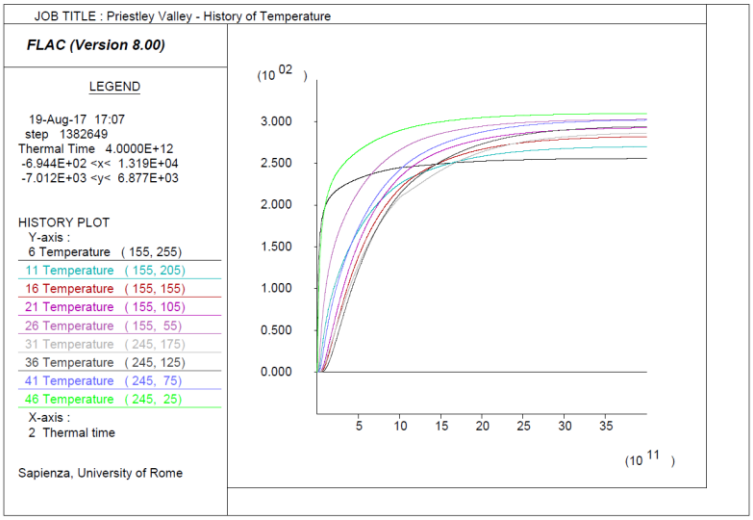

Fig. 80 - Temperature vs. Thermal time curve at different point along two monitored vertical. Absence of ice in the glacial trough. Temperature are expressed in Kelvin.

In a second stage, the presence of a cold glacial mass within the U-shaped valley was established, setting an inner initial temperature condition starting by dimensionless steady-state profiles with no strain heating proposed by (Clarke et al.,

1977). Temperature profiles were defined by parameters θ and ξ which refers to scaled temperatures and scaled heights above the bed, respectively (Fig. 81). Different curves express the temperature profiles at different values of advection parameter (γ), which express the vertical velocity due to advection within the ice mass. Positive values of γ indicate accumulation zone, while the negatives refer to ablation.

Higher vertical velocities, resulting from higher accumulation rates at the surface, increase the thickness of the isothermal zone surficial zone. With higher rates of advection (higher vertical velocities), the heat supplied can warm a smaller fraction of the descending ice, so the whole ice column is colder.

Given the position of the defined cross section, a precautionary transitional behaviour was considered and γ=0 assumed. This profile is consistent with most of temperature profiles derived by Engelhardt et al. since 1993 in WAIS.

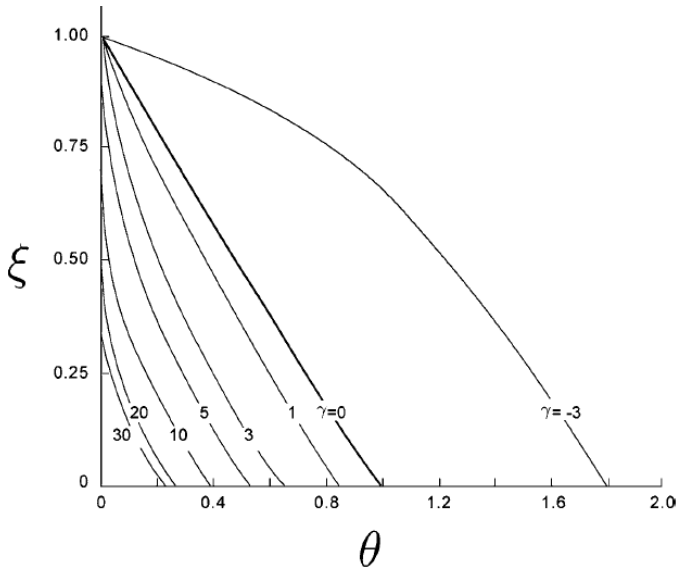

Fig. 81 - Dimensionless steady temperature profiles for various values of the advection parameter (γ). From Cuffey and Paterson, Physics of Glacier, 2010, adapted from Clarke, 1977.

To take into account the horizontal velocity of the ice mass within the glacial trough and consider the continuous renewal of glacial mass, a suite of thermal analysis was conducted considering the transit of ice through the modelled cross section varying the ice velocity.

Ice mass, because of its movement, is continuously in a transient thermal non-equilibrium with the bedrock. The movement of the ice from the ice-sheet to the outlet at various velocity, was represented in the 2D-model by different time duration of thermal calculation, expressing the maximum elapsed time required for "new" ice to move from the accumulation zone (i.e. ice-sheet) through the section. This time represent the maximum time in which the ice mass can be thermalised by geothermal heat flux.

At the arrival of new "cold" mass, the temperature profile was re-initialised according to the above described standard profile (Fig. 82), leaving the mass free to warms up. The duration of this temperature-update time-interval reflects the range of possible velocities of the ice mass. Hence, the faster the ice flow, the shorter was the stationing time within the cross section and thus, in the numerical domain.

The time duration lasted for the renewal of the ice mass was calculated considering the distance of the cross-section from the ice-sheet, under velocity assumption of 0.5, 5 and 50 m/day.

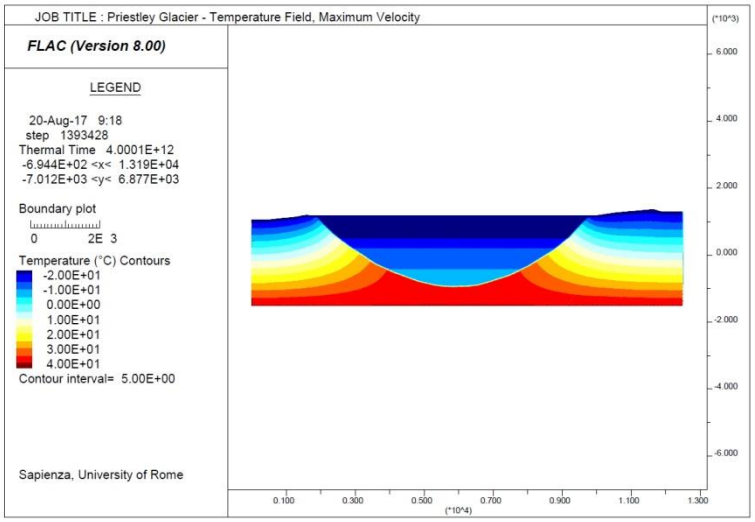

Fig. 82 - Temperature field in glacial valley in presence of cold ice mass moving with the modelled maximum velocity.

The comparison of temperature field derived in the glacial valley in the hypothesis of maximum (Fig. 82) and minimum (Fig. 83) velocity, evidenced the effect

of longer stationing time of the ice masses, which are heated from below by geothermal flux.

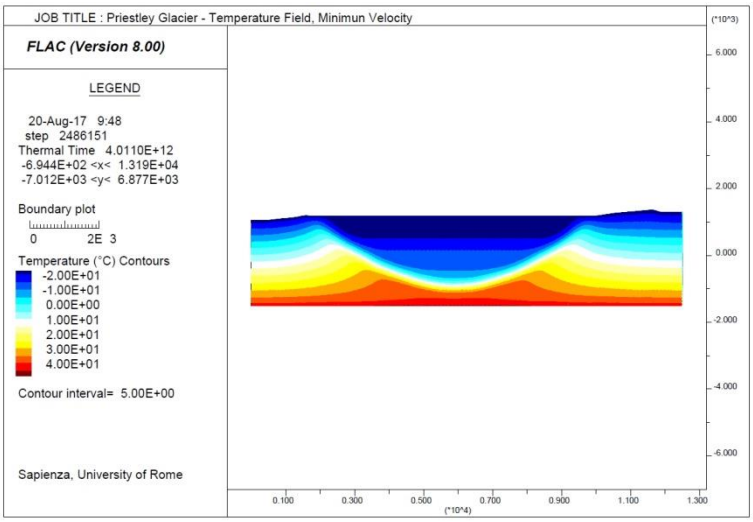

Fig. 83 - Temperature field in glacial valley in presence of cold ice mass moving with a modelled minimum velocity.

In the maximum velocity hypothesis (50 m/day) the ice mass has no sufficient time to warms up and the temperature field appears unaffected by the presence of a cold mass. On the contrary, under minimum velocity (0.5 m/day) the time required for the ice mass to transit through the cross-section is sensibly higher and sufficient to cause perturbation of the isotherms in the wall-rocks (Fig. 83).

To assess the role of geothermal heat flux as possible factor controlling the glacial system response in terms of physic states of the ice, a sensitivity analysis was conducted in the hypothesis of crustal heat flux variations (under 2D-conditions) and transit velocities of the ice. The analysis was conducted to evaluate the role of geothermal heat flux in the documented transition from wet- to dry-based glacier. This preliminary sensitivity analysis was performed with constant geometries in the glacial valley, i.e. under constant glacial loading.

The thermal modelling allowed to evaluate the response of the ice mass to heat flux reductions, evidencing the effects on the thermalisation of the valley. These thermal perturbations could led towards the conditions required for ice pressure-

temperature (P-T) phase transition. To this aim a specific FISH (FLAC®) script able to check the P-T melting conditions was defined, imposing transition thresholds in agreement with the phase diagram of water (Kamb, 1965). To visualise the regions where melting occurred, an indicator parameter was arbitrarily fixed.

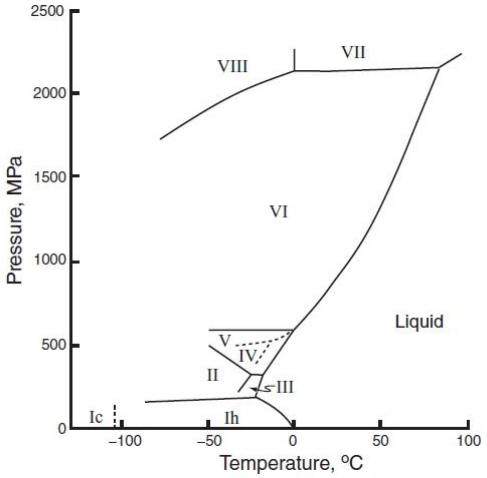

Fig. 84 - Phase diagram of water, after Kamb, 1965.

The parametric analysis was performed for the velocity hypothesis above mentioned, under initial heat fluxes of 120 and 90 mW/m², giving solution to three distinct ice velocities (Fig. 85). The heat flux was then reduced from the initial values to 90, 70 and 50 mW/m² respectively, according to the resolving scheme reported in Fig. 85.

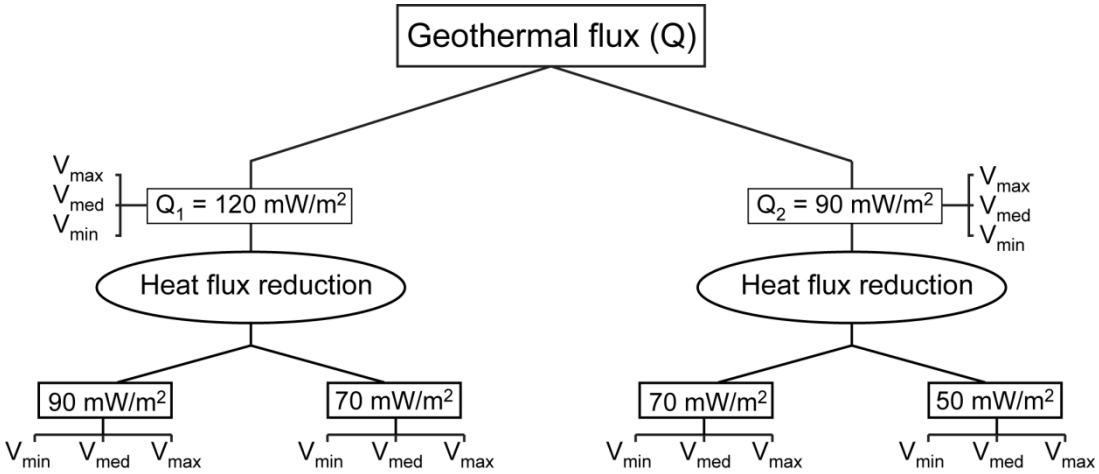

Fig. 85 - Flow chart of geothermal heat flux sensitivity analysis under various ice mass velocity.

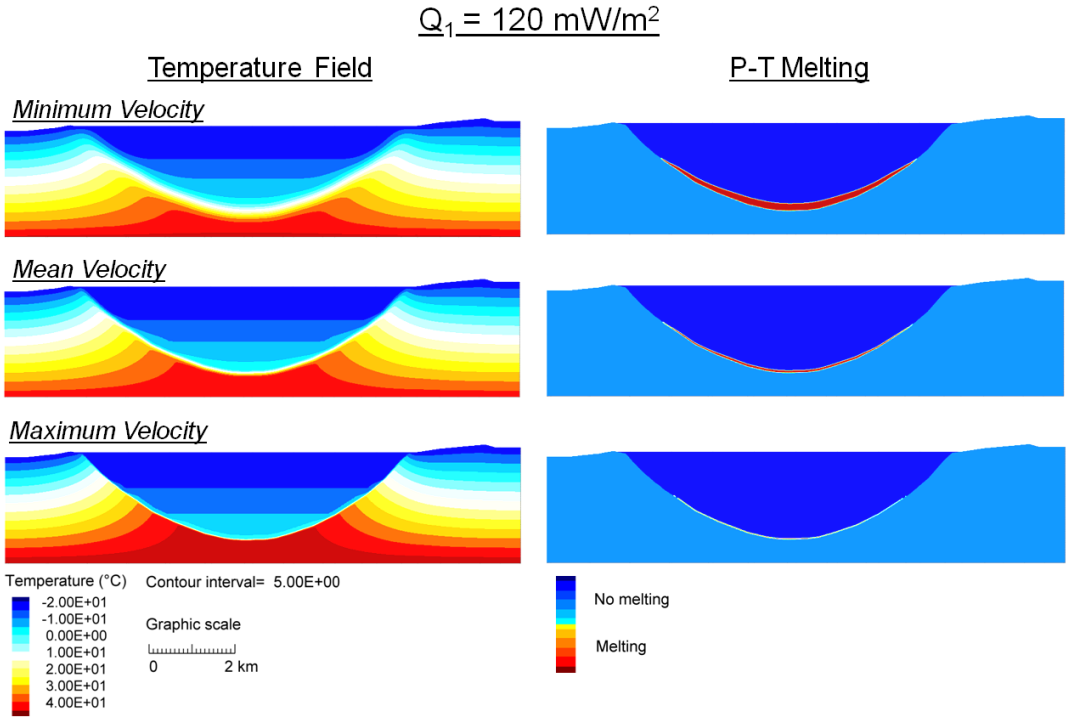

Fig. 86 - Temperatures field contour under initial heat flux Q_1=120mW/m² for three velocity hypotheses. P-T melting distribution at glacier base is reported.

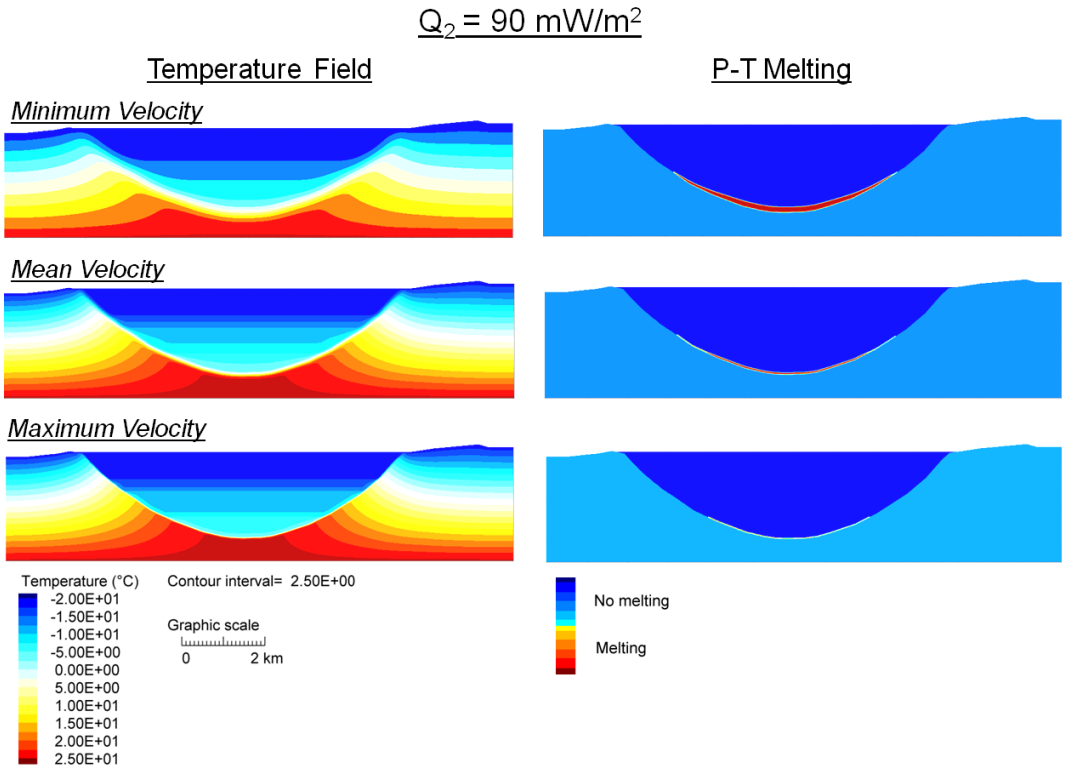

Fig. 87 - Temperatures field contour under initial heat flux Q_2=90mW/m² for three velocity hypotheses. P-T melting distribution at glacier base is reported.

The performed analysis highlights the close relation between ice velocity and thermalisation of the valley, showing a linearity between transit-time and heating of both ice and rock masses.

For both the geothermal heat flux assumed as initial condition, the temperature distribution in depth is able to cause melting at the base of the ice mass, which volumes increase (defined as area×unitary length) at decreasing velocity (Fig. 86, Fig. 87). The contour plots also show higher temperature as the heat flux increases, supporting the (conceivable) effect of thermal perturbation on the slope system (Fig. 87).

The heat flux was then reduced from the initial values of 120 and 90 mW/m² of two steps, respectively towards 90 and 70 mW/m² for the first (Fig. 88), and 70 and 50 mW/m² for the latter (Fig. 89). The reduction of geothermal heat flux from 120 to 90 mW/m², is high enough to cause the transition from wet to dry based glacier only for velocity greater than 5 m/day, because the continuous fast renovation of ice mass

makes the heating too slow to cause melting. At minimum velocity, in fact, a reduction of heat flux of only one step (from 120 to 90 mW/m²) is not sufficient to induce ice phase transition (Fig. 88). To ensure the transition from wet- to cold-based glacier a consistent reduction of the heat flux to 70 mW/m² is required (right side of Fig. 88).

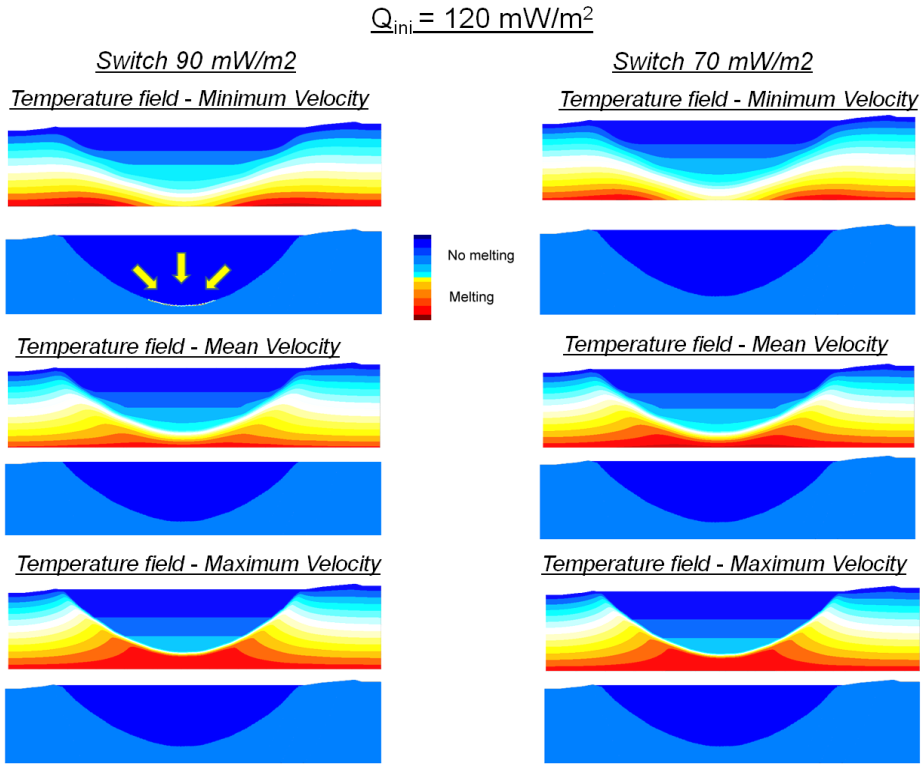

Fig. 88 -Temperatures field and melting conditions deriving by the heat flux reduction from 120 mW/m², under varied ice velocity conditions. P-T melting conditions was still verified under 90 mW/m² and minimum ice velocity conditions.

Starting from initial heat flux of 90 mW/m² the phase transition occurred in all the heat flux reduction and velocity hypothesis (Fig. 89), suggesting that the derived variation in thermal flux represent the minimum perturbation required to cause phase transition at base of the glacier.

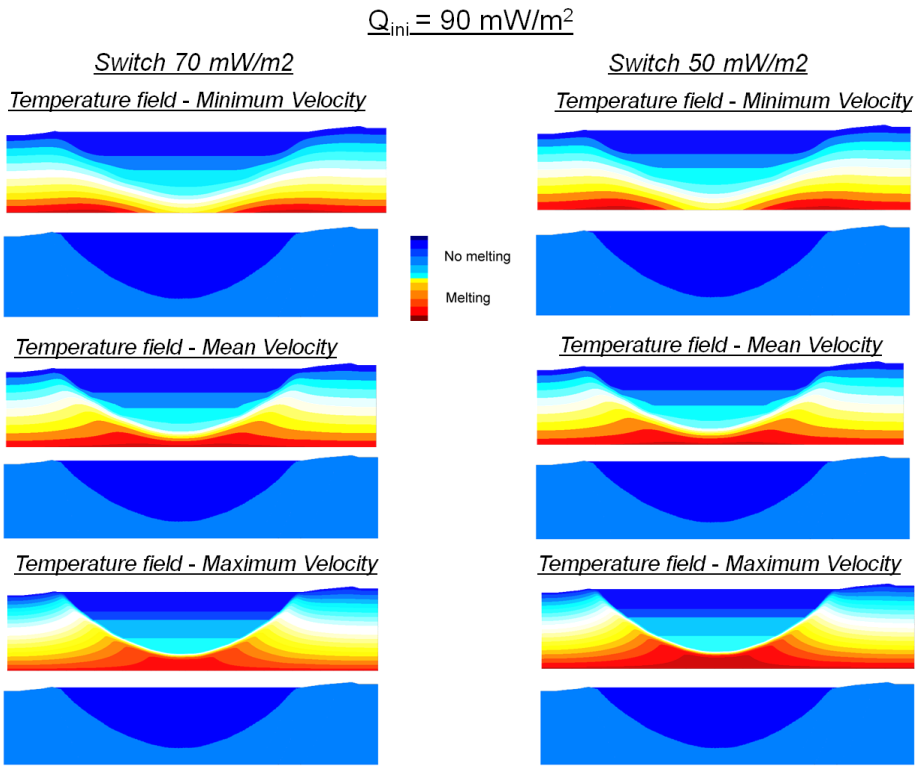

Fig. 89 - Temperatures field and melting conditions deriving by the heat flux reduction from 90 mW/m², under varied ice velocity conditions.

After the switch from high to lower heat flux conditions, the analysis was continued until the achievement of new thermal equilibrium. During the period elapsed until the reaching of a new steady-state, the temporal profiles within the glacial mass were continuously re-initialised, as evidenced by the sawtooth-like curve derived by time-history of temperature within the glacier (Fig. 90).

The heat flux contribution can be deduced by the analysis of Time-History of temperatures for two point located inside and below the ice mass (Fig. 90). The effect on temperatures induced by heat flux reduction from 120 mW/m² to 90 and 70 mW/m² is clearly shown by curves, which evidence a marked decay of temperature for the major heat flux reduction (orange curve on Fig. 90). Only for a decrease of heat flux down to 70 mW/m², the temperature curve of ice (grey line) decrease below the P-T melting conditions (dashed red line on Fig. 90).

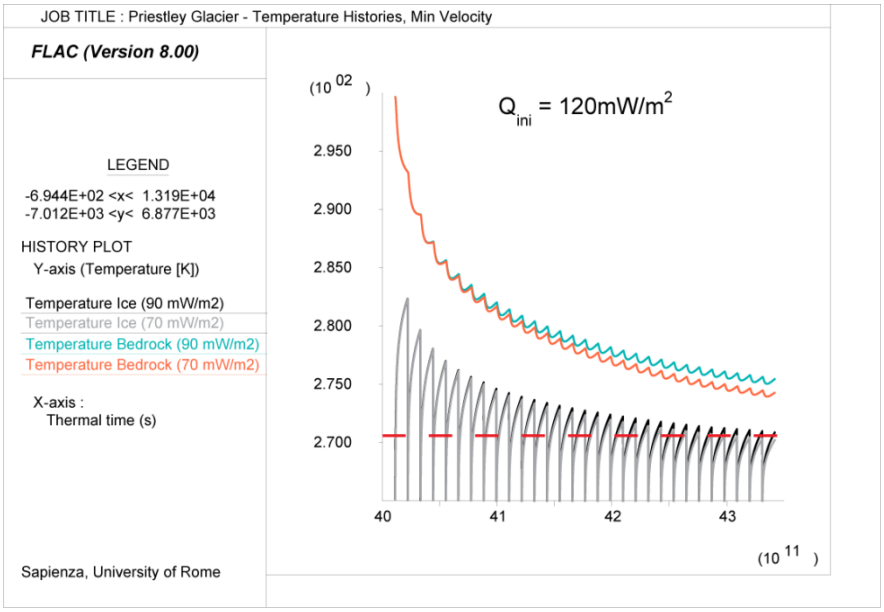

Fig. 90 - Time-history of temperature for two point located inside (coloured curves) and below (gray scale curves) the ice mass. The curve indicates the effect on temperature induced by heat flux reduction from 120 mW/m² to 90 (light blue line) and 70 (orange line) mW/m². The sawtooth signal indicates the continuous initialisation of temperature profile in the glacial mass. Only for a decrease of heat flux up to 70 mW/m² the temperature curve of ice (grey line) decrease below the P-T melting conditions (dashed red line).

Under such a hypothesis it can be deduced how reduced variation of geothermal flux might be responsible for sensible thermal perturbation at the base of the glacier and within the rock mass. Such behaviour can control the physic state of ice influencing the glacial dynamics and potentially controlling the gravitational effect on slope enhancing slope instabilities. The derived values for geothermal heat fluxes required for ice melting at glacial base are in good agreement with the magnitude of thermal perturbations inferred by Seroussi et al., 2017 as direct consequence of volcanism in the West Antarctic Ice Sheet (WAIS).

The numerical thermal analysis was then extended to the entire temporal evolution of the valley system, by the reproduction of the defined morpho-evolutionary model and the modelling of thermal effects induced by advance and retreat pulses of the Priestley glacier.

To this aim, the evolution of the Priestley glacier was transferred in the numerical domain by imposing temporal and geometric variations in a time-span of couple of hundreds of thousands of years.

The morpho-evolutionary model reported in Fig. 35 was transposed in thermal model in FLAC® 8.0 environment, keeping constant the geothermal flux applied to the lower boundary of the domain, and assuming invariant climatic conditions at the top of the model.

The thermal model of the valley evolution was reconstructed for the last 1.2 Ma, assuming a thermal time-step duration of 3×10^6 s, maximum value to ensure numerical stability of thermal calculation.

The glacial advance or retreat phases derived by the definition of morpho-evolutionary model were summarized in Fig. 91, where the geometric variation in the main stage are expressed as stationing elevation (in m a.s.l.) of the glacier within the valley. The effect of glacial perturbation on the thermal evolution of the rock slopes can be derived by the analysis of temperature time-histories derived by monitoring points located below the valley bottom within the bedrock, along two monitoring verticals (indexed at nodal point i=245 and i=335; Fig. 92). The position of monitoring point was defined according to the isotherm distribution.

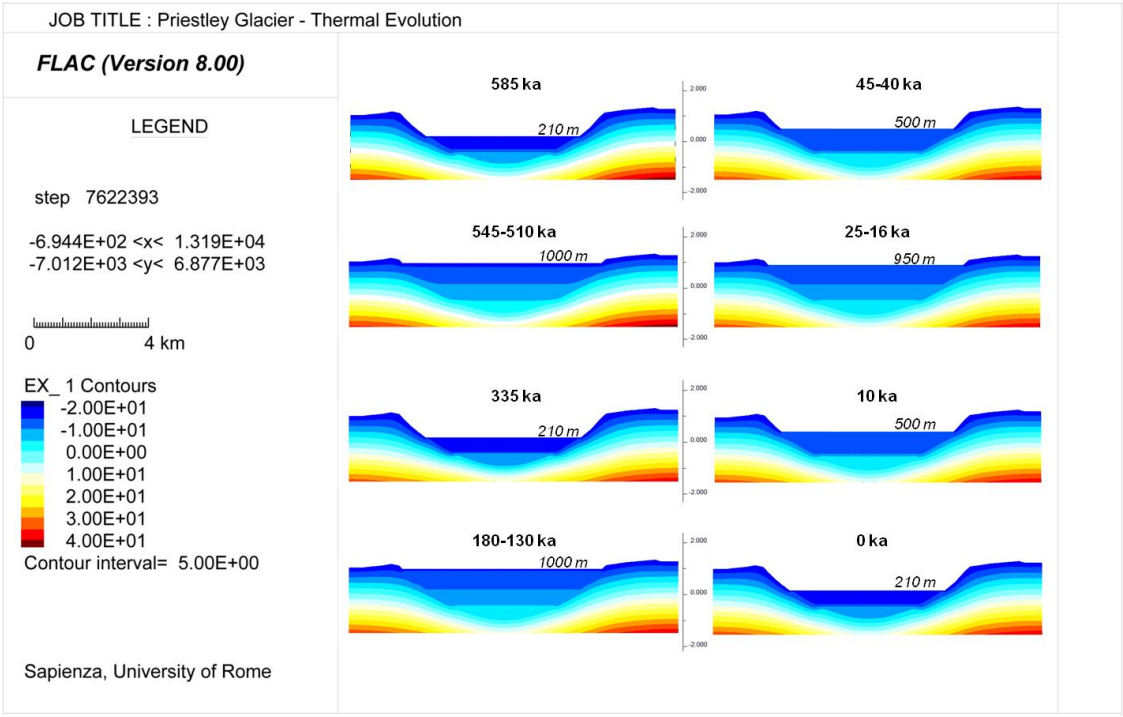

Fig. 91 - Thermal evolution of the Priestley Glacier valley during the main exemplary stage of advance and retreat reconstructed by morpho-evolutionary model. Elevation in m a.s.l.

The most surficial points (black and grey curves) show significant temperature variations induced by the pulsation of the glacier, which reflects in temperature decrease as the ice becomes thinner and the cold upper boundary condition moves downward. The point closest to the glacier is also affected by the continuous thermal fluctuations introduced to simulate the movement of glacial mass through the section (inlayer in Fig. 92). As depth rise, the temperature variations induced by the pulsation of the glacier, becomes progressively smaller (couples orange-light blue and green-red), reducing up to variation limited within 1-2 °C at elevation approximately 1500 m below the ice mass (purple curve) (Fig. 92).

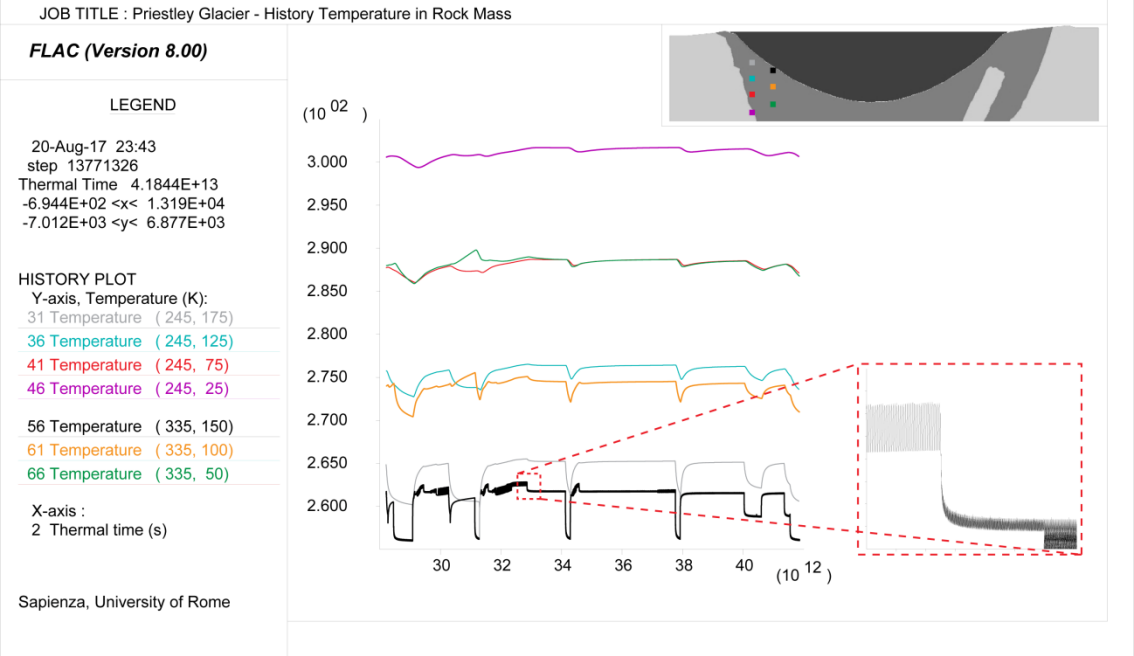

Fig. 92 - Temperature time-histories derived by monitoring points within the rock mass, below the valley bottom. Temperature are referred to two monitoring verticals (i=245 and i=335) respectively located farther and closer to the ice mass. Each curve represents the temperature conditions of different point (represented by the same colour) located at different depth and position in the cross-section.

The temperature variations derived at the deepest monitoring point allow to assert that the thermal effects induced by the presence a glacial "cold" mass are not limited to shallow depth, constraining, given all the specificity of the case study, the maximum depth of resentment to 1500 m below the base of glacier.

6.2.3. 2D Elasto-plastic and visco-plastic sequences

In order to evaluate the mechanical response of the slope system to glacial thickness variation as well as regional and local thermal perturbation, elasto-plastic and visco-plastic multi-stage sequences were modelled by the results of laboratory characterisation and geomorphological and chronological investigations.

With the same geometries defined in FLAC for thermal modelling, the numerical domain was set in mechanical configuration and an infinite half-space assumed. Horizontal displacements were avoided along the lateral boundaries, while

both vertical and horizontal displacements at the base of the numerical domain were avoided. An initial static equilibrium was reached under perfectly-elastic conditions by applying the gravitational acceleration. An elasto-plastic static equilibrium was secondarily reached by attributing a Mohr-Coulomb constitutive law, updating elastic moduli by FISH scripting as function of the lithostatic loads (Fig. 93). Strength and deformability parameters adopted in stress-strain numerical modelling for Antarctic case study are reported in Annexed Tables 3 and 4.

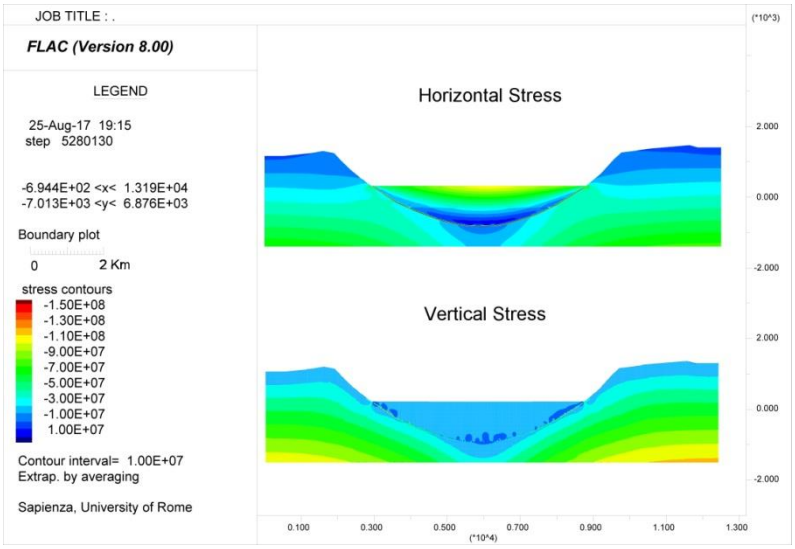

Fig. 93 - Vertical and horizontal stress contours derived for the Priestley glacier valley.

The morpho-evolution of the system was reconstructed in a sequential scheme by reproducing discrete geometric variations within the model. These variations were assumed to be reached instantaneously, therefore assuming that morphological variation occurred in a time period sufficiently short to lead viscous and thermal processes to evolve under constant boundary conditions.

The vertical and horizontal displacement cumulated at the end of the modelled morpho-evolution of Priestley Glacier show a maximum vertical component of about 7 m on ridges bounding the valley system (Fig. 94). The contour of horizontal displacement shows negligible effects on slopes, with a maximum of horizontal deformation below the base of glacial valley (Fig. 94). No plasticity occurred in the model under elasto-plastic conditions.

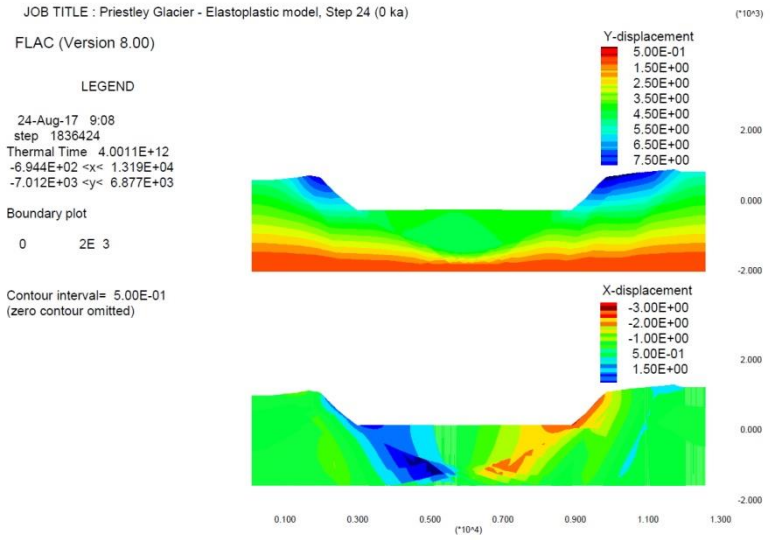

Fig. 94 - Vertical (Y) and horizontal (X) displacement derived by elasto-plastic model.

With the same approach adopted for the Ischia case study, the effect of time-dependent deformation was computed by assuming a visco-plastic rheological model. Given the lacks of literature data about viscosity, the rock mass parameters was assumed with regards of the involved lithologies, considering rheological parameters derived by back-analysis of slope-scale gravitational deformation (Bozzano et al., 2016; Della Seta et al., 2017; Esposito et al., 2013). Two series of analysis was conducted in the range of viscosity between 10^{21} and 10^{22} Pa·s.

The introduction of a Burger-creep rheology led to considerable deformation in the rock slopes, directed towards the valley and located above the actual glacial trimlines. Under viscosity hypothesis of 10^{22} Pa·s, it doubles the ones resulted by elasto-plastic model, covering a larger volume enveloped by circular shaped geometry.

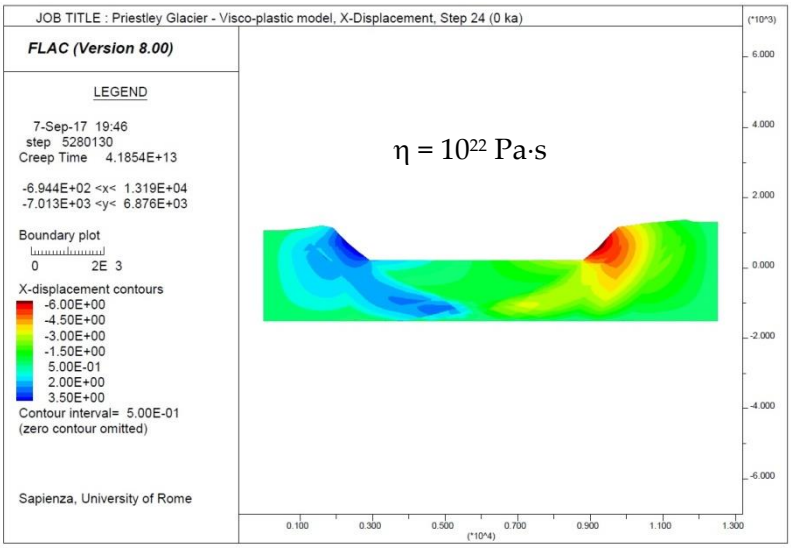

Fig. 95 - Horizontal displacement contour plot derived by visco-plastic model at the end of the modelled time-sequence (step 24). Viscosity hypothesis of 10^{22} Pa·s.

Under lower rock mass viscosity, the deformations within both slopes reached an order of magnitude greater involving progressively deeper zone located below the glacial valley bottom (Fig. 96). Vertical displacements compensated the horizontal strain of slopes, by a maximum displacement of 15 m. Although no plasticity occurred even under this rheological condition.

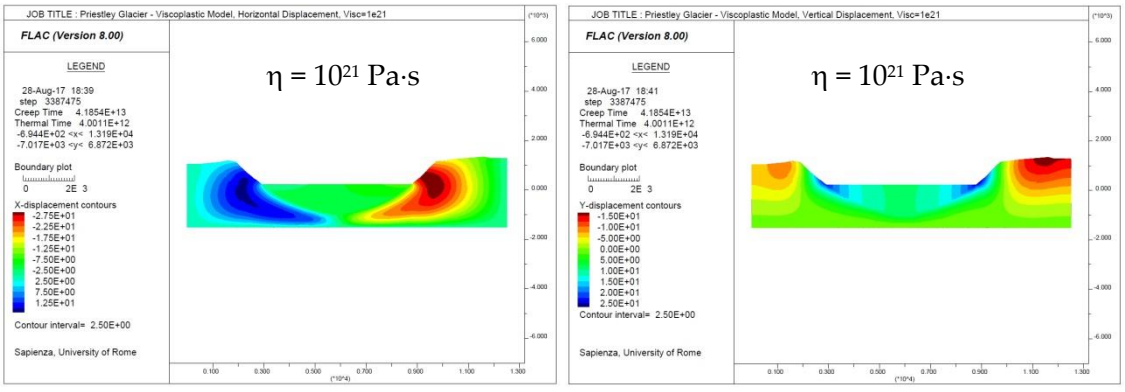

Fig. 96 - Horizontal (left) and vertical (right) displacement contour plot derived by visco-plastic model at the end of the modelled time-sequence (step 24). Viscosity hypothesis of 10^{21} Pa·s.

Time history of horizontal displacement along the hydrographical right bank of the glacier (left of the model) evidenced the creep-like deformative evolution of the slopes, which, after an initial stage of elasto-plastic deformation, evolved diminishing the strain rate up to a minimum. As the secondary stage begins, strain rate becomes constant and deformations evolves in a steady state, perturbed only by pressure

variations related to the morphological evolution of the valley (Fig. 97). This pattern is evidenced even at lower viscosity at higher strain rates (Fig. 98).

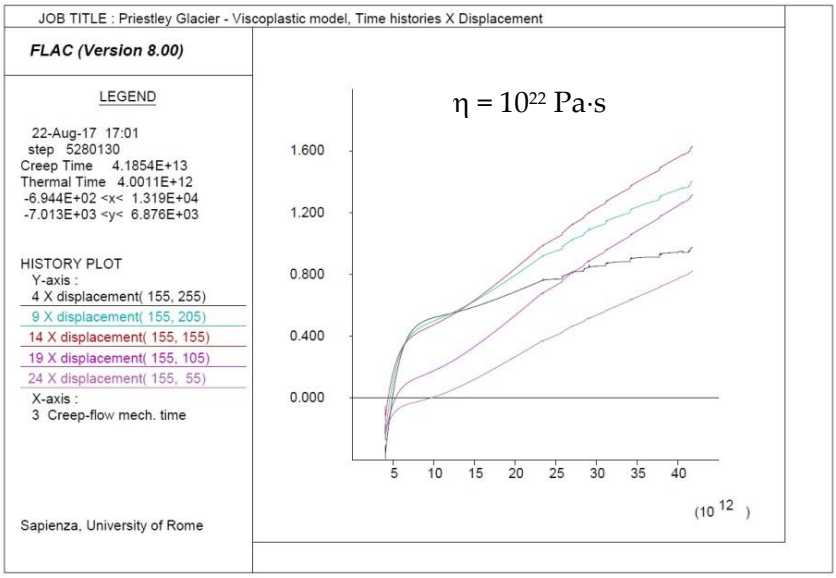

Fig. 97 - Time histories of horizontal displacement (X-disp) derived along monitoring vertical on the left slope of the model. Typical creep-like curves were obtained. Viscosity hypothesis of 10^{22} Pa·s.

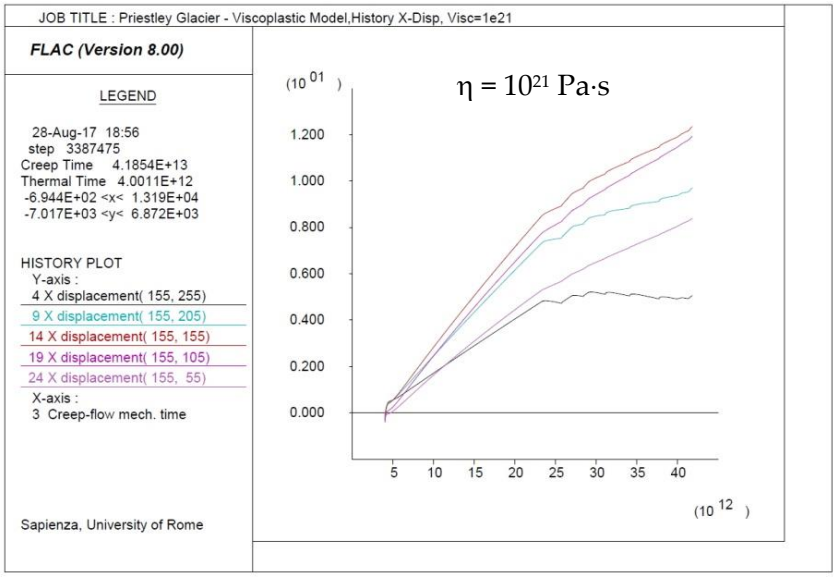

Fig. 98 - Time histories of horizontal displacement (X-disp) derived along monitoring vertical on the left slope of the model. Typical creep-like curves were obtained. Viscosity hypothesis of 10^{21} Pa·s.

6.2.4. 2D Thermo-mechanical modelling of Priestley Glacier valley

The numerical analysis conducted was then extended to the evaluation of thermo-mechanic effects deriving by the combination of regional heat flux and local thermal anomalies due to the presence of a glacial "cold" mass.

The thermo-mechanic model was derived starting from the results of visco-plastic model, reproducing at the same time the 2D-thermal evolution of the Priestley glacier previously discussed.

The analysis of thermal state of the system clearly evidenced the continuous thermal non-equilibrium between the bedrock and the glacial mass. The continuous transitory state of the system is also confirmed by the temperature time-histories reported in Fig. 92, demonstrating that after fast morphological (and thermal) variations the rock mass does not always have enough time to reach a new stationary equilibrium (evidenced by flat portions of temperature vs. time curves).

Because of the transitory features of the forcing actions in the observation time-window, given the time-scale of evolution of thermal process, a statement of quasi-stationarity in the modelled system cannot be assumed, therefore a fully coupled analysis is required.

In the adopted coupled analysis, each discrete stage of the numerical analysis thermal and mechanical fields evolved continuously and relative constitutive relations of both physics were considered at the same time (Fig. 5).

Thermo-mechanic modelling was conducted under two regional heat flux conditions (70 and 90 mW/m^2) under the viscosity hypothesis assumed in visco-plastic creep models (10^{21} and 10^{22} Pa·s).

The comparison of thermo-mechanic and visco-plastic sequence evidenced the presence of high deformations induced by temperature gradients and thermal expansions effects, directly related to the consideration of geothermal and local glacial

thermal perturbations. These thermally-induced effects enucleated below the minimum level of ice stationing (210 m a.s.l.) (Fig. 99), where higher horizontal thermal gradients exist. As confirmed temperature field contours, isotherms converge to the centre of the valley producing the highest temperature horizontal gradients (Fig. 83), able to induce significant horizontal thermo-mechanic deformations. Such deformation contours are divergent from the centre of the valley (Fig. 99), contrary to what observed by visco-plastic modelling where positive (right directed) and negative (left directed) deformation occurred on left and right slope of the model, respectively (Fig. 95).

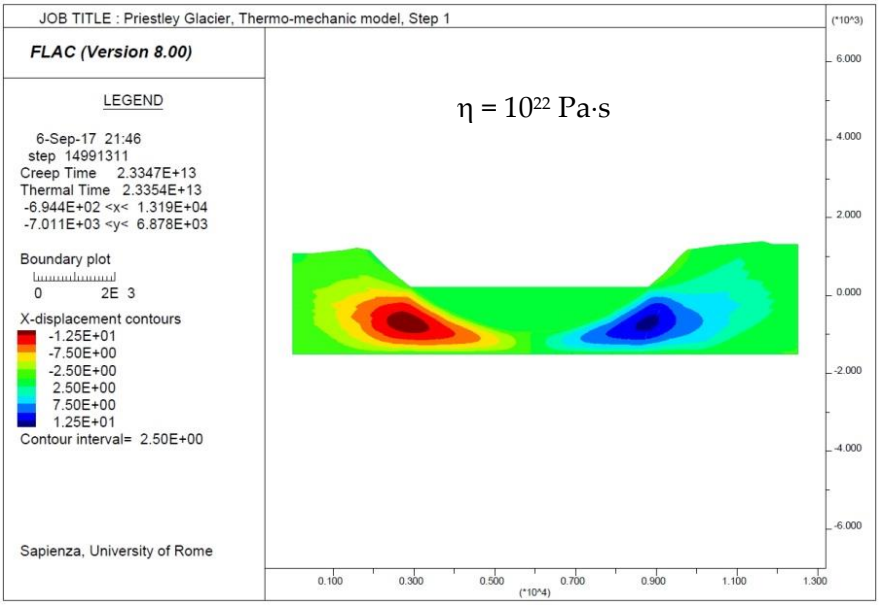

Fig. 99 - Horizontal displacement contour under thermo-mechanical modelling assumptions. The contour map, oppositely to what observed by temperature-independent visco-plastic modelling, shown two maximums of deformations divergent from the centre of the valley related to thermo-mechanic effects, and able to mask creep deformations. Viscosity hypothesis of 10^{22} Pa·s.

At higher viscosity (10^{22} Pa·s), where time-dependent creep deformation remain limited, thermo-mechanic effect induced by the stable presence of a cold mass and significant geothermal gradients, appear predominant and able to mask the creep-deformation (Fig. 99). This effect was ascribed to thermal expansion effects which, below the glacial base level, cumulated deformation up to 10 m in the horizontal direction where consistent horizontal thermal gradients exists.

Comparison of time-series of horizontal displacement along the left slope of the model confirm this behaviour, evidencing the inverse trend of deformations induced by thermal interactions in the rock mass. Under higher viscosity values (10^{22} Pa·s), thermal expansion led to considerable displacements, becoming greater than gravity-induce deformations, which, at such depths, appeared masked by thermally induced deformations (Fig. 100). Negligible influences have been proved in horizontal displacement within the upper slope, where isotherm contours are parallel to the uppermost surface and thermal fluxes are vertically oriented (Fig. 99).

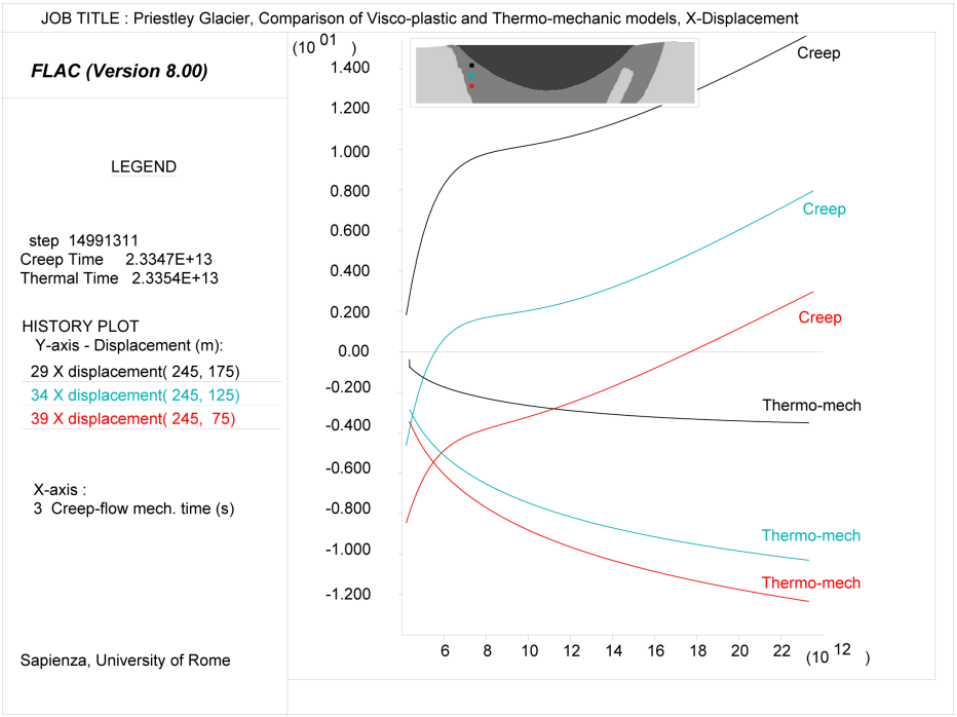

Fig. 100 - Comparison of time histories of horizontal displacements at different heights along the left slope of the glacial valley under visco-plastic ("Creep" curves) and thermo-mechanic ("Thermo-mech" curves) modelling assumptions. Viscosity equals to 10^{22} Pa·s.

On the vertical direction, instead, Y-displacement contour plot relative to the upper part of slopes bounding the glacial valley (Fig. 101), clearly shown the role thermo-mechanic effects in slope deformation and evidencing incremental displacement over time in the initial stage of creep processes. These displacements have been cumulated along the vertical component, aligning with the direction of thermal flow, as result of thermal expansions perpendicular to the isotherms.

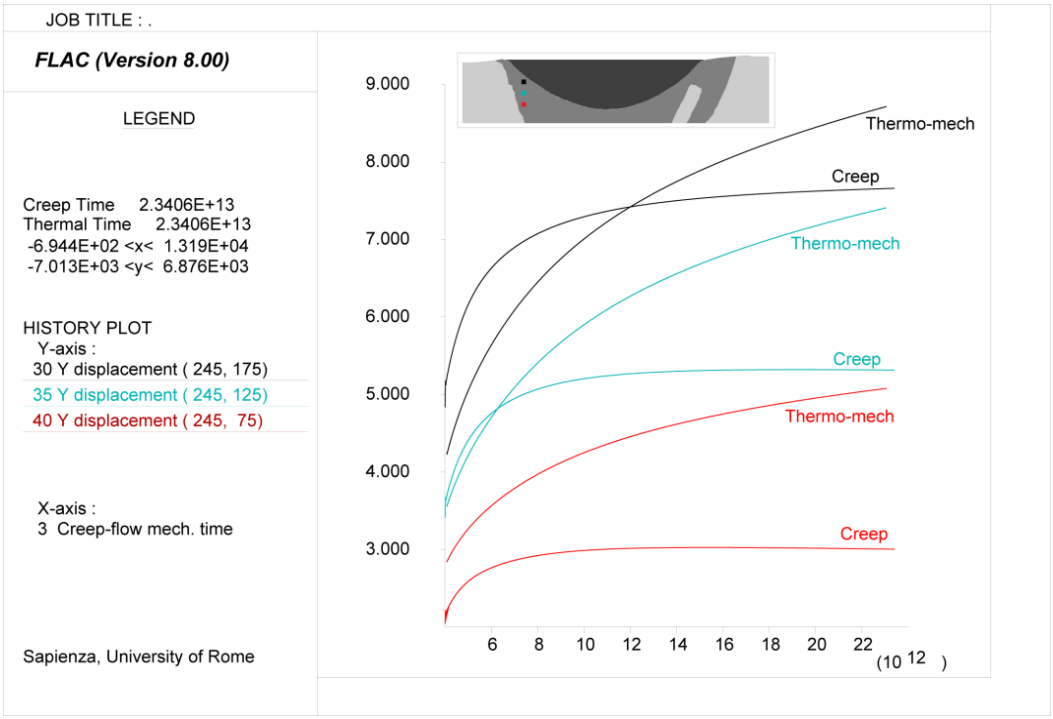

Fig. 101 - Comparison of time histories of vertical displacements at different heights along the left slope of the glacial valley under visco-plastic ("Creep" curves) and thermo-mechanic ("Thermo-mech" curves) modelling assumptions. Viscosity equals to 10^{22} Pa·s.

As viscosity decreased, creep deformations reached orders of magnitude of tens of meters (Fig. 102), confining thermo-mechanical effects induced in the upper slope to a secondary role in the cumulated slope deformations. In both slopes, above the stationing level of ice, gravity-induced deformations with maximum of approximately 9 meters were reached, with direction of movement towards the centre of the valley and opposite to the deep thermally induced deformations (Fig. 102).

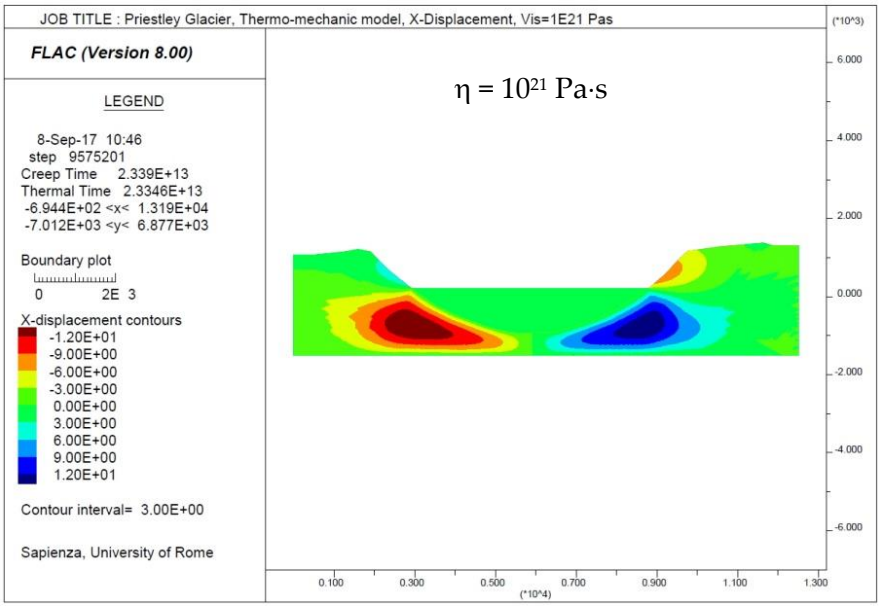

Fig. 102 - Horizontal displacement contour under thermo-mechanical modelling assumptions. The contour map, oppositely to what observed by temperature-independent visco-plastic modelling, shown two maximums of deformations divergent from the centre of the valley related to thermo-mechanic effects. Under lower viscosity hypothesis (10^{21} Pa·s) creep horizontal deformation in the upper slope growth directing toward the centre of the valley.

Under lower viscosity hypothesis, at the same monitoring point, after an initial stage where thermal expansion (i.e. negative displacement on left slope of the model) prevailed, visco-plastic creep deformation becomes predominant, overcoming the thermally induced deformations and reversing the direction of movement. The creep deformations remain in stationary creep (Fig. 103).

The presence of a local thermal perturbations due to the glacier ice represents the main conditioning feature respect to the regional variations of heat fluxes variations, which even though capable of condition the physic-state at the base of the glacier, are not sufficient to invoke considerable thermo-mechanic effects.

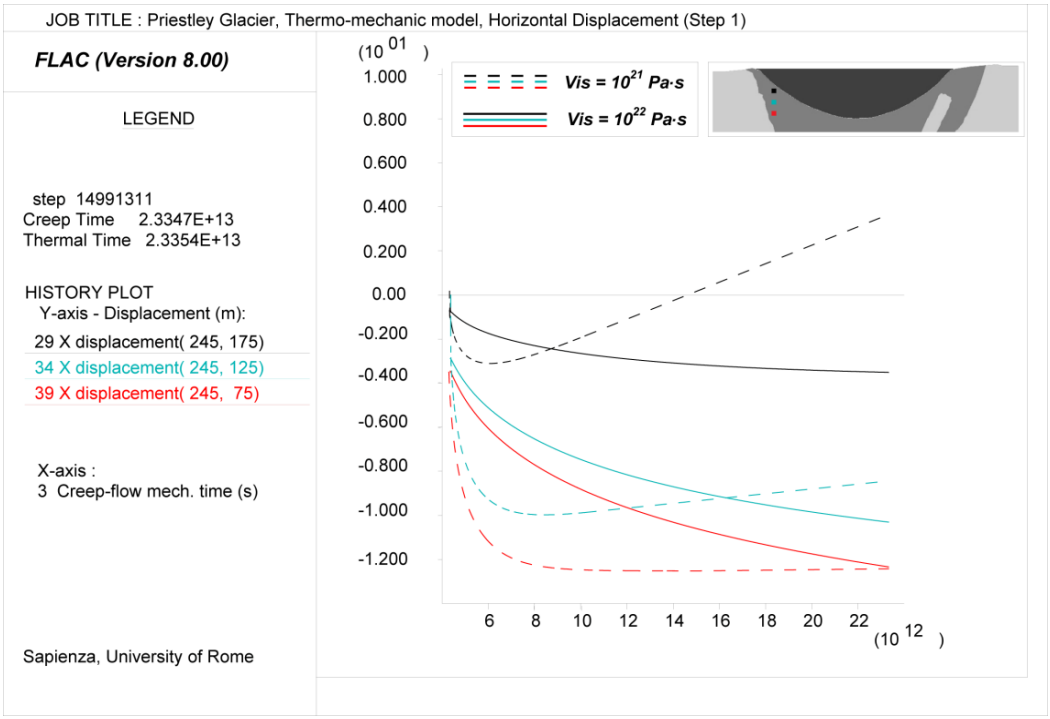

Fig. 103 - Comparison of time histories of horizontal displacements at different heights along the left slope of the glacial valley derived by thermo-mechanic modelling under viscosity values equals to 10^{21} Pa·s (dashed curves) and 10^{22} Pa·s (solid curves).

The comparison between two heat flux hypotheses under constant viscosity, revealed how the variation of regional heat flux appear irrelevant for thermo-mechanic effects. Temperature differences induced in bedrock by heat flux variations are in fact limited in a couple of tens degrees, and unable to influence the deformation pattern within the slope (Fig. 104).

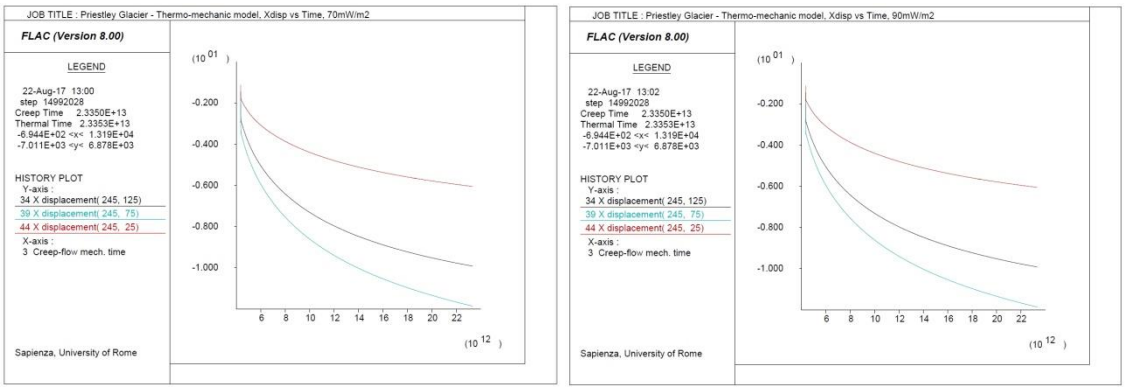

Fig. 104 - Time-histories of horizontal displacement derived by thermo-mechanical model of the Priestley glacier valley under geothermal heat flux hypothesis of 70 (left) and 90 (right) mW/m². Viscosity hypothesis of 10^{22} Pa·s.

6.2.5. Salient features of the Priestley Glacier case study

The Antarctic region experienced variations of geothermal heat fluxes as consequences of its geodynamic history and related volcanism. Furthermore, the simultaneous occurrence of glacial conditions has made the case study functional to the research.

In order to compute the role of deep geothermal perturbations on shallower slope systems (i.e. in this case an entire valley system) similarly to the "warm" case study (see Chapter 5.1.) a combination of multiple model at different scales was adopted (Fig. 105). Starting from a 1D-log representative of the Northern Victoria Land crust, a parametric analysis on deep thermal perturbation was conducted back-analysing the geothermal flux calculated as output. The solution was reached by a single-physics solution (Fig. 105) assuming pure conductive heat transfer under steady-state conditions.

The output of 1D thermal model was applied as boundary conditions to the 2D thermal model of the valley system, imposing a constant output heat flux to the shallow system. The 2D model was resolved by transient analysis, simulating by a multi-stage sequential modelling the temporal evolution of the glacial system over the last 1.2 Ma. This evolution was summarised in a sequential morpho-evolutionary model, which constrained the stationing position of the ice mass in the valley and supported the timing of morphological and thermal variations (i.e. stages) to be modelled.

Starting from the defined morpho-evolutionary model, a sequential mechanical modelling was performed under elasto-plastic and visco-plastic behaviour. Both models converged for the definition of a 2D Thermo-mechanical model.

The 2D thermal model highlighted how after fast morphological variations the system does not have enough time to reach a steady state conditions. Because of transiency of the systems after glacial fluctuations, given the observation time-window

of analysis (i.e. minimum time-range within gravitational processes can evolve), a steady state assumption cannot be done for the multi-physical modelling. From these statements results the choice of fully coupled solution for thermo-mechanical model.

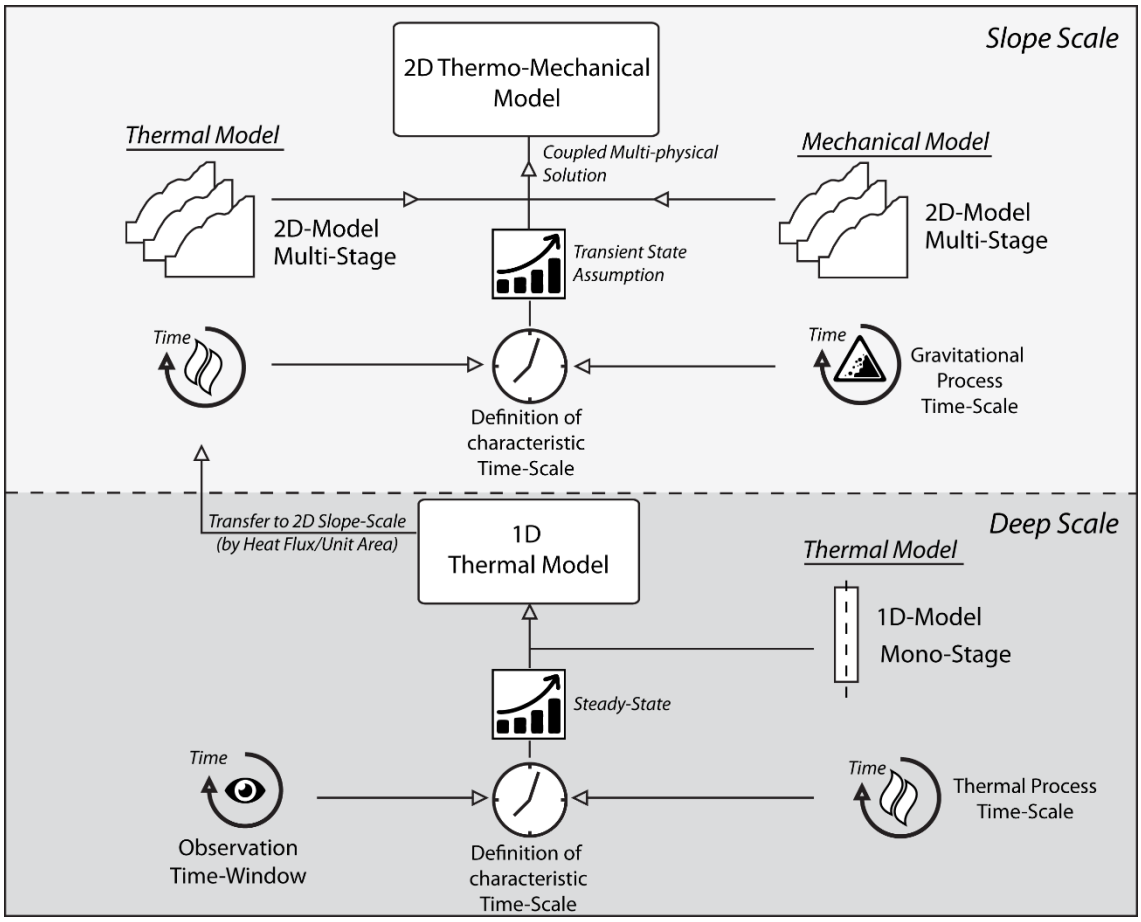

Fig. 105 - Summary flow chart of multi-physical numerical modelling performed for the Antarctic case study.

For this case study the combination of deep crustal model and valley-slope model was adopted to evaluate the heating conditions perturbing the glacial systems, deriving the total heat flux to be applied to the slope-scale model. Because single physical process was considered in the deep scale modelling, no multi-physical couplings were considered.

The coupled solving scheme adopted to reproduce transient thermal states during the sequential morpho-evolution of the glacial valley, allow to reproduce

thermo-mechanical interactions in valley-slopes related to both geothermal and local perturbations due to the presence of the glacial mass.

The numerical modelling required memory-intensive and long-lasted calculations, making too heavy the coupled solution over time-interval greater than hundreds of thousands of years. For this reason, on such wide time-interval, a steady-state assumption must be accepted and uncoupled solutions preferably adopted.

7. Inferences from modelling results

The results derived for the two selected case studies clearly evidenced the role of thermal fields on slope-scale deformations, showing peculiar characters depending on the specificity of the involved systems.

In particular, the analysis of thermo-mechanic effects induced by regional heat flux as well as the presence of local thermal anomalies highlighted the role of thermal perturbations in the entity and spatial distribution of gravitational deformations, which appear controlled by the temperature distribution in the slopes.

Thermo-mechanic effects resulted non-negligible respect to the intensity of slope deformations, which appear more relevant at higher viscosity, where low strain rate occur. In time-dependent analysis under wide time-scale, in fact, creep deformations are predominant and thermo-mechanic effects becomes negligible.

Because no proper thermo-mechanic effects on mechanical and rheological parameters deriving by thermal degradation were considered, strain rate remains unaffected by thermal dilation. The amount of thermally-induced deformations was ascribed to be related to elasto-plastic deformation, or confined in the primary stages of creep deformations.

The role of thermo-mechanic interaction in the evolution of DSGSD was approached and tested by the application of multi-physical approach, through the definition of a combination of multi-scale models (i.e. deep crustal scales and shallow slope scales), able to define inner forces or boundary conditions to be applied to the slope system.

This cascade of modelling represented a key factor to manage model of natural systems evolving at different space- and time-scales, allowing to combine models of deep thermal or hydrothermal systems at steady state, with transient processes acting on at slope scale.

The proposed multi-physical approach based on the definition of intermediate thermal, hydrodynamic and mechanical models, supported by field-surveys and laboratory investigations. The multi-physical models, designed according to the peculiarities of case studies, both have examined the sensitivity of the systems (deep or shallow) to variation of physical state parameters, as well as to inner or boundary conditions.

In both cases, the numerical analysis started from the definition of a simplified model of the deep systems. On this model sensitivity analysis on parameter or external conditions were performed, trying to validate a model representative of the conditions existing in the past, in which gravitational process could have evolved. To this aim, the validated solutions were transferred to slope-scale, in which parametric analyses was performed on mechanical and rheological parameters. In these parametric analyses, the temporal evolution of gravitative processes was assessed, trying to back-analyse the ongoing processes on the basis of the reconstructed engineering-geological and conceptual models (e.g. Ischia case study). For the Antarctic case study, this kind of back-analysis was not carried out because of lacks data suitable for validation.

The numerical analyses, once validated, can be extend to the future, analysing possible evolution over time of ongoing processes maintaining unaltered boundary conditions (i.e. Forward analysis), or assessing future physically-based scenarios deriving by changes of internal forcing (i.e. Scenario analysis) (Fig. 106).

Different present-scenarios can be derived simulating the evolution of the system since the past, considering different parameters or physical conditions (e.g. ones resulting from performed sensitivity analysis). Solutions retained inadmissible for the back-analysis of ongoing processes can be used to perform analysis of scenario (e.g. extreme thermal condition in Ischia hydrothermal system), extending from the past to the future the sensitivity analysis.

Several scenarios, deriving by different parameters or physical conditions, were defined assuming variations acting on either deep-scale (e.g. crustal geothermal fluxes) or slope-scale (e.g. ice velocities in glacial valleys) (Fig. 106).

Physical variations affecting the evolution of deep-scale processes in the past, can results at present-time in new deep scenario which must be transferred to slope-scale to assess their effects on gravitational deformations, and then, eventually, ponder future scenarios (Fig. 106). Future-scenarios of the only deep-scale models were not evaluated because not of interest for slope stability topics.

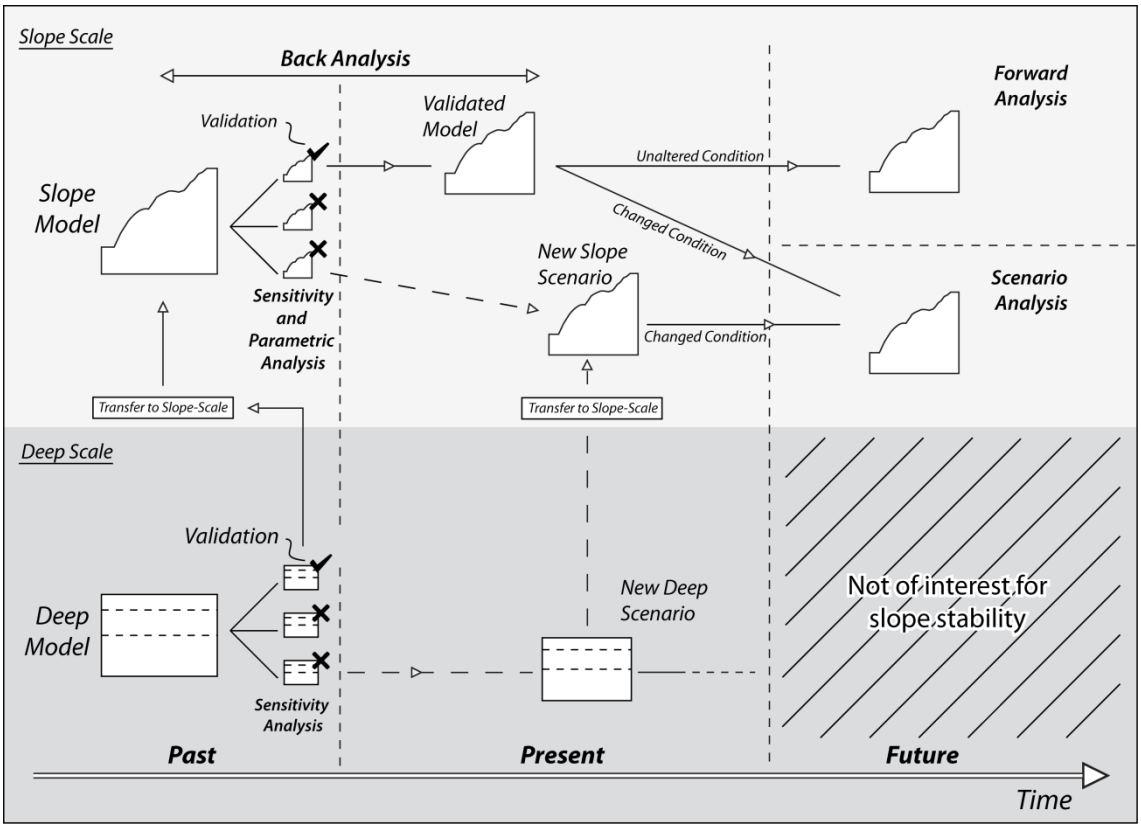

Fig. 106 - Synthetic workflow of the performed analysis over the modelled time.

The two solving analysis approaches (coupled or uncoupled) were tested for numerical analysis in different solving schemes by the support of two codes able to resolve multiple physics constitutive laws. Coupled or uncoupled schemes were used as function of the stationary or transitory state of the system respect the observation time-window (here referred to the state of activity of slope scale gravitational

processes). Where stationarity or quasi-stationarity assumption can be verified in the time-scales of observation, an uncoupled solving scheme has been chosen and each physics solved sequentially (Baroni et al., 2014).

The uncoupled solving scheme has revealed the best solution to reproduce slope deformations evolving in complex multi-physical systems over wide time-scales.

On the contrary, where quasi-stationarity cannot be assumed because of the specificity of the systems, a fully coupled solution must be adopted to compute mutual effect of physical interactions.

Although a coupled approach was adopted for the solutions of strict physical interactions in transient states, on large time-scales the numerical modelling resulted in time- and memory- intensive calculations. For this reason, in these cases, the uncoupled solutions should be preferred. Fully coupled algorithms instead, appear limited to the modelling of scenarios in small time-scales, within which short-term forcing can act in transient states.

The fully coupled algorithm applicability is thus reduced to small geometric- and temporal-scale, as example in the modelling of the cyclic influence solar radiation on rock deformations (Bakun-Mazor et al., 2013; Collins and Stock, 2016; Gischig et al., 2011; Gunzburger et al., 2005; Gunzburger and Merrien-Soukatchoff, 2011) where, given the time-windows of observation and the nature of thermal perturbations, transient strict interaction exists.

The uncoupled solutions revealed also suitable for sequential modelling, in which multiple stages of an evolutionary sequence were reproduced (e.g. discrete variations in the positioning of the ice mass).

The proposed approach tested the combination of just few physics, analysing the applicability of both schemes in the reproduction of physical systems where DSGSD can be involved. If several physics are considered (e.g. dynamic transient input in a multi-physical thermo-hydrodynamic system) the numerical solution can require a

combination of both the solving approach, switching from uncoupled to coupled solution as function of the processes evolution time-scales.

The combination of multiple geometric scales of analysis will allow to define the impact of perturbation of the deep system on slope levels, ensuring that a proper geometric resolution is maintained to perform stress-strain analyses and infer the deformative behaviour of rock masses.

At the same time a test for the combination of multiple codes (FDM and FEM) for numerical analysis was experimented to test their capabilities and take advantage of their specific features.

In order to evaluate the reproducibility of numerical analysis and the accuracy of both techniques in the description of coupled processes, the resolved model will be reproduced (i.e. computed) adopting alternative schemes by coupled or uncoupled solutions in the same case studies.

The multi-physical approach was also extended to the definition of scenario analyses. These scenarios, here proposed in a first analysis for the sole thermal interactions, could be reinforced through the definition of thermo-hydro-mechanical model considering thermal and pore-pressure coupling, evolving over the short- or the long-terms.

Despite the potential of the multi-physical approach in the analysis of gravitational slope deformation deriving by possibility to combine different physics with different scales adopting specific resolving schemes, main issues resides in the correct validation of a physical model representative of the conditions existing in the past and constituting the starting point of the modelling. In the case of a multi-physical analysis, in fact, the problem of the representativeness of an adopted model is extended not only to the geometries or engineering-geological model, but also to the description of concomitant physical processes acting in the system.

8. Conclusions

Natural systems are often characterised by physic complexities which can condition and control the time-space evolution of gravitational processes. The role of stationary or transient groundwater circulation in the stability of rock slope was took into account since decades. In the recent time the attention of scientific community moved to the analysis of the combination of multiple physics to justify observed deformations, which can control the plastic deformations and affect the evolution of slope up to failure. Among them, the thermo-mechanic interaction with the rock masses could play the clearest effect in exposed quarry or rocky cliff, where high temperature deriving by solar radiation exists. Despite this growing interest, application to thermo-mechanic analysis to large scale slope deformation are still limited, because of the difficult to manage multiple physical interactions on such a large spatial and temporal scales.

In order to try to encompass these effects on the spatial and temporal evolution of DSGSD, a suite of numerical analysis was conducted by the adopted multi-physical approach on selected case study representative of volcanic and glacial environments. In these geological contexts the lack of considerations of all disturbance forces acting on slopes could led to an underestimation of slope deformations and a wrong interpretations of modelling results.

This research aimed to evaluate the applicability of multi-physical numerical analysis in the modelling of gravitational instability processes at slope scale, testing the potential of modelling cascades in reproducing thermo-mechanical behaviour of rock-masses. Case studies where non-negligible physical interactions exist were selected, testing the response of the adopted approach with large spatial scales (up to kilometric scales), and wide time-intervals (up to 1 Million of Years).

Thermal models were defined for slope systems involved in conductive and convective heat transfer. At the same time mechanical elasto-plastic and visco-plastic

models was calibrated to be merged with thermal model of slope systems. These models were based on engineering geological model reconstructed by means field and laboratory investigations and constrained by geophysical and geothermal data. These preparatory models were then moved into multi-physical models, solved by coupled or uncoupled solve, as function of the stationarity or transient evolution of thermodynamic systems in the observation time-window.

Once calibrated this multi-physical approach were also borrowed for the definition of future scenario resulting by variation in parameters or physical boundary conditions or, maintaining unaltered the state of the system, to the picturing of predictive models in deferred time.

The adopted approach evidenced the applicability conditions of the two solving schemes (coupled or uncoupled), highlighting:

- Ability of uncoupled solutions in the reproduction of multi-physical interactions under stationarity assumption.
- Easy management of multi-physical interactions under multi-stage sequential modelling.
- Possibility to combine multi-scale modelling (i.e. deep crustal scales and slope scale) with different dimensions (1D and 2D) and spatial resolutions.
- Limitation of fully coupled solutions to the modelling of few physical interactions on narrow time-intervals (< hundreds of thousands of years).
- Exportability of multi-physical approach to scenario or generical forward analysis.

The choice of the more suitable numerical solution for the simulation of gravitational processes evolving in multi-physical systems was based on a comparison between the variability over time of the physical variables characterising the physical process involved in the system. The definition of the characteristic time of the analysis was thus defined considering the difference in the derivative term over time of the physical variables in the given time and space (Fig. 107). Where this difference is large (e.g.

gravitational processes evolving with an own rate under constant deep thermal perturbations) the numerical analysis can be achieved under invariance over time of the thermal conditions and the uncoupled scheme adopted. Instead, where the variables of the involved physical process are similar, no assumptions of steady-state conditions can be done and a coupled multi-physical solution preferred.

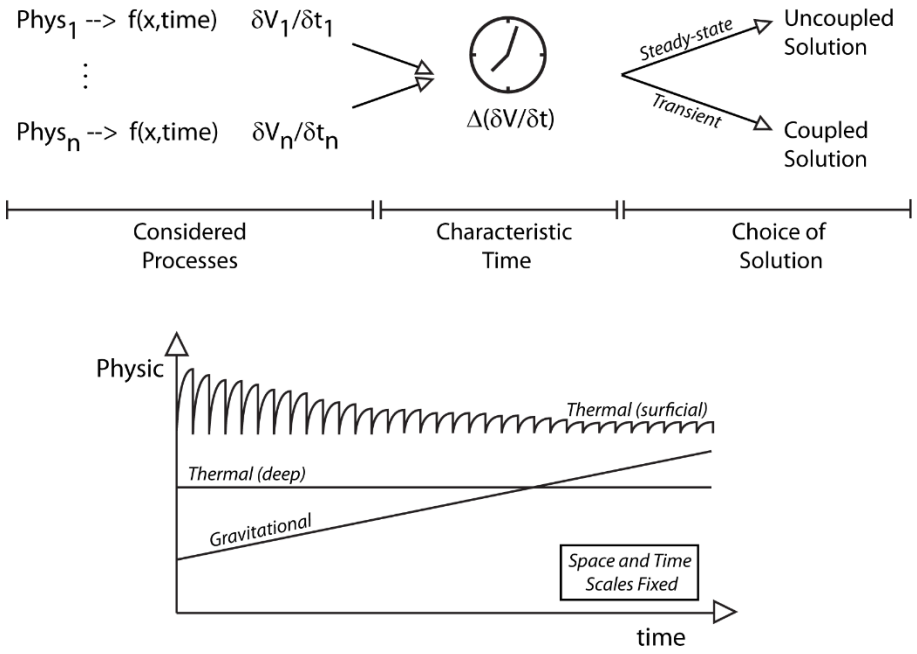

Fig. 107 – Criterion for the choice of the proper numerical solution for the modelling of multiple physical interactions in a given space and time scales.

These models once constrained on geological, physical and geotechnical monitoring data, will represent robust tools for the analysis of possible scenarios of evolution of DSGSDs towards generalised flank failure.

The definition of a broad-spectrum multi-physical model for analysis of gravitational slope deformations represents nowadays a useful tool for comprehension of factor inducing slope instabilities. Because of its ability to induced paroxysmal multi-hazard scenarios and the worldwide diffusion of slopes prone to instabilities, these analyses represent a crucial topic in the management of natural risks.

References

Ablay, G., Hürlimann, M., 2000. Evolution of the north flank of Tenerife by recurrent giant landslides. J. Volcanol. Geotherm. Res. 103, 135–159. doi:10.1016/S0377-0273(00)00220-1.

Acocella, V., Funiciello, R., 1999. The interaction between regional and local tectonics during resurgent doming: the case of the island of Ischia, Italy. J. Volcanol. Geotherm. Res. 88, 109–123. doi:10.1016/S0377-0273(98)00109-7

Agliardi, F., Crosta, G., Zanchi, A., 2001. Structural constraints on deep-seated slope deformation kinematics. Eng. Geol. 59, 83–102. doi:10.1016/S0013-7952(00)00066-1

Alley, R.B., 1989. Water-pressure coupling of sliding and bed deformation: I. Water System. J. Glaciol. 35, 108– 118.

Alm, O., Jaktlund, L. L., Shaoquan, K. 1985. The influence of microcrack density on the elastic and fracture mechanical properties of Stripa granite. Physics of the Earth and Planetary Interiors, 40(3), 161-179.

Alonso, E.E.Ã., Zervos, A., Pinyol, N.M.Ã., 2016. Thermo-poro-mechanical analysis of landslides: from creeping behaviour to catastrophic failure 202–219.

Alonso, E.E., Pinyol, N.M., 2010. Criteria for rapid sliding I . A review of Vaiont case. Eng. Geol. 114, 198–210. doi:10.1016/j.enggeo.2010.04.018

Altaner, S., Demosthenous, C., Pozzuoli, A., Rolandi, G., 2013. Alteration history of Mount Epomeo Green Tuff and a related polymictic breccia, Ischia Island, Italy: Evidence for debris avalanche. Bull. Volcanol. 75, 1–13. doi:10.1007/s00445-013-0718-1

Ambrosi, C., Crosta, G.B., 2011. Valley shape influence on deformation mechanisms of rock slopes. In: Jaboyedoff, M. (Ed.), Slope Tectonics. Geological Society, London, pp. 215–233.

Appleton, J.D., 1972. Petrogenesis of potassium rich lavas from the Roccamonfina volcano, RomanRegion, Italy. J. Petrol. 13, 425–456.

Apuani, T., Corazzato, C., 2009. Numerical model of the Stromboli volcano (Italy) including the effect of magma pressure in the dyke system. Rock Mech. Rock Eng. 42, 53–72. doi:10.1007/s00603-008-0163-1

Apuani, T., Corazzato, C., Merri, A., Tibaldi, A., 2013. Understanding Etna flank instability through numerical models. J. Volcanol. Geotherm. Res. 251, 112–126. doi:10.1016/j.jvolgeores.2012.06.015

Armienti P, Civetta L, Innocenti F, Manetti P, Tripodo A, Villari L, De Vita G., 1991. New petrological and geochemical data on Mt. Melbourne volcanic Field, Northern Victoria Land Antarctica (II Italian Antarctic Expedition). Mem Soc Geol Ital 46:397‑424.

Armienti, P., Baroni, C., 1999. Cenozoic climatic change in Antarctica recorded by volcanic activity and landscape evolution. Geology 27, 617–620. doi:10.1130/0091-7613(1999)027<0617:CCCIAR>2.3.CO;2

Armienti, P., Perinelli, C., 2010. Cenozoic thermal evolution of lithospheric mantle in northern Victoria Land (Antarctica): Evidences from mantle xenoliths. Tectonophysics 486, 28–35. doi:10.1016/j.tecto.2010.02.006

Arora, V.K., 1987. Strength and deformational behaviour of jointed rocks. PhD thesis, IIT Delhi, India.

Aydin A, Basu A. The Schmidt hammer in rock material characterization. Eng Geol 2005;81:1–14.

Aydin, A., 2009. ISRM Suggested method for determination of the Schmidt hammer rebound hardness: Revised version. Int. J. Rock Mech. Min. Sci. 46, 627–634. doi:10.1016/j.ijrmms.2008.01.020

Bächler, D., Kohl, T., Rybach, L., 2003. Impact of graben-parallel faults on hydrothermal convection-Rhine Graben case study. Phys. Chem. Earth 28, 431–441. doi:10.1016/S1474-7065(03)00063-9.

Bader, H., 1964. Density of ice as a function of temperature and stress. Cold Regions Research and Engineering Laboratory, US Army Material Command.

Bakun-Mazor, D., Hatzor, Y.H., Glaser, S.D., Carlos Santamarina, J., 2013. Thermally vs. seismically induced block displacements in Masada rock slopes. Int. J. Rock Mech. Min. Sci. 61, 196–211. doi:10.1016/j.ijrmms.2013.03.005

Ballantyne, C.K., 2002. Paraglacial geomorphology. Quat. Sci. Rev. 21, 1935–2017. doi:10.1016/S0277-3791(02)00005-7

Barbour, S. L., & Krahn, J. 2004. Numerical modelling–Prediction or process. Geotechnical News, 22(4), 44-52.

Baroni, C., Frezzotti, M., Salvatore, M.C., Meneghel, M., Tabacco, I.E., Vittuari, L., Bondesan, A., Biasini, A., Cimbelli, A., Orombelli, G., 2004. Antarctic geomorphological and glaciological 1: 250 000 map series: Mount Murchinson quadrangole, northern Victoria Land. Explanatory notes. Ann. Glaciol. 39,

256–264.

Baroni C. (ed.), Biasini A., Bondesan A., Denton G.H., Frezzotti M., Grigioni P., Meneghel, M., Orombelli G., Salvatore M.C., Della Vedova A.M. & Vittuari L., 2005. Mount Melbourne Quadrangle, Victoria Land, Antarctica 1:250,000 (Antarctic Geomorphological and Glaciological Map Series). In: Haeberli W., Zemp M., Hoelzle M., Frauenfelder R. & Kääb A. (eds.), 2005, Fluctuations of Glaciers 1995- 2000 (Vol. VIII). IUGG (CCS) / UNEP / UNESCO, World Glacier Monitoring Service, Zurich, Switzerland: 288 pp.

Baroni, C., Fasano, F., 2006. Micromorphological evidence of warm-based glacier deposition from the Ricker Hills Tillite (Victoria Land, Antarctica). Quaternary Science Reviews 25(9–10), 976–992.

Baroni, C., Fasano, F., Giorgetti, G., Salvatore, M.C., Ribecai, C., 2008. The Ricker Hills Tillite provides evidence of Oligocene warm-based glaciation in Victoria Land, Antarctica. Global Planetary Change 60(3–4), 457–470.

Baroni C., 2013. Climate Change Impacts on Cold Climates. In: Shroder, J., Giardino, M., Harbor, J. (Eds.), Treatise on Geomorphology. Academic Press, San Diego, CA, vol. 8, Glacial and Periglacial Geomorphology, pp. 430-459.

Baroni, C., Martino, S., Salvatore, M.C., Scarascia Mugnozza, G., Schiliro`, L., 2014. Thermomechanical stress-strain numerical modelling of deglaciation since the Last Glacial Maximum in the Adamello Group (Rhaetian Alps, Italy). Geomorphology 226, 278–299. doi:10.1016/j.geomorph.2014.08.013

Barton N, Choubey V, 1977. The shear strength of rock joints in theory and practice. Rock Mech 10:1–54.

Bastoncelli D. (2004). Phd Thesis Analisi geomorfica quantitativa di forme del rilievo relitte e sepolte per la ricostruzione della storia glaciale cenozoica della Terra Vittoria Settentrionale (Antartide). Tutor: Carlo Baroni. XVII ciclo del dottorato in Scienze Polari, Università di Siena.

Beck, A.C. 1968. Gravity faulting as a mechanism of topographic adjustment. New Zealand Journal of Geology and Geophysics 11, 191–199.

Benko, B., Stead, D., 1998. The Frank slide: a reexamination of the failure mechanism. Can. Geotech. J. 35, 299–311. doi:10.1139/cgj-35-2-299

Bérard, T., Cornet, F.H., 2003. Evidence of thermally induced borehole elongation: A case study at Soultz, France. Int. J. Rock Mech. Min. Sci. 40, 1121–1140. doi:10.1016/S1365-1609(03)00118-7

Bianchi Fasani, G., Di Luzio, E., Esposito, C., Martino, S., Scarascia-Mugnozza, G., 2011. Numerical modelling of Plio-Quaternary slope evolution based on geological constraints: a case study from the Caramanico Valley (Central Apennines, Italy). Geol. Soc. London, Spec. Publ. 351, 201–214. doi:10.1144/SP351.11

Bieniawski, Z.T., 1988. The Rock Mass Rating (RMR) system (geomechanics classification) in engineering pratice. In: Kirkaldie, Louis (Ed.), Rock Classification Systems for Engineering Purposes, pp. 17–34.

Bigot-Cormier, F., Braucher, R., Bourlès, D., Guglielmi, Y., Dubar, M., Stéphan, J.F., 2005. Chronological constraints on processes leading to large active landslides. Earth Planet. Sci. Lett. 235, 141–150. doi:10.1016/j.epsl.2005.03.012

Bonaccorso, A., Bonforte, A., Gambino, S., 2010. Thermal expansion-contraction and slope instability of a fumarole field inferred from geodetic measurements at Vulcano. Bull. Volcanol. 72, 791–801. doi:10.1007/s00445-010-0366-7

Bonaccorso, A., Currenti, G., Del Negro, C., 2013. Interaction of volcano-tectonic fault with magma storage, intrusion and flank instability: A thirty years study at Mt. Etna volcano. J. Volcanol. Geotherm. Res. 251, 127–136. doi:10.1016/j.jvolgeores.2012.06.002

Borselli, L., Capra, L., Sarocchi, D., De la Cruz-Reyna, S., 2011. Flank collapse scenarios at Volcan de Colima, Mexico: A relative instability analysis. J. Volcanol. Geotherm. Res. 208, 51–65. doi:10.1016/j.jvolgeores.2011.08.004

Boulton, G.S., Caban, P.E., van Gijssel, K., 1995. Groundwater flow beneath ice sheets. Part I — large scale patterns. Quat. Sci. Rev. 14, 545– 562.

Bozzano, F., Della Seta, M., Martino, S., 2016. Time-dependent evolution of rock slopes by a multi-modelling approach. Geomorphology 263, 113–131. doi:10.1016/j.geomorph.2016.03.031

Bozzano, F., Gaeta, M., Lenti, L., Martino, S., Paciello, A., Palladino, D.M., Sottili, G., 2013. Modeling the effects of eruptive and seismic activities on flank instability at Mount Etna, Italy. J. Geophys. Res. Solid Earth 118, 5252–5273. doi:10.1002/jgrb.50377

Bozzano, F., Lenti, L., Martino, S., Montagna, A., Paciello, A., 2011. Earthquake triggering of landslides in highly jointed rock masses: Reconstruction of the 1783 Scilla rock avalanche (Italy). Geomorphology

129, 294–308. doi:10.1016/j.geomorph.2011.02.025

Bozzano, F., Martino, S., Montagna, A., Prestininzi, A., 2012. Back analysis of a rock landslide to infer rheological parameters. Eng. Geol. 131–132, 45–56. doi:10.1016/j.enggeo.2012.02.003

Bozzano, F., Bretschneider, A., and Martino, S., 2008. Stress–strain history from the geological evolution of the Orvieto and Radicofani cliff slopes (Italy). Landslides, 5(4), 351-366.

Brantut, N., Heap, M.J., Meredith, P.G., Baud, P., 2013. Time-dependent cracking and brittle creep in crustal rocks: A review. J. Struct. Geol. 52, 17–43. doi:10.1016/j.jsg.2013.03.007

Brinkman, H. C., 1949. A calculation of the viscous force exerted by a flowing fluid on a dense swarm of particles. Applied Scientific Research. 1: 27–34. doi:10.1007/BF02120313.

Brown, R.J., Orsi, G., De Vita, S., 2008. New insights into Late Pleistocene explosive volcanic activity and caldera formation on Ischia (southern Italy). Bull. Volcanol. 70, 583–603. doi:10.1007/s00445-007-0155-0

Bruel D., Modelling heat extraction from forced fluid flow through stimulated fractured rock masses: evaluation of the Soultz-sousforets site potential. Geothermics 1995;24(3):439–50.

Buchner, G., Italiano, a., Vita-Finzi, C., 1996. Recent uplift of Ischia, southern Italy. Geol. Soc. London, Spec. Publ. 110, 249–252. doi:10.1144/GSL.SP.1996.110.01.19

Burland, J.B. 1987. Nash Lecture: The Teaching of Soil Mechanics – a Personal View. Proceedings, 9th ECSMFE, Dublin, Vol. 3, pp 1427-1447.

Carlino, S., 2012. The process of resurgence for Ischia Island (southern Italy) since 55 ka: The laccolith model and implications for eruption forecasting. Bull. Volcanol. 74, 947–961. doi:10.1007/s00445-012-0578-0

Carlino, S., Somma, R., Troiano, A., Di Giuseppe, M.G., Troise, C., De Natale, G., 2014. The geothermal system of Ischia Island (southern Italy): Critical review and sustainability analysis of geothermal resource for electricity generation. Renew. Energy 62, 177–196. doi:10.1016/j.renene.2013.06.052 Review

Carmignani L.; Ghezzo C.; Gosso G.; Lombardo B.; Meccheri M.; Montrasio A.; Pertusati P.C.; Salvini F., 1989. Geology of the Wilson Terrane in the area between David and Mariner Glaciers, Victoria Land (Antarctica). Mem. Soc. Geol. It. 33: 77–97.

Carson, C.J., McLaren, S., Roberts, J.L., Boger, S.D., Blankenship, D.D., 2014. Hot rocks in a cold place: high sub-glacial heat flow in East Antarctica. J. Geol. Soc. London. 171, 9–12. doi:10.1144/jgs2013-030

Casini, S., Martino, S., Petitta, M., Prestininzi, A., 2006. A physical analogue model to analyse interactions between tensile stresses and dissolution in carbonate slopes. Hydrogeol. J. 14, 1387–1402. doi:10.1007/s10040-006-0064-x

Castaldo, R., Gola, G., Santilano, A., De Novellis, V., Pepe, S., Manzo, M., Manzella, A., Tizzani, P., 2017. The role of thermo-rheological properties of the crust beneath Ischia Island (Southern Italy) in the modulation of the ground deformation pattern. J. Volcanol. Geotherm. Res. doi:10.1016/j.jvolgeores.2017.03.003

Cataldi, R., Mongelli, F., Squarci, P., Taffi, L., Zito, G., Calore, C., 1991. Geothermal ranking of Italian territory. Geothermics 24:115–129.

Cecinato, F., Zervos, A., 2012. Influence of thermomechanics in the catastrophic collapse of planar landslides 225, 207–225. doi:10.1139/T11-095

Cecinato, F., Zervos, A., Veveakis, E., 2011. A thermo-mechanical model for the catastrophic collapse of large landslides 1507–1535. doi:10.1002/nag

Celico P, Stanzione D, Esposito L, Formica F, Piscopo V, De Rosa BM. La complessità idrogeologica di un'area vulcanica attiva: l'Isola d'Ischia (Napoli-Campania). Boll Soc Geol It 1999;118:485e504.

Chen, L., Wang, C.P., Liu, J.F., Liu, Y.M., Liu, J., Su, R., Wang, J., 2014. A damage-mechanism-based creep model considering temperature effect in granite. Mech. Res. Commun. 56, 76–82. doi:10.1016/j.mechrescom.2013.11.009

Chigira, M., 1992. Long-term gravitational deformation of rocks by mass rock creep. Eng. Geol. 32, 157–184. doi:10.1016/0013-7952(92)90043-X

Chiodini, G., Avino, R., Brombach, T., Caliro, S., Cardellini, C., De Vita, S., Frondini, F., Granirei, D., Marotta, E., Ventura, G., 2004. Fumarolic and diffuse soil degassing west of Mount Epomeo, Ischia, Italy. J. Volcanol. Geotherm. Res. 133, 291–309. doi:10.1016/S0377-0273(03)00403-7

Civetta, L., Gallo, G., Orsi, G., 1991. Sr- and Nd-isotope and trace-element constraints on the chemical evolution of the magmatic system of Ischia (Italy) in the last 55 ka. J. Volcanol. Geotherm. Res. 46,

213–230. doi:10.1016/0377-0273(91)90084-D

Clarke, G.K.C., Nitsan, U., Paterson, W.S.B., 1977. Strain heating and creep instability in glaciers and ice sheets. Rev. Geophys. 15, 235–247. doi:10.1029/RG015i002p00235.

Coletta C.B., 2016. Modellazione geologico-tecnica e numerica di processi deformativi in atto in corrispondenza dell'abitato di Corniolo (Santa Sofia, FC). MSc Thesis

Collins, B.D., Stock, G.M., 2016. Rockfall triggering by cyclic thermal stressing of exfoliation fractures. Nat. Geosci. 9, 395–400. doi:10.1038/ngeo2686

Comsol Multiphysics: University of Rome Sapienza. License Number 1029647

Cossart, E., Braucher, R., Fort, M., Bourlès, D.L., Carcaillet, J., 2008. Slope instability in relation to glacial debuttressing in alpine areas (Upper Durance catchment, southeastern France): Evidence from field data and 10Be cosmic ray exposure ages. Geomorphology 95, 3–26. doi:10.1016/j.geomorph.2006.12.022

Crosta, G., 1996. Landslide, Spreading, Deep Seated Gravitational Deformation: Analysis, examples, Problems and proposal. Geogr. Fis. e Din. Quat. 19, 297–313.

Crosta, G.B., Frattini, P., Agliardi, F., 2013. Deep seated gravitational slope deformations in the European Alps. Tectonophysics 605, 13–33. doi:10.1016/j.tecto.2013.04.028

Cundall, P. A., 1976. Explicit Finite Difference Methods in Geomechanics. in: Numerical Methods in Engineering (Proceedings of the EF Conference on Numerical Methods in Geomechanics, Blacksburg, Virginia) Vol. 1, pp. 132-150.

Cundall, P.A., 1989. Numerical experiments on localization in frictional materials. Ing. arch 59: 148. https://doi.org/10.1007/BF00538368

Cundall, P.A., 2014. Explicit finite-difference method in geomechanics. Numerical Methods in Geomechanics, ASCE,.

Currenti, G., Napoli, R., Coco, A., Privitera, E., 2017. Effects of hydrothermal unrest on stress and deformation: insights from numerical modeling and application to Vulcano Island (Italy). Bull. Volcanol. 79. doi:10.1007/s00445-017-1110-3

David, C., Menendez, B., Darot, M., 1999. Influence of stress-induced and thermal cracking on physical properties and microstructure of La Peyratte granite. Int. J. Rock Mech. Min. Sci. 36, 433–448. doi:10.1016/S0148-9062(99)00010-8

Davies, M.C.R., Hamza, O., Harris, C., 2001. The Effect of Rise in Mean Annual Temperature on the Stability of Rock Slopes Containing Ice-Filled Discontinuities. Permafr. Periglac. Process. 12, 137–144. doi:10.1002/ppp378

de Vita, S., Sansivero, F., Orsi, G., Marotta, E., 2006. Cyclical slope instability and volcanism related to volcano-tectonism in resurgent calderas: The Ischia island (Italy) case study. Eng. Geol. 86, 148–165. doi:10.1016/j.enggeo.2006.02.013

DeConto, R.M., Pollard, D., 2003. Rapid Cenozoic glaciation of Antarctica induced by declining atmospheric CO2. Nature 421(6920), 245–249.

del Potro, R., Hürlimann, M., 2009. The decrease in the shear strength of volcanic materials with argillic hydrothermal alteration, insights from the summit region of Teide stratovolcano, Tenerife. Eng. Geol. 104, 135–143. doi:10.1016/j.enggeo.2008.09.005

del Potro, R., Hürlimann, M., 2008. Geotechnical classification and characterisation of materials for stability analyses of large volcanic slopes. Eng. Geol. 98, 1–17. doi:10.1016/j.enggeo.2007.11.007

Del Potro, R., Hürlimann, M., Pinkerton, H., 2013. Modelling flank instabilities on stratovolcanoes: Parameter sensitivity and stability analyses of Teide, Tenerife. J. Volcanol. Geotherm. Res. 256, 50–60. doi:10.1016/j.jvolgeores.2013.02.003

Del Ventisette, C., Casagli, N., Fortuny-Guasch, J., Tarchi, D., 2012. Ruinon landslide (Valfurva, Italy) activity in relation to rainfall by means of GBInSAR monitoring. Landslides 9, 497–509. doi:10.1007/s10346-011-0307-3

Della Seta, M., Esposito, C., Marmoni, G.M., Martino, S., Paciello, A., Perinelli, C., Sottili, G., 2015. Geological constraints for a conceptual evolutionary model of the slope deformations affecting Mt. Nuovo at Ischia (Italy). Ital. J. Eng. Geol. Environ. 2, 15–29. doi:10.4408/IJEGE.2015-02.O-02

Della Seta, M., Esposito, C., Marmoni, G.M., Martino, S., Scarascia Mugnozza, G., Troiani, F., 2017. Morpho-structural evolution of the valley-slope systems and related implications on slope-scale gravitational processes: New results from the Mt. Genzana case history (Central Apennines, Italy). Geomorphology 289, 60–77. doi:10.1016/j.geomorph.2016.07.003

Della Seta, M., Marotta, E., Orsi, G., de Vita, S., Sansivero, F., Fredi, P., 2012. Slope instability induced by volcano-tectonics as an additional source of hazard in active volcanic areas: The case of Ischia island (Italy). Bull. Volcanol. 74, 79–106. doi:10.1007/s00445-011-0501-0

Della Vedova, B., Pellis, G., and Lawver, L.A., 1992, Heat fl ow and active tectonics of the western Ross Sea, in Yoshida, Y., Kaminuma, K., and Shiraishi, K., eds., Proceedings of the 6th ISAES: Saitama, Japan, p. 627–637

Della Vedova, B., Ramigni, M., Brancolini, G., 1994. Cenozoic tectonic activity and thermal regime of the Victoria Land Basin (Ross Sea, Antarctica). Terra Antart. 1, 125–126.

Denton, G.H., Prentice, M.L., Burckle, L.H., 1991. Cainozoic history of the Antarctic ice sheet. In: Tingey, R.J. (Ed.), The geology of Antarctica. Oxford University Press, Oxford, pp. 365–433.

Di Luzio, E., Saroli, M., Esposito, C., Bianchi-Fasani, G., Cavinato, G.P., Scarascia-Mugnozza, G., 2004. Influence of structural framework on mountain slope deformation in the Maiella anticline (Central Apennines, Italy). Geomorphology 60, 417–432. doi:10.1016/j.geomorph.2003.10.004

Di Napoli, R., Aiuppa, A., Bellomo, S., Brusca, L., D'Alessandro, W., Candela, E.G., Longo, M., Pecoraino, G., Valenza, M., 2009. A model for Ischia hydrothermal system: Evidences from the chemistry of thermal groundwaters. J. Volcanol. Geotherm. Res. 186, 133–159. doi:10.1016/j.jvolgeores.2009.06.005

Di Napoli, R., Martorana, R., Orsi, G., Aiuppa, A., Camarda, M., De Gregorio, S., Gagliano Candela, E., Luzio, D., Messina, N., Pecoraino, G., Bitetto, M., De Vita, S., Valenza, M., 2011. The structure of a hydrothermal system from an integrated geochemical, geophysical, and geological approach: The Ischia Island case study. Geochemistry, Geophys. Geosystems 12, 1–25. doi:10.1029/2010GC003476

Di Napoli, R., Federico, C., Aiuppa, A., D'Antonio, M., Valenza, M., 2013. Quantitative models of hydrothermal fluid-mineral reaction: The Ischia case. Geochim. Cosmochim. Acta 105, 108–129. doi:10.1016/j.gca.2012.11.039

Di Nicola L., Strasky S., Schlüchter C., Salvatore M.C., Akçar N., Kubik P.W., Christl M., Kasper H.U., Wieler R., & Baroni C., 2009. Multiple cosmogenic nuclides document complex Pleistocene exposure history of glacial drifts in Terra Nova Bay (northern Victoria Land, Antarctica). Quaternary Research, 71 (1), 83-92. doi: 10.1016/j.yqres.2008.07.004.

Di Nicola, L., Baroni, C., Strasky, S., Salvatore, M.C., Schlüchter, C., Akçar, N., Kubik, P.W., Wieler, R., 2012. Multiple cosmogenic nuclides document the stability of the East Antarctic Ice Sheet in northern Victoria Land since the Late Miocene (5-7 Ma). Quat. Sci. Rev. 57, 85–94. doi:10.1016/j.quascirev.2012.09.026

Discenza, M.E., Esposito, C., Martino, S., Petitta, M., Prestininzi, A., Mugnozza, G.S., 2011. The gravitational slope deformation of Mt. Rocchetta ridge (central Apennines, Italy): Geological-evolutionary model and numerical analysis. Bull. Eng. Geol. Environ. 70, 559–575. doi:10.1007/s10064-010-0342-7

Discenza, M.E., Martino, S., Mugnozza, G.S., Stedile, L., 2013. Rheological behavior of jointed rock masses inferred from an analogue laboratory testing approach 411–416.

Dow, J. A. S., & Neall, V. E., 1974. Geology of the lower Rennick Glacier, northern Victoria Land, Antarctica. New Zealand Journal of Geology and Geophysics, 17(3), 659-714

Draebing, D., Haberkorn, A., Krautblatter, M., Kenner, R., Phillips, M., 2017. Thermal and Mechanical Responses Resulting From Spatial and Temporal Snow Cover Variability in Permafrost Rock Slopes, Steintaelli, Swiss Alps. Permafr. Periglac. Process. 28, 140–157. doi:10.1002/ppp.1921

Draebing, D., Krautblatter, M., Dikau, R., 2014. Interaction of thermal and mechanical processes in steep permafrost rock walls: A conceptual approach. Geomorphology 226, 226–235. doi:10.1016/j.geomorph.2014.08.009

Dramis, F., Sorriso-Valvo, M., 1994. Deep-seated gravitational slope deformations, related landslides and tectonics. Eng. Geol. 38, 231–243. doi:10.1016/0013-7952(94)90040-X

Eberhardt, E., Stead, D., Coggan, J.S., 2004. Numerical analysis of initiation and progressive failure in natural rock slopes-the 1991 Randa rockslide. Int. J. Rock Mech. Min. Sci. 41, 69–87. doi:10.1016/S1365-1609(03)00076-5

Engelhardt, H., Humphrey, N., Kamb, B., Fahnestock, M., 1990. Physical Conditions at the Base of a Fast Moving Antarctic Ice Stream. Science (80-.). 248, 57–59. doi:10.1126/science.248.4951.57

Engelhardt, H. and Kamb B. 1993. Vertical Temperature Profile of Ice Stream B. Antarctic J. U.S., 28(5),63-66

Engelhardt, Hermann. 2004a. Ice Temperature and High Geothermal Heat Flux at Siple Dome, West

Antarctica, from Borehole Measurements. J. Glaciol. 50(169), 251-256.

Engelhardt, Hermann. 2004b. Thermal Regime and Dynamics of the West Antarctic Ice Sheet. Ann. Glaciol. 39, 85-92.

Eppelbaum, L., Kutasov, I., & Pilchin, A., 2014. Thermal properties of rocks and density of fluids. In Applied geothermics (pp. 99-149). Springer Berlin Heidelberg

Esposito, C., Bianchi Fasani, G., Martino, S., Scarascia-Mugnozza, G., 2013. Quaternary gravitational morpho-genesis of Central Apennines (Italy): Insights from the Mt. Genzana case history. Tectonophysics 605, 96–103. doi:10.1016/j.tecto.2013.06.023

Esposito, C., Martino, S., Mugnozza, G.S., 2007. Mountain slope deformations along thrust fronts in jointed limestone: An equivalent continuum modelling approach. Geomorphology 90, 55–72. doi:10.1016/j.geomorph.2007.01.017

Feda, J., 1973. Stability of natural slopes. Proc. 8th Int. Conf. Smfe, Session 6, Oral Discussion, Moskva.

Ferrero, A.M., Migliazza, M., Spagnoli, A., Zucali, M., 2014. Micromechanics of intergranular cracking due to anisotropic thermal expansion in calcite marbles. Eng. Fract. Mech. 130, 42–52. doi:10.1016/j.engfracmech.2014.01.004

Fisher, A.T., Mankoff, K.D., Tulaczyk, S.M., Tyler, S.W., 2015. High geothermal heat flux measured below the West Antarctic Ice Sheet 1–9.

Flac 2D 8.0. Itasca Consulting Group, license number 213-039-0127-30821 Sapienza University of Rome.

Fredrich, J.T., Wong, T., 1986. Micromechanics of thermally induced cracking in three crustal rocks. J. Geophys. Res. 91, 12743. doi:10.1029/JB091iB12p12743

Fretwell, P., Pritchard, H.D., Vaughan, D.G., Bamber, J.L., Barrand, N.E., Bell, R., Bianchi, C., Bingham, R.G., Blankenship, D.D., Casassa, G., Catania, G., Callens, D., Conway, H., Cook, A.J., Corr, H.F.J., Damaske, D., Damm, V., Ferraccioli, F., Forsberg, R., Fujita, S., Gim, Y., Gogineni, P., Griggs, J.A., Hindmarsh, R.C.A., Holmlund, P., Holt, J.W., Jacobel, R.W., Jenkins, A., Jokat, W., Jordan, T., King, E.C., Kohler, J., Krabill, W., Riger-Kusk, M., Langley, K.A., Leitchenkov, G., Leuschen, C., Luyendyk, B.P., Matsuoka, K., Mouginot, J., Nitsche, F.O., Nogi, Y., Nost, O.A., Popov, S. V., Rignot, E., Rippin, D.M., Rivera, A., Roberts, J., Ross, N., Siegert, M.J., Smith, A.M., Steinhage, D., Studinger, M., Sun, B., Tinto, B.K., Welch, B.C., Wilson, D., Young, D.A., Xiangbin, C., Zirizzotti, A., 2013. Bedmap2: Improved ice bed, surface and thickness datasets for Antarctica. Cryosphere 7, 375–393. doi:10.5194/tc-7-375-2013.

Frezzotti, M., & Mabin, M. C. G., 1994. 20th century behaviour of Drygalski Ice Tongue, Ross Sea, Antarctica. Annals of Glaciology, 20(1), 397-400.

Frolova, J., Ladygin, V., Rychagov, S., Zukhubaya, D., 2014. Effects of hydrothermal alterations on physical and mechanical properties of rocks in the Kuril-Kamchatka island arc. Eng. Geol. 183, 80–95. doi:10.1016/j.enggeo.2014.10.011

Giordano, G., Lucci, F., Phillips, D., Cozzupoli, D., & Runci, V., 2012. Stratigraphy, geochronology and evolution of the Mt. Melbourne volcanic field (North Victoria Land, Antarctica). Bulletin of volcanology, 74(9), 1985-2005.

Giraud A, Rousset G. Thermoelastic and thermoplastic response of a porous space submitted to a decaying heat source. Int J Rock Mech Min Sci 1995;19:475–95.

Gischig, V.S., Moore, J.R., Evans, K.F., Amann, F., Loew, S., 2011. Thermomechanical forcing of deep rock slope deformation: 1. Conceptual study of a simplified slope. J. Geophys. Res. Earth Surf. 116, 1–18. doi:10.1029/2011JF002006

Glicken, H., 1998. Rockslide-debris avalanche of May 18, 1980, Mount St Helens volcano, Washington. Bull. Geol. Soc. Jpn. 49, 55–106.

Grämiger, L.M., Moore, J.R., Gischig, V.S., Ivy-Ochs, S., Loew, S., 2017. Beyond debuttressing: Mechanics of paraglacial rock slope damage during repeat glacial cycles. J. Geophys. Res. Earth Surf. 1004–1036. doi:10.1002/2016JF003967

Greif, V., Brcek, M., Vlcko, J., Varilova, Z., Zvelebil, J., 2016. Thermomechanical behavior of Pravcicka Brana Rock Arch (Czech Republic). Landslides 1–15. doi:10.1007/s10346-016-0784-5

Gudlaugsson, E., Humbert, A., Kleiner, T., Kohler, J., Andreassen, K., 2016. The influence of a model subglacial lake on ice dynamics and internal layering. Cryosphere 10, 751–760. doi:10.5194/tc-10-751-2016

Gudmundsson, A., 2012. Strengths and strain energies of volcanic edifices: Implications for eruptions, collapse calderas, and landslides. Nat. Hazards Earth Syst. Sci. 12, 2241–2258. doi:10.5194/nhess-12-

2241-2012

Gudmundsson, A., 2009. Toughness and failure of volcanic edifices. Tectonophysics 471, 27–35. doi:10.1016/j.tecto.2009.03.001

Gunzburger, Y., Merrien-Soukatchoff, V., 2011. Near-surface temperatures and heat balance of bare outcrops exposed to solar radiation. Earth Surf. Process. Landforms 36, 1577–1589. doi:10.1002/esp.2167

Gunzburger, Y., Merrien-Soukatchoff, V., Guglielmi, Y., 2005. Influence of daily surface temperature fluctuations on rock slope stability: Case study of the Rochers de Valabres slope (France). Int. J. Rock Mech. Min. Sci. 42, 331–349. doi:10.1016/j.ijrmms.2004.11.003

Hall, K., 1999. The role of thermal stress fatigue in the breakdown of rock in cold regions. Geomorphology 31, 47–63. doi:10.1016/S0169-555X(99)00072-0

Hambrey, M.J., Glasser, N.F., McKelvey, B.C., Sugden, D.E., Fink, D., 2007. Cenozoic landscape evolution of an East Antarctic oasis (Radok Lake area, northern Prince Charles Mountains), and its implications for the glacial and climatic history of Antarctica. Quaternary Science Reviews 26(5–6), 598–626.

Hansen, I., and R. Greve (1996), Polythermal modelling of steady states of the Antarctic ice sheet in comparison with the real world, Ann. Glaciol., 23, 382–387.

Haque, U., Blum, P., da Silva, P.F., Andersen, P., Pilz, J., Chalov, S.R., Malet, J.P., Auflic, M.J., Andres, N., Poyiadji, E., Lamas, P.C., Zhang, W., Peshevski, I., Petursson, H., Kurt, T., Dobrev, N., Garcia-Davalillo, J.C., Halkia, M., Ferri, S., Gaprindashvili, G., Engstr??m, J., Keellings, D., 2016. Fatal landslides in Europe. Landslides 1–10. doi:10.1007/s10346-016-0689-3

Heap, M.J., Baud, P., Meredith, P.G., 2009. Influence of temperature on brittle creep in sandstones. Geophys. Res. Lett. 36, 1–6. doi:10.1029/2009GL039373

Heap, M.J., Baud, P., Meredith, P.G., Vinciguerra, S., Bell, A.F., Main, I.G., 2011. Brittle creep in basalt and its application to time-dependent volcano deformation. Earth Planet. Sci. Lett. 307, 71–82. doi:10.1016/j.epsl.2011.04.035

Heap, M.J., Mollo, S., Vinciguerra, S., Lavall??e, Y., Hess, K.U., Dingwell, D.B., Baud, P., Iezzi, G., 2013. Thermal weakening of the carbonate basement under Mt. Etna volcano (Italy): Implications for volcano instability. J. Volcanol. Geotherm. Res. 250, 42–60. doi:10.1016/j.jvolgeores.2012.10.004

Hoek, E., 1983. Strength of jointed rock masses. Geotechnique 23, 187–223. doi:10.1680/geot.1983.33.3.187

Hoek, E., Carranza-Torres, C.T., Corkum, B., 2002. Hoek–Brown failure criterion—2002 edition. In: Hammah, R., Bawden, W., Curran, J., Telesnicki, M. (Eds.), Proceedings of the Fifth North American Rock Mechanics Symposium (NARMS-TAC). University of Toronto Press, Toronto, pp. 267–273.

Holm, K., Bovis, M., Jakob, M., 2004. The landslide response of alpine basins to post-Little Ice Age glacial thinning and retreat in southwestern British Columbia. Geomorphology 57, 201–216. doi:10.1016/S0169-555X(03)00103-X

Homand-Etienne, F., R. Houpert. Thermally induced microcracking in granites: characterization and analysis. International Journal of Rock Mechanics and Mining Sciences & Geomechanics Abstracts. Vol. 26. No. 2. Pergamon, 1989.

Hutchinson, J.N., 1988. General report: morphological and geotechnical parameters of landslides in relation to geology and hydrogeology. Final Proc. 5th International Symposium on Landslides, vol. 1. Lausanne, Switzerland, pp. 3 –35.

Ingebritsen, S. E., S. Geiger, S. Hurwitz, and T. Driesner, 2010 - Numerical simulation of magmatic hydrothermal systems, Rev. Geophys., 48, RG1002.

I.S.R.M., 1978. Suggested methods for the quantitative description of discontinuities in rock masses. International Journal of Rock Mechanics and Mining Sciences & Geomechanics.Vol. 15, 319–368.

Jia, H., Xiang, W., Krautblatter, M., 2015. Quantifying Rock Fatigue and Decreasing Compressive and Tensile Strength after Repeated Freeze-Thaw Cycles. Permafr. Periglac. Process. 26, 368–377. doi:10.1002/ppp.1857

John, D.A., Sisson, T.W., Breit, G.N., Rye, R.O., Vallance, J.W., 2008. Characteristics, extent and origin of hydrothermal alteration at Mount Rainier Volcano, Cascades Arc, USA: Implications for debris-flow hazards and mineral deposits. J. Volcanol. Geotherm. Res. 175, 289–314. doi:10.1016/j.jvolgeores.2008.04.004

Kamb, B., 1965. Structure of ice VI. Science, 150(3693), 205-209.

Karato, S.I., 2008. Deformation of earth materials (Chapter 19). An Introduction to the Rheology of Solid

Earth. Cambridge University Press.
Kennett, J.P., 1977. Cenozoic evolution of Antarctic glaciation, the circum-Antarctic Ocean, and their impact on global paleoceanography. J. Geophys. Res. 82, 3843–3860. doi:10.1029/JC082i027p03843
Kyle, P. R., 1990. A. McMurdo Volcanic Group Western Ross embayment. Volcanoes of the Antarctic plate and southern Oceans, 18-145.
Larour, E., Morlighem, M., Seroussi, H., Schiermeier, J., Rignot, E., 2012. Ice flow sensitivity to geothermal heat flux of Pine Island Glacier, Antarctica. J. Geophys. Res. F Earth Surf. 117, 1–12. doi:10.1029/2012JF002371
Lénat, J.F., Bachélery, P., Peltier, A., 2012. The interplay between collapse structures, hydrothermal systems, and magma intrusions: The case of the central area of Piton de la Fournaise volcano. Bull. Volcanol. 74, 407–421. doi:10.1007/s00445-011-0535-3.
Lekhnitskii, S.G., 1963. Theory of Elasticity of an Anisotropic Elastic Body. Holden Day, Inc., San Francisco.
Lewis, A.R., Marchant, D.R., Ashworth, A.C., et al., 2008. Mid-Miocene cooling, the extinction of tundra in continental Antarctica. Proceedings of the National Academy of Sciences of the United States of America 105(31), 10676–10680.
Lewis, A.R., Marchant, D.R., Ashworth, A.C., Hemming, S.A., Machlus, M.L., 2007. Major middle Miocene global climate change: evidence from East Antarctica, the Transantarctic Mountains. Geological Society of America Bulletin 119, 1449–1461.
Lopez, D.L., Williams, S.N., 1993. Catastrophic Volcanic Collapse: Relation to Hydrothermal Processes. Sci. New Ser. Jstor 260, 1794–1976.
Lyle, M., Gibbs, S., Moore, T.C., Rea, D.K., 2007. Late Oligocene initiation of the Antarctic circumpolar current: evidence from the South Pacific. Geology 35(8), 691–694.
Maffei, A., Martino, S., Prestininzi, A., 2005. From the geological to the numerical model in the analysis of gravity-induced slope deformations: An example from the Central Apennines (Italy). Eng. Geol. 78, 215–236. doi:10.1016/j.enggeo.2004.12.009
Mahr, T., 1977. Deep-Reaching gravitational deformations of high mountain slopes. Bull. Int. Assoc. Eng. Geol. 16, 121–127. doi:10.1007/BF02591467
Manzo, M., Ricciardi, G.P., Casu, F., Ventura, G., Zeni, G., Borgström, S., Berardino, P., Del Gaudio, C., Lanari, R., 2006. Surface deformation analysis in the Ischia Island (Italy) based on spaceborne radar interferometry. J. Volcanol. Geotherm. Res. 151, 399–416. doi:10.1016/j.jvolgeores.2005.09.010
Marchant, D.R., Swisher, C.C., Lux, D.R., West, D.P., Denton, G.H., 1993. Pliocene paleoclimate, East Antarctic ice sheet history from surficial ash deposits. Science 260, 667–670.
Marmoni, G.M., Martino, S., Heap, M.J., Reuschlé, T., 2017. Multiphysics Laboratory Tests for Modelling Gravity-driven Instabilities at Slope Scale, in: Procedia Engineering. doi:10.1016/j.proeng.2017.05.165
Marmoni G.M., Martino S., Heap M.J., Reuschlé T. (2017).Gravitational slope-deformation of a resurgent caldera: New insights from the mechanical behaviour of Mt. Nuovo tuffs (Ischia Island, Italy). Journal of Volcanology and Geothermal Research 345:1-20. https://doi.org/10.1016/j.jvolgeores.2017.07.019;
McCalpin, J.P., Irvine, J.R. (1995). Sackungen at the Aspen Highlands ski area, Pitkin County, Colorado. Environmental and Engineering Geoscience 1, 277–290.
McGuire, W.J., 1996. Volcano instability: a review of contemporary themes. Geol. Soc. London, Spec. Publ. 110, 1–23. doi:10.1144/GSL.SP.1996.110.01.01
McKenna, J.R., Blackwell, D.D., 2004. Numerical modeling of transient Basin and Range extensional geothermal systems. Geothermics 33, 457–476. doi:10.1016/j.geothermics.2003.10.001
Mencl, V., 1968. Plastizitatslehre und das wirkliche Verhalten von Gebirgsmassen. Felsmech. U. Ing. Geol., Suppl. IV, 1-8.
Molin, P., Acocella, V., Funiciello, R., 2003. Structural, seismic and hydrothermal features at the border of an active intermittent resurgent block: Ischia Island (Italy). J. Volcanol. Geotherm. Res. 121, 65–81. doi:10.1016/S0377-0273(02)00412-2
Molnar, P., 2004. Interactions among topographically induced elastic stress, static fatigue, and valley incision. J. Geophys. Res. 109, 1–9. doi:10.1029/2003JF000097
Morin, R.H., Williams, T., Henrys, S. a., Magens, D., Niessen, F., Hansaraj, D., 2010. Heat Flow and Hydrologic Characteristics at the AND-1B borehole, ANDRILL McMurdo Ice Shelf Project, Antarctica. Geosphere 6, 370–378. doi:10.1130/GES00512.1

Moro, M., Saroli, M., Salvi, S., Stramondo, S., Doumaz, F., 2007. The relationship between seismic deformation and deep-seated gravitational movements during the 1997 Umbria-Marche (Central Italy) earthquakes. Geomorphology 89, 297–307. doi:10.1016/j.geomorph.2006.12.013

Nara, Y., Meredith, P.G., Yoneda, T., Kaneko, K., 2011. Influence of macro-fractures and micro-fractures on permeability and elastic wave velocities in basalt at elevated pressure. Tectonophysics 503, 52–59. doi:10.1016/j.tecto.2010.09.027

Oberholzer, P., Baroni, C., Salvatore, M.C., Baur, H., Wieler, R., 2008. Dating late Cenozoic erosional surfaces in Victoria Land, Antarctica, with cosmogenic neon in pyroxenes. Antarct. Sci. 20, 89–98. doi:10.1017/S095410200700079X

Oberholzer, P., Baroni, C., Schaefer, J.M., Orombelli, G., Ochs, S.I., Kubik, P.W., Baur, H., Wieler, R., 2003. Limited Pliocene/Pleistocene glaciation in Deep Freeze Range, northern Victoria Land, Antarctica, derived from in situ cosmogenic nuclides. Antarct. Sci. 15, 493–502. doi:10.1017/S0954102003001603

Orombelli, G., Baroni, C., Denton, G.H., 1990. Late Cenozoic Glacial History of the Terra Nova Bay Region, Northern Victoria Land, Antarctica. Geogr. Fis. e Din. Quat. 13, 139–163.

Orsi, G., de Vita, S., Di Vito, M., Isaia, R., Nave, R., Heiken G., 2003. Facing volcanic and related hazards in the Neapolitan area, in: American Geophysical Union (Special Publication) (Ed.), Earth Science in the City A Reader. Washington, pp. 121–170.

Orsi, G., Gallo, G., Zanchi, A., 1991. Simple-shearing block resurgence in caldera depressions. A model from Pantelleria and Ischia. J. Volcanol. Geotherm. Res. 47, 1–11. doi:10.1016/0377-0273(91)90097-J

Orsi, G., Piochi, M., Campajola, L., D'Onofrio, A., Gialanella, L., Terrasi, F., 1996. 14C geochronological constraints for the volcanic history of the island of Ischia (Italy) over the last 5000 years. J Volcanol Geotherm Res 71, 249–257. doi:10.1016/0377-0273(95)00067-4

Palis, E., Lebourg, T., Tric, E., Malet, J.P., Vidal, M., 2016. Long-term monitoring of a large deep-seated landslide (La Clapiere, South-East French Alps): initial study. Landslides 1–16. doi:10.1007/s10346-016-0705-7

Palmstrom A., 1995. RMi – a rock mass characterization system for rock engineering purposes. Ph. D. Thesis, University of Oslo, Norway, pp 350.

Pan, E., Amadei, B., Savage, W.Z., 1995. Gravitational and tectonic stresses in anisotropic rock with irregular topography. Int. J. Rock Mech. Min. Sci. 32, 201–214. doi:10.1016/0148-9062(94)00046-6

Pánek, T., Mentlík, P., Ditchburn, B., Zondervan, A., Norton, K., Hradecký, J., 2015. Are sackungen diagnostic features of (de)glaciated mountains? Geomorphology 248, 396–410. doi:10.1016/j.geomorph.2015.07.022

Pánek, T., Mentlík, P., Engel, Z., Braucher, R., Zondervan, A., 2017. Late Quaternary sackungen in the highest mountains of the Carpathians. Quat. Sci. Rev. 159, 47–62. doi:10.1016/j.quascirev.2017.01.008

Pasten, C., Garcia, M., Cortes, D.D., 2015. Physical and numerical modelling of the thermally induced wedging mechanism. Geotech. Lett. 5, 186–190. doi:http://dx.doi.org/10.1680/jgele.15.00072

Perinelli, C., Armienti, P., Dallai, L., 2011. Thermal evolution of the lithosphere in a rift environment as inferred from the geochemistry of mantle cumulates, Northern Victoria Land, Antarctica. J. Petrol. 52, 665–690. doi:10.1093/petrology/egq099

Perinelli, C., Gaeta, M., Armienti, P., 2017. Cumulate xenoliths from Mt. Overlord, northern Victoria Land, Antarctica: A window into high pressure storage and differentiation of mantle-derived basalts. Lithos 268–271, 225–239. doi:10.1016/j.lithos.2016.10.027

Pertusati P.; Musumeci G.; Carosi R.; Meccheri M.; Baroni C.; Capponi G.; Carmignani L.; Castelli D.; Colombo F.; Crispini L.; Di Vincenzo G.; Ghezzo C.; Gosso G.; Lombardo B.; Montomoli C.; Montrasio A.; Oggiano G.; Perchiazzi N.; Ricci C.A.; Rocchi S.; Salvini F.; Skinner D.N.B.; Talarico F.; Tessensohn F., 2012. Antarctic Geological 1:250000 Map series. Mount Melbourne Quadrangle, (Victoria Land). GIGAMAP-German Italian Geological Antarctic Map Program, PNRA.

Petley, D., 2012. Global patterns of loss of life from landslides. Geology 40, 927–930. doi:10.1130/G33217.1

Petley, D.N., Higuchi, T., Petley, D.J., Bulmer, M.H., Carey, J., 2005. Development of progressive landslide failure in cohesive materials. Geology 33, 201–204. doi:10.1130/G21147.1

Petrenko, V., and Whitworth, R., 1991 Physics of Ice. : Oxford University Press. Retrieved 16 Oct. 2017, from http://www.oxfordscholarship.com/view/10.1093/acprof:oso/9780198518945.001.0001/acprof-9780198518945.

Pinyol, M., Alonso, E.E., 2016. Internal Progressive Failure in Deep-Seated Landslides 2317–2332. doi:10.1007/s00603-015-0888-6

Pisani, G., Castelli, M., Scavia, C., 2010. Hydrogeological model and hydraulic behaviour of a large landslide in the Italian Western Alps. Nat. Hazards Earth Syst. Sci. 10, 2391–2406. doi:10.5194/nhess-10-2391-2010

Poland, M.P., Peltier, A., Bonforte, A., Puglisi, G., 2017. The spectrum of persistent volcanic flank instability: A review and proposed framework based on Kīlauea, Piton de la Fournaise, and Etna. J. Volcanol. Geotherm. Res. 339, 63–80. doi:10.1016/j.jvolgeores.2017.05.004

Pollard, D., DeConto, R.M., Nyblade, A.A., 2005. Sensitivity of Cenozoic Antarctic ice sheet variations to geothermal heat flux. Glob. Planet. Change 49, 63–74. doi:10.1016/j.gloplacha.2005.05.003

Radbruch-Hall, D.H., 1978. Gravitational creep of rock masses on slopes. In: Voight, B. (Ed.), Rockslides and Avalanches. Develop. Geotec. Eng, vol. 14. Elsevier, Amsterdam, pp. 607–658.

Ramamurthy, T., 1994. Strength and modulus responses of anisotropic rocks. Rock Engineering by Hudson J.A., 1(13), 313–329.

Reid, M.E., 2004. Massive collapse of volcano edifices triggered by hydrothermal pressurization. Geology 32, 373–376. doi:10.1130/G20300.1

Reid, M.E., Sisson, T.W., Brien, D.L., 2002. Volcano collapse promoted by hydrothermal alteration and edifice shape, Mount Rainier, Washington. Geology 29, 779–782. doi:10.1130/0091-7613(2001)029<0779:VCPBHA>2.0.CO;2

Reuschlé, T., Haore, S. G., Darot, M. 2006. The effect of heating on the microstructural evolution of La Peyratte granite deduced from acoustic velocity measurements. Earth and Planetary Science Letters, 243(3), 692-700.

Rippin, D.M., Bamber, J.L., Siegert, M.J., Vaughan, D.G., Corr, H.F.J., 2003. Basal topography and ice flow in the Bailey/Slessor region of East Antarctica. J. Geophys. Res. 108 (F1), 6008. doi: 10.1029/2003JF000039.

Risk, G.F., and Hochstein, R., 1974, Heat fl ow at Arrival Heights, Ross Island, Antarctica: New Zealand Journal of Geology and Geophysics, v. 17, p. 629–644.

Rittmann, A., 1930. Geologie der Insel Ischia. Z f Vulkanol Er-ganzungsband 6.

Rittmann A., 1948. Origine e differenziazione del magma ischitano. Bull Suisse Mineral Petrogr 28:643–698

Ritz, C., V. Rommelaere, and C. Dumas, 2001. Modeling the evolution of Antarctic ice sheet over the last 420,000 years: Implications for altitude changes in the Vostok region, J. Geophys. Res., 106, 31,943–31,964.

Rocchi, V., Sammonds, P.R., Kilburn, C.R.J., 2004. Fracturing of Etnean and Vesuvian rocks at high temperatures and low pressures. J. Volcanol. Geotherm. Res. 132, 137–157. doi:10.1016/S0377-0273(03)00342-1

Rocchi, V., Sammonds, P.R., Kilburn, C.R.J., 2003. Flow and fracture maps for basaltic rock deformation at high temperatures. J. Volcanol. Geotherm. Res. 120, 25–42. doi:10.1016/S0377-0273(02)00343-8

Rosas-Carbajal, M., Komorowski, J.-C., Nicollin, F., Gibert, D., 2016. Volcano electrical tomography unveils edifice collapse hazard linked to hydrothermal system structure and dynamics. Sci. Rep. 6, 29899. doi:10.1038/srep29899

Rutqvist, J., 2011. Status of the TOUGH-FLAC simulator and recent applications related to coupled fluid flow and crustal deformations. Comput. Geosci. 37, 739–750. doi:10.1016/j.cageo.2010.08.006

Rutqvist, J., Börgesson, L., Chijimatsu, M., Nguyen, T.S., Jing, L., Noorishad, J., Tsang, C.F., 2001. Coupled thermo-hydro-mechanical analysis of a heater test in fractured rock and bentonite at Kamaishi Mine - comparison of field results to predictions of four finite element codes. Int. J. Rock Mech. Min. Sci. 38, 129–142. doi:10.1016/S1365-1609(00)00069-1

Salari G., 2017 - Petrographic characterization and calorimetric measurements of igneous and metamorphic rocks from Deep Freeze Range area (northern Victoria Land, Antarctica). MSc Thesis.

Salvini F., Brancolini G., Busetti M., Storti F., Mazzarini F., Coren F., 1997. Cenozoic geodynamics of the Ross Sea region, Antarctica: crustal extension, intraplate strike–slip faulting, and tectonic inheritance. Journal of Geophysical Research, 102 (24) (1997), pp. 669-696.

Salvini F., Storti F., 1999.Cenozoic tectonic lineaments of the Terra Nova Bay region, Ross Embayment, Antarctica. Global and Planetary Change, 23:129-144

Savage, W.Z., Varnes, D.J. 1987. Mechanics of gravitational spreading of steep-sides ridges (sackung). International Association of Engineering Geologists Bulletin 35, 31–36.

Sbrana, A., Toccaceli, R.M., 2011. Carta Geologica della regione Campania - Foglio 464, Isola di Ischia. Litografia artistica cartografica, Firenze.

Scarascia, G., Bianchi Fasani, G., Esposito, C., Saroli, M., Di Luzio, E., Evans, S.G., 2006. Rock Avalanche and Mountain Slope Deformation in a. S.G. Evans al. (eds.), Landslides from Massive Rock Slope Fail. Landslides, 357–376.

Schröder, H., Paulsen, T. & Wonik, T. 2011. Thermal properties of the AND-2A borehole in the southern Victoria Land Basin, McMurdo Sound, Antarctica. Geosphere, 7, 1324–1330.

Semenza, E., Ghirotti, M., 2000. History of the 1963 Vaiont slide: the importance of geological factors. Bull. Eng. Geol. Environ. 59, 87–97. doi:10.1007/s100640000067

Sepe, V., Atzori, S., Ventura, G., 2007. Subsidence due to crack closure and depressurization of hydrothermal systems: A case study from Mt Epomeo (Ischia Island, Italy). Terra Nov. 19, 127–132. doi:10.1111/j.1365-3121.2006.00727.x.

Seroussi, H., Ivins, E. R., Wiens, D.A., Bondzio, J., 2017. Influence of aWest Antarcticmantle plume on ice sheet basal conditions. Journal of Geophysical Research: Solid Earth. doi: 10.1002/2017JB014423.

Siebert, L., 1984. Large volcanic debris avalanches: characteristics of source areas, deposits, and associated eruptions. J. Volcanol. Geotherm. Res. 22, 163–197.

Sitharam, T.G., Latha, G.M., 2002. Simulation of excavations in jointed rock masses using a practical equivalent continuum approach. Int. J. Rock Mech. Min. Sci. 39, 517–525. doi:10.1016/S1365-1609(02)00024-2

Sitharam, T.G., Sridevi, J., Shimizu, N., 2001. Practical equivalent continuum characterization of jointed rock masses. Int. J. Rock Mech. Min. Sci. 38, 437–448. doi:10.1016/S1365-1609(01)00010-7

Sherrod, D.R., Scott, W.E., and Stauffer, P.H., eds., 2008. A volcano rekindled; the renewed eruption of Mount St. Helens, 2004-2006: U.S. Geological Survey Professional Paper 1750, 856 p.

Smellie, J.L., Rocchi, S., Gemelli, M., Di Vincenzo, G., Armienti, P., 2011. A thin predominantly cold-based late miocene east antarctic ice sheet inferred from glaciovolcanic sequences in northern victoria land, antarctica. Palaeogeogr. Palaeoclimatol. Palaeoecol. 307, 129–149. doi:10.1016/j.palaeo.2011.05.008

Smith G.D., 1978. Numerical Solution of Partial Differential Equations: Finite Difference Methods, Oxford University Press, Oxford

Sridevi, J., Sitharam, T.G., 2000. Analysis of strength and moduli of jointed rocks. Geotech. Geol. Eng. 18, 3–21. doi:10.1023/A:1008992621515

Strasky S., Di Nicola L., Baroni C., Salvatore M. C., Baur H., Kubik P. W., Schlüchter C., Wieler R., 2009. Surface exposure ages imply multiple low-amplitude Pleistocene variations in East Antarctic Ice Sheet, Ricker Hills, Victoria Land. Antarctic Science, 21 (1), 59-69. doi: 10.1017/S0954102008001478 Published online by Cambridge University Press 09 Jul 2008.

Sugden, D., Denton, G., 2004. Cenozoic landscape evolution of the Convoy Range to Mackay Glacier area, Transantarctic Mountains: onshore to offshore synthesis. Geological Society of America Bulletin 116, 840–857.

Takeda, A., S. Cox, and A. Payne (2002), Parallel numerical modelling of the Antarctic ice sheet, Comp. Geosci., 28, 723–734.

Tabacco, I.E., Bianchi, C., Chiappini, M., Passerini, A., Zirizzotti, A., Zuccheretti, E., 1999. Latest improvements for the echo sounding system of the Italian radar glaciological group and measurements in Antarctica. Ann. Di Geofis. doi:10.4401/ag-3722

Tabacco, I.E., Bianchi, C., Zirizzotti, A., Zuccheretti, E., Forieri, A., Della Vedova, A., 2002. Airborne radar survey above Vostok region, east-central Antarctica: Ice thickness and Lake Vostok geometry. J. Glaciol. 48, 62–69. doi:10.3189/172756502781831656

Terzaghi K. and Fröhlich O. K., "Theorie der Setzung von Tonschichte," Franz Deuticke, Leipzig/Wien, 1936.

Thomas, M.E., Petford, N., Bromhead, E.N., 2004. The effect of internal gas pressurization on volcanic edifice stability: Evolution towards a critical state. Terra Nov. 16, 312–317. doi:10.1111/j.1365-3121.2004.00567.x

Tibaldi, A., Vezzoli, L., 2004. A new type of volcano flank failure: The resurgent caldera sector collapse, Ischia, Italy. Geophys. Res. Lett. 31, 2–5. doi:10.1029/2004GL020419

Tibaldi, A., Vezzoli, L., 1998. The space problem of caldera resurgence: an example from Ischia Island, Italy. Geol. Rundschau 87, 53–66. doi:10.1007/s005310050189

Tomlinson, E.L., Albert, P.G., Wulf, S., Brown, R.J., Smith, V.C., Keller, J., Orsi, G., Bourne, A.J., Menzies, M.A., 2014. Age and geochemistry of tephra layers from Ischia, Italy: Constraints from proximal-distal correlations with Lago Grande di Monticchio. J. Volcanol. Geotherm. Res. 287, 22–39.

doi:10.1016/j.jvolgeores.2014.09.006.

Van Dusen M.S. 1929. Thermal conductivity of non-metallic solids. (In Washburn, E. W., ed. Intemational critical tables of numerical data, physics, chemistry and technology. New York and London, McGraw-Hill. Vol. 5, 2-16.

Van Wyk de Vries, B., Kerle, N., Petley, D., 2000. Sector collapse forming at Casita volcano, Nicaragua. Geology 28, 167–170. doi:10.1130/0091-7613(2000)28<167:SCFACV>2.0.CO;2

Vargas EA Jr, Chavez E, Gusma˜o LG, Amaral CP, 2009. Is thermal fatigue a possible mechanism for failure of some rock slopes in Rio de Janeiro, Brazil? 43rd US Rock Mechanics Symposium. American Rock Mechanics Association ARMA, Asheville, North Carolina, paper 09-126

Vargas, E., Velloso, R.Q., Chávez, L.E., Gusmão, L., Do Amaral, C.P., 2013. On the effect of thermally induced stresses in failures of some rock slopes in Rio de Janeiro, Brazil. Rock Mech. Rock Eng. 46, 123–134. doi:10.1007/s00603-012-0247-9

Varnes, D.J., Radbruch-Hall, D., Savage, W.Z., 1989. Topographic and structural conditions in areas of gravitational spreading of ridges in the Western United States. United States Geological Survey Professional Paper 1496 (28 pp.).

Varnes, D. J. 1978. Slope movement types and processes. In: Special Report 176: Landslides: Analysis and Control (Eds: Schuster, R. L. & Krizek, R. J.)

Veevers, J.J., 2012. Reconstructions before rifting and drifting reveal the geological connections between Antarctica and its conjugates in Gondwanaland. Earth-Science Rev. 111, 249–318. doi:10.1016/j.earscirev.2011.11.009

Verman, M., Singh, B., Viladkar, M.N., Jethwa, J.L., 1997. Effect of tunnel depth modulus of deformation of rock mass. Rock Mechanics and Rock Engineering 30, 121–127.

Villarraga, C.J., Gendre, V., 2016. The effect of thermal fatigue in a limestone — a laboratory study 1987–1993.

Vinciguerra S., Trovato C., Meredith P.G., Benson P.M., 2005. Relating seismic velocities, thermal cracking and permeability in Mt. Etna and Iceland basalts. International Journal of Rock Mechanics and Mining Sciences 42, 900–910

Vezzoli, L., 1988. Island of Ischia. - In: Vezzoli L (ed) CNR Quaderni de "La ricerca scientifica", 114-10, 122.

Vita, S. De, Sansivero, F., Orsi, G., 2010. caldera (Italy) over the past 10 k . y . 2464, 193–241. doi:10.1130/2010.2464(10).

Vlcko, J., Greif, V., Grof, V., Jezny, M., Petro, L., Brcek, M., 2009. Rock displacement and thermal expansion study at historic heritage sites in Slovakia. Environ. Geol. 58, 1727–1740. doi:10.1007/s00254-008-1672-7

Voight, B., Elsworth, D., 1997. Failure of volcano slopes. Géotechnique 47, 1–31. doi:10.1680/geot.1997.47.1.1

Voight, B., Faust, C., 1982. Frictional heat and strength loss in some rapid landslides. Géotechnique 32, 43–54. doi:10.1680/geot.1982.32.1.43

Wagner, W., Saul, A., and Pruss, A., 1994. International equations for the pressure along the melting and along the sublimation curve of ordinary water substance. Journal of Physical and Chemical Reference Data, 23, 515–27. [11, 254]

Wörner, G., 1999. Lithospheric dynamics and mantle sources of alkaline magmatism of the Cenozoic West Antarctic Rift System. Glob. Planet. Change 23, 61–77. doi:10.1016/S0921-8181(99)00051-X

Wyering, L.D., Villeneuve, M.C., Wallis, I.C., Siratovich, P.A., Kennedy, B.M., Gravley, D.M., Cant, J.L., 2014. Mechanical and physical properties of hydrothermally altered rocks, Taupo Volcanic Zone, New Zealand. J. Volcanol. Geotherm. Res. 288, 76–93. doi:10.1016/j.jvolgeores.2014.10.008

Ye, G. lin, Nishimura, T., Zhang, F., 2015. Experimental study on shear and creep behaviour of green tuff at high temperatures. Int. J. Rock Mech. Min. Sci. 79, 19–28. doi:10.1016/j.ijrmms.2015.08.005

Young, D.A., Wright, A.P., Roberts, J.L., et al., 2011. A dynamic early East Antarctic Ice Sheet suggested by ice-covered fjord landscapes. Nature 474(7349), 72–75.

Zachos, J., Pagani, M., Sloan, L., Thomas, E., Billups, K., 2001. Trends, rhythms, and aberrations in global climate 65 Ma to present. Science 292, 686–693.

Zienkiewicz O.C. 1971. The Finite Element Method in Engineering Science, McGraw-Hill, London

Zischinsky, U. 1966. On the deformation of high slopes. Proc. lst Conf. Int. Soc. Rock Mech., Lisbon, Sect., 2, pp. 179–185.

Zischinsky, U., 1969.Uber sackungen. Rock Mech 1 (1), 30-52

Zorzi, L., Massironi, M., Surian, N., Genevois, R., Floris, M., 2014. How multiple foliations may control large gravitational phenomena: A case study from the Cismon Valley, Eastern Alps, Italy. Geomorphology 207, 149–160. doi:10.1016/j.geomorph.2013.11.001.

Annexes

Sample	Connected Porosity (%)	Bulk Density (kg/m³)	Intact permeability (m²)	Test type	Saturation condition (Dry/Wet)	Thermal stressing temperature (°C)	Confining pressure (MPa)	Pore fluid pressure (MPa)	Effective pressure (MPa)	Peak differential stress (MPa)	Differential stress at C* (MPa)
UGT_2	45.3	1341	2.5 × 10-13	Triaxial	Wet	room	15	10	5	-	1.45
UGT_6	46	1330	1.4 × 10-13	Triaxial	Wet	room	12	10	2	-	2.6
UGT_7	45.7	1346	2.4 × 10-13	Triaxial	Wet	room	11	10	1	-	3.7
UGT_8	48.2	1287	1.0 × 10-13	Uniaxial	Dry	room	-	-	-	5.3	-
UGT_9	44.4	1376	6.6 × 10-14	Uniaxial	Wet	room	-	-	-	3.55	-
UGT_10	47	1341	1.9 × 10-13	Triaxial	Dry	room	1	0	1	6.2	-
UGT_11	48.5	1309	2.5 × 10-13	Uniaxial	Wet	room	-	-	-	1.8	-
UGT_15	46.4	1360	3.9 × 10-14	Triaxial	Dry	room	0.5	0	0.5	5.8	-
UGT_20	43.4	1449	-	Hydrostatic	Dry	room	-	-	-	-	11 (P*)
UGT_21	46.1	1381	1.2 × 10-13	Uniaxial	Dry	100	-	-	-	4.9	-
UGT_22	47	1332	2.2 × 10-13	Triaxial	Dry	room	5	0	5	-	2.6
UGT_23	46.3	1385	-	Uniaxial	Dry	200	-	-	-	4.9	-
UGT_25	46.4	1374	-	Uniaxial	Dry	300	-	-	-	6.4	-
UGT_26	47	1354	1.0 × 10-13	Triaxial	Dry	room	2	0	2	4.6	-
UGT_L_2	44.6	1384	-	Uniaxial	Dry	room	-	-	-	4.4	-
LGT_1	20.7	2031	1.1 × 10-16	Triaxial	Wet	room	11	10	1	27.4	-
LGT_3	20.5	2057	1.5 × 10-16	Triaxial	Dry	room	5	0	5	40.8	-
LGT_6	21.1	2051	3.2 × 10-16	Uniaxial	Dry	room	-	-	-	37.8	-
LGT_7	21.7	2022	-	Uniaxial	Dry	200	-	-	-	33.1	-
LGT_9	21.7	2049	1.1 × 10-15	Uniaxial	Dry	100	-	-	-	26.9	-
LGT_11	20.7	2058	1.3 × 10-16	Triaxial	Wet	room	15	10	5	-	25.7
LGT_12	21.8	2041	-	Uniaxial	Dry	300	-	-	-	34.5	-
LGT_14	21	2069	-	Uniaxial	Dry	room	-	-	-	33.5	-
LGT_16	20.7	2095	1.9 × 10-16	Triaxial	Dry	room	1	0	1	39.6	-

LGT_17	20.4	2106	1.4 × 10-16	Triaxial	Wet	room	12	10	2	34	-
LGT_18	21.4	2076	6.3 × 10-16	Uniaxial	Wet	room	-	-	-	26	-
LGT_20	20.4	2041	1.1 × 10-16	Triaxial	Dry	room	2	0	2	35	-
LGT_31	22.7	2057	1.2 × 10-16	Triaxial	Dry	room	10	0	10	-	41
LGT_L_2	20.2	2039	-	Uniaxial	Dry	room	-	-	-	30	-

Annexed Table 1. Experimental summary for the laboratory mechanical experiments performed for the Mt. Nuovo (Ischia) DSGSD case study.

Rock Mass Deformability parameters adopter in numerical modelling											
lithology	σ_c	J_v	n	r	J_f	$\|E\|_i$	$\|E\|_j$	$\|G\|_i$	$\|B\|_i$	$\|G\|_j$	$\|B\|_j$
	MPa	m^{-3}			m^{-3}	MPa	MPa			MPa	MPa
MEGT	0.5	12	0.82	0.45	32.52	2.82E+03	1.94E+03	1.83E+03	3.76E+02	1.26E+03	2.59E+02
		42	0.82	0.45	113.82		7.62E+02			4.95E+02	1.02E+02
	1	12	0.82	0.45	32.52	2.26E+03	1.55E+03	1.47E+03	3.01E+02	1.01E+03	2.07E+02
		42	0.82	0.45	113.82		6.10E+02			3.96E+02	8.13E+01
	2	12	0.82	0.45	32.52	2.43E+03	1.67E+03	1.58E+03	3.24E+02	1.09E+03	2.23E+02
		42	0.82	0.45	113.82		6.57E+02			4.27E+02	8.76E+01
	5	12	0.82	0.45	32.52	6.73E+02	4.63E+02	4.37E+02	8.97E+01	3.01E+02	6.17E+01
		42	0.82	0.45	113.82		1.82E+02			1.18E+02	2.42E+01
LGT	1	12	0.82	0.8	18.29	1.57E+04	1.27E+04	1.02E+04	2.09E+03	8.27E+03	1.70E+03
		42	0.82	0.8	64.02		7.52E+03			4.89E+03	1.00E+03
	2	12	0.82	0.8	18.29	9.00E+03	7.29E+03	5.85E+03	1.20E+03	4.74E+03	9.73E+02
		42	0.82	0.8	64.02		4.31E+03			2.80E+03	5.75E+02
	5	12	0.82	0.8	18.29	8.60E+03	6.97E+03	5.59E+03	1.15E+03	4.53E+03	9.29E+02
		42	0.82	0.8	64.02		4.12E+03			2.68E+03	5.49E+02
	10	12	0.82	0.8	18.29	1.50E+04	1.21E+04	9.74E+03	2.00E+03	7.89E+03	1.62E+03
		42	0.82	0.8	64.02		7.17E+03			4.66E+03	9.57E+02
LIS	0.5	12	0.82	0.95	15.40	1.84E+04	1.5413E+04	1.2E+04	2.45E+03	1.0018E+04	2.06E+03
	1	12	0.82	0.95	15.40	1.84E+04	1.5414E+04	1.2E+04	2.45E+03	1.0019E+04	2.06E+03
	2	12	0.82	0.95	15.40	1.84E+04	1.5541E+04	1.2E+04	2.45E+03	1.0101E+04	2.07E+03
	5	12	0.82	0.95	15.40	1.84E+04	1.8061E+04	1.2E+04	2.45E+03	1.1739E+04	2.41E+03
	10	12	0.82	0.95	15.40	1.84E+04	2.4977E+04	1.2E+04	2.45E+03	1.6235E+04	3.33E+03
	20	12	0.82	0.95	15.40	1.84E+04	4.0435E+04	1.2E+04	2.45E+03	2.6283E+04	5.39E+03

Annexed Table 2. Mechanical deformability parameters adopted in stress-strain numerical modelling for Ischia Tuffs (MEGT and LGT) and Trachytic lavas (LIS).

Rock Mass Strength parameters adopter in numerical modelling									
	σc	ϱ, γ_d	σ_v	Δσ	B	E	φ	c	t
lithology	MPa	kN/m3	MPa	MPa	MPa	MPa	°	MPa	MPa
MEGT	1	13.15	7.08	6.08	1.90E+03	2257	21	1.9	0.99
MEGT	0.5	13.34	6.12	5.62	2.40E+03	2820	21	1.9	0.99
MEGT	5	13.07	9.38	4.38	5.60E+02	673	21	1.9	0.99
MEGT	2	13.29	6.42	4.42	2.03E+03	2431	21	1.9	0.99
LGT	5	20.18	22.2	17.2	7.20E+03	8601	33	9.1	3.7
LGT	1	20.55	19.9	18.9	1.30E+04	15707	33	9.1	3.7
LGT	2	20.02	17	15	7.50E+03	9002	33	9.1	3.7
LGT	10	20.18	33.4	23.4		14980	33	9.1	3.7

Annexed Table 3. Strength parameters adopted in stress-strain numerical modelling for Ischia Tuffs (MEGT and LGT).

Lithology	Sample	Sampling	Jv	b	Jf	γ (N/m3)	σci	Ei (s3=0)	σcj	ϕp	c	t	ν
		(dd/mm/yyyy)					(Pa)	(Pa)	(Pa)	(°)	(Pa)	(Pa)	
Anphibolite	FP_12	04/01/1987	-	-	-	2.90E+04	1.19E+08	2.42E+11	-	40	6.00E+07	9.42E+07	0.25
Granodiorite	AB3	15/01/1987	-	-	-	2.68E+04	1.60E+08	9.21E+10	-	38	7.00E+07	1.10E+08	0.25

Annexed Table 4. Strength parameters adopted in stress-strain numerical modelling for Antarctic case study. Strength parameters for both Anphibolite and Gradiorite were derived by literature in Chang et al. (2000) and Dayre and Giraud (1986), respectively.

			Confining Pressure (MPa)											
Lithology	Sample	Sampling	1			2			5			10		
			Ei (σ3)	Gi (σ3)	Ki (σ3)	Ei (σ3)	Gi (σ3)	Ki (σ3)	Ei (σ3)	Gi (σ3)	Ki (σ3)	Ei (σ3)	Gi (σ3)	Ki (σ3)
		(dd/mm/yyyy)	(Pa)	(Pa)	(Pa)	(Pa)	(Pa)	(Pa)	(Pa)	(Pa)	(Pa)	(Pa)	(Pa)	(Pa)
Anphibolite	FP_12	04/01/1987	9.63E+11	3.85E+11	6.4228E+11	1.46E+12	5.84E+11	9.74E+11	2.53E+12	1.01E+12	1.69E+12	3.84E+12	1.53E+12	1.28E+12
Granodiorite	AB3	15/01/1987	3.67E+11	1.47E+11	2.44E+11	5.56E+11	2.22E+11	3.70E+11	9.63E+11	3.85E+11	6.42E+11	1.46E+12	5.84E+11	9.73E+11

Annexed Table 5. Deformability parameters adopted in stress-strain numerical modelling for Antarctic case study and derived by UCS tests on samples collected in previous Antarctic Expeditions.